THE
PHYSICAL REVIEW

A journal of experimental and theoretical physics established by E. L. Nichols in 1893

SECOND SERIES, VOL. 74, No. 1 JULY 1, 1948

Range of Protons from $N^{14}(n,p)C^{14}$

I. C. CORNOG, W. FRANZEN, AND W. E. STEPHENS
Randal Morgan Laboratory, University of Pennsylvania, Philadelphia, Pennsylvania
(Received March 12, 1948)

The mean range of protons emitted in the slow neutron disintegration of nitrogen has been measured in a cloud chamber to be 1.00 cm of air, in good agreement with other observers. It is suggested that this range and the energy (561 kev) of the emitted protons as deduced from the $n-H$ mass difference and the extrapolated end point of the C^{14} beta-ray spectrum be used to establish a reliable point on the proton range-energy curve. This point lies on Bethe's original 1937 range-energy curve, but disagrees with Bethe's curve revised to fit the ionization chamber range of artificially accelerated protons.

1. INTRODUCTION

IT has been pointed out[1] that the cycle

$$_0n^1+{}_7N^{14}\rightarrow{}_6C^{14}+{}_1H^1+Q$$
$$_6C^{14}\rightarrow{}_7N^{14}+\beta_-+E$$

leads to

$$n-H=E+Q,$$

and that the best values of these energies known in 1946 were incompatible. Recent work has tended to confirm the suspicion that the proton range-energy curve was at fault.

In order to investigate this cycle in detail, a program was undertaken in this laboratory to measure the carbon 14 beta-ray end point and the range of the protons from the (n,p) reaction. Preliminary values of the C^{14} end point have been published.[2]

Here we wish to describe our measurements on the $N^{14}(n,p)$ protons and to discuss the implications of these data.

[1] W. E. Stephens, Rev. Mod. Phys. **19**, 19 (1947).
[2] W. E. Stephens and Margaret N. Lewis, Phys. Rev. **72**, 526A (1947); Margaret N. Lewis and Miriam Paul, Phys. Rev. **73**, 1269 (1948).

2. OBSERVATIONS

An 800 millicurie radium-beryllium neutron source was surrounded by paraffin and placed near a 15-cm horizontal cloud chamber filled with nitrogen plus n-propyl alcohol and water vapor to a total pressure of one atmosphere. Approximately 4000 stereoscopic photographs were taken and reprojected through the same camera and mirror. 92 protons which had an angle of less than 30° with the horizontal plane of the chamber and greater than 30° with the normal to the mirror were selected for measurement. Figure 1a shows a histogram obtained by grouping the tracks in 0.07-cm groups, and Fig. 1b shows an integral number range curve.

The most probable location of the peak of the differential straggling curve as obtained from the observed track lengths by the method of least squares and in agreement with the value obtained graphically is 1.005 cm. The straggling as estimated from Fig. 1b is 0.065 cm; this compares with a value of 0.03 cm to be expected theoretically.

The stopping power of the gas was determined

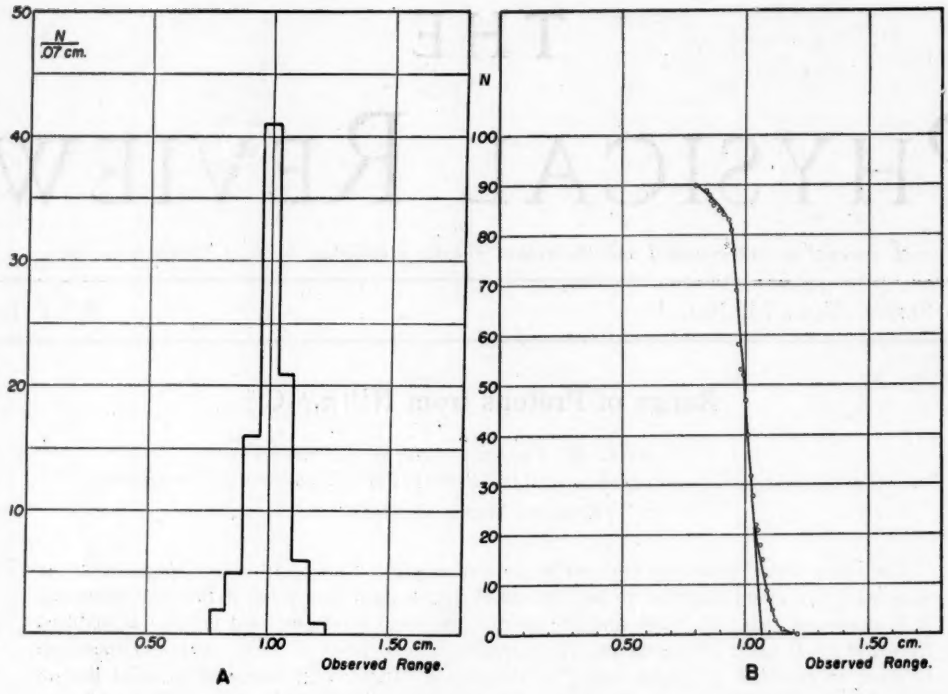

FIG. 1. A. Histogram obtained by grouping $N^{14}(n,p)$ proton tracks in 0.07-cm groups.
B. Integral number range curve obtained for $N^{14}(n,p)$ proton tracks.

by observation of the range of Po alpha-particles emitted by a thick source placed in the chamber. The mean range of the alpha-particles was found by extrapolating an integral straggling curve for the particles and equating the extrapolated range thus obtained to the mean range on the assumption that the source was thick.[3] Figure 2 shows the experimental points obtained. The value of the stopping power calculated from the mean range given by this method (3.773 cm) and the known air range of the alpha-particles[4] (3.842 cm) is 1.018. This value must be increased by 0.3 percent to account for the difference in stopping power of the vapor for polonium alpha-particles and 1.00-cm protons as estimated from Bethe's table[5] of stopping powers and particle velocities. We thus obtain a stopping power of 1.022. This value is in good agreement with a value of 1.03 calculated independently from the known temperature and pressure of the gas before expansion, the expansion ratio, and the estimated composition of the vapor mixture.

From this range in normal air of 1.026 cm we must subtract the range of the recoiling C^{14} nucleus. This range can be estimated to be 0.035 cm by use of Blackett's relation[6]

$$R = kmZ^{-\frac{1}{3}}f(v)$$

and Wrenshall's[7] ranges of C^{12} nuclei. A more reliable value of the range of the C^{14} recoil is obtained from the works of Boggild[8] and Hughes and Eggler[9] who observed 0.03 cm and 0.025 cm, respectively. Assuming 0.03 cm for C^{14}, we obtain a range of 0.996 cm for the range of the proton. The uncertainty in this value can be estimated to be 1 percent for measurement and 1 percent for calibration.

3. DISCUSSION

The proton range observed in these measurements agrees well with results obtained by other

[3] Livingston and Bethe, Rev. Phys. **9**, 287 (1937).
[4] Holloway and Livingston, Phys. Rev. **54**, 18 (1938).
[5] Livingston and Bethe, Rev. Mod. Phys. **9**, 274 (1937).
[6] P. M. S. Blackett, Proc. Roy. Soc. **A107**, 349 (1925).
[7] G. A. Wrenshall, Phys. Rev. **57**, 1095 (1940).
[8] J. K. Boggild, D. Kgl. Danske Vid. Selskab, mat-fys. Medd. **23**, 22 (1945).
[9] Hughes and Eggler, Phys. Rev. **73**, 809 (1948). We are indebted to Dr. D. J. Hughes for measuring his C^{14} recoils and informing us of his results.

observers. Bonner and Brubaker[10] reported a range of 1.06 cm but did not take the C^{14} recoil into account; if a correction for this recoil is applied, one obtains 1.03 cm. Boggild[8] who studied the $N^{14}(n,p)$ reaction incidental to his beautiful and extensive investigation of the slow neutron disintegration of B^{10}, obtained a range of 1.00 cm for the protons emitted in the nitrogen reaction. His cloud chamber was filled with air and methyl-alcohol vapor to a pressure of 18-cm Hg. The resulting low stopping power enabled Boggild to see the C^{14} recoil track and to subtract its observed range (0.03 cm) from the observed total track length. The straggling in track lengths (0.03 cm) in his case is just equal to the theoretical value, or approximately one-half of the value observed in our experiment. (This is presumably due to the greater accuracy of measurement attainable at lower pressures with resulting longer track lengths.) Recent work, also done with low pressure air, reported by Hughes and Eggler[9] gives a value of 0.991 cm for the proton range. In this case, the proton ranges were measured by disregarding the portion of the track identified as due to the recoiling C^{14} by its denser ionization. All these results are consistent with a range of 1.00 cm for the proton produced in the slow neutron disintegration of nitrogen.*

Several measurements have been made with ionization chambers of the disintegration energy Q of the $N^{14}(n,p)C^{14}$ reaction with slow neutrons. Huber reports two values, 0.57 ± 0.04 Mev[11] and 0.63 ± 0.01 Mev.[12] However, it appears probable that a more reliable value of Q can be obtained by means of the transmutation cycle mentioned previously. For this it is necessary to know the $n-H$ mass difference and the C^{14} beta-ray spectrum end point.

A value of 755 ± 16 kev is derived in reference 1 for the $n-H$ mass difference by averaging the results of three reliable experiments in which the threshold for the photo-disintegration of the deuteron was determined with different methods of detection. (This value is slightly higher than the value of 751 ± 6 kev sometimes quoted.[13] The lower value is based on a measurement of the $D(e,n)$ threshold,[14] the accuracy of which depends on the calibration of the electron energy used. In the absence of details relating to this calibration, it is not possible to estimate the reliability of the quoted error.)

Several experiments on the end point of the C^{14} beta-ray spectrum now allow an estimate of E. Assuming the validity of the Fermi theory of beta-decay, we can define E as the extrapolated end point on a Kurie plot; this end point is independent of the neutrino mass.[15] The extrapolated end point of the C^{14} beta-ray spectrum has been determined in a beta-ray spectrograph as

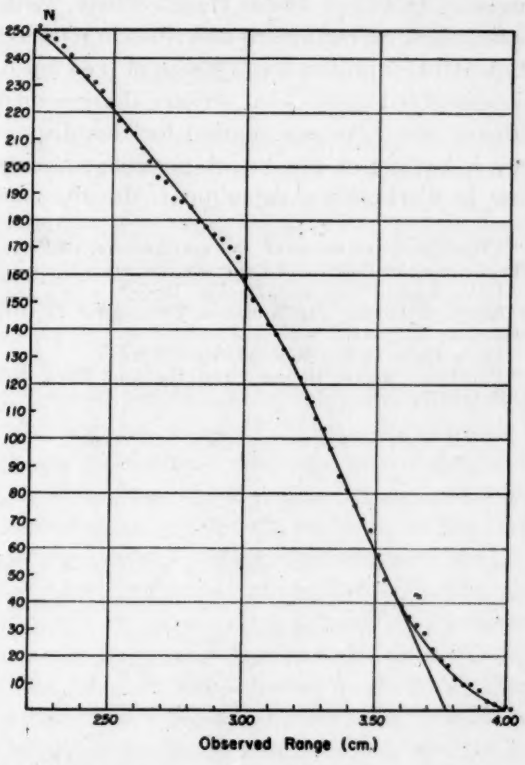

FIG. 2. Integral number range curve obtained for polonium alpha-particles emitted by thick source placed in chamber.

[10] Bonner and Brubaker, Phys. Rev. **49**, 778 (1936).

* *Note added in proof:*—Another determination of the range of the N^{14} (n,p) protons was reported by Cüer (J. de Phys. et Rad. VIII–8, 83 (1947)), who exposed a photographic emulsion impregnated with NaN_3 to slow neutrons and observed the transmutation tracks in the emulsion. He observed a range of 0.985 cm with an estimated uncertainty of 5 percent due to grain straggling and stopping power calibration. This is consistant with our conclusions.

[11] Huber, Huber, and Scherrer, Helv. Phys. Acta **13**, 209 (1940).

[12] Huber and Stebler, Phys. Rev. **73**, 85 (1948).

[13] D. J. Hughes, Phys. Rev. **70**, 219 (1946).

[14] Wiedenbeck and Marhoefer, Phys. Rev. **67**, 54 (1945).

[15] O. Kofoed-Hansen, Phys. Rev. **71**, 451 (1947).

153±5 kev (photographic detection)[16] and 154 kev (counter detection).[17] These values agree with an absorption curve end point of 154 kev.[18] A value of 154±5 kev seems reasonable from these data.

Using $n-H=755\pm16$ kev and $E=154\pm5$ kev, gives $Q=601\pm17$ kev. The proton gets 14/15 of the energy or 561±16 kev. These data seem now to be reliable and consistent enough to establish a point on the proton range-energy curve such that a proton of 561 kev has a range of 1.00 cm with an accuracy of probably better than 3 percent.

Such a point disagrees with the unpublished but blue-printed curve set up by Bethe[19] from the work of Parkinson, Herb, Bellamy, and Hudson[20] on the range of protons accelerated in a statitron. Parkinson's data give ionization extrapolated ranges at 0°C and 76-cm Hg and have to be corrected to compare with the mean ranges at 15°C and 76-cm Hg used here. Bethe applied these corrections as described in reference 19. A 560-kev proton has a range of 0.83 cm on this corrected curve, in serious disagreement with our data. An explanation for this discrepancy is lacking at present. A possible source of error in Parkinson's experiment already mentioned by him is the actual temperature of the gas in the beam which may have been higher than measured due to heating by the beam; the correction that this requires would, however, increase rather than decrease the disagreement.

The 561-kev−1.00-cm point agrees very closely with Bethe's original curve[21] which was computed from Blackett and Lees' experiments[22] on the ranges of low energy alpha-particles. In these computations the rule $R_H(v)=1.0072R_\alpha(v)-0.20$ cm was used. If the revised 1938 alpha-particle range-energy curve[23] is used instead of Blackett and Lees' results, only an inappreciable change results.

Consequently the part of Bethe's original curve near 1 cm may be regarded as more nearly correct than the curve revised by use of Parkinson's data. However, the very close agreement at this point may be fortuitous as indicated by the fact that the revised curve fits data on the disintegration of the deuteron[19] by Th C″ gamma-rays considerably better than the original curve. The desirability of new experiments to establish a reliable proton range-energy curve in the low energy region is evident from these observations.

This research was supported in part by the Office of Naval Research. We wish to thank Miss Grace Marmor for assistance in reading the films.

[16] Unpublished estimate of the extrapolated end point from the work of Lewis and Paul; see reference 2.
[17] P. W. Levy, Phys. Rev. **72**, 248 (1947).
[18] Solomon, Gould, and Anfinsen, Phys. Rev. **72**, 1097 (1947).
[19] H. A. Bethe, Phys. Rev. **53**, 313 (1938).
[20] Parkinson, Herb, Bellamy and Hudson, Phys. Rev. **52**, 79 (1937).
[21] Livingston and Bethe, Rev. Mod. Phys. **9**, 268 (1937).
[22] Blackett and Lees, Proc. Roy. Soc. **A134**, 658 (1932).
[23] Holloway and Livingston, Phys. Rev. **54**, 30 (1938).

PHYSICAL REVIEW VOLUME 74, NUMBER 1 JULY 1, 1948

The Emission of Protons from Light Nuclei on Bombardment with α-Particles of Short Range

F. C. CHAMPION AND R. R. ROY
King's College, University of London, England

(Received February 16, 1948)

The expansion chamber method is used to obtain tracks of protons ejected in 67 disintegrations of fluorine and 121 disintegrations of neon while both gases are under α-particle bombardment. The energetics of the reaction are in good agreement with the mass data, and protons corresponding to transitions to the ground state of the residual nuclei are found with both elements. No disintegrations are detected until the energies of the α-particles reach 3.7 and 4.4 Mev in fluorine and neon, respectively. These are the only energy levels recorded.

The ranges of the protons from fluorine vary within wide limits (an indication of several excited states of the residual nucleus), while those from neon show only one range corresponding to the ground state. In all cases the angular distribution of the ejected protons is anisotropic, and evidence is given that the low energy α-particles responsible for the disintegrations all make off-center collisions and therefore possess angular momentum about the nuclear center. A simple model of the collision process is suggested to account for these results and also for the relative yields which are in the ratio 1:0.5:2 for nitrogen, fluorine, and neon, respectively. A possible cause of the apparent disintegration of nitrogen by α-particles of very low energy is discussed.

I. INTRODUCTION

A CONSIDERABLE quantity of data is now available on the proton emission accompanying the disintegration of light nuclei by α-particle bombardment.[1] Most of the experiments have hitherto been performed with α-particles of 5- to 8-Mev energy using electrical methods of recording. We have now applied the expansion chamber method to examine the disintegration of the three elements, nitrogen, fluorine, and neon by α-particles of energies 0–5 Mev.

The information which could be derived from such experiments would ideally comprise (1) establishment of resonance levels and a measurement of their energy and breadth, (2) demonstration of the existence and the nature of the selection rules governing nuclear disintegration, and (3) measurement of the absolute yield of the disintegration process. The quantities measured experimentally are the numbers and ranges of the emitted protons and of the incident α-particles, together with the angular distribution of the direction of ejection of the protons with respect to the direction of the incident α-particles. We have already presented[2] some results for nitrogen which showed that the angular distribution of the group of protons emitted, when the remaining range R_a of the incident α-particles in air at S.T.P. was 2.1 cm, had a pronounced maximum when $\theta \approx 90°$, where θ is the angle between the direction of emission of the proton and the direction of the incident α-particle. While disintegration experiments with nitrogen have been undertaken with success by several workers, the disintegration of fluorine and neon by α-particle bombardment has not hitherto been demonstrated by the expansion chamber method.

II. EXPERIMENTAL METHOD

The expansion chamber used was larger than in the previous experiment with nitrogen for it was now 16.5 cm in diameter and about 4 cm high. It enclosed a thin cylinder of Cellophane mounted coaxially and of diameter 10 cm. The stopping power of the Cellophane was about 3 cm of air. Such an arrangement allowed the estimation of the range of protons which would otherwise have been uncertain because of their passage out of the expansion chamber. This improvement was only partially successful for it introduced straggling up to 1 cm because the protons passed through the cylinder at varying angles. Uncertainties also arose from possible inhomogeneity in thickness of the Cellophane and condensation of water vapor on the Cellophane surface.

[1] M. S. Livingston and H. A. Bethe, Rev. Mod. Phys 9, 299 (1937).
[2] F. Champion and R. Roy, Proc. Roy. Soc. **A191**, 269 (1947).

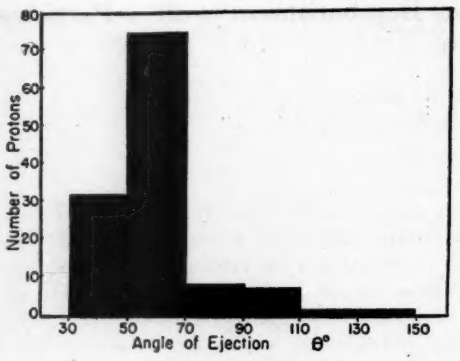

FIG. 1. Angular distribution of protons ejected from neon under α-particle bombardment.

The slit and shutter system were also improved with a view to obtaining a finer and more rectangular beam of condensation, but certain difficulties still remain which can only be remedied by the construction of a chamber working at lower pressure. For example, the fact that the neon was contaminated with 20 percent helium and also that the fluorine, in the form of carbon tetrafluoride, had to be diluted with helium in order to give a suitable stopping power resulted in a broadening of the condensation beam even more than in the previous experiment with nitrogen. This was partly caused by the greater mobility of the ions in helium, but it resulted mainly from the long ranges of the projected helium nuclei and the α-particles scattered by the various nuclei present. To avoid including projected protons arising from possible hydrogen contamination, protons ejected with $\theta<30°$ were neglected. This precaution at small angles, together with the mechanical interference at large angles produced by the presence of the slit system on back-projected protons, restricted the effective angular range of examination to between 30° and 120°.

III. RESULTS

A. Fluorine

In 1775 photographs in 25 percent carbon tetrafluoride and 75 percent helium, with minor impurities of not more than 2 percent nitrogen, carbon dioxide, fluorine oxide, and oxygen, 67 disintegrations were obtained. In the only other expansion chamber experiment on record,[3] a much weaker source of α-particles was used and no disintegrations were found in 6265 photographs. The ranges of the ejected protons had all values from 8 cm upwards, with 19 examples in which the range exceeded the confines of the expansion chamber. No disintegrations were found for $R_\alpha<1.9$ cm and all those registered lay between this limit and $R_\alpha=2.3$ cm. The angular distribution of the whole 67 tracks of all ranges was roughly isotropic over the angular range 30° to 120°. No effective separation of the protons into discrete groups was possible with the resolution available. However, the angular distribution of the 19 protons which passed out of the expansion chamber was examined separately and found to show a preponderance at the smaller angles.

B. Neon

In 1200 photographs in about 80 percent neon, 20 percent helium, and less than 2 percent nitrogen, 121 disintegrations were recorded. The protons were all of range 8 cm with a spread of about 1 cm. This spread may be due to more than one energy of emission of the protons but the resolving power of the apparatus is too poor to establish this. All protons were emitted soon after the α-ray beam emerged from the slit system when R_α lay between 2.6 and 3 cm. The angular distribution is shown in Fig. 1.

IV. DISCUSSION

According to the mass data,[4] the fluorine reaction is exothermic for the ground state with $Q=+1.57$ Mev. From our observations with $R_\alpha=2.3$ cm corresponding to $E_\alpha=3.7$ Mev, the maximum range of the protons emitted should be about 35 cm. These could correspond to the 19 examples where the range of the protons exceeded the size of the expansion chamber. Those of smaller range would correspond to a number of excited levels of the residual nucleus formed in the reaction. Several of them are known to exist from the reports of other workers.[1]

With neon, the mass data indicate a value of $Q=-1.7$ Mev. From our observations, the energy of the protons emitted is about 2.1 Mev

[3] N. Feather, Proc. Roy. Soc. **A141**, 194 (1933).

[4] G. Mattauch, *Nuclear Physics Tables* (Interscience Publishers, Inc., New York, 1946).

and of the α-particles responsible for the disintegration $E_\alpha = 4.4$ Mev. We therefore conclude that we are observing the protons from the ground state. Apart from the initial report,[5] the only other experiment[6] on the disintegration of neon used electrical methods of recording. With α-particles of up to 8-Mev energy, these workers found a value of $Q = -2.54$ Mev, which indicated an excited state of the residual nucleus. These faster α-particles passed over the top of the potential barrier whereas our protons come from a resonance disintegration. The results clearly support the view that the ground state of the nucleus is more likely to be in evidence the lower the energy of the bombarding particles.

The angular distribution of all the protons ejected from fluorine is approximately isotropic when examined as a whole. It is difficult to extract as much information as is desirable in this case because of our inability to resolve the energies of the individual proton groups. However, some interesting conclusions can be drawn if attention is confined to the long-range protons possibly corresponding to the ground state. The distribution of these 19 protons shows a maximum at the smallest angle, that is at 30°, and then shows a gradual decrease at larger angles, no protons being recorded for $\theta > 60°$. In this group, therefore, the distribution is anisotropic and, since the total distribution of all the ranges is approximately isotropic, by subtraction one at least of the remaining groups must also be anisotropic. With neon, Fig. 1 shows that the angular distribution has a pronounced maximum at $\theta \approx 60°$. The relatively large number which also occurs at angles close to 30° should almost certainly be reduced, for some of these tracks were on the short-range side and were probably protons projected from hydrogen contamination. A few tracks were recorded at high angles but, as has already been explained, the present experimental arrangement is not very suitable for reliable recording of protons ejected at much more than 90°. Therefore, we are unable to state definitely that the theoretically fundamental requirement for resonance disintegrations from a single level is fulfilled, namely, that the angular distribution should be symmetrical in the forwards and backwards direction. The results in nitrogen have been shown to be in fair agreement with this requirement but as the distribution rose rather sharply to a maximum at $\theta \approx 90°$ in that case, the evidence is not entirely conclusive. Our general impression with fluorine is that there are fewer particles emitted in the backward than in the forward direction, but this may be explicable in terms of interference effects resulting from a complex level system.[7]

Attempts which we have made to explain the results in terms of an α-particle substructure of the nuclei concerned have been completely unsuccessful. In our last paper we suggested that nuclei containing equal numbers of neutrons and protons possessed symmetrically arranged nucleons with the protons closer to the nuclear surface than the neutrons. Off-center collisions by α-particles possessing angular momentum with respect to the nuclear center would then result in impact on a particular proton, which would leave the nucleus after a time sufficient to allow appreciable nuclear rotation to occur, according to the principle of the conservation of angular momentum. Such a simple picture would predict a rotation in neon somewhat less than in nitrogen for incident α-particles of the same impulse. Consequently, ejection would occur at smaller angles in neon than in nitrogen; the experimental results show $\theta = 60°$ and 90°, respectively. For fluorine which contains ten neutrons and nine protons the symmetry is lacking, and the protons are likely to be less close to the nuclear surface. For proton emission, therefore, an α-particle must make a nuclear collision which is relatively less off-center and, consequently, less angular momentum should be imparted to the nucleus. Less rotation should result and, in agreement with experiment, protons should be ejected mainly at smaller angles. We are aware that such a picture is not easy to reconcile with present theoretical views of nuclear disintegration, according to which the incident particle is completely absorbed in the nucleus for an appreciable time before disintegration occurs and according to which the nu-

[5] E. Rutherford, J. Chadwick, and C. Ellis, *Radiations from Radioactive Substances* (Cambridge University Press, Teddington, 1930), p. 293.

[6] E. Pollard and C. J. Brasefield, Phys. Rev. **51**, 8 (1937).

[7] S. Rubin, Phys. Rev. **72**, 1176 (1947).

cleon which is first struck bears no relation to the nucleon which is finally emitted. We wish to emphasize that more data are required on the back-projected protons before a final decision can be reached on this point.

The strength of the polonium source in these experiments was 4 mc and an approximate comparison of the yields with the three elements shows them to be in the ratio 1:0.5:2 for nitrogen, fluorine, and neon, respectively. The high yield with neon is perhaps surprising but several factors could account for this. For example, the energy of the α-particles responsible for the neon disintegration is somewhat higher than with the other two elements. On the other hand, the smaller yield with fluorine is explicable by the simple picture that we have suggested, in which the protons are less close to the nuclear surface and hence the nucleus presents an effectively smaller cross section for proton emission resulting from the impact of α-particles which have made off-center collisions.

It is interesting to note that all the angular distributions recorded are anisotropic and the implication is that probably none of the disintegrations produced by these low energy α-particles corresponds to an s-state. Earlier evidence[8] has been given in this respect in that the width of the resonance levels in fluorine have been shown to require disintegration from a p-level when α-particles of low energy are used.

One outstanding difference exists between the observations in nitrogen and the other two gases. With fluorine and neon no disintegrations were observed when the α-particle range fell below 2 cm, whereas in nitrogen several such cases were found. We have explained that the intense source of α-particles which was used resulted in a condensation beam of some breadth and this limited the accuracy with which R_α could be determined, unless $\theta=90°$. However, under this ideal condition, three cases were found where $R_\alpha<1.4$ cm. Now from the mass data it follows that if energy and momentum are conserved in all disintegrations, it is impossible for protons of range such as that shown in our previous paper, Fig. 7, Plate 19, to be produced by α-particles with $R_\alpha<1.4$ cm. Previous workers[1] have, on many occasions, found Q values for nitrogen much larger than that calculated from the mass data. In particular, technically good photographs[9] have recorded a value as high as $+0.94$ Mev, whereas the value calculated from the mass data is -1.2 Mev. The suggestion made to account for this discrepancy was that the recoil nucleus made an unresolved collision with another nucleus, although the chances against such an event were 200:1. We too can explain our anomaly in a similar fashion. For example, the anomalous protons might be those liberated in a forward direction within the collimating slits by α-particles of high energy. At some point of their path, before they emerge from the end of the condensation beam, these protons might be deflected by a nuclear encounter and emerge from the beam at a high angle at some point close to the end of the range of the α-particles. They would thus give the appearance of having been generated close to the end of the range. It seems only reasonable to point out, however, that if this explanation is the correct one, it is difficult to understand why such behavior is not found with fluorine and neon.

V. ACKNOWLEDGMENTS

We thank the Medical Research Council Radon Centre for the generous gift of old radon tubes from which we extracted the polonium and Imperial Chemical Industries for the donation of the carbon tetrafluoride.

[8] J. Chadwick and J. Constable, Proc. Roy. Soc. **A135**, 49 (1932).

[9] P. Blackett and D. Lees, Proc. Roy. Soc. **A136**, 325 (1932).

PHYSICAL REVIEW VOLUME 74, NUMBER 1 JULY 1, 1948

Internal Friction in the Interstitial Solid Solutions of C and O in Tantalum*

T'ING-SUI KÊ
Institute for the Study of Metals, The University of Chicago, Chicago, Illinois

(Received February 5, 1948)

A strongly temperature-dependent type of internal friction is observed in tantalum specimens containing a small amount of carbon or oxygen. Internal friction peaks occur, respectively, around 150°C and 170°C for carbon and oxygen when the frequency of vibration is about one cycle per second. The activation energies associated with these relaxations are found to be 25,000 calories per mole for carbon and 29,000 calories per mole for oxygen. These observations are consistent with the viewpoint that the relaxations observed are associated with the anelasticity caused by the stress-induced preferential distribution of C or O among the various interstitial positions which have tetragonal symmetry in body-centered cubic tantalum. Such a picture has been proposed by Snoek in interpreting the relaxation phenomena observed in alpha-iron (body-centered cubic) containing small amounts of carbon or nitrogen. The observations in tantalum might thus indicate that such relaxations are characteristic of all interstitial solid solutions of body-centered cubic metals. It has been further found that the carbon relaxation peak can be interpreted in terms of a relaxation process having a single relaxation time with a unique activation energy while the oxygen peak can not. This suggests that the interstitial atoms responsible for the observed relaxation peaks in tantalum are situated at the octahedral positions in the case of carbon and at both octahedral and tetrahedral positions in the case of oxygen.

I. INTRODUCTION

A STRONGLY temperature-dependent type of internal friction has been observed in iron for many years. An internal friction peak occurs around room temperature when the frequency of vibration is of the order of one cycle per second. Recently, Snoek[1] proposed that this internal friction is due to the anelasticity associated with the stress-induced preferential distribution of carbon or nitrogen atoms in primary solid solution of alpha-iron. Let us consider the octahedral interstitial positions in the lattice of alpha-iron which has a body-centered cubic structure. If carbon or nitrogen atoms go into these positions, tetragonal deformation will be introduced in the lattice with the tetragonal axis along one of the three ⟨100⟩ directions. When a tensile stress is applied along one of these axes, there will be a greater probability that a solute atom be in an interstitial position with tetragonal axis along this axis. The establishment of this preferential distribution of solute atoms causes a relaxation phenomenon and will manifest itself as internal friction and related effects.

It can be seen that no anelastic effects are to be expected when the tensile stress is applied along a ⟨111⟩ direction, for then all interstitial positions are equivalent. This high anisotropy of the anelasticity in single crystals of alpha-iron has been confirmed by Dijkstra,[2] who showed that the relaxation strength along a ⟨111⟩ direction is only about 5 percent of that along a ⟨100⟩ direction.

If the above picture is correct, this type of strongly temperature-dependent anelastic effects observed in alpha-iron should also occur in the primary solid solution of other body-centered cubic metals containing interstitial solute atoms. On the other hand, accepting this picture of stress-induced preferential distribution of solute atoms, information can be derived from measurements of anelastic effects as to the properties of the interstitial solid solutions in other body-centered cubic metals.

As far as the author is aware, there is no experimental information in the literature about the interstitial solid solutions of tantalum which has a body-centered cubic structure. The purpose of the present paper is to describe some internal friction measurements from which the conclusion can be drawn that carbon and oxygen do form interstitial solutions with tantalum. This observation is the first evidence that oxygen forms interstitial solid solution with a metal. A discussion is made of the location of C and O in the octahedral or tetrahedral position in the tantalum lattice.

* This research has been supported by ONR Contract No. N-6ori-20-IV.

[1] J. L. Snoek, Physica 8, 711 (1941).

[2] L. J. Dijkstra, Philips Research Reports 2, 357 (1947).

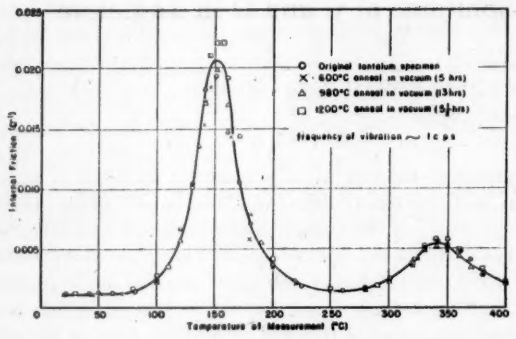

FIG. 1. Variation of internal friction with temperature in tantalum specimens (containing 0.013 percent of carbon) annealed in vacuum at various temperatures. Frequency of vibration is about one cycle per second.

II. INTERNAL FRICTION IN TANTALUM CONTAINING CARBON

The tantalum used in the measurements was 99.9 percent pure and was received in annealed form in wires having a diameter of 0.03 inch. It was fine-grained and had a rather uniform grain size. A wire of about one foot long was cut from the spool and straightened by stretching. It was mounted in the furnace for torsional measurements. A description of the torsional apparatus has been given before.[3] The natural frequency of the vibrating system, including the specimen and the auxiliary inertia member, was about 1.2 cycles per second and the total longitudinal load on the wire was about 28 g. As the Young's modulus of tantalum is 2.7×10^{7} pounds per square inch, this load corresponds to a longitudinal elastic strain of the order of magnitude of 10^{-6}. This is smaller than the average shearing strain, which is about 10^{-5}, applied to the wire during the dynamic torsional measurements. Under these conditions it has been found that the internal friction in the specimen is independent of the stress amplitude.

All the internal friction measurements were taken in an atmosphere of argon having a purity of 99.8 percent. The temperature of the specimen was controlled and measured with a relative accuracy of 1°C with a Tag Celectray indicating temperature controller.

The variation of internal friction with temperature in this tantalum wire is shown in Fig. 1. The internal friction curve does not change by annealing in vacuum at various temperatures. This indicates that the internal friction peaks observed have nothing to do with cold-working. With a frequency of about one cycle per second, the first internal friction peak or the lower temperature peak occurs at a temperature of about 150°C and the second peak or the higher temperature peak occurs at about 350°C. Let us first confine ourselves to the lower temperature peak. The physical origin of the higher temperature peak will be discussed in a later paper.

The heat of activation associated with the lower temperature peak was determined by taking measurements at two different frequencies. The internal friction curves corresponding to these two frequencies are shown in Fig. 2. The lower frequency used was about 0.3 cycles per second. It is shown in Fig. 3 that these two curves can be superposed on each other by a horizontal shift of the $1/T$ scale through 0.105×10^{-3}. As the two frequencies of vibration have a constant ratio of 3.81 over the whole temperature range concerned, this gives a heat

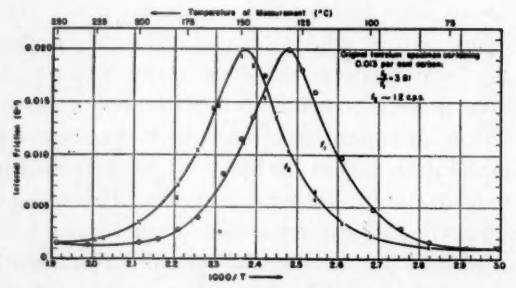

FIG. 2. Internal friction curves for tantalum specimen (containing 0.013 percent of carbon) with two frequencies of vibration having a ratio of 3.81.

[3] T. S. Kê, Phys. Rev. 71, 533 (1947).

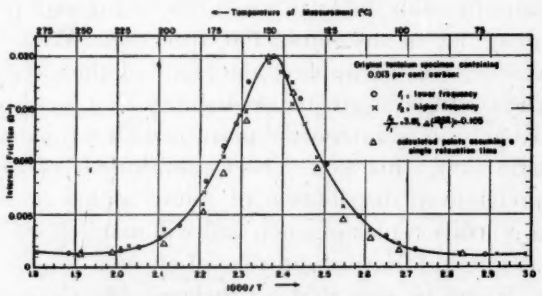

FIG. 3. Determination of heat of activation associated with the lower temperature peak shown in Fig. 1 by a horizontal shift of the two internal friction curves shown in Fig. 2. The two curves were superposed on each other by a relative shift of the $1000/T$ scale through 0.105. This gives a heat of activation of 25,000 calories per mole. The triangles indicate the calculated points assuming a single relaxation time and a unique heat of activation.

of activation of 25,000 calories per mole following similar calculations made before.[4]

In relaxation processes having a single relaxation time, τ, the internal friction Q^{-1} associated with this relaxation is given, if the relaxation is small, by the following well-known relation:

$$Q^{-1}=\Delta_M(\tau\omega/1+\tau^2\omega^2), \quad (1)$$

where Δ_M is the total relaxation strength and ω is the angular frequency of vibration. It can be shown that the internal friction will reach its maximum value when

$$\tau\omega=1, \quad (2)$$

and Eq. (1) becomes

$$Q^{-1}=2Q_{\max}{}^{-1}(\tau\omega/1+\tau^2\omega^2). \quad (3)$$

The temperature dependence of the relaxation time can be represented by the expression

$$\tau=\tau_0 e^{H/RT}, \quad (4)$$

where H is the heat of activation, R the gas constant, and τ_0 a coefficient which can be determined from Eqs. (2) and (4) and the known value of H. As H has been found to be 25,000 calories per mole and the frequency of vibration is 1.24 c.p.s. at the optimum temperature 148°C (421°K), we have

$$\tau_0=1.6\times10^{-14} \text{ sec.} \quad (5)$$

The theoretical internal friction at various temperatures for a relaxation process having a single relaxation time can thus be calculated according to Eq. (3). In our present case these calculated points are indicated by the triangles in Fig. 3. They lie fairly close to the observed curve. This shows that the observed relaxation phenomenon (the lower temperature peak) has a single relaxation time.

In order to confirm this conclusion, the internal friction curve shown in Fig. 3 was plotted in Fig. 4 with the logarithm of Q^{-1} against $1/T$. The two straight-line asymptotes shown have slopes of equal magnitude but of opposite sign, and the heat of activation H determined from both slopes is 25,000 calories per mole, which is identical with the value previously obtained by a different method. These two straight lines intersect at a point where the internal friction is 0.04, which is twice as much as the maximum

[4] T. S. Kê, Phys. Rev. **72**, 41 (1947).

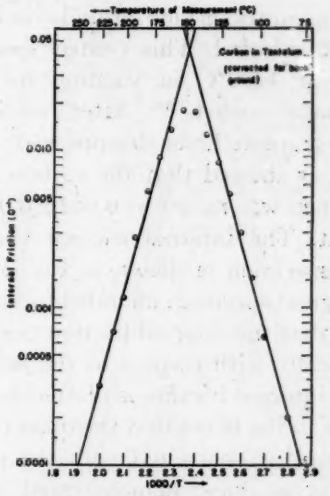

FIG. 4. Internal friction in tantalum specimen containing 0.013 percent of carbon with log Q^{-1} plotted against $1/T$. The straight-line asymptotes have slopes of equal magnitude but of opposite sign. The heat of activation calculated from these slopes is 25,000 calories per mole.

internal friction. All these results are in conformity with Eq. (1), indicating a single relaxation time.

The existence of a single relaxation time suggests that the observed relaxation phenomenon is associated with a diffusion process having a definite and unique diffusion distance.

Chemical analysis of the carbon content in the tantalum specimen by combustion method showed 0.013±0.003 percent of carbon by weight.** This specimen was enriched in carbon

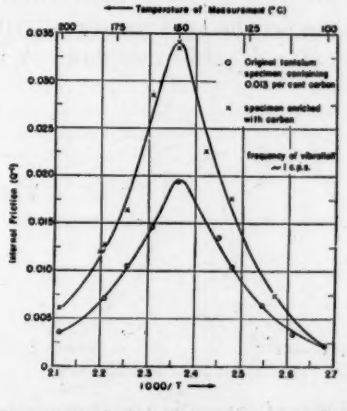
Temperature of Measurement (°C)
Original tantalum specimen containing 0.013 per cent carbon
Specimen enriched with carbon
Internal Friction (Q⁻¹)
1000/T

FIG. 5. Internal friction curve for tantalum specimen enriched with carbon compared with the curve for the original specimen containing 0.013 percent of carbon. The symmetrical increase of the original curve indicates that the internal friction peak concerned is due to carbon.

** Thanks are due Mr. R. E. Fryxell and Dr. N. H. Nachtrieb of this Institute for making this analysis.

by painting on its surface a thin layer of colloidal graphite in alcohol. This coated specimen was annealed at 1200°C in vacuum for 48 hours and furnace cooled.*** After such a treatment the graphite layer disappeared, and chemical analysis showed that the carbon content in the specimen was raised to 0.062 ± 0.003 percent by weight. The internal friction curve of the enriched specimen is shown in Fig. 5 with that of the original specimen included for comparison. It is seen that the internal friction peak increases symmetrically with respect to the original peak when the internal friction is plotted against $1/T$. This leads to the belief that the observed internal friction peak is connected with the presence of carbon. As we have demonstrated above that the relaxation process has a single relaxation time, this means that the observed internal friction peak (lower temperature peak in Fig. 1) is due to carbon alone.

In the case of alpha-iron, the carbon peak occurs around 35°C when the frequency of vibration is about one cycle per second. As the melting point of tantalum is higher than that of iron, the relaxation peak for carbon would be expected to occur at a higher temperature in tantalum than in alpha-iron. This was found to be the case as the carbon peak in tantalum occurs around 150°C. Thus, with reference to the previous work on alpha-iron, it is reasonable to infer that the observed internal friction peak is due to the stress-induced preferential distribution of C among the various interstitial positions in body-centered cubic tantalum. A corroboration of this inference by stress relaxation measurements will be described in a later paper.

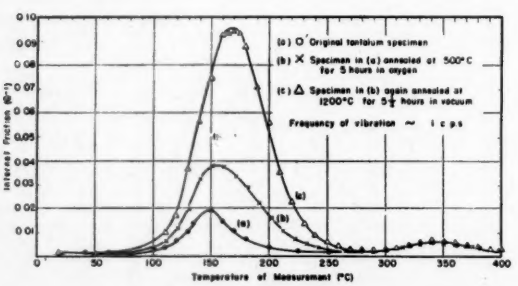

FIG. 6. Effect of oxygen in tantalum upon the internal friction peak observed in tantalum specimen containing 0.013 percent of carbon. The original internal friction curve was raised and shifted toward higher temperatures because of the addition of oxygen.

*** Thanks are due Mr. Harold H. Hirsch of this Institute for help in treating the specimen.

The higher temperature internal friction peak shown in Fig. 1 was found not to change with the amount of carbon in tantalum. Accordingly, it is not connected with the presence of carbon.

It should be mentioned that the internal friction peak for the specimen enriched with carbon (Fig. 5) is not stable, and all the measurements should be made as rapidly as possible. Thus it has been found that when the temperature of the specimen is raised, the internal friction increases with annealing time at a given temperature. This indicates that segregation of carbon from the solid solution has taken place when the specimen was furnace cooled from 1200°C to room temperature during the treatment. As the temperature of the specimen is raised during the measurement, some carbon will redissolve, resulting in the increase of internal friction, until the saturation value is reached. It is evident, then, that the carbon content in the specimen as determined by chemical analysis (0.062 percent) is more than the saturation value at 150°C. Taking the lower curve in Fig. 5 as standard (containing 0.013 percent of carbon), estimation can be made from the relative height of the two peaks that the solubility of carbon in tantalum at 150°C is approximately 0.02 percent assuming that the internal friction is linear with the carbon concentration in the specimen concerned.

III. INTERNAL FRICTION IN TANTALUM CONTAINING OXYGEN

The effect of oxygen in tantalum upon the internal friction peak described in the last section is shown in Fig. 6. Curve *a* shows the internal friction observed in the original tantalum specimen containing 0.013 percent of carbon. This specimen was annealed in an atmosphere of oxygen at 500°C for five hours. Such a treatment resulted in the formation of a thin oxide layer on the surface of the specimen. The internal friction peak (curve *b*) for this specimen was raised and shifted toward higher temperatures relative to the original curve. This indicates that some oxygen atoms have diffused into the specimen during the annealing to form interstitial solid solution with tantalum. According to this viewpoint, the new internal friction peak

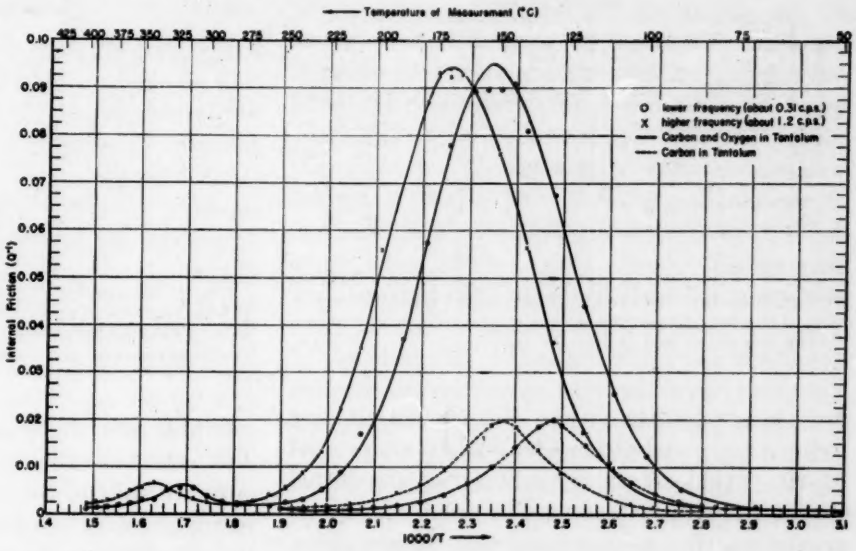
Temperature of Measurement (°C)
O lower frequency (about 0.31 c.p.s.)
X higher frequency (about 1.2 c.p.s.)
Carbon and Oxygen in Tantalum
Carbon in Tantalum
Internal Friction (Q⁻¹)
1000/T

FIG. 7. Internal friction curves for original tantalum specimen (dotted curves) and for the oxygen-enriched specimen (solid curves). Both were determined with two frequencies of vibration.

is a combination of the original carbon peak and an additional oxygen peak with its maximum at a higher temperature. This viewpoint is strengthened by the finding that the raise and shift toward higher temperatures of the internal friction peak are much more marked (curve *c*) after the oxide-coated specimen was again annealed in vacuum at 1200°C and furnace cooled. After such a treatment, the oxide layer originally formed on the surface of the specimen disappeared. As the weight of specimen remains unchanged before and after the treatment at 1200°C, the surface layer must have been diffused into the specimen. The increase in weight of the specimen compared with the original specimen was about 0.06 percent. If all this oxygen goes into solution, then the oxygen content in solution will be about 0.06 percent by weight. From Fig. 6, the internal friction curve for this specimen reaches a maximum value of about 0.1, which is higher than any internal friction peak so far reported in the literature. This internal friction peak has been found to be very stable, indicating that the oxygen content in solution can be further increased. The solubility of oxygen in tantalum is thus greater than 0.06 percent at 170°C.

The higher temperature peak (Figs. 1 and 6) has been found to be independent of the oxygen content in tantalum.

The question may arise that some nitrogen may have been introduced into the tantalum specimen during the annealing in oxygen. However, later experiments show that nitrogen does not give a relaxation peak anywhere close to this lower temperature peak. It may be mentioned here that the higher temperature peak shown in Figs. 1 and 6 has been found to be connected with the presence of nitrogen in tantalum.

Let us assume that curve *c* in Fig. 6 is a combination of a carbon peak and an oxygen peak. We should be able, then, to resolve this curve into its components. In Fig. 7 the dotted curves indicate the carbon peak determined at two frequencies of vibration. The solid curves

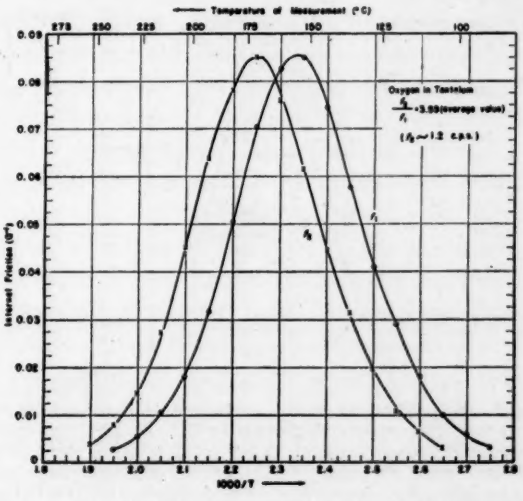

FIG. 8. Internal friction curves resulting from oxygen in tantalum obtained by subtracting the dotted curves from the corresponding solid curves shown in Fig. 7.

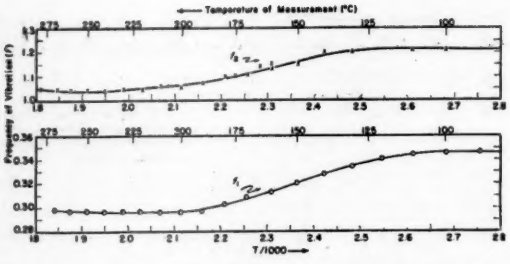

FIG. 9. Variation of natural frequencies of vibration with temperature for the oxygen-enriched tantalum specimen. The two curves correspond to the two solid internal friction curves shown in Fig. 7.

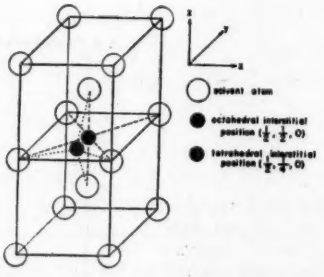

FIG. 11. Examples illustrating the octahedral and tetrahedral interstitial positions in a body-centered cubic lattice. The closest atoms to these positions were indicated by dashed and dotted lines.

are the composite curves determined at two frequencies of vibration identical to those used for the dotted curves. By subtracting the dotted curves from the corresponding solid curves, we get the contribution attributable to oxygen alone. This is shown in Fig. 8. We can see that the internal friction peak occurs at a temperature of about 20°C higher in the case of oxygen than in carbon.

Figure 9 gives the temperature variation of the natural frequencies of vibration corresponding to the two solid internal friction curves shown in Fig. 7. The frequency decreases with a rise of temperature, and the variation is considerable over the temperature range concerned. This is because the relaxation concerned is rather large. In spite of the variation of frequency with temperature, it has been found that the ratio of the two frequencies at any given temperature changes very slightly with temperature and that the average ratio of the two frequencies is 3.59. As the contribution of oxygen to the solid curves shown in Fig. 7 is by far greater than that of carbon, we can take this frequency ratio of 3.59 in the evaluation of the heat of activation associated with the oxygen relaxation from the two curves shown in Fig. 8. The horizontal shift in $1/T$ scale to bring these two curves to superpose on each other was found to be 0.0875×10^{-3} (Fig. 10), and this gives a heat of activation of about 29,000 calories per mole which is higher than the value for carbon.

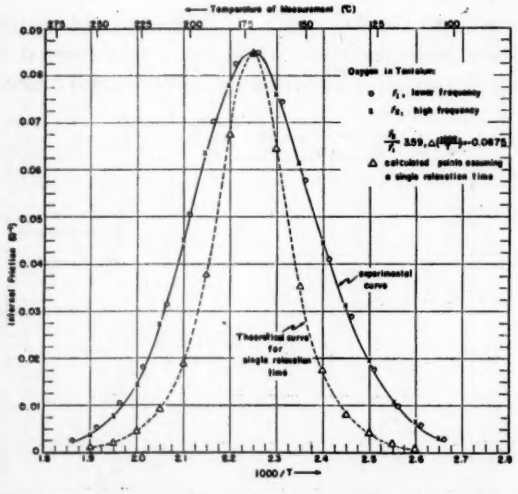

FIG. 10. Determination of heat of activation associated with the oxygen peak by a horizontal shift of the two internal friction curves shown in Fig. 8. The two curves were superposed on each other by a relative shift of the $1000/T$ scale through 0.0875. Taking the frequency ratio to be 3.59, this gives a heat of activation of 29,000 calories per mole. The triangles indicate the calculated points assuming a single relaxation time and a unique heat of activation.

It can be seen from Fig. 10 that the internal friction in the oxygen peak reaches its maximum value at 172°C (445°K) and the frequency of vibration at this temperature is 1.11 c.p.s. according to the upper curve of Fig. 9. Using the heat of activation of 29,000 calories per mole, we find that

$$\tau_0 = 1.0\times10^{-15} \text{ sec.}$$

Following similar procedures as made in the case of carbon, the theoretical curve for a single relaxation time was calculated and is shown by the dotted curve in Fig. 10. It is much narrower than the observed curve. This indicates that the observed oxygen peak cannot be interpreted in terms of a single relaxation time with a unique activation energy. A discussion of this point will be given in the next section.

IV. DISCUSSION

The condition for stress-induced preferential distribution of interstitial solute atoms is that an unsymmetrical distortion be introduced in the lattice when the solute atoms go into the interstitial positions. In a body-centered cubic lattice there are two kinds of interstitial positions for the solute atoms. One kind is octahedral, situated at the center of the faces or the middle of the edges of an elementary cell. A typical example of such positions is shown in Fig. 11, which has the coordinates $(\frac{1}{2}, \frac{1}{2}, 0)$. The other kind is tetrahedral, situated at the center of a tetrahedron constituted by two corner and two center atoms. It can be seen that in both kinds of interstitial positions there are three *types* of positions each having tetragonal axis along one of the principal axes. Therefore, as far as the mechanism of the stress-induced preferential distribution of the solute atoms is concerned, all the arguments are valid for both kinds of interstitial positions, octahedral or tetrahedral. However, the unsymmetrical distortion introduced in the lattice is much greater in cases where a solute atom goes into an octahedral position. Consequently the internal friction peak should also be greater.

In the case of carbon in alpha-iron reference can be made to the case of martensite, for which it has been shown that the carbon atoms occupy the octahedral positions.[5] This may indicate that it is easier to push away the two nearest atoms around an octahedral position to make room for the carbon atom than to push away all the four atoms around a tetrahedral position, although the octahedral position is smaller than the tetrahedral position as far as the two nearest neighbors are concerned. As the metallic radius of tantalum is larger than that of iron, we can assume that carbon atoms can also go into the octahedral positions in tantalum. Now we have demonstrated above that the observed carbon peak around 150°C has a single relaxation time with a unique heat of activation. This indicates that this peak can be associated with only the stress-induced preferential distribution among the various types of interstitial positions of one single kind: octahedral or tetrahedral. If the observed 150°C peak is associated with the carbons in the tetrahedral positions, then there should be another relaxation peak of larger magnitude associated with the carbon atoms in the octahedral positions. As no other conspicuous relaxation peak the presence of carbon in tantalum was observed within the wide temperature range from −75°C to 550°C, we may assume that the observed peak is associated with the carbon atoms in octahedral positions.

The situation in the case of oxygen is different because the relaxation curve observed cannot be interpreted in terms of a single relaxation time with a unique activation energy. This may indicate that the relaxation process does not consist of a single relaxation time or that there is more than one activation energy involved in the relaxation process. The observed relaxation time and activation energy are thus only the mean values. This leads us to assume that oxygen, probably with metallic bond, can go into both the octahedral and tetrahedral positions, as the metallic radius of oxygen is about 12 percent smaller than that of carbon.[6]

It can be seen from Fig. 11 that each octahedral position is surrounded by four tetrahedral positions. When a solute atom at the octahedral position $(\frac{1}{2}, \frac{1}{2}, 0)$ having a tetragonal axis along z axis diffuses into the octahedral position $(\frac{1}{2}, 0, 0)$ having a tetragonal axis along x axis, it must pass through the tetragonal position $(\frac{1}{2}, \frac{1}{4}, 0)$. If, in non-quantum-mechanical language, the tetrahedral position cannot accommodate the solute atom, then the solute atom can only accomplish its journey by one single jump with a unique value of activation energy. A single relaxation time is thus involved in the process. This may correspond to the case of the carbon relaxation. However, if the tetrahedral position can also accommodate the oxygen as we assumed above, then the stress-induced diffusion among the octahedral positions may be accomplished by two intermediate steps having different heats of activation. Accordingly, the relaxation process involved is much complicated with a broadened relaxation curve.

[5] N. J. Petch, J. Iron and Steel Inst. **147**, 221 (1943); H. Lipson and A. M. B. Parker, *Ibid.* **149**, 123 (1944).

[6] Linus Pauling, J. Am. Chem. Soc. **69**, 542 (1947).

Stress Relaxation by Interstitial Atomic Diffusion in Tantalum*

T'ING-SUI KÊ
Institute for the Study of Metals, The University of Chicago, Chicago, Illinois

(Received March 22, 1948)

In a preceding article, it was shown that the internal friction peaks observed in tantalum containing small amounts of C and O are caused by the stress-induced preferential distributions of C or O among the interstices in tantalum. In order to further elucidate this viewpoint, the relaxation strength associated with these relaxations has been determined by rigidity and stress relaxation measurements in torsion covering a wide range of temperature. When the reciprocal of relaxation strength is plotted against absolute temperature, the graph is a straight line passing through the origin. This linear relationship agrees with that predicted by theory assuming a model of stress-induced preferential distribution. The finding that the extrapolated line passes through absolute zero temperature shows that the interaction between solute atoms is negligibly small. This implies that the critical temperature for self-induced preferential distribution of solute atoms is close to absolute zero.

I. INTRODUCTION

IN a preceding article[1] it was shown that the internal friction peaks observed in tantalum containing small amounts of C and O are consistent with the viewpoint that C and O form an interstitial solid solution in tantalum, and hence lead to local distortions having tetragonal symmetry just in the same manner as C and N lead to local distortions having tetragonal symmetry when dissolved in alpha-iron,[2] which likewise has a body-centered cubic structure. When a tensile stress is applied to the specimen along a given direction, this tetragonal deformation will lead to a preferential distribution of the C or O among the various interstices having tetragonal axes along different directions. The establishment of such a stress-induced preferential equilibrium distribution of C and O requires some time. Consequently, strain lags behind the stress and gives rise to internal friction and related effects.

In the theoretical analysis of relaxation phenomena, it is often convenient to describe the magnitude of the relaxation in terms of a quantity known as the relaxation strength. It is defined by

$$\Delta_M = (M_U - M_R)/M_R, \tag{1}$$

where M_U and M_R are, respectively, the unrelaxed and relaxed elastic moduli. When the relaxation arises from a stress-induced preferential distribution of solute atoms, it may be shown that the temperature dependence of the relaxation strength is given by[3]

$$\Delta_M = T_0/(T - \alpha T_0). \tag{2}$$

In this relation, T is the absolute temperature; α is a numerical coefficient taking account of the interaction between solute atoms—it corresponds to the Weiss factor in the theory of ferromagnetism; and T_0 is a temperature-independent term which increases with the concentration of the solute atoms and the tetragonal distortion introduced in the lattice due to the presence of the solute atom.

Equation (2) is inapplicable at temperatures below αT_0. However, before this temperature is reached from above, there is a critical temperature below which there will be a spontaneous ordering of the solute atoms under zero stress. At this temperature the interaction between the solute atoms reduces the energy of one of them if it goes to an interstices having a tetragonal axis parallel to the preponderant ones of the others. This is analogous to the Curie temperature below which the magnetic moments of the atoms, or, rather, the spins of the electrons in a ferromagnetic domain are orientated in such a way as to point all along the same direction at zero magnetic field. The critical temperature T_c

* This research has been supported by ONR (Contract No. N6ori-20-IV).

[1] T. S. Kê, Phys. Rev. **74**, 9 (1948).

[2] J. L. Snoek, Physica **8**, 711 (1941).

[3] C. Zener, *Elasticity and Anelasticity of Metals* (The University of Chicago Press, Chicago, 1948) p. 113. A somewhat different approach was given by D. Polder, Philips Research Reports 1, 5 (1945).

for such a self-induced preferential distribution of interstitial solute atoms in body-centered cubic lattices has been computed by Zener to be

$$T_c = 1.05\alpha T_0, \qquad (3)$$

and he pointed out that the persistence of the tetragonal structure of freshly quenched martensite at room temperature can be interpreted only as due to such a self-induced preferential distribution of carbon atoms in iron.[4] Assuming α to be of the order of magnitude of unity, the critical temperature for such a spontaneous ordering was raised, according to Zener, to above the room temperature as the carbon content in iron reaches 0.14 percent by weight.

Before the concept of preferential distribution of solute atoms in alpha-iron was proposed by Snoek, early work of Richter[5] on the elastic after-effect of carbonyl iron had shown that the relaxation observed had a temperature coefficient of 0.003 at room temperature, a temperature coefficient which is consistent with Eq. (2). However, his conditions of measurement were such that an estimate of the interaction constant α could not be obtained.

The purpose of this paper is to subject the theoretical Eq. (2) to an experimental test, and in particular, to obtain an estimate of the interaction parameter α. It is very difficult to test Eq. (2) over a wide temperature range by working with the C–Fe system. The solubility of C in iron is extremely small and segregation will take place even at room temperature when a fair amount of carbon was "loaded" in iron in solid solution. On the contrary, the interstitial solid solutions of C and O in tantalum are appropriate for such a study as, according to the observations described in the preceding article, the solubility of C and O in tantalum is fairly high and no perceptible segregation takes place up to a fairly high temperature.

II. RELAXATION STRENGTH BY RIGIDITY MEASUREMENTS

The relaxation strength was determined by rigidity (Section II) and stress relaxation measurements (Section III) in torsion. As we have demonstrated that the superposition principle is valid in the relaxation processes concerned,[1] Eq. (2) holds for torsional stress as well as for tensile stress.

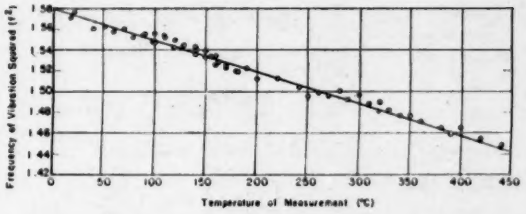

FIG. 1. Variation of "rigidity" with temperature in high purity tantalum.

The variation of rigidity with temperature of high purity tantalum** was determined by measuring the frequency of the free torsional vibration of a wire specimen at various temperatures with an apparatus which has been described before.[6] The observations are shown in Fig. 1. The rigidity was plotted in arbitrary units. It is seen that the rigidity decreases linearly with temperature up to 450°C, the highest temperature of measurement. This is in conformity with the finding of a number of workers that if no relaxation processes occur, the normal variation of the elastic coefficients with temperature is linear over a wide range of temperature.[7]

In the following study of the relaxation phenomena caused by the presence of C and O in

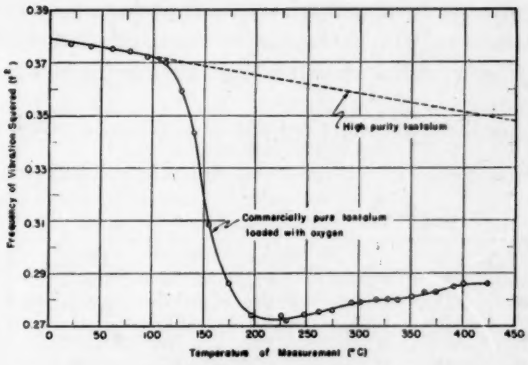

FIG. 2. Variation of "rigidity" with temperature in tantalum containing C and O.

[4] C. Zener, Trans. A.I.M.E. **167**, 550 (1946).
[5] G. Richter, Ann. d. Physik **32**, 683 (1938).

** Thanks are due to Fansteel Metallurgical Corporation for supplying the high purity tantalum.

[6] T. S. Kê, Phys. Rev. **71**, 533 (1947).
[7] F. Rose, Phys. Rev. **49**, 50 (1936); M. A. Durand, Phys. Rev. **50**, 449 (1936); S. L. Quinby and S. Siegel, Phys. Rev. **54**, 293 (1936); S. Birch and D. Bancroft, J. Chem. Phys. **8**, 642 (1940); S. Siegel and R. Cummerrow, J. Chem. Phys. **8**, 847 (1940); T. S. Kê, see reference 6.

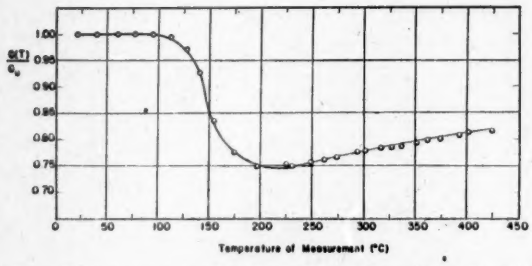

FIG. 3. Rigidity relaxation in tantalum containing C and O.

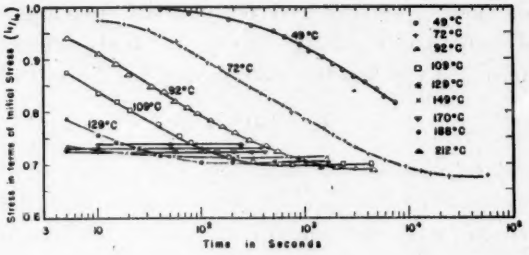

FIG. 4. Stress relaxation at constant strain at various temperatures in tantalum containing C and O.

tantalum, the tantalum specimen used was of commercial purity. It contained 0.013 percent carbon by weight. This specimen was loaded with oxygen by a special diffusion procedure as described in the preceding article. Microscopic examination of the specimen after this treatment showed that no perceptible oxide was precipitated along the grain boundaries and inside the grains. The oxygen content in the specimen is about 0.06 percent by weight, assuming all the oxygen goes into solid solution in tantalum.

The temperature variation of rigidity of the tantalum specimen described above is shown in Fig. 2. The rigidity curve is a straight line up to a temperature around 100°C above which a sudden drop occurs. The internal friction also begins to rise around this temperature. According to the analysis made in the preceding paper, this sudden drop in rigidity is caused by the stress-induced preferential distribution of C and O among the various interstices in tantalum. The dotted line shown in Fig. 2 gives the rigidity curve for high purity tantalum. It was converted from Fig. 1.

The ratio $G(T)/G_U$ was determined from Fig. 2 and utilized the relationship

$$G(T)/G_U=(f_T/f_U)^2, \tag{4}$$

where f_T and $G(T)$ are, respectively, the observed frequency and rigidity at a given temperature T; f_U and G_U are, respectively the unrelaxed frequency and rigidity at the same temperature obtained from the dotted line. This ratio is plotted as a function of temperature in Fig. 3, which shows that the relaxation is essentially complete at a temperature around 225°C. Accordingly, the value of $G(T)/G_U$ at 225°C is equal to G_R/G_U at that temperature. At still higher temperatures, the ratio G_R/G_U increases with a rise of temperature. As the relaxation has been complete at these temperatures, this increase tells us the temperature dependence of the ratio G_R/G_U. The values of G_R/G_U and Δ_G, the relaxation strength in torsion, at various temperatures are summarized in Table I. It is seen that the relaxation strength decreases with an increase of temperature in agreement with the theoretical relationship given by Eq. (2).

TABLE I. Temperature dependence of relaxation strength from rigidity measurements.

T (°C)	T (°K)	f_R^2	f_U^2	G_R/G_U	Δ_G	$1/\Delta_G$
225	498	0.274	0.364	0.753	0.32_8	3.0_5
230	503	0.272	0.362	0.749	0.33_6	2.9_8
248	521	0.274	0.362	0.757	0.32_2	3.1_1
262	535	0.275	0.361	0.762	0.31_3	3.2_0
274	547	0.276	0.360	0.766	0.30_5	3.2_8
293	566	0.279	0.359	0.777	0.28_7	3.4_9
302	575	0.279	0.358	0.799	0.28_4	3.5_2
317	590	0.280	0.357	0.784	0.27_6	3.6_2
327	600	0.280	0.357	0.785	0.27_4	3.6_5
337	610	0.280	0.356	0.787	0.27_1	3.6_9
351	624	0.281	0.355	0.792	0.26_3	3.8_0
363	636	0.283	0.354	0.799	0.25_1	3.9_8
374	647	0.283	0.353	0.801	0.24_8	4.0_3
392	665	0.285	0.352	0.809	0.23_5	4.2_5
401	674	0.286	0.352	0.813	0.22_9	4.3_6
423	696	0.286	0.350	0.817	0.22_4	4.4_6

TABLE II. Temperature dependence of relaxation strength from stress relaxation measurements.

T (°C)	T (°K)	$S_R/S_0=G_R/G_U$	Δ_G	$1/\Delta_G$
72	345	0.675	0.48_1	2.0_8
92	365	0.690	0.45_0	2.2_2
109	382	0.699	0.43_9	2.2_8
129	402	0.707	0.41_3	2.4_2
149	422	0.715	0.39_8	2.5_1
170	443	0.726	0.37_9	2.6_4
188	461	0.736	0.35_8	2.7_9
212	485	0.750	0.33_3	3.0_0

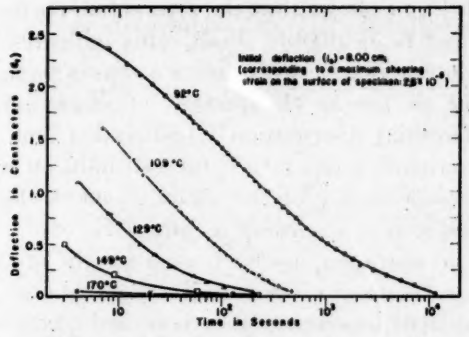

FIG. 5. Some typical examples of the recovery curves at various temperatures in tantalum containing C and O, initial deflection (D_0) = 8.00 cm.

III. RELAXATION STRENGTH FROM STRESS RELAXATION MEASUREMENTS

By the rigidity measurements described above, we can only determine the relaxation strength at temperatures at which the relaxation has been essentially completed in a half-cycle of the period of vibration. Thus, for the case described above in which the period of vibration is about one second, we could only determine the relaxation strength for temperatures above 225°C. To extend the measurement below this temperature, it is most appropriate to measure the stress relaxation at constant strain with the so-called torsional stress relaxometer developed in this laboratory.[6] This stress relaxometer utilizes the principle of a moving coil galvanometer with the test specimen as the suspension fiber. The current passing through the galvanometer is a measure of the torque, S, acting on the wire; and the deflection, D, of the galvanometer is a measure of the shear strain. The specimen was twisted through a given amount, D_0, by passing a suitable amount of current, i_0, through the moving coil. In order to maintain the twist to the constant amount D_0, the current was continuously reduced and its value, i_t, recorded as a function of time. We have then

$$i_t/i_0 = S_t/S_0. \tag{5}$$

In the measurements at different temperatures, it is desirable to twist the specimen through the same angle. As the rigidity of the wire decreases with a rise of temperature, the initial current i_0 required to twist the specimen through D_0 also decreases with a rise of temperature. When the temperature of measurement is low, the relaxation is slow and the initial current, i_0, can be easily determined by visual observation. At higher temperatures, however, it is difficult to locate the instantaneous deflection as creep starts immediately after the wire was twisted. Thus at those temperatures, we determine the corresponding value of i_0 from the static rigidity curve for high purity tantalum. This curve has an identical slope with the dynamic rigidity curve shown in Fig. 1.

The stress relaxation curves at various temperatures are shown in Fig. 4, in which the ratio i_t/i_0, which is equal to S_t/S_0, is plotted against the logarithm of time. The constant twist, D_0, maintained at all temperatures was 8 cm on a scale three meters away from the specimen. This corresponds to a maximum shear strain of 2.8 $\times 10^{-5}$ on the surface of the specimen. These curves flattened out after a certain length of time depending on the temperature at which the measurement was taken. The flat portion of each curve gives the relaxed value of S_t/S_0, which is S_R/S_0. Table II summarizes the values of S_R/S_0 at different temperatures. The relaxation strength Δ_G can be calculated from S_R/S_0 as we have the relationship

$$S_R/S_0 = G_R/G_U. \tag{6}$$

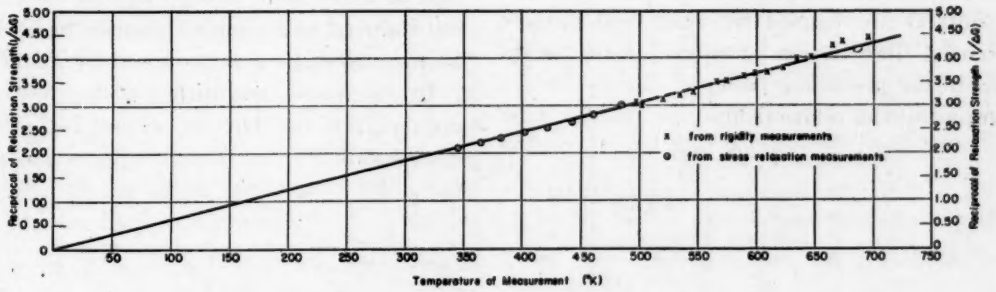
Reciprocal of Relaxation Strength (1/Δ$_G$)
Reciprocal of Relaxation Strength (1/Δ$_G$)
× from rigidity measurements
○ from stress relaxation measurements
Temperature of Measurement (°K)

FIG. 6. Temperature dependence of the relaxation strength in tantalum containing C and O.

In these measurements, the temperature was controlled and measured with a Tag Celectray indicating temperature controller to a relative accuracy of 1°C. In measuring the current, we used a microammeter shunted with a suitable resistance. This set-up gives a relative accuracy of within one percent. We are, therefore, justified to include three significant figures in the calculated values of S_R/S_0. On the other hand, we have only two significant figures for the relaxation strength, as subtraction was involved in its calculation.

After the stress relaxation had been completed at each temperature, the stress was suddenly relieved and the residual deflection observed as a function of time. Some typical examples of the recovery curves so obtained are given in Fig. 5, showing that the relaxation phenomena concerned are recoverable under the experimental conditions.

IV. TEMPERATURE DEPENDENCE OF RELAXATION STRENGTH AND CONCLUSIONS

To compare the experimentally observed temperature dependence of relaxation strength with the theoretical relation

$$\Delta_G = T_0/(T-\alpha T_0),$$

it is convenient to plot the reciprocal of relaxation strength against the absolute temperature. The values of $1/\Delta_G$ in torsion, which are included in the last column of Tables I and II, are plotted in Fig. 6 against the absolute temperature. These include the results from both rigidity and stress relaxation measurements. It is seen that the experimental points lie closely along a straight line passing through the origin. The fact that Fig. 6 gives a straight line supports the viewpoint that the relaxation phenomena observed in tantalum containing a small amount of C and O are caused by the stress-induced preferential distribution of solute atoms as described in the preceding paper.

Comparing the relationship

$$1/\Delta_G = T/T_0 - \alpha \qquad (7)$$

with Fig. 6 shows that the interaction coefficient α must be negligibly small. This indicates that the interaction between solute atoms is negligibly small as far as the process of stress-induced preferential distribution is concerned and that the critical temperature for self-induced spontaneous ordering of the solute atoms is close to absolute zero according to Eq. (3).

The tantalum specimen used for the study of the relaxation processes described above contains 0.013 percent of carbon and about 0.06 percent of oxygen by weight. The relaxation observed is, according to the analysis made in the preceding article, principally due to oxygen. As T_0 in Eq. (2) increases linearly with the concentration of solute atoms,[3] the question may arise that a higher concentration of oxygen might give rise to an observable critical temperature if the coefficient α is not exactly zero. Actually, the atomic concentration of O in the tantalum specimen is 0.68 percent which is already higher than the atomic concentration of C in iron (0.65 atomic percent corresponding to 0.14 percent by weight) necessary for the formation of tetragonal martensite above room temperature. On the other hand, the experimental accuracy involved in the determination of the straight line relationship shown in Fig. 6 leads us to believe that this line, if not passing exactly through the origin, can only give a very small value of α; and therefore, according to Eq. (3), T_c must be close to absolute zero even if T_0 is very much increased by raising the concentration of the solute atoms.

We believe, thus, no spontaneous ordering can occur in the interstitial solid solutions of C and O in tantalum. If we generalize this conclusion to the case of the interstitial solid solution of carbon in iron, we can say that the formation of martensite is not likely to be due to the self-induced preferential distribution of carbon atoms in iron as was proposed by Zener.

In conclusion, the author wishes to express his appreciation to Dr. C. Zener for stimulating discussions.

PHYSICAL REVIEW VOLUME 74, NUMBER 1 JULY 1, 1948

Theory of the Lithium Two-Alpha-Reactions. I. Angular Distribution of $Li^7(p,\alpha)\alpha$

D. R. INGLIS
Department of Physics, The Johns Hopkins University, Baltimore, Maryland
(Received March 16, 1948)

The reactions $Li^7(p,\alpha)\alpha$ and $Li^6(d,\alpha)\alpha$ have a special interest because the Bose statistics and consequent even parity of the final pair of alphas simplifies the analysis. It is assumed on reasonable grounds that Li^7 has odd parity and Li^6 even. This means that only $p, f\cdots$ protons entering Li^7 are relevant to this reaction and only entering $s, d\cdots$ deuterons of Li^6. An expression for the energy variation of the angular distribution in the Li^7 reaction is derived from the dispersion formula, with the specific assumption that only two levels of the compound nucleus, having angular momentum 0 and 2, are important in the range of energies employed in the experiments. (An alternative assumption is investigated but is more involved and it is considered less plausible.) The angular factor is $1+A(E)\cos^2\theta+B(E)\cos^4\theta$. A formula for $A(E)$ as far as it results from entering p waves has been derived previously by Critchfield and Teller, but it may not be adjusted to fit the data in the energy range up to 3 Mev even within the rather large experimental uncertainty. The effect of entering f waves is also included in the present analysis, and this contribution is not only essential to the existence of $B(E)$ but also makes it possible to obtain agreement with the recent measurements of $A(E)$. Certain matrix elements are treated as arbitrary parameters in obtaining this fit. In addition to the low-energy node apparent in the early data, a second node of $A(E)$ is required at higher energy. The formula derived for $B(E)$ contains the same resonance denominator as does $A(E)$ and is compatible with the present experimental results. The contrasting facts, first that the easy entrance of s waves makes the $Li^6(d,\alpha)\alpha$ reaction symmetric at very low energies and second that the p waves responsible for the Li^7 reaction at low energies may introduce asymmetry, are associated in a simple way with the qualitative experimental observation that both $A(E)$ and $B(E)$ rise more quickly in the Li^7 reaction than in the Li^6 reaction as the bombarding energy is increased from zero. Presentation of a detailed formulation of the Li^6 reaction is deferred until a later paper.

I. INTRODUCTION

THE nuclear reactions $Li^7(p,\alpha)\alpha$ and $Li^6(d,\alpha)\alpha$ are unique in having two alphas as their end products, and the Bose statistics obeyed by these alphas simplifies the theoretical treatment on the basis of the dispersion formula to a point where some measure of interpretation of the angular distributions is easily possible. The angular distribution of the $Li^7(p,\alpha)\alpha$ reaction was first investigated experimentally by Young, Ellett, and Plain,[1] and theoretically by Critchfield and Teller.[2] The angular distribution seemed to be of the form $1+A(E)\cos^2\theta$, with the value of $A(E)$ approaching a maximum at the top bombarding energy E of 400 kev. The form $1+A(E)\cos^2\theta$ follows most simply from the assumption that only p protons enter and are responsible for the reaction, f protons being repelled by the Coulomb barrier and s and d protons being ineffective because of the assumed odd parity of the target nucleus and the even parity of the final configuration. A form for $A(E)$ rising to a maximum and gradually tailing off to small values at high energies (through a node or not, depending on the existence of an unobserved node at very low energies) was shown to follow from the assumption of a broad s state and a narrow d state of the compound nucleus. Both the appearance of a maximum of $A(E)$ at 400 kev and the detection of a corresponding resonance maximum in the yield curve (relative to penetration factor) constructed from the yield data then available seem to have been spurious. The sensitivity of this inferred maximum in relative yield to the assumed nuclear radius has been discussed briefly by Eisner.[3]

Later experimental investigations[4–6] have shown that $A(E)$ increases to a maximum value of about 2 at about 1 Mev, and then decreases steadily but remains positive to the highest energies of the observations (3 Mev). The latest observations[6] show moreover that there is also a

[1] V. J. Young, A. Ellett, and G. J. Plain, Phys. Rev. **48**, 498 (1940).
[2] C. L. Critchfield and E. Teller, Phys. Rev. **60**, 10 (1941).
[3] E. Eisner, Phys. Rev. **65**, 85 (1944).
[4] C. D. Swartz, H. H. Rossi, B. Jennings, and D. R. Inglis, Phys. Rev. **65**, 80 (1944).
[5] S. Rubin, W. A. Fowler, and C. C. Lauritsen, Phys. Rev. **71**, 212 (1947).
[6] N. P. Heydenburg, C. M. Hudson, D. R. Inglis, and W. D. Whitehead, Jr., Phys. Rev. **73**, 241 (1948).

term in $\cos^4\theta$: that the angular distribution is more accurately of the form $1+A(E)\cos^2\theta+B(E)\cos^4\theta$. The experiments are not yet sufficiently accurate to fix the dependence of the coefficient B on energy very well, but it is definitely negative and of the order of magnitude $-\frac{1}{2}$ throughout at least most of the range from 1 Mev to 3 Mev.

The reaction $Li^6(d,\alpha)\alpha$ involves the formation of the same compound nucleus Be^8 as is formed in $Li^7(p,\alpha)\alpha$ but the binding energy of a deuteron to Li^6 is 4.96 Mev higher than the binding energy of a proton to Li^7, so the compound nucleus is in a more highly excited state in the Li^6 reaction than in the Li^7 reaction, for comparable bombarding energies. The Li^6 spectrum thus makes it possible to explore a different part of the Be^8 spectrum than that explored as yet by the Li^7 reaction. Observations on the angular distribution of the alphas from the Li^6 reaction have been made recently by Heydenburg, Hudson, Inglis, and Whitehead.[7] The excitation curve displays a broad dip between a peak at 0.7 Mev and one above 3.5 Mev, the highest energy of the observations. Here again the angular distribution is limited to even powers of $\cos\theta$ by the Bose statistics of the product alphas, and the observations indicate that $A(E)$ rises, starting near 0.7 Mev, to a broad maximum of about unity at 2 Mev, while $B(E)$ is absent to almost 1.5 Mev and is small and positive at the higher energies.

Even though the validity of nuclear models, such as the alpha-model and the central-field model, for the calculation of finer details seems at present extremely questionable, the parities deduced on the basis of these models are almost beyond doubt, and it is assumed throughout this work that the parity of the ground state of Li^7 is odd while that of Li^6 is even. The results show that the data are compatible with these assumptions. Only in the case of flagrant disagreement would it seem to us worth while to investigate the contrary assumption.

In this paper we extend the theoretical interpretation of the Li^7 reaction to include the effects of entering f protons, and we shall present a similar interpretation of the Li^6 reaction in a subsequent paper. Some characteristic differences appear in the two reactions. The protons which enter the Li^7 reaction most easily, the p protons, are themselves responsible for the $\cos^2\theta$ term, so the necessity of penetrating a barrier does not make the asymmetry vanish at zero bombarding energy. The observed vanishing of $A(E)$ near $E=0$ is caused by a pure coincidence in the placing of the resonant state of the compound nucleus. In the Li^6 reaction, on the contrary, the deuterons which enter most easily are s deuterons which by themselves give spherical symmetry, and the penetration of d deuterons is necessary for the appearance of the asymmetry, so the coefficient $A(E)$ rises from zero for a more natural reason as E increases from zero, and this makes the rise more gradual than Li^7 as is observed. This qualitative agreement is perhaps the simplest experimental verification we have of the validity of the parities as given by the nuclear models.

A similar simple correlation is found between the theoretical expectation arising from the assumed parities of the two target nuclei and the qualitative features of the observed behavior of $B(E)$. The penetration of the f waves may be expected to be more meager than the penetration of the p waves in the Li^7 reaction by a factor of the same order of magnitude as the penetration of the d waves relative to the s waves in the Li^6 reaction. The product of a p wave and an f wave (which appears because the incoming matrix element is contained quadratically or bilinearly in the dispersion formula (1)) introduces a degree of complexity in the rotational properties sufficient to account for a $\cos^4\theta$ term, and this product term is rendered small by the penetration factor to the same degree as is the product term between s and d waves in the Li^6 reaction. The latter product only introduces a term as high as $\cos^2\theta$, and the square of the d wave involving the square of the penetration factor is required to make the $\cos^4\theta$ term, leaving the $\cos^4\theta$ term less prominent in the Li^6 reaction, as observed.

[7] N. P. Heydenburg, C. M. Hudson, D. R. Inglis, and W. D. Whitehead, Jr., Bull. Am. Phys. Soc. **23**, No. 3 (1948).

II. CALCULATION OF ANGULAR DISTRIBUTIONS FROM THE DISPERSION FORMULA

The calculation is based on the Breit-Wigner dispersion formula[8] extended to several compound states, which for a system prepared in a well defined initial state P may be written

$$\sigma(E,\theta)\sim\lambda^2|\sum_r(P/H/r)(r/H/Q)/[E_p-E_r+(i/2)\Gamma_r]|^2. \quad (1)$$

The fact that the cross section is the square of a sum gives rise to interference between various states r of the compound nucleus. The "incoming" state P is characterized first by some quantization of the spin directions of the particle spin s and the target-nucleus "spin" I. A possible representation is that defined by the projections (along the beam direction) m_s and m_I. A more convenient and equivalent representation is that in which the sum of these two "spins" is given by a quantum number S, where

$$\mathbf{S}=\mathbf{s}+\mathbf{I}, \quad (2)$$

and by its projection m. In discussing the applications of (1), we first imagine that such a well defined initial state has been selected. The wave function of the prepared incoming state P is the product of a "spin" function $Z_m^{(S)}$ and a plane wave describing the orbital motion:

$$P_m^{(S)}=Z_m^{(S)}\sum_{l=0}^{\infty}i^l(2l+1)\psi_l(kr)P_l(\cos\theta_p)=\sum_{l=0}^{\infty}(lS0m/). \quad (3)$$

The functions $(lSm_lm/)=Z_m^{(S)}P_l(\cos\theta_p)e^{im_l\phi}\times i^l(2l+1)\psi_l(kr)$ are the normalized spin and angle factors of the incoming waves, each multiplied by a radial function depending on l. These functions do not describe proper states of the angular momentum j_r, since they diagonalize the projections of $\mathbf{l}$ and $\mathbf{S}$ separately rather than the vector sum of $\mathbf{l}$ and $\mathbf{S}$. However, any one of the states $(lS0m/)$ appearing in (3) could be used, along with the other $(lSm_lm'/)$ having $m_l+m'=m$, to make up by linear combination a wave function of a proper state of the angular momentum j, for any j between $l-S$ and $l+S$. The transformation coefficient from $(lS0m/)$ to such a proper state of the angular momentum we call $(lS0m/lSjm)$. We may then write for the "incoming" matrix element,

$$(P/H/r)=\sum_l(lS0m/lSj_rm)(lSj_r/H/r). \quad (4)$$

The numerical factors $i^l(2l+1)$ are considered contained in $(lSj_r/H/r)$ and this matrix element also involves a radial integration over $\psi_l(kr)$ along with other factors. This $(lSj_r/H/r)$ might have been written $(lSj_rm/H/rm)$ but both wave functions diagonalize j so the matrix element is independent of m. $(lSj_r/H/r)$ then transforms from an incoming proper function of the angular momentum, having $j=j_r$ and a given l, to the resonant state r of the compound nucleus. No simple model which might allow the assignment of values of S and l to the nuclear states is to be expected to be valid, especially in the very highly excited states r of the compound nuclei encountered in nuclear reactions. The state r is rather to be thought of as a complicated mixture of states having various values of S and l, in such a way that neither of these possible quantum numbers would have any meaning. Even if the spin angular momentum S and the orbital angular momentum l were to have a meaning in a specific state r, the transformation from the incoming state S, l would in general involve transformation coefficients mixing spin and orbit because the "spin" I of the target nucleus generally contains orbital contributions. The vector-coupling situation for the transformation of the incoming state to the compound state r is thus a complicated one, usually involving a complex coefficient. If, for a given value of l, there are n values of S which combine with it to give a certain value of j_r, the n incoming proper wave functions $(Slj_r/)$ may be combined in n orthogonal linear combinations, $n-1$ of which have zero matrix elements of H with r and the other of which, X_{lr}, has a value of this matrix element $(X_{lr}/H/r)$. Then we may write

$$(lSj_r/H/r)=[lSj_r/X_{lr}](X_{lr}/H/r), \quad (5)$$

and this incoming matrix element may be

[8] G. Breit and E. Wigner, Phys. Rev. **49**, 519 (1936); H. A. Bethe and G. Placzek, Phys. Rev. **51**, 450 (1937); H. A. Bethe, Rev. Mod. Phys. **9**, 71 (1937); G. Breit, Phys. Rev. **58**, 506 (1940). Cf. also H. Feshbach, D. C. Peasley, and V. F. Weiskopf, Phys. Rev. **71**, 145, 564 (1947).

further factored thus:[2]

$$(X_{lr}/H/r)=\phi_l(E)\alpha_{lr}', \tag{6}$$

where $\phi_l(E)$ is real and α_{lr}' is in general complex. The vector-coupling coefficients are expected to be complex but not to depend much on energy as one passes through a resonance, so they are contained almost entirely in α_{lr}', while the energy dependence of $\phi_l(E)$ arises almost entirely from the penetration of the Coulomb barrier. (In certain simple cases encountered in nuclear models α_{lr}' might be real, such as the case in which both incoming state and compound state are the same Russell-Saunders state, that is, in a transition with the magnitudes of spin and orbital momenta separately conserved and with no admixtures of other configurations of the compound nucleus.) Both of the reactions here considered are so highly exoergic that the "outgoing" matrix element $(r/H/Q)$ is assumed to be independent of energy during the passage of even a broad resonance. (A slow dependence of this factor on energy could also be included in $\phi_l(E)$.)

In Eq. (1), the angle θ which appears explicitly on the left side is implied in the final state Q on the right side. This means that the matrix element $(r/H/Q)$ describes not only the transition to the state of two alphas whose orbital motion is characterized by angular momentum matching that of the compound state, $L=j_r$ and $M_L=m$, but also describes the fact that observations are made at an angle θ, which brings in as a factor the angular wave function of this final state at θ, the associated Legendre polynomial $P_L^m(\cos\theta)$. Formally, the observed final state is a plane wave in the θ direction, and this angle factor is the angle part of the transformation coefficient from the outgoing radial wave (which includes an angle factor $P_L^m(\cos\alpha)e^{im\beta}$) to the plane wave Q, arising from the expansion

$$e^{ik\cdot R}=\sum_{n=1} i^n(2n+1)j_n(kR)\Big\{P_n(\cos\alpha)P_n(\cos\theta)$$

$$+2\sum_{n=0}^{n}\frac{(n-m)!}{(n+m)!}P_n^m(\cos\alpha)P_n^m(\cos\theta)\cos m(\phi-\beta)\Big\},$$

wherein α and β are the colatitude and azimuth angles of the position vector R, θ and ϕ those of the observation direction k.

Because products of incoming and outgoing matrix elements appear in (1), we combine the complex factors in one complex number α_{lr} defined as the product of α_{lr}' and all of $(r/H/Q)$ except the angle factor $P_j^m(\cos\theta)$. Then we have

$$\sigma_P(E,\theta)=4\pi\lambda^2\Big|\sum_{lr}\{(lS0m/lSj_rm)$$

$$\times[lSj_r/X_{lr}]\phi_l(E)\alpha_{lr}P_{j_r}^m(\cos\theta)/$$

$$(E-E_r+(i/2)\Gamma_r)\}\Big|^2. \tag{7}$$

The preparation of the system into well defined states for the application of (1) would involve orienting the spins in just one quantized fashion before the impact, which is not done in the experiments. An unpolarized beam hitting an unpolarized target is equivalent to a repetition of the experiment equal numbers of times in the various possible prepared states P, and the cross section for finding an alpha in a small element of solid angle at θ is

$$\sigma(E,\theta)=\sum_P\sigma_P(E,\theta). \tag{8}$$

Equations (7) and (8) together form the basis for the interpretation of the experiments for which rather extensive results have recently become available.

III. ANGULAR DISTRIBUTION OF THE Li^7+PROTON REACTION

In the reaction $Li^7(p,\alpha)\alpha$, the proton spin is $s=\frac{1}{2}$, the target nucleus has angular momentum $I=\frac{3}{2}$, and these combine to give "spin" states $S=1$ and $S=2$. The ground state of Li^7 is assumed to be odd, so incoming $p, f, h\cdots$ waves may give the even states of the compound nucleus required for the reaction, and the successively higher values of l find penetration more and more difficult, so it will suffice to consider only $l=1$ and $l=3$. The Bose statistics of the product alphas demands that the compound states of interest have not only even parity but also even angular momentum j_r. With $l=1$, the "spin" state $S=1$ leads to $j_r=0$ or 2, while $S=2$ leads only to $j_r=2$. With the incoming f wave, $S=1$ and $S=2$ each lead to $j_r=2$ or 4. We are then free to assume such disposition of virtual levels of the compound

TABLE I. Transformation coefficients $(l S 0 m / l S j_r m)$.

m	$(110m/112m)$	$(120m/122m)$	$(310m/312m)$	$(320m/322m)$	$(4/5)^{\frac{1}{2}}P_2^m(x)$
2	0	$-(2/3)^{\frac{1}{2}}$	0	$-14^{-\frac{1}{2}}$	$(3/2)^{\frac{1}{2}}(1-x^2)$
1	$2^{-\frac{1}{2}}$	$-6^{-\frac{1}{2}}$	$7^{-\frac{1}{2}}$	$2/14^{\frac{1}{2}}$	$6^{\frac{1}{2}}x(1-x^2)^{\frac{1}{2}}$
0	$(2/3)^{\frac{1}{2}}$	0	$-(3/7)^{\frac{1}{2}}$	0	$(1-3x^2)$
-1	$2^{-\frac{1}{2}}$	$6^{-\frac{1}{2}}$	$7^{-\frac{1}{2}}$	$-2/14^{\frac{1}{2}}$	
-2	0	$(2/3)^{\frac{1}{2}}$	0	$14^{-\frac{1}{2}}$	

nucleus, having $j_r=0$, 2, or 4, as may be necessary to account for the observations. The main trends of the observations may be attributed to an entering p wave, involving levels having not more than $j_r=0$ and 2, and it is rather gratifyingly found unnecessary to introduce any further states in order to explain the finer details arising from the f wave. That is, it may be assumed, in the interest of simplicity, that the f wave reacts only with the $j_r=2$ state(s), without invoking $j_r=4$.

The transformation coefficients $(lS0m/lSj_rm)$ appearing in (7) transform from a representation in which the projections of l and S are diagonal to that in which the total angular momentum is diagonal, and are the same as are used to describe Russell-Saunders states in the theory of atomic spectra. They have indeed been tabulated in a form convenient for the present work in the book of Condon and Shortley.[9] (Investigators preferring to make their own calculations complete from the beginning can do so without writing as many matrix elements as are listed in reference 2 by using a sum rule introduced by Breit and Darling[10] for the purpose of confining attention to those coefficients having $m_l=0$ in just such calculations as these.) The coefficients (9) for the states that concern us are evaluated in Table I. (Those with $l=1$ are also listed in reference 2.)

Our first set of assumptions about the compound nucleus is that it has just two states which contribute appreciably to the reaction in the energy range investigated, a state numbered $r=0$ having $j_0=0$ and having its half-width Γ_0 considerably greater than the range of energies covered by the experiments so that the energy variation of its "resonance denominator" may be neglected, and a state number 2 having $j_2=2$ and Γ_2 small enough to account for the rather rapid energy variation of the angular distribution of the product alphas. These are the assumptions about the compound states made in reference 2. With these states, the cross section given by (1) and (8) is

$$\begin{aligned}\sigma(E,\theta)&=4\pi\lambda^2\sum_{S,m}|H_0{}^PH_Q{}^0/(i\Gamma_0/2)\\&\qquad+H_2{}^PH_Q{}^2/(E-E_2+i\Gamma_2/2)|^2\\&=(16\pi\lambda^2/\Gamma_2{}^2)\sum_{S,m}|(\Gamma_2/i\Gamma_0)H_0{}^PH_Q{}^0\\&\qquad+H_2{}^PH_Q{}^2/(\epsilon+i)|^2\\&=[(16\pi\lambda^2/\Gamma_2{}^2)/(\epsilon^2+1)]\\&\times\sum_{S,m}|(\Gamma_2/i\Gamma_0)(\epsilon+i)H_0{}^PH_Q{}^0+H_2{}^PH_Q{}^2|^2.\end{aligned}\tag{9}$$

Here we have put

$$(E-E_2)/(\Gamma_2/2)=\epsilon,$$

which then measures the energy deviation from resonance with the state $r=2$ in units of its half-width. The summation indices S and m are implicit in the initial state P. Putting this in the more explicit notation of Eq. (7), we have

$$\begin{aligned}\sigma(E,\theta)&=[(16\pi\lambda^2/\Gamma_2{}^2)/(\epsilon^2+1)]\sum_{S,m}|(\Gamma_2/i\Gamma_0)(\epsilon+i)\phi_1\alpha_{10}\delta(S/1)\delta(m/0)\\&\qquad+\sum_{l=1,3}(lS0m/lS2m)[lS2/l2]\alpha_{l2}\phi_lP_2{}^m(\cos\theta)|^2\\&=[(16\pi\lambda^2/\Gamma_2{}^2)/(\epsilon^2+1)]\Big\{\sum_{m=-2}^{2}|\sum_{l=1,3}(l20m/l22m)[l22/l2]\alpha_{l2}\phi_l|^2(P_2{}^m)^2+\sum_{m=\pm1}|\sum_{l=1,3}(l10m/l12m)\\&\qquad\times[l12/l2]\alpha_{l2}\phi_l|^2(P_2{}^m)^2+|(\Gamma_2\alpha_{10}/i\Gamma_0)(\epsilon+i)\phi_1+\sum_{l=1,3}(l100/l120)[l12/l2]\alpha_{l2}\phi_lP_2{}^0|^2\Big\}.\end{aligned}\tag{10}$$

[9] E. U. Condon and G. H. Shortley, *Theory of Atomic Spectra* (Oxford University Press, New York, 1935), pp. 76, 77.
[10] G. Breit and B. T. Darling, Phys. Rev. 71, 402 (1947).

TABLE II. Sums used in the Li^7 reaction with $j_r=0$ and 2.

l_1	l_2	$(4/5)\sum_{m=-2}^{2}(l_1 20m/l_2 2m)\times(l_2 20m/l_2 2m)(P_2^m)^2$	$(4/5)\sum_{m=-1}^{1}(l_1 10m/l_2 1m)\times(l_2 10m/l_2 1m)(P_2^m)^2$
1	1	$2(1-x^2)$	$(2/3)(1+3x^2)$
1	3	$(3/7)^{\frac{1}{2}}(1-x^2)(1-5x^2)$	$-(2/7)^{\frac{1}{2}}(1-12x^2+15x^4)$
3	3	$(3/28)(1-x^2)(1+15x^2)$	$(3/7)(1-4x^2+7x^4)$

The sums over m appearing here (and more explicitly in Eq. (12)) are easily evaluated by use of Table I with the results shown in Table II (in which we put $\cos\theta=x$). The use of these sums is helpful in consolidating the result expressed in (10), but we are still left with a rather distressing number of arbitrary constants in addition to the energy-dependent factors ϕ_l which we consider to be just the penetration factors of the incoming waves penetrating the Coulomb barrier. At least we may first note that the first row of Table II contains no powers of x higher than x^2, and this leads immediately to the result that for $\phi_3=0$ the cross section varies with angle as $1+A(E)\cos^2\theta$, as may also be obtained from the transformation properties of the entering p wave. We further note in Table II that the $\cos^4\theta$ term comes in with the first power of ϕ_3, as anticipated in the introductory paragraphs above, and that there are no higher powers of $\cos\theta$ with ϕ_3^2.

The most conspicuous contributions to the angular distribution at fairly low energies are made by the terms in ϕ_1 alone, and with only these terms the analysis involves the arbitrary complex constants

$$[122/12]\alpha_{12},\quad [112/12]\alpha_{12},\quad \Gamma_2\alpha_{10}/i\Gamma_0,$$

and also the common factor $(16\pi\lambda^2/\Gamma_2^2)$ in which we need not be interested if we confine our attention to the angular distribution. The number of constants appearing in the equation and essential to the angular distribution may be reduced by dividing through by one of them, say by $[112/12]\alpha_{12}$ as was done in reference 2. This procedure, which simplifies the leading terms, neither simplifies nor complicates the terms in ϕ_3. In carrying it out, we define the remaining arbitrary constants in terms of their real parts R and imaginary parts I:

$$\begin{aligned}\Gamma_2\alpha_{10}/i\Gamma_0[112/12]\alpha_{12}&=R_0+iI_0,\\ [122/12]/[112/12]&=R_1+iI_1,\\ [312/32]\alpha_{32}/[112/12]\alpha_{12}&=R_2+iI_2,\\ [322/32]\alpha_{32}/[112/12]\alpha_{12}&=R_3+iI_3.\end{aligned}\tag{11}$$

With these definitions, the first summation in the last member of (10), for example, can be developed as follows:

$$\begin{aligned}&\sum_{m=-2}^{2}\Big|\sum_{l=1,3}(l20m/l22m)\phi_l(R_l+iI_l)\Big|^2(P_2^m)^2\\ &=\sum_m\{[\sum_l(l20m/l22m)\phi_lR_l]^2\\ &\qquad+[\sum_l(l20m/l22m)\phi_lI_l]^2\}(P_2^m)^2\\ &=(R_1^2+I_1^2)\phi_1^2\sum_m(120m/122m)^2(P_2^m)^2\\ &\quad+2(R_1R_3+I_1I_3)\phi_1\phi_3\sum_m(120m/122m)\\ &\quad\times(320m/322m)(P_2^m)^2+(R_3^2+I_3^2)\\ &\qquad\times\phi_3^2\sum_m(320m/322m)^2(P_2^m)^2.\end{aligned}\tag{12}$$

When the other terms are treated similarly and evaluations made by use of Tables I and II, Eq. (10) becomes

$$\begin{aligned}\sigma\sim(\epsilon^2+1)^{-1}\{&[(5/2)(R_1^2+I_1^2)(1-x^2)\\ &+(5/6)(1+3x^2)+(R_0^2+I_0^2)(1+\epsilon^2)\\ &+(10/3)^{\frac{1}{2}}(R_0\epsilon-I_0)(1-3x^2)]\phi_1^2\\ &+(3/7)^{\frac{1}{2}}[(5/2)(R_1R_3+I_1I_3)(1-x^2)(1-5x^2)\\ &-(5/6^{\frac{1}{2}})R_2(1-12x^2+15x^4)-5^{\frac{1}{2}}((R_0R_2+I_0I_2)\epsilon\\ &+R_0I_2-R_2I_0)(1-3x^2)]\phi_1\phi_3\\ &+(15/112)[(R_3^2+I_3^2)(1-x^2)(1+15x^2)\\ &\quad+4(R_2^2+I_2^2)(1-4x^2+7x^4)]\phi_3^2\}.\end{aligned}\tag{13}$$

It is clear from Eqs. (8) and (10), among others, that there are no interference terms between the incoming states with $S=1$ and $S=2$, and consequently the phase of (R_1+iI_1) relative to (R_0+iI_0) cannot affect the result. If we consider these as entirely arbitrary parameters, we might without loss of generality of the result set $I_1=0$ (as suggested by footnote 9 of reference 2), and this is reflected in the form of (13). We prefer instead to keep our parameters uniquely defined in terms of the matrix elements even though these matrix elements are not in practice calculable, since expressing the parameters, which are handled as arbitrary, in this conceptually clearer

way does not interfere with the usefulness of the formulas. With the equation for the cross section in the form (13), it appears expedient to rename some of the combinations of arbitrary constants thus:

$$\begin{aligned} a&=(5/2)(R_1^2+I_1^2),\\ b&=(5/2)(3/7)^{\frac{1}{2}}(R_1R_3+I_1I_3),\\ c&=(5/14^{\frac{1}{2}})R_2,\\ d&=(15/7)^{\frac{1}{2}}(R_0R_2+I_0I_2),\\ e&=(15/112)(R_3^2+I_3^2). \end{aligned} \tag{14}$$

R_0 and I_0 together with these five are used as the seven independent real parameters. Among them, a and e are necessarily positive (or at least not negative). The formula for the cross section may then be written in the form

$$\sigma=C(\epsilon)[1+A(\epsilon)\cos^2\theta+B(\epsilon)\cos^4\theta], \tag{15}$$

with

$$\begin{aligned} A(\epsilon)&=[5/2-a-(30)^{\frac{1}{2}}(R_0\epsilon-I_0)\\ &\quad+3(2b+4c+d\epsilon+\alpha)\Phi\\ &\quad+(14e-4\gamma)\Phi^2]/D(\epsilon),\\ B(\epsilon)&=[5(b-3c)\Phi-(15e-7\gamma)\Phi^2]/D(\epsilon),\\ C(\epsilon)&=\pi(4\lambda[112/12]\alpha_{12}\phi_1/2^{\frac{1}{2}})^2D(\epsilon)/(\epsilon^2+1),\\ D(\epsilon)&=(R_0^2+I_0^2)(\epsilon^2+1)+5/6+a\\ &\quad+2(2/3)^{\frac{1}{2}}(R_0\epsilon-I_0)+(b-c-d\epsilon-\alpha)\Phi\\ &\quad+(e+\gamma)\Phi^2, \end{aligned} \tag{16}$$

where

$$\Phi=\phi_3/\phi_1$$

is the ratio of the penetration amplitudes of the incoming f and p waves, and the auxiliary constants α and γ (which were introduced as abbreviations for $(15/7)^{\frac{1}{2}}(R_0I_2-R_2I_0)$ and $(15/28)(R_2^2+I_2^2)$, respectively) may be expressed in terms of the independent parameters thus:

$$\begin{aligned} \alpha&=(R_0d-(6/5)^{\frac{1}{2}}(R_0^2+I_0^2)c)/I_0,\\ \gamma&=(3/10)\{c^2+((5/6)^{\frac{1}{2}}d-cR_0)^2/I_0^2\}. \end{aligned} \tag{17}$$

The common factor $C(\epsilon)$ contains a further matrix element not included in our listed parameters, but it need not necessarily be considered in a study of the angular distribution. It must be remembered that ϵ is related to the bombarding energy (in c.m. coordinates) and the resonant energy through the relation $\epsilon=2(E-E_2)/\Gamma_2$ so that the E_2 and Γ_2 must be considered as further arbitrary parameters. With no entering f wave, Φ reduces to zero and makes $B(E)=0$, as has been noted above, and the parameters involved in the determination of $A(E)$ are five: E_2, Γ_2, R_0, I_0, and a, of which Γ_2 and a are limited to positive values. When the terms in Φ but not those in Φ^2 are taken into account, we have the three additional arbitrary parameters, b, c, and d, and the terms in Φ^2 bring in the last parameter, e, which is positive.

The algebra is here presented more explicitly than is required to derive the form of the results used in the experimental comparisons below. This is done in order to display the extent to which the integrals originally appearing in the theory in principle determine, or from the empirical viewpoint are determined by, the final parameters which are adjusted to fit the data.

IV. COMPARISON WITH THE EXPERIMENTAL RESULTS

Since it depends on arbitrary assumptions about the compound nucleus, the theory here presented should be considered as merely the simplest of several alternative theories, and its adequacy must be judged by comparison with experiment. Unfortunately, the experimental determination of the coefficient $A(E)$ and particularly of $B(E)$ depend on taking rather small differences of observations subject to statistical and in some cases probably systematic errors, and the measurements at present available, which have only recently exhibited the term in $\cos^4\theta$ at all, must be regarded as preliminary. Under these circumstances the comparison between detailed theoretical and experimental results must be regarded more as a test whether the theoretical formula has sufficient flexibility to fit a typical experimental trend than as a final adjustment of the theory to the data. If the final data should require a more complicated theory, the understanding of it will have been aided by a study of the insufficient flexibility of the simpler theory. It is nevertheless gratifying that the theory here presented appears to have adequate flexibility to account for the general trend of the data over the fairly wide energy range in which they are now available.

The experimental measurements on $A(E)$ made by four different groups of investigators in partially overlapping energy regions are not in very close accord on the details of the curve. In reference 1 an S-shaped curve was drawn through the data up to 400 kev, and this does not seem

to join in a reasonable way with the curves of either reference 4 or 5. This *S*-shaped curve is reproduced as the short curve near the origin of Fig. 1. References 4 and 5 disagree by about 150 kev on the position of the principal steep ascent of the curve. However, these minor discrepancies leave little doubt that the main trend of the curve includes a sharp rise from practically zero at a small positive energy to a rather broad peak at about 1 Mev and a somewhat more gradual descent toward higher energies. The lower curve in Fig. 1 is drawn to fit all the data reasonably well with emphasis on avoiding sharp bends and inflections and with the knowledge that the theory does not require it to go to zero at zero bombarding energy. The only point which deviates from this compromise curve by more than 0.3 in A is the point whose originally plotted limits of uncertainty are reproduced by the vertical broken line in Fig. 1, the point from reference 4 at 875 kev, and it may be seen clearly in Fig. 3 of that paper that the reason this point was plotted too low was a prejudice against the possibility of a term in $\cos^4\theta$. (On the $\cos^2\theta$ plot, the 90° point was so far below a straight line through the others, probably the combined effect of experimental fluctuations and of the negative value of $B(E)$, that it was ignored in determining the slope, since repetition of the observation had become impossible because of the advent of the war.) The curve avoids the inflections of the *S*-shaped curve at low energies and is consequently drawn with a node at about 100 kev. In reference 1, there seems to be a little evidence of a very natural prejudice against the possible appearance of negative values of A at low energies: the lowest point at 100 kev seems to be plotted in their Fig. 3 with an indication of the upper limit but with no indication of a lower limit. The scatter of points on their Fig. 2 would seem to permit a slightly negative A at 100 kev. The intensity is so low at these energies that the observations have unfortunately not been extended to energies sufficiently below 100 kev to have detected the negative value of $A(E)$ which would be expected there if there is a node near 100 kev. Experimental proof of the existence of a node rather than a gradual approach to zero would be desirable as a test of the theory.

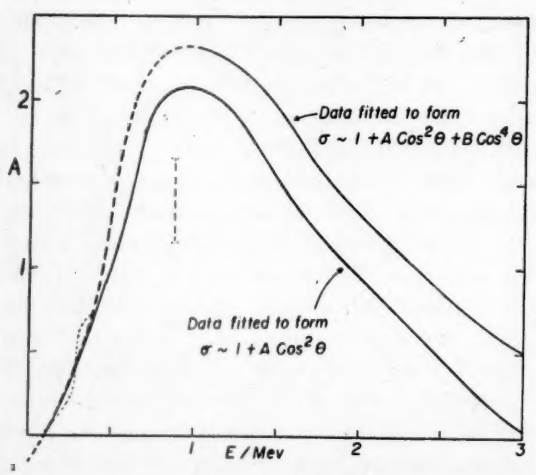

FIG. 1. The coefficient of the term in $\cos^2\theta$: curves summarizing the general trend of the observed angular distribution of $Li^7(p,\alpha)\alpha$ with varying energy. The lower curve is drawn in keeping with the interpretation of the earlier experimental papers, in which the term in $\cos^4\theta$ was not recognized. That these curves are uncertain in detail is indicated by discrepancies of overlapping data in the low energy part and by difficulties encountered in discriminating against scattered protons at the high energy end. The upper curve gives the general trend of the part of the angular distribution attributed to the $\cos^2\theta$ term after a part has been attributed to the term in $\cos^4\theta$.

The lower curve in Fig. 1 is based on fitting the data as well as possible to the simplified form of the angular distribution $1+A(E)\cos^2\theta$, with neglect of the observations at 10° and 20° when these were available in the more recent data in order to facilitate a comparison with the older data.

The upper curve in Fig. 1 represents $A(E)$ as determined by fitting the data to the more adequate form for the angular distribution $1+A(E)\cos^2\theta+B(E)\cos^4\theta$. This is, of course, the curve for $A(E)$ which should correspond to the theoretical expression (16). The part above 1 Mev is taken from reference 6, where this fit was carried out. The broken portion of the curve below 1 Mev is an arbitrary extrapolation guided by the lower curve, the data in this region being inadequate for any determination of $B(E)$. (Preparations are being made for further observation of this region.) The upper curve is expected to approach the lower curve closely at very low energies, where $B(E)$ is expected to vanish, so this curve also has a node at 100 kev.

Since $A(E)$ is observed to have its most rapid variation and pass through its maximum in the

range of energies up to not much over 1 Mev, in which Φ is expected to remain well below unity, it may be expected that the gross features of the curve for $A(E)$ may be reproduced by the approximation neglecting terms in Φ. On the face of it, it would seem that almost any general form of curve could be reproduced over a fairly limited range by a formula containing as many as five parameters. The equation for $A(\epsilon)$ when $\Phi=0$,

$$A(\epsilon)=\frac{5/2-a-2(6)^{\frac{1}{2}}(R_0\epsilon-I_0)}{(R_0^2+I_0^2)(\epsilon^2+1)+5/6+a+2(2/3)^{\frac{1}{2}}(R_0\epsilon-I_0)} \tag{18}$$

(which corresponds[11] to Eq. (12) of reference 2), does, however, seem to have a peculiar fitness for reproducing a curve which rises to a single maximum and falls to a node at one end of the observed range and to a small value but not a node at the other end. The numerator is linear in ϵ and thus has only one node, which can be made to match the experimental node[1,4] at about $E=100$ kev in the laboratory coordinate system.[12] For convenience in plotting a curve to compare with the experimental curve, Eq. (18) may be written with fewer terms:

$$A(E)=(C_1E+C_2)/(E^2+C_3E+C_4), \quad (18.1)$$

where the four parameters are expressed in the previous five parameters a, R_0, I_0, E_2, and Γ_2 as follows:

$$\begin{aligned}
&C_1=-6^{\frac{1}{2}}R_0\Gamma_2/\rho, \quad \rho=R_0^2+I_0^2,\\
&C_2=[(5/2-a+2(6)^{\frac{1}{2}}I_0)(\Gamma_2/4)\\
&\qquad\qquad +6^{\frac{1}{2}}E_2R_0]\Gamma_2/\rho, \quad (19)\\
&C_3=(2/3)^{\frac{1}{2}}R_0\Gamma_2/\rho-2E_2,\\
&C_4=(5/6+a-2(2/3)^{\frac{1}{2}}I_0)\Gamma_2^2/4\rho\\
&\qquad -(2/3)^{\frac{1}{2}}(R_0\Gamma_2/\rho)E_2+E_2^2+\Gamma_2^2/4.
\end{aligned}$$

The shape of the curve thus depends on only these four parameters and the previous five parameters are not uniquely determined by fitting the curve to the experimental data, even in this approximation which neglects terms in Φ.

This curve is plotted as curve *II* in Fig. 2, with the constants determined to match the experimental curve in the following respects: $A(0.1\text{ Mev})=0$, $A(3\text{ Mev})=\frac{1}{2}$, $E_{\max}=0.95$ Mev, $A(E_{\max})=2.32$. This curve has a considerably sharper maximum than the experimental curve *I* of Fig. 2, the latter being a copy of the upper curve in Fig. 1 which was drawn simply as a reasonable compromise between the slightly divergent and uncertain data. The constants C for curve *II* are $C_1=0.92$ Mev, $C_2=-0.092$ (Mev)^2, $C_3=-1.5$ Mev and $C_4=0.86$ (Mev)^2. A typical set of the previous five parameters compatible with this curve is

$$\begin{aligned}
&E_2=0.6\text{ Mev}; \quad \Gamma_2=0.1\text{ Mev};\\
&R_0=-0.04; \quad I_0=-0.1;\\
&a=(5/2)(R_1^2+I_1^2)=0.23.
\end{aligned}$$

The domain over which these sets of parameters may vary is limited by the requirement that a be

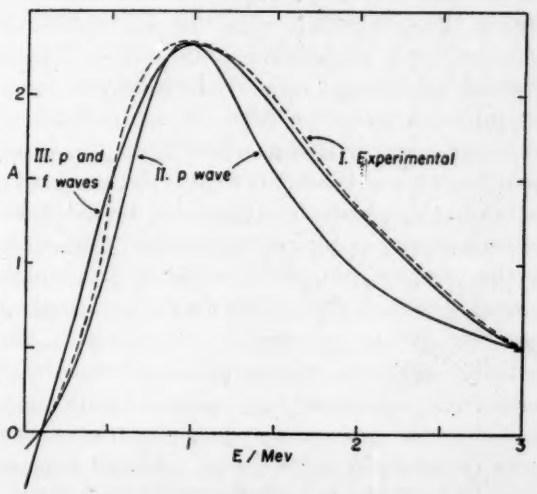

FIG. 2. The coefficient of the term in $\cos^2\theta$: comparison between theory and experiment. The curve taken to represent the rather uncertain experimental results is the same as the upper curve of Fig. 1. The theory resulting from only entering p waves gives too sharp a peak when fitted at the low energy node, at the peak, and at the highest energy. The theory including entering f waves is sufficiently adaptable to fit the experimental trend satisfactorily over this energy range.

[11] The correspondence between the coefficients becomes clear if one puts $\cos 2\xi=1-2\sin^2\xi$ and notes that $a=(5/2)\tan^2\xi$ and that the terms in β^2 in numerator and denominator have the ratio 3 when $\sin\xi=a=0$ and the ratio -1 when $\sin\xi=1$ (or $a=\infty$).

[12] For convenience in comparison with experiment, at this point we consider the definition $\epsilon=2(E-E_2)/\Gamma_2$ to hold in the laboratory system, which is permitted since Γ_2 is now treated as an arbitrary parameter. This parameter Γ_2 is then (8/7) times the half-width appropriate to the theory, and for consistency a factor $(8/7)^3$ should henceforth be inserted in the expression in (16) defining $C(\epsilon)$.

TABLE III. Barrier penetrabilities for p and f waves.

$\frac{R}{e^2/mc^2}$	E/mc^2	1	1.5	2	3	4	6
1.5	C_1	1.73	1.23	0.90	0.51	0.28	0.04
	C_3	6.53	5.54	4.87	3.97	3.35	2.52
	Φ	0.0055	0.0087	0.0121	0.0193	0.0266	0.0381
	$5.06+2\ln\phi_1$	0.70	1.73	2.44	3.32	3.92	4.90
2.25	C_1	1.00	0.58	0.33	0.07		
	C_3	4.17	3.38	2.80	2.07	1.58	0.96
	Φ	0.028	0.038	0.050	0.065		
	$3.34+2\ln\phi_1$	0.83	1.81	2.44	2.56		
	$\ln Y(90°)$	1.61	2.10	2.44	3.20	4.26	

positive. E_2 remains fixed, and the rapidity of variation of the other parameters is indicated by the statement that, while a varies from 0 to 0.5, Γ_2 varies from 0.2 Mev to 0, R_0 from -0.07 to 0, and the ratio I_0/R_0 from 2.6 to 2.4. The smallness of $R_0^2+I_0^2$ relative to $R_1^2+I_1^2$ presumably arises primarily from the small ratio Γ_2/Γ_0, rather than from the other coefficients appearing in Eqs. (11), since the latter contain complicated integrals having no apparent reason to be very much larger for one state than another.

The next step in increasing complexity is to take into account the effect of the f wave of entering protons by including the terms containing Φ in the expression for $A(\epsilon)$ in Eq. (16). As we have noted above, Φ is essentially the ratio of the penetrabilities of the f and p wave functions (not probability amplitudes). These penetrabilities should properly be computed from the amplitudes, at the edge of the nucleus, of the regular and irregular solutions of the wave equation with a Coulomb field. Of these, only the regular solutions are at present available for f waves in the published literature.[13] We shall for the present content ourselves with a rough indication of their variation with energy obtained from the WKB approximation, which is admittedly unreliable for energies near the top of the barrier such as we are concerned with here. In Table III are shown data on the energy variation of $\Phi=\phi_3/\phi_1$, for two assumed nuclear radii, $R=1.5e^2/mc^2$ and $R=2.25e^2/mc^2$. These about span the range of uncertainty of R—they correspond to $\frac{1}{2}A^{\frac{1}{3}}e^2/mc^2$ plus half the range of the internuclear interaction and to about $0.7A^{\frac{1}{3}}e^2/mc^2$ plus the full range of the interaction, respectively. The data are computed from Eq. (631) of Bethe's *Nuclear Dynamics* article[14] by putting our ϕ_l equal to $(B_l-E)^{-\frac{1}{4}}e^{-C_l}$, where $B_l=U_l(R)$ is the height of the barrier. Here $U_l(r)=l(l+1)\hbar^2/(2Mr^2)+3e^2/r$, with M the reduced mass, and $C_l=2(M/\hbar^2)\int(U_l-E)^{\frac{1}{2}}dr$ integrated through the barrier. With $R=1.5e^2/mc^2$, B_1 is $7.19mc^2$ and B_3 is $33mc^2$. With $R=2.25e^2/mc^2$, B_1 is $3.6mc^2$ and B_3 is $15mc^2$, and with this large radius an energy of even $4mc^2$ is over the p wave barrier. In the table are also given the values of $\log\phi_1^2$ within a constant made to match the experimental data for $\log Y(90°)$ (taken from Fig. 4 of reference 6) at $E=2mc^2$. Equations (15) and (16) above show that the 90° yield can have a complicated dependence on energy through the explicit appearance of ϵ in $C(\epsilon)$ and $D(\epsilon)$, but because of the exponential nature of the penetration factor a large part of this energy variation is still expected to arise from the factor ϕ_1^2. For the sake of making this comparison, the experimental data for $\log Y(90°)$ are displayed as the last row of Table III. These data are taken from Fig. 4 of reference 6 (after converting energies from the center-of-mass system in mc^2 to the laboratory system in Mev). The traditional way of plotting $\log Y$ against $E^{-\frac{1}{2}}$ as followed in that figure arises from the expectation of a straight line in a much cruder approximation than we have used here, valid only even further below the top of the barrier, and the comparison of yields in Table III is more significant than the deviation from a straight line in that figure.

In the comparison between $\ln\phi_1^2$ and $\ln Y(90°)$ in Table III the two R's both lead to the expectation of a sharper variation with energy than is observed in the region below $2mc^2$, as though the existence of a resonance, presumably the state $j_r=2$ at 0.6 Mev, elevates the observed value there through the resonance denominator in $C(\epsilon)$. Aside from this, the value $R=1.5e^2/mc^2$ provides as satisfactory agreement as can be expected from the WKB approximation in a light nucleus. (The larger value or R might show up better, too, were it not that the approach to the top of the barrier invalidates the estimates completely at intermediate energies.)

[13] F. L. Yost, J. A. Wheeler and G. Breit, Terr. Mag. 40, 443 (1935).

[14] H. A. Bethe, Rev. Mod. Phys. 9, 178 (1937).

The main purpose of Table III is to exhibit the variation of Φ with energy. With the smaller radius, the relative penetrability Φ varies almost linearly with energy (or more nearly as the 1.1 power). With the larger radius the more questionable calculation gives a variation more nearly like the 0.85 power of the energy, which at least suggests that the variation is probably not very far from linear for a small range of radii R in the neighborhood of $1.5e^2/mc^2$.

In Eq. (16) we may then put

$$\Phi = KE/mc^2. \tag{20}$$

Since this is multiplied everywhere by arbitrary constants, the exact value of the numerical coefficient K is of no importance, though its order of magnitude is of considerable interest because one would presume offhand that several of the larger ratios of matrix elements in (14) would have the same order of magnitude, and that the coefficients of Φ in (16) would be of the same order of magnitude as the terms without Φ, except where fortuitous cancellations of the matrix elements cause some combinations of coefficients to vanish. The experimental fact is that $B(\epsilon)$, which contains Φ as a factor, is, in the energy range 2 to $6mc^2$, about one-fourth to half as large in magnitude as is $A(\epsilon)$, which has a leading term without Φ. The leading term in A cannot be fortuitously small at all these energies (it is known to be so at 100 kev), so Φ is expected to be of order of magnitude $\frac{1}{2}$ at $4mc^2$, for example, suggesting that one would prefer to find K of order of magnitude $\frac{1}{10}$, rather than 0.006 to 0.03 as suggested by the calculations for $R=1.5$ to $2.25e^2/mc^2$. While one might take this as indicative of a large nuclear radius, our ignorance of the matrix elements involved actually allows us to conclude only that the coefficient $5(b-3c)$ which determines the size of $B(\epsilon)$ in (16) is probably considerably larger in magnitude than, say, $2(6)^{\frac{1}{2}}R_0$ which is responsible for the size of $A(\epsilon)$.

The linear relation (20) in (15) and (16) yields

$$A(E)=(C_0E^2+C_1E+C_2)/(E^2+C_3E+C_4) \tag{21}$$

in place of (18.1), and for the coefficient of the $\cos^4$ term

$$B(E)=(C_5E^2+C_6E)/(E^2+C_3E+C_4). \tag{22}$$

These new coefficients C_n are no longer defined by (19) but instead involve the additional arbitrary parameters b, c, d, and e, as well as the constant K. Equation (21) which includes the effect of an entering f wave contains one more arbitrary coefficient C_n than does (18.1), which resulted from an entering p wave only. Whereas (18.1) gave somewhat too sharp a peak to fit the experimental data, the additional freedom provided by the C_0 term in (21) is sufficient to make a satisfactory fit with the data. This is shown by curve *III* in Fig. 2, which represents Eq. (21) with the constants[15] chosen to satisfy the following requirements: $A(0.1\ \text{Mev})=0$, $A(3\ \text{Mev})=\frac{1}{2}$, $A(2\ \text{Mev})=1.6$, $E_{\max}=1$ Mev, $A(E_{\max})=2.3$. While these requirements are stated in "round numbers" and may not give the best possible fit to the experimental curve *I*, the curve does show that (21) permits freedom to make the peak rather broad as required by the experimental results. Raising the curve as we have done on the high energy side of the peak raises it on the low energy side also and makes it steeper at very low energies than suggested by the low energy experiments. A slightly better fit with the various low energy experiments could perhaps be obtained by placing the node at about 200 kev and the peak at about 900 kev. In view of the tentative and discrepant nature of the experimental results below 1 Mev, which have not yet been analyzed for a term in $\cos^4\theta$, the agreement of curve *III* with curve *I* may be considered satisfactory, and a distinct improvement over curve *II*.

The f wave was included primarily in order to explain the $\cos^4\theta$ term, but we see now that the additional freedom that it introduces also helps to account for the energy dependence of the $\cos^2\theta$ term, insofar as the rather preliminary experimental data at present available may be trusted. Our assumptions about the states of the compound nucleus and about the barrier penetration must also be regarded as tentative, but within the limitations of these assumptions it should be noted that the inclusion of the f wave results not simply in additional freedom to fit the data within a limited energy range but also requires quite different behavior of $A(E)$ over

[15] They are $C_0=-0.99$, $C_1=4.34$ $C_2=,-0.43$, $C_3=-0.98$, $C_4=1.24$.

an extended energy range. In particular, the quadratic form of the numerator of (21) requires either no nodes or two, and the interpretation of the low-energy data in terms of a node near 100 kev requires another node at some higher energy. The available experimental data at the high energy end of the curve, near 3 Mev, are particularly uncertain because of the inconvenient range of scattered protons at those energies, but they seem at least to be compatible with a descent toward a node. Another important aspect of the greater freedom introduced by the f wave is that the correlation between the angular distribution and the expected position of a resonance in the excitation curve has been lost. Whereas with only a p wave curve *II* of Fig. 2 required a resonance (not observed) in the 90° yield at about 0.6 Mev, the number of parameters E_2, Γ_2, R_0, a, b, etc., has been increased by four in including the f wave, while the number of coefficients C_n uniquely determined by the data has been increased by only one, so it may unfortunately no longer be expected that the "parameters" E_2, Γ_2, etc., may be determined or even seriously limited.

As for the energy variation of $B(E)$, comparison of (22) with (16) and (20) shows that C_5 contains a factor K^2, so that C_5E^2 may be expected to be much smaller than C_6E, at least at energies below 1 or 2 Mev, since the coefficient $5(b-3c)$ may not be fortuitously small as we have seen above. Because the experimental determination of B depends on taking second differences of values subject to statistical and other fluctuations (and because the observation at the highest energy, 3 Mev, is made more doubtful than the rest by interference from scattered protons), the trend of B with energy is far from well established. The curves resulting from a couple of trial values of C_6 and C_5 (one with $C_5=0$ and the other with C_5 relatively much larger than would seem most likely) are shown in Fig. 3, along with the scattered experimental points. The resonance denominator here contains the same constants[15] as used for curve *III* of Fig. 2. The form of the curves gives hope of obtaining agreement with more definite experimental data if they should become available.

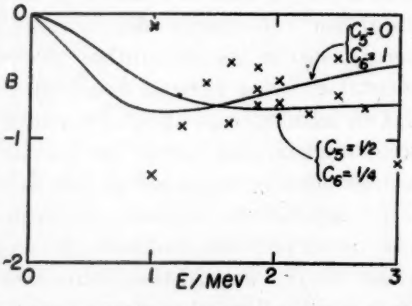

FIG. 3. The coefficient of the term in $\cos^4\theta$. Plausible variations of the two remaining arbitrary parameters would be expected to leave the theoretical curve between or near the two curves shown. The scattered preliminary experimental points are also shown.

V. ALTERNATIVE SET OF COMPOUND STATES

The assumption investigated above, that the angular distribution is to be attributed to a broad state of the compound nucleus with $j_r=0$ and a narrower state with $j_r=2$, seems to us the simplest and most natural basis for the interpretation of the experimental results, simplest because it involves fewest arbitrary parameters, and most natural because the gradual energy dependence of the angular distribution suggests a low density of levels of the compound nucleus Be^8 in this region of excitation, and one expects to encounter low angular momenta at those energies where the density of levels is very low. The great breadth of the state with $j_r=0$ is naturally associated with the ease with which such a state is expected to break up into two alphas.

It must however be recognized that the possibility of fitting the data with the above assumptions does not constitute a complete demonstration of the validity of those assumptions, and this investigation would be very incomplete without a display of some of the qualitative features of results obtainable from alternative assumptions. The simplest modification of the assumptions used above is to drop the requirement that Γ_0 be very large. This alteration complicates all the formulas considerably, but the development parallels so closely the calculation already carried out that we wish here only to note that its final formula for $A(E)$ is analogous to (21) with the numerator including powers of E up to the fifth and the denominator up to a term in E^4, the latter being small of order K^2.

We consider here in more detail the possibility

that there are two virtual states of the compound nucleus, each having $J_r=2$, but differing in E_r and Γ_r. We develop from Eqs. (7) and (8) as before, and the incoming states are the same as considered above. We find for the factor in the cross section which determines the angular distribution,

$$\begin{aligned}\sigma\sim&\{[\textstyle\sum C_{111r}/(\epsilon_r^2+1)+((\epsilon_1\epsilon_2+1)D_{111}\\&+(\epsilon_1-\epsilon_2)E_{111})/(\epsilon_1^2+1)(\epsilon_2^2+1)](1/3+x^2)\\&+[\textstyle\sum C_{112r}/(\epsilon_r^2+1)+((\epsilon_1\epsilon_2+1)D_{112}\\&+(\epsilon_1-\epsilon_2)E_{112})/(\epsilon_1^2+1)(\epsilon_2^2+1)](1-x^2)\}\\&-7^{-\frac{1}{2}}\{2^{\frac{1}{2}}[\textstyle\sum C_{131r}/(\epsilon_r^2+1)+((\epsilon_1\epsilon_2+1)D_{131}\\&+(\epsilon_1-\epsilon_2)E_{131})/(\epsilon_1^2+1)(\epsilon_2^2+1)](1-12x^2\\&+15x^4)+3^{\frac{1}{2}}[\textstyle\sum C_{133r}/(\epsilon_r^2+1)+((\epsilon_1\epsilon_2+1)D_{133}\\&+(\epsilon_1-\epsilon_2)E_{133})/(\epsilon_1^2+1)(\epsilon_2^2+1)](1-6x^2\\&+5_x^4)\}\Phi+(3/28)\{[\textstyle\sum C_{331r}/(\epsilon_r^2+1)\\&+((\epsilon_1\epsilon_2+1)D_{331}+(\epsilon_1-\epsilon_2)E_{331})/(\epsilon_1^2+1)\\&\times(\epsilon_2^2+1)](1+14x^2-15x^4)+4[\textstyle\sum C_{333r}/\\&(\epsilon_r^2+1)+((\epsilon_1\epsilon_2+1)D_{333}+(\epsilon_1-\epsilon_2)E_{333})/\\&(\epsilon_1^2+1)(\epsilon_2^2+1)](1-4x^2+7x^4)\}\Phi^2.\end{aligned}$$

The wealth of constants appearing here are defined as follows in terms of the integrals originally entering the theory:

$$\begin{aligned}&C_{abSr}=R_{aSr}R_{bSr}+I_{aSr}I_{bSr},\\&D_{abS}=R_{aS1}R_{bS2}+R_{aS2}R_{bS1}+I_{aS1}I_{bS2}+I_{aS2}I_{bS1},\\&E_{abS}=R_{aS1}I_{bS2}-I_{aS1}R_{bS2}+R_{bS1}I_{aS2}-I_{bS1}R_{aS2},\\&R_{lSr}+iI_{lSr}=(\Gamma_1/\Gamma_r)[lSj_r/lj_r]\alpha_{lr}/[11j_1/1j_1]\alpha_{11}.\end{aligned}$$

We then have the conditions

$$R_{111}=1,\quad I_{111}=0,$$

and the other R_{lSr} and I_{lSr} may be considered as arbitrary parameters, which amounts to the same thing as treating the C's, D's, and E's as arbitrary parameters with the conditions

$$C_{111}=1,\quad C_{1112}=E_{111}^2+D_{111}^2/4.$$

Neglecting terms containing Φ, we obtain $\sigma\sim 1+A\cos^2\theta$ as the result of an entering p wave, with

$$A=\frac{b(\epsilon_2^2+1)+d(\epsilon_1\epsilon_2+1)+f(\epsilon_1-\epsilon_2)+\{\frac{3}{4}[(c+d)^2+(e+f)^2]-g\}(\epsilon_1^2+1)}{a(\epsilon_2^2+1)+c(\epsilon_1\epsilon_2+1)+e(\epsilon_1-\epsilon_2)+g(\epsilon_1^2+1)}.$$

Here we have renamed the parameters to simplify the appearance of the equation, and of them, $a\geqslant\frac{1}{8}$ and $g\geqslant 0$. This contains seven parameters explicitly, and there are four more implicit in the definitions of the ϵ's, as compared with three explicit and two implicit parameters in Eq. (18) above. With so many parameters there is without doubt much more freedom than is required to fit the experimental results and any correlation achieved would seem less significant than with the fewer parameters of the simpler interpretation presented above. It is, of course, still possible that future more accurate data might require this greater freedom, or perhaps even a more complicated set of assumptions involving a state of the compound nucleus with $j_r=4$.

Energy Quanta Emitted in Disintegration of Ground State of Ba^{133}

FU-CHUN YU AND J. D. KURBATOV
The Ohio State University, Columbus, Ohio

(Received March 19, 1948)

The ground state of radioactive Ba^{133} was correlated with metastable state of Ba^{133*}. It was found that after K-electron capture occurs, there are two excited states in Cs^{133*} corresponding to observed two photons of 320 ± 10 kev and 85 ± 5 kev. Both gamma-rays are converted. The conversion ratios for these two photons are $N_e/N_\gamma \approx 0.02$ and ≈ 0.34, respectively. The change in angular momenta of the excited states of Cs^{133*} due to emission of 320-kev and 85-kev photons is calculated to be $L=2$ and $L=1$. Attempts to observe a third gamma-ray of $\sim$405 kev did not yield positive results. The calculated intensity of the 405-kev photon, if it is emitted, is estimated as equal to 0.001 of the intensity of the 320-kev photon.

1. INTRODUCTION

THE scheme of disintegration of the species Ba^{133} has been investigated by several authors. In the past Ba^{133} was obtained by $(d,2n)$ or (p,n) reactions of cesium. This mode of activation always produced a period of about 39 hours, which was followed by partially converted quanta of 276.4 kev and by K, L, M, x-rays of barium.[1] In accord with these observations, this period has been described as one of the excited states of radioactive Ba^{133}.

Concerning the scheme of disintegration of the ground state of Ba^{133}, the available information is not in sufficient agreement. In older work[1] it was suggested that the ground state of Ba^{133}, of half-life $T\sim340$ hours, disintegrates into stable cesium by K-electron capture followed by K x-radiation of cesium and soft gamma-rays of 17 kev. In more recent works[2–4] the latter was not confirmed.

It was proposed[2] that Ba^{133}, obtained by activation with slow neutrons, disintegrates by K-electron capture, its half-life exceeding 20 years, and leads to the excited state of Cs^{133*}. The latter emits a single photon of 360 kev into the ground state of Cs^{133}.

Independently, observations have been made by other authors that by activation of barium with slow neutrons in a cyclotron the (n,γ) reaction yields a period of $T\sim30$ hours accompanied by quanta of $\sim$250 kev.[3] The 30-hour period in barium has been verified by (d,p) reaction on barium.[4] However, due to the existence of the 39-hour period in Ba, the 30-hour period with close photon energy was mistaken for the 39-hr. Ba^{133*}. Only the 39-hr. period of Ba^{133*} is listed at present in all tables of radioactive species.

2. EXPERIMENTAL RESULTS

In the present study, the radioactive species of barium were obtained by prolonged activation of barium with slow neutrons, and by activation of cesium and of barium with deuterons.

The prolonged activation of barium with slow neutrons yielded after chemical purification several periods in barium that were identified as follows: $T=29$ hr.; $T=39$ hr.; $T=12$ days, and a long period. After 200 days the activated barium was used for studying the radiations of the long period.

The cesium was twice removed from barium in an interval of fifteen days, and since in both separations no activity in the cesium fraction was observed, it was confirmed that Ba^{133} cannot be the mother substance of Cs^{131}, $T=10$ days.

In spite of the low specific activity of barium activated with slow neutrons, it was possible, by means of absorption measurements with a Wulf electrometer, to establish two gamma-rays of $\sim$310 kev and $\sim$80 kev. The same energy values were obtained by using copper and tin absorbers. In Fig. 1 are shown the results on absorption in lead of the radiations from Ba^{133} and for purpose of comparison from Ba^{133*},

[1] J. M. Cork and Gail P. Smith, Phys. Rev. **60**, 480 (1941).
[2] Seymour Katcoff, Phys. Rev. **72**, 1160 (1947).
[3] D. C. Kalbfell and R. A. Cooley, Phys. Rev. **58**, 81 (1940).
[4] K. E. Weimer, M. L. Pool, and J. D. Kurbatov, Phys. Rev. **63**, 59A (1943).

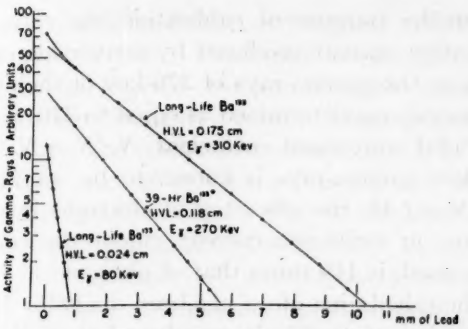

FIG. 1. Lead absorption showing gamma-rays of 270 kev in the 39-hr. period and gamma-rays of 80 kev and 310 kev in the long-life period.

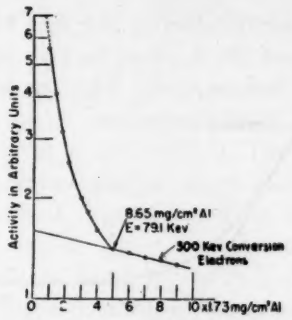

FIG. 2. Long-life Ba^{133}. Absorption of low energy electrons in aluminum.

$T = 38.9$ hr. (since the exact energy of 276.4 kev has been established by the beta-spectrometer for Ba^{133*}). The metastable state of Ba^{133*} was secured by the activation of cesium, Cs^{133}, with deuterons.

The low specific activity of Ba^{133} produced by slow neutrons prohibited the use of a spectrometer; consequently, parallel to adsorption a study of Ba^{133} was made in a cloud chamber. The results obtained with the cloud chamber confirmed the existence of two photons from Ba^{133}. In addition, it was possible to obtain a ratio of photo-electron tracks of the photons of ~ 310 kev and of ~ 80 kev. A full account of the work with the cloud chamber will be presented later.

Independently, it has been found that the total ionization current produced in an electrometer by electrons and by photons is predominantly due to the conversion electrons of ~ 80-kev photons. This made it possible to obtain information on the conversion coefficient of the 80-kev photon in K and L shells and to evaluate more exactly its energy as 85 ± 5 kev. In Fig. 2 are given the results of absorption of electrons in aluminum, where there is a sudden change of slope in the curve between the L shell conversion electrons of 85 kev and conversion electrons of 310 kev. A more exact absorption curve of conversion electrons is given in Fig. 3. From this curve, it was possible to estimate the conversion ratio in L and K shells of 85-kev photon. The value of N_K/N_L was found to be between 9 and 11. Making use of the curve given by Hebb and Nelsen, the ratio $N_K/N_L = 9$ was obtained which corresponds to one unit change in angular momentum. For an angular momentum change of two units[5] the ratio N_K/N_L would drop to a value of 3.

The K-conversion coefficient was calculated for the 85-kev photon of cesium. It was found that $\alpha_K = 0.306$; then $\alpha_K + \alpha_L = 0.34$ or $N_e/N_\gamma = 0.34$. It can be noted that in case $L = 2$, $\alpha_K \sim 2$, which is not consistent with experimental observation.

In order to establish the mass number of the long-life barium and to evaluate better the energy of the photons emitted, a strong activation of cesium was made with deuterons. The barium fraction was separated from the activated cesium without the addition of carrier, that is, all barium atoms produced by (d,n) and $(d,2n)$ reactions were undiluted by common barium or any other carrier.[6]

By following the disintegration of gamma-rays of 276.4 kev, emitted by the 38.9-hr. period, it was established that the photon intensity of the long-life barium was rising (see Fig. 4). The

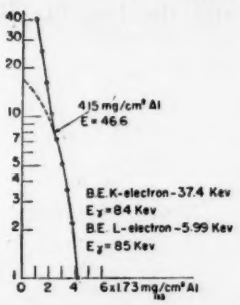

FIG. 3. Long-life Ba^{133} absorption of low energy electrons in aluminum.

[5] M. H. Hebb and E. Nelsen, Phys. Rev. **58**, 486 (1940), S. M. Dancoff and P. Morrison, Phys. Rev. **55**, 122 (1939).
[6] M. H. Kurbatov, Fu-Chun Yu, and J. D. Kurbatov, Chem. Phys. **16**, 87 (1948).

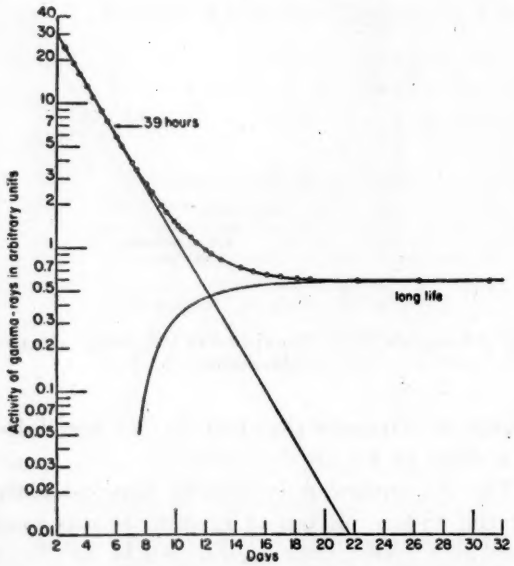

FIG. 4. The genetic relation between the gamma-ray of 276 kev of 38.9-hr. period of Ba^{133*} and that of 320 kev of the long-life Ba^{133}.

energies of the photons of long-life barium have been determined to be equal to 330 kev and 80 kev. In this case a very high specific activity was measured. The energies of conversion electrons corresponding to these two photons were found to be equal to 300 kev and 79 kev for the L shell conversion. Thus it has been determined that the long-life period of barium, obtained by prolonged activation with slow neutrons on barium, possesses the same energy photons as the long-life period in barium, that was obtained by activation of cesium. Therefore, the genetic relation between the metastable state of the 38.9-hr. period Ba^{133*} and the long-life Ba^{133} has been established.

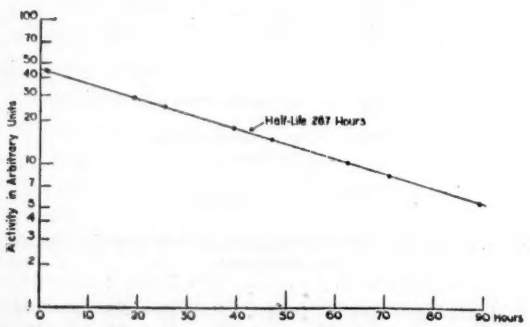

FIG. 5. Decay of Ba^{133*} half-life 28.7 hr., produced by Ba(d,p) reaction.

For the purpose of calibration the ratio of ionization current produced by conversion electrons to the gamma-rays of 276 kev of the 38.9-hr. period was determined as equal to 270. Since the total conversion coefficient N_e/N_e+N_γ for 276-kev gamma-rays is known to be $=0.71$ or $N_e/N_\gamma=2.45$, the efficiency of electrons in producing an ionization current, under the conditions used, is 110 times that of photons.

The calculation of α_K has been made for 38.9-hr. period of Ba^{133*}. It was found that $N_e/N_\gamma=2.32$, taking the change in angular momentum as four. Thus, the calculated value is in good agreement with the experimentally observed $N_e/N_\gamma=2.45$.

The current produced in the ionization chamber (at the same geometry) by conversion electrons of 330-kev gamma-ray was found to be about twice as much as the current produced by the gamma-ray itself. The efficiency of electrons of 300 kev in producing ionization current in the electrometer is approximated as 100 times that of gamma-rays of the same energy. Thus the ratio $N_e/N_\gamma=0.02$ was obtained. The calculated conversion ratios $\alpha_K=N_K/N_\gamma$ for different values of change in angular momenta, L, are:

if $\alpha_K=$	0.0060,	0.019,	0.051,	0.13,	0.33,
$L=$	1,	2,	3,	4,	5.

Therefore, it is reasonable to assume that the change in angular momentum, associated with a photon of 330 kev is two units.

In addition to the activities described above in Ba^{133}, the period of 28.7 hr. was confirmed in barium. The activation of barium with deuterons in a cyclotron resulted in no observation of the 38.9-hr. period of Ba^{133}. In contrast, the period of 28.7 hr. was clearly defined (see Fig. 5). Due

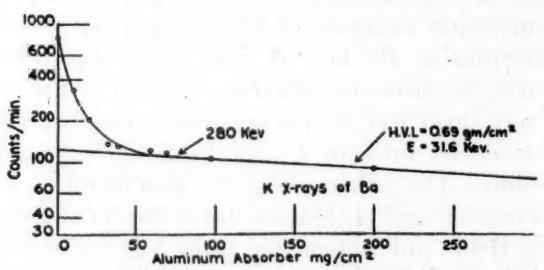

FIG. 6. Aluminum absorption of conversion electrons of 28.7-hr. period Ba^{135}.

to very intense radiation of the short period of Ba^{139}, $T=86$ min., the study of the 28.7-hr. period was limited to the determination of monochromatic electron energy, which proved to be 280 kev, and to the determination of K x-rays of barium (see Fig. 6). Gamma-rays of very weak intensity were also found. Due to the existence of x-ray of barium, of monochromatic electrons, and other experimental observations previously reported,[4] it is postulated that this period is a metastable state of Ba^{135}. However, other assignments of mass number are not entirely eliminated.

3. DISCUSSION OF RESULTS

The ratio of the number of conversion electrons to the number of quanta for 85-kev photon of Ba^{133*} was found to be 0.34, that for 320 kev, 0.02; it can be approximated that the ratio of the number of 320-kev gamma-quanta to 85-kev gamma-quanta is $1.34/1.02=1.31$. These two gamma-rays are assumed to be emitted in cascade. The following experimental evidence has been obtained to this effect. The ratio of the ionization current produced by the 320 kev to that of 85-kev photon was 2.5; this, after correction for efficiency due to the geometry of sample, seems to be in fair agreement with the above. The cloud-chamber data showed that the ratio of the number of conversion electron tracks corresponding to the 85-kev photon to the conversion electron tracks of 320-kev photons is less than twenty.

The spin of the ground state of cesium[7] is given as 7/2; the change in angular momenta of 85-kev photon and 320-kev photon are estimated to be one and two, respectively. Thus, the transition from the excited state of 405 kev above the ground level may be accompanied by a total change in angular momentum from 1/2 to 7/2, or alternately from 13/2 to 7/2. The attempt to observe experimentally a third gamma-ray of 405 kev resulted negatively. This may undermine the possible alternate total change in angular momenta from 9/2 to 7/2, since in this case the emission of photon of 405 kev becomes highly probable.

Calculations were made for the probability of emission of photons of 85 kev, 320 kev, and 405 kev. The results obtained were $T=3.2\times10^{-17}$ sec.; $T=3.8\times10^{-15}$ sec., and $T=6.0\times10^{-12}$ sec., respectively. Therefore, it can be estimated that the intensity of 405-kev photon is about 0.001 of the intensity of 320-kev photon.

The chemical separation of cesium from long-life barium made within a few minutes did not yield any gamma-rays in the cesium fraction; this is accepted as a confirmation of the non-existence of a metastable state in cesium. The critical absorption of x-rays emitted by the long life barium gave consistent results of K x-rays of cesium.

ACKNOWLEDGMENT

The help received from the Alumni Fund of The Ohio State University in securing research equipment is deeply appreciated by the authors. One of the authors is greatly indebted to The Industrial Research Foundation of The Ohio State University for the grant of a fellowship.

We thank the Isotopes Research Division of the U. S. Atomic Energy Commission for neutron activation.

[7] H. Kopfermann, *Kernmoments* (Akademiche Verlagsgesellschaft, Leipzig, 1940).

Experiments on the Separation of Low Energy Mesotrons from Electrons

P. C. BHATTACHARYA*
Institute of Nuclear Physics, Calcutta University, Calcutta, India
(Received January 26, 1948)

For the separation of low energy mesotrons from the electrons a block of lead 1.25 cm thick was placed above a pair of anticounters such that any electron which generates a shower in it is removed by the anticounters. An additional block of lead was also placed below the anticounters to absorb any electron which escaped the system without producing a shower in the upper lead piece. The mesotrons thus separated from the electrons were examined in a Wilson chamber having a 2-cm block of lead across the center. 937 single tracks were observed to traverse the 2-cm lead block and all these tracks were ascribed to mesotrons. There was a case of a shower of three particles found to be generated in the lead piece inside the chamber and this shower was attributed to a knock-on process. It was also found out that the additional lead block whose thickness was to be 4 cm, according to Bhabha, could be reduced to 2 cm at sea level without disturbing the efficiency of the system.

By an experiment with counters it was also found out that 1.25 cm of lead corresponds to the maximum for showers of two or more particles initiated only by electrons in lead.

I. INTRODUCTION

IT is known that the mesotrons occur only in cosmic radiation—in fact, the penetrating component consists practically of mesotrons while the soft component consists of electrons, positrons, and photons. The soft component is absorbable in a few centimeters of lead and produces cascades in traversing dense material like lead. It is only for these properties that the electrons can be eliminated from the mesotrons. In order to get rid of them the usual practice is to put 10 cm of lead between Geiger-Müller counters but the defect of this method is that the filter while absorbing the soft component absorbs also all the mesotrons of range up to 10 cm of lead, i.e., of energy up to 2.4×10^8 ev as can be seen from the range-energy curves of Rossi and Greissen.[1] The number of these low energy mesotrons increases with altitude. Experiments of Malcolm Correll[2] suggest that the slow mesotrons of energy between 8×10^7 ev and 2×10^8 ev at 11,500 ft are produced by a neutral radiation although the more energetic mesotrons are believed to be produced by the protons. Similarly, the other characteristics of slow mesotrons are likely to be quite interesting. But most of these low energy mesotrons are lost in the thick absorber in the process of separation. In order to study their properties it was decided to undertake first of all, experiments to separate the mesotrons from the electrons using as little of lead absorber as possible. Furthermore, in balloon experiments for measuring mesotron intensity at high altitude it will be an advantage if we can use smaller thickness of lead as filter.

Recently Bhabha[3] suggested a method for the removal of electrons by making the most effective use of the cascade process. In this method a block of lead 1.25 cm thick was used to produce showers. It was placed just below the topmost counter of the telescope and over a counter tray containing two sets of counters attached to an anticoincidence circuit such that any shower produced in the lead piece were suppressed by the anticounters. A second piece of lead, 4 cm thick was placed below the anticounters but above the lowest counter of the telescope. The function of the second lead piece was to absorb any low energy electron which escaped the system without producing a shower in the upper lead block. Thus, with this arrangement one is expected to have mesotrons of energy as low as 1.6×10^8 ev, i.e., of range 5.25 cm of lead.

It will be interesting to test experimentally with a Wilson chamber to see how far this suggested arrangement is correct. For this purpose the four-centimeter lead block of Bhabha

* I.C.I. (India) Research Fellow under the auspices of the National Institute of Sciences of India.

[1] Bruno Rossi and Kenneth Greissen, Rev. Mod. Phys. **13**, 240 (1941).

[2] M. Correll, Bull. Am. Phys. Soc. **22**, 27 (1947).

[3] H. J. Bhabha, Proc. Ind. Acad. Sci. **19**, 23 (1944).

was further divided into two pieces of 2 cm each, and one of them was placed across the middle of the Wilson chamber while the other one was placed just above the lowest counter. The lead piece across the chamber served to distinguish between electrons and mesotrons. An electron has a large probability of producing secondaries in traversing the lead block while a mesotron will come out as a single particle.

In regard to the thickness of the upper lead block an experiment with counters was carried out to ascertain the exact thickness of lead corresponding to the shower maximum of more than one particle and more than two particles initiated by electrons in lead. Calculations of the probabilities of showers of more than one particle and more than two particles were also carried out by the author.[4] These calculations were made on the assumption that fluctuations obey Poisson distribution and that the energy spectrum of the electrons incident on the top lead block is of the form $J(K/E)^{\alpha}$ where J and K are suitable constants and $\alpha=2.9$ at sea level. It is shown in that paper that the probability curves show a maximum at absorber thickness of 1 to 2 radiation units and that the maximum depends on the lower limit of the energy spectrum. It is further shown there that we can have a number of theoretical curves for showers of more than one particle and more than two particles corresponding to the different low energy limits of the energy spectrum and that the curves which fit well with the experimental one can give an idea of the low energy limit of the incident electron spectrum.

II. EXPERIMENTAL

A. Counter Experiment for Showers

The Geiger-Müller counters used in these experiments were each 15 cm long and 4 cm in diameter; the outer electrode was of thin copper foil and the central one was of 3–4 mil-tungsten wire. They were sealed in Pyrex glass tubes with a mixture of alcohol vapor and argon. The starting potential of these counters was about 1000 volts with a plateau of about 300 volts. The efficiency of these counters was found to be in the range 98.6 to 99.8 percent. The counters were used in Rossi parallel connection and the resolving time of the circuit was found to be of the order of 10^{-5} sec.

FIG. 1. Arrangement of counters for determining the shower maximum for more than one particle and more than two particles in lead. Each of the counters 1, 2, 4, and 5 are, in fact, two counters joined in parallel.

In order to determine the shower maximum of more than one particle and more than two particles, the counters were arranged as in Fig. 1. Each of the counters 1, 2, 4, and 5 were, in fact, two counters joined in parallel. The circuits were used in such a way that the coincidences C_{12345} or $C_{123(4+5)}$ were recorded simultaneously with coincidences C_{123}. For recording the coincidences $C_{123(4+5)}$ the counters C_4 and C_5 were joined in parallel. Lead blocks of different thicknesses were placed at t and records taken in a cyclic manner so as to avoid any instrumental selectivity. Further, the coincidences C_{123} due to

TABLE I. Data for side showers, etc. for different thicknesses of lead.

Lead in cm	Fourfold coincidences $C_{123(4+5)}$ No. of counts	Time in hours	Rate (counts per hour)	Fivefold coincidences C_{12345} No. of counts	Time in hours	Rate (counts per hour)
0	217	221	0.982±0.0449	91	201	0.4527±0.0318
1	208	204	1.020±0.0473	96	207	0.4637±0.0317
2	212	210	1.009±0.0464	92	200	0.4601±0.0321
4	218	220	0.991±0.0447	89	197½	0.4506±0.0320

[4] Proc. Nat. Inst. Sci., India, *in press*.

TABLE II. Data for showers of two or more particles.

Lead in cm	No. of counts	Time in hours	Fourfold coincidences $C_{123(4+5)}$ Counting rate per hour	Counting rate corrected for showers, etc.
0.0	514	140½	3.659±0.1081	2.677±0.1170
0.5	387	60	6.449±0.2197	5.429±0.2247
1.0	439	61½	7.139±0.2282	6.119±0.2328
1.5	394	63	6.255±0.2111	5.235±0.2160
2.0	355	71	5.000±0.1778	3.991±0.1835
2.5	385	89	4.326±0.1477	3.317±0.1546
3.5	207	74	2.688±0.1252	1.697±0.1323
4.5	176	77	2.286±0.1154	1.295±0.1233

TABLE III. Data for showers of three or more particles.

Lead in cm	No. of counts	Time in hours	Fivefold coincidences C_{12345} Counts per hour	Counting rate corrected for showers, etc.
0.0	255	278	0.917±0.0385	0.465±0.0499
0.5	273	139	1.964±0.0797	1.500±0.0860
1.0	210	90	2.333±0.1079	1.869±0.1123
1.5	233	122	1.910±0.0838	1.446±0.0894
2.0	288	175	1.646±0.0649	1.185±0.0721
2.5	149	102	1.461±0.0802	1.001±0.0860
3.5	192	175	1.097±0.0531	0.647±0.0616
4.5	155	172	0.901±0.0485	0.451±0.0583

single particles were recorded simultaneously either with C_{12345} or with $C_{123(4+5)}$ as a check on the data for showers. The side showers, etc., were determined by shifting the counter 2 to a distance denoted by a dotted line in the figure, other counters being kept at their previous position. These counting rates were subtracted from the experimental rate of showers to get the real shower rate. The shower correction for intermediate thicknesses of lead, *viz.*, 0.5, 1.5 cm, etc., were made from the graphical interpolation. The data for side showers, etc., are given in Table I while the experimental results are given in Tables II and III. These results are plotted in Fig. 2. The top curve shows the shower of two or more particles and the bottom one the shower of three or more particles. The dotted curves show the theoretical results for different low

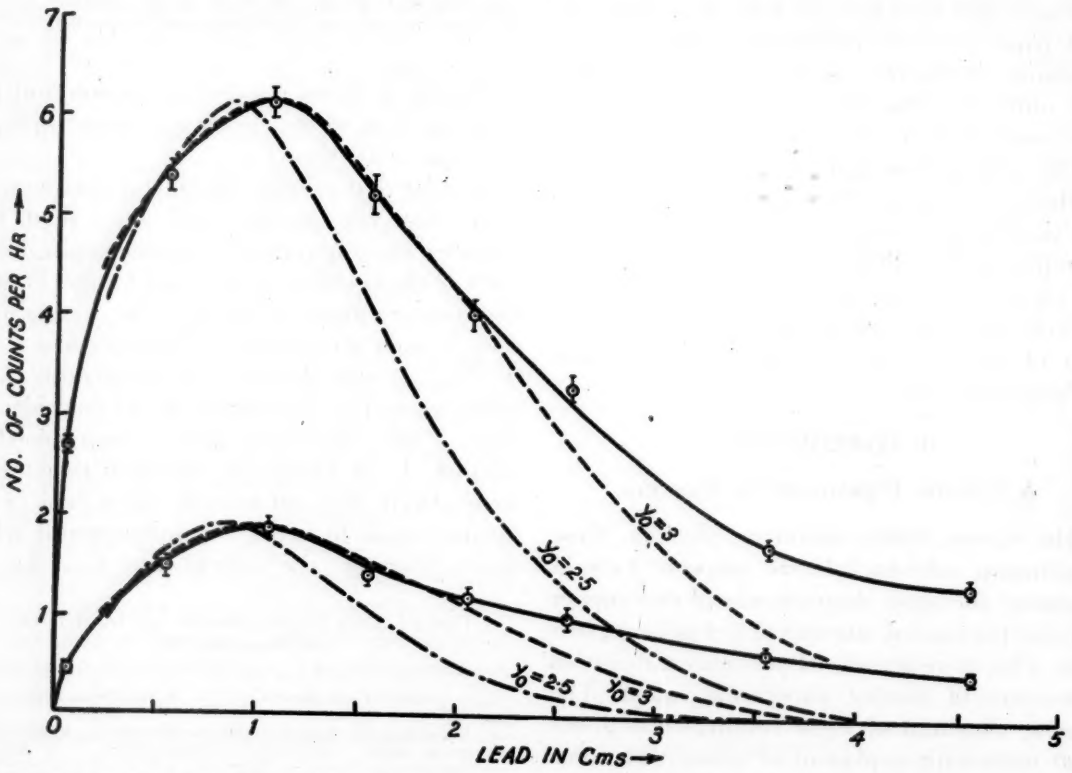

FIG. 2. The top solid curve shows the experimental result for showers of two or more particles in lead and the bottom one for showers of three or more particles. The dotted curves denote the theoretical results for different low energy limits of the incident electron spectrum corresponding to different values of y_0. Since $E=\beta e^{y_0}$ where $\beta=6.9\times10^8$ ev in lead, we find that $y_0=3$ corresponds to electrons of energy 1.4×10^8 ev.

energy limits of the incident electron spectrum corresponding to different values of y_0 which are written on the curves themselves. These theoretical curves were normalized at the maximum, and while comparing these curves with the experimental ones proper care was taken regarding their abscissa. To convert the abscissa of the calculated curves in thicknesses of lead, they are to be multiplied by 0.52 cm.

From the experimental curves for showers of more than one particle and more than two particles it will be seen that about 1.25 cm of lead corresponds to the shower maximum of both the curves. It will be also seen that the calculated curves corresponding to $y_0=3$ for more than one particle and more than two particles practically coincide in the neighborhood of the maximum of both the experimental curves. In the tail of the transition curves the deviation of the theoretical curves from the experimental ones is very pronounced, as it should be. The theoretical curves drop practically to zero between 4 and 5 cm of lead while the experimental ones maintain some high level. As $y_0=3$ corresponds to electrons of energy 1.4×10^8 ev, the lower limit of the energy spectrum of electrons incident on the top of the upper lead block appears to be equal to 1.4×10^8 ev. But electrons of energy lower than this are known to exist at sea level from the experiments of Williams[5] and others. The discrepancy may be due to the fact that the theoretical calculations do not hold well at such low energy. Moreover, the experiment was carried out in the room of a one-story building and, consequently, some of the low energy electrons were cut off. It can be seen also that our experimental arrangement is likely to miss some showers.

B. Experiment with Counter Controlled Wilson Chamber

In order to examine the mesotrons separated from the electrons a lead block 2 cm in thickness was placed across the Wilson chamber and the relative positions of counters and lead blocks with respect to the chamber are shown in Fig. 3. A particle which traverses the 2-cm lead plate as a single particle without appreciable deflection is taken to be a mesotron.

[5] E. J. Williams, Proc. Roy. Soc. 172, 194 (1939).

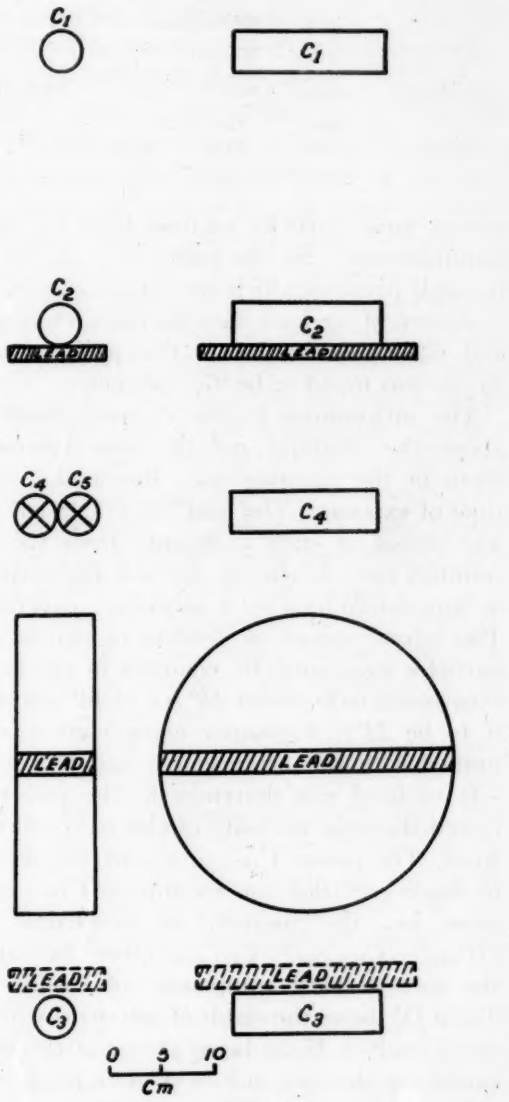

FIG. 3. Side and front view of the arrangement of counters, etc., with respect to the Wilson chamber. C_4 and C_5 are the counters connected to the anticoincidence circuit. The lower lead block shown dotted was removed in some of the observations.

The counters C_4 and C_5 were connected to a circuit such that the coincidence pulse C_{45} was reversed by a valve and fed to the grid of a thyratron through a condenser. The coincidence pulse C_{123} is also fed to the grid of the same thyratron through another condenser. The pulses C_{45} and C_{123} are in opposite phase so that if they arrive at the grid at the same instant there will be no record, i.e., the system will not register any single particle accompanied by a shower of

TABLE IV.

Coincidences	No. of counts	Time in hours	Counts per hour	Soft:hard
C_{123}	160	17	9.4	22 percent
$C_{123-(45)}$	154	20	7.7	

two or more particles exciting both C_4 and C_5 simultaneously. So the pulses $C_{123-(45)}$ are due to single particles which are not accompanied by a shower of at least two particles exciting C_4 and C_5. The efficiency of this anticoincidence circuit was found to be 97.7 percent.

The anticounters C_4 and C_5 were placed just above the chamber and the area covered by them in the chamber was illuminated at the time of exposure. The lead block 1.25 cm thick was placed at such a distance from the anticounters that the shower rate was the maximum as was determined by a subsidiary experiment. The lateral spread of showers of two or more particles was found by counters in the present experiment to be about 24° (cf. Held[6] who found it to be 22°). A counter experiment was performed with this arrangement and the ratio of soft to hard was determined. The pulses C_{123} record the total intensity of electrons and mesotrons. The pulses $C_{123-(45)}$ record the intensity of single particles not accompanied by secondaries, i.e., the intensity of mesotrons. Thus $[(C_{123})-(C_{123-(45)})]/C_{123-(45)}$ gives the ratio of the soft to hard component of cosmic rays. Table IV shows the result of soft:hard with 3.25 cm of lead—1.25 cm being placed at the top for producing showers and 2 cm piece being placed at the middle of the Wilson chamber.

TABLE V

	1.25-cm lead at the top and 2-cm block across the chamber	No. of photos	Time in hours	Information extracted
1	2-cm lead over the counter C_3	523	86	435 single particles traversed the lead plate with one three-particle shower produced in the lead plate.
2	Without lead over the counter C_3	620	100	502 single particles traversed the lead plate without producing any shower in it.

[6] Held, result not published, see Geiger, Ergeb. d. exakt. Naturwiss **14**, 42 (1934).

The Wilson cloud chamber was of the Blackett type. It was 30 cm in diameter and 10 cm in depth. It contained oxygen and air at a pressure of about 96 cm mercury and the liquid mixture was of alcohol and water. Eight 100-watt, 110-volt, straight filament lamps were used for the illumination. The beam was collimated by eight spherical lenses. Normally the filaments were kept dull red, but they were "flashed" by putting instantaneously 220 volts at the moment when a cosmic particle traversed the chamber. The camera was normally kept open in the dark and after each exposure the film was wound by a mechanical device driven by a motor. The camera lenses were Aldis F/3, 5-cm focal length, and the film was the Kodak panchromatic super XX, 35 mm-size.

The working of the Wilson chamber was automatic and the expansion of the chamber was controlled by the pulses $C_{123-(45)}$. After each expansion the chamber remained inactive for about 120 sec., when three slow expansions occurred to clear the chamber from old ions. There was no magnetic field in the chamber. Table V shows the result of two runs. The expansion of the cloud chamber per hour were little less than the counting rate and this is expected as the chamber remained inactive for sometime after each expansion. 937 single tracks were observed to traverse the 2-cm lead piece at the middle of the Wilson chamber but only one shower of three particles was found to be generated in the lead piece. This shower might be due to a knock-on process, i.e., a mesotron while traversing the lead block knocked out an electron imparting sufficient energy to it and that electron might produce the shower by the cascade process.

There were 15 cases in which one secondary was found to accompany the primary in the upper half of the chamber. This might be caused by the inefficiency of the anticounter circuit. This might also happen when both the shower particles pass through any one of the anticounters, *viz.*, C_4 or C_5, when there would not be any coincident pulse C_{45} so that the particle would be recorded as due to the pulse $C_{123-(45)}$. This defect seems to be inherent in the present arrangement of counters.

III. DISCUSSION

Schein, Jesse, and Wollan[7] also used side counters to eliminate the electrons which produced showers in the lead block. The distance of the lead block from the side counters was not mentioned by them. It is found here that the relative position of the lead block and the counters is very important. The upper lead block of 1.25-cm thickness should be placed at such a distance from the anticounters that the showers generated in it have the maximum chance of operating the anticounters. In the present investigation this distance was found to be about 15 cm.

The method of separation of mesotrons by placing 1.25 cm of lead above a pair of anticounters and another lead piece of 4-cm thickness below the anticounters, as was originally suggested by Bhabha, was found to be quite efficient in sorting out the mesotrons. With this arrangement we can study mesotrons of energy as low as 1.6×10^8 ev, i.e., of range 5.25 cm of lead. This arrangement can be used for measuring the mesotron intensity at high altitudes.

Now the question arises as to whether the additional block of lead of 4-cm thickness is absolutely necessary or whether it can be reduced or totally dispensed with in case we want to study mesotrons of range lower than 5 cm of lead.

We have found 15 cases in which a secondary was found to accompany the primary in the upper half of the Wilson chamber. The probable causes for these have already been discussed. The most plausible reason is that all the particles of the shower pass through either of the anticounters C_4 or C_5 and in such cases the anticoincidence circuit does not give any pulse, so that we get a pulse $C_{123-(45)}$ which is ascribed to a mesotron although it is due to a shower particle. It is also shown in my paper (in press) that the chance of missing such showers increases with showers of fewer particles. Such cases will be more frequent if we totally discard the lower lead block. Thus the lower lead block appears to be indispensible for absorbing these showers of fewer particles and also for absorbing the low energy electrons which escape the system without producing a shower in the top lead block.

As regards the thickness of this lead block we have seen that at sea level it can be reduced to 2 cm without affecting the efficiency in the system, i.e., mesotrons.

In conclusion, the author expresses his indebtedness to Professor M. N. Saha for his kind interest and encouragement throughout the progress of the work. Thanks are also due to Dr. N. Das Gupta and Mr. S. K. Ghosh for discussions and criticisms and also for the latter's assistance in taking some of the observations.

[7] M. Schein, W. P. Jesse, and E. O. Wollan, Phys. Rev. 59, 615 (1941).

Radioactive Europium, Gadolinium, and Terbium

N. L. KRISBERG* AND M. L. POOL
The Ohio State University, Columbus, Ohio

AND

CARL T. HIBDON
The University of Colorado, Boulder, Colorado

(Received March 29, 1948)

An activity with a half-life of 18.0±0.2 hours and a weaker one of 5.5±0.2 days have been produced by neutron bombardment of gadolinium, resulting in a saturation intensity ratio of 25. A deuteron bombardment of gadolinium gave a ratio of 3 and produced 72-day Tb^{160} with a saturation intensity equal to that of the 5.5 day. The 18.0-hour activity decays by the emission of negative β-particles of 0.85 Mev and a γ-ray of 0.3 Mev. The 5.5-day activity decays by the emission of negative β-particles of 0.5 Mev and γ-rays of 1.28 Mev. Neither the 18.0-hour nor the 5.5-day substance is produced by fast neutron bombardment of Tb, but there is some evidence that both are produced by fast neutron bombardment of dysprosium. In accordance with the above data both the 18.0-hour and the 5.5-day activities are assigned mass 161. An activity with a minimum half-life of 20 years and one with a minimum half-life of 75 days have been produced by a deuteron bombardment of europium. The decay of the 20-year activity is by the emission of β-particles of 1.4 Mev and a γ-ray. The 75-day activity is probably attributable to Gd^{153} and the 20-year activity to Eu^{151}.

I. INTRODUCTION

USING neutrons from a radon beryllium source, several investigations of neutron induced activities in the rare earth elements have been made.[1–4] Later, using cyclotron techniques, experiments were performed using both neutrons and deuterons as bombarding particles.[5–7] Because of the difficulties of obtaining very pure rare earths, there remains some disagreement as to the radioactive isotopes existing in these elements. In addition, certain known activities of the rare earths have not yet been firmly placed because of the difficulty of obtaining chemical separation of these elements from each other.

It is the purpose of this paper to report a series of experiments in the europium, gadolinium, and terbium region which have extended over the past six years. Some of the characteristic radiations associated with the above-mentioned activities are described. Although the experiments give some evidence as to the isotopic location of the activities, exact placing has not been done.

Unless otherwise stated, Hilger materials were used. For all neutron bombardments the sample material was passed directly from the original shipping container to a gelatin capsule. At the conclusion of the bombardment the sample was removed from the capsule for decay readings and the capsule checked for activity.

II. THE 72-DAY ACTIVITY

An activity which decayed with a half-life of 72 days was produced in the rare earth fraction of a deuteron bombardment of gadolinium. Cloud-chamber observations showed that decay occurred by the emission of negative β-particles. By means of aluminum absorption measurements the energy of the β-particle was determined to be 0.71 Mev. Lead absorption measurements indicated that a γ-ray was associated with this decay. The above data are in agreement with the known[8] characteristic radiations of Tb^{160}. This activity is therefore presumed to have been produced by the reaction $Gd^{160}(d,2n)Tb^{160}$.

III. THE 5.5-DAY ACTIVITY

Figure 1 shows the decay of a 5.5-day activity produced by a neutron bombardment of Gd_2O_3.

* Lt. Col. U.S.A.F. Research under auspices of Air University, Maxwell Field, Alabama.

[1] E. Amaldi, O. D'Agostino, E. Fermi, B. Pontecorvo, F. Rasetti, and E. Segrè, Proc. Roy. Soc. **149A**, 523 (1935).

[2] J. K. March and S. Sugden, Nature **136**, 102 (1935).

[3] G. Hevesy and Hilde Levi, Kgl. Danske Vid. Sels. Math-Fys. Medd. **14**, No. 5 (1936); S. Sugden, Nature **135**, 469 (1935).

[4] J. C. McLennan and W. H. Rann, Nature **136**, 831 (1935).

[5] M. L. Pool and L. L. Quill, Phys. Rev. **53**, 437 (1938).

[6] A. W. Tyler, Phys. Rev. **56**, 125 (1939).

[7] K. Fajans and A. F. Voigt, Phys. Rev. **60**, 533 (1941).

[8] W. Bothe, Naturwiss. **31**, 551 (1943).

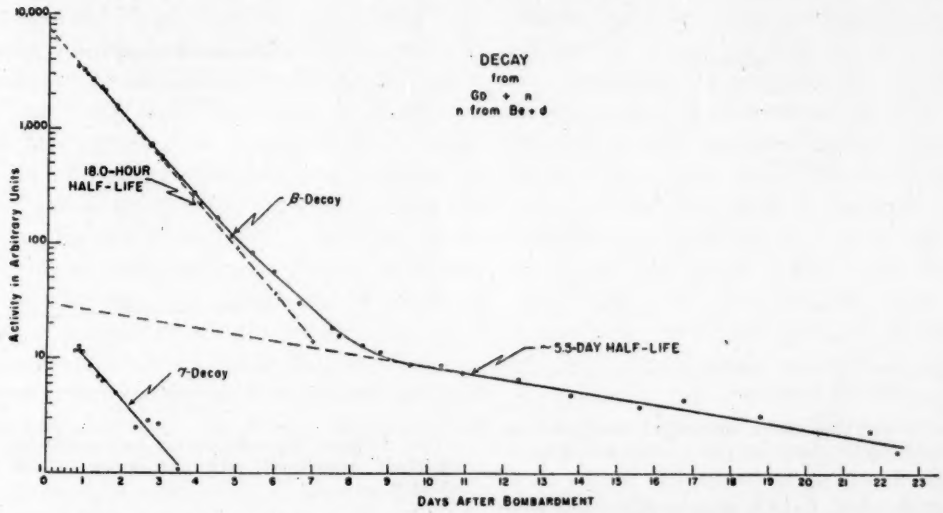

FIG. 1. Decay curve of the β-particle and γ-ray activity induced in Gd_2O_3 by neutrons produced from a deuteron bombardment of beryllium.

The neutron flux was obtained from a deuteron bombardment of beryllium. The beryllium target was made sufficiently thick to completely intercept the deuteron beam, and the Gd_2O_3 was placed directly behind the target. Within experimental error an identical decay curve was obtained using the neutron flux from a deuteron bombardment of lithium.

Figure 2 shows the γ-ray decay of the rare earth activity produced when Gd_2O_3 was bombarded with deuterons. A similar curve was obtained for the β-particle decay. From the lead absorption measurements shown in Fig. 3 the energy of the γ-ray was found to be 1.28 Mev. Cloud-chamber observations showed that decay occurred with the emission of negative β-particles. The energy was determined to be 0.5 Mev by aluminum absorption measurements.

A sample of very pure Tb was exposed for 7.5 hours to an intense neutron flux produced by a deuteron bombardment of lithium. No 5.5-day activity was observed. When Dy was similarly bombarded there was some evidence that this half-life was present in the resulting activity.

IV. THE 18.0-HOUR ACTIVITY

A sample of Gd_2O_3 was placed in the center of a four-foot cube of paraffin with a 500-millicurie radon-beryllium source and allowed to remain for thirty days. No measurable activity was obtained.

When a similar sample enclosed in 5 inches of paraffin was placed near the target section of the cyclotron during a deuteron bombardment of lithium, the induced activity decayed with a half-life of approximately 18 hours.

As shown in Fig. 1 this activity was produced also by a neutron bombardment of Gd_2O_3 when the neutron flux was obtained from a deuteron bombardment of beryllium. A γ-ray of low intensity was found to be associated with this decay. Cloud-chamber observations showed that decay took place by the emission of negative β-particles. By means of aluminum absorption measurements the energy was found to be 0.85 Mev. Within experimental error identical results

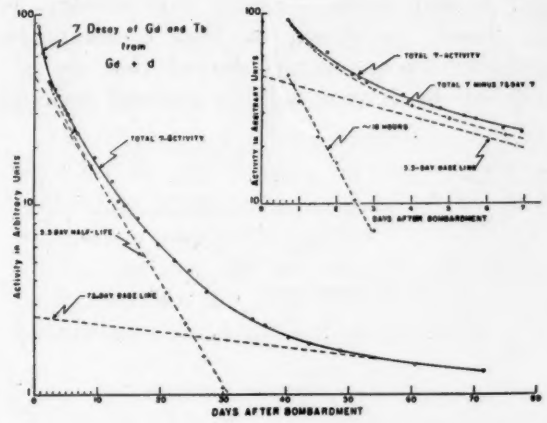

FIG. 2. γ-ray activity induced on the rare earth fraction by a deuteron bombardment of Gd_2O_3.

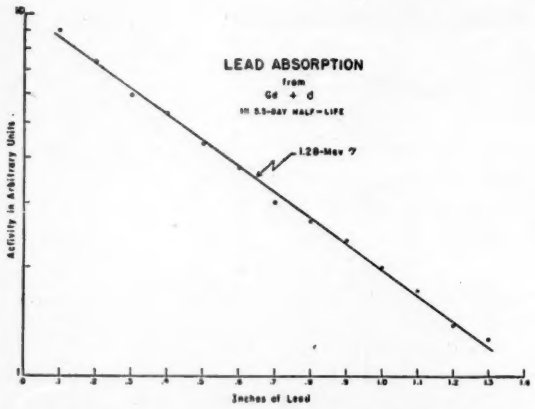

FIG. 3. Lead absorption curve showing 1.28-Mev γ-ray associated with the decay of the 5.5-day activity.

were obtained when Gd_2O_3 was bombarded with neutrons produced by a deuteron bombardment of lithium.

This activity was observed in the rare earth fraction of a deuteron bombardment of Gd_2O_3, as shown in the insert of Fig. 2. From the lead absorption measurements shown in Fig. 4 the energy of the γ-ray was found to be 0.3 Mev. No evidence of internal conversion of this γ-ray was found. The energy of the negative β-particle emitted was found to be 0.85 Mev, as shown in Fig. 5.

V. THE 75-DAY AND THE 20-YEAR ACTIVITY

Figure 6 shows the decay of the rare earth fraction of a deuteron bombardment of europium. The 20-year half-life is estimated as the minimum half-life of this activity from the decay observed. The very strong 9.2-hour activity of Eu^{152} present during the early part of decay is not shown. As shown by Fig. 7, aluminum absorption measurements showed that the activity of the 20-year half-life material decayed

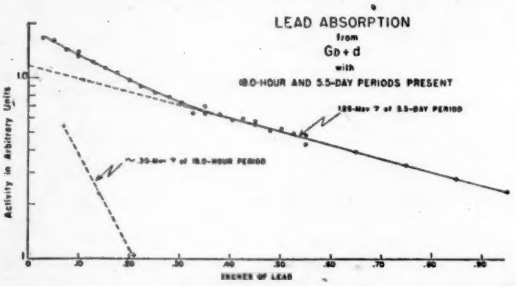

FIG. 4. Lead absorption curve showing 0.3-Mev γ-ray associated with the decay of the 18.0-hour activity.

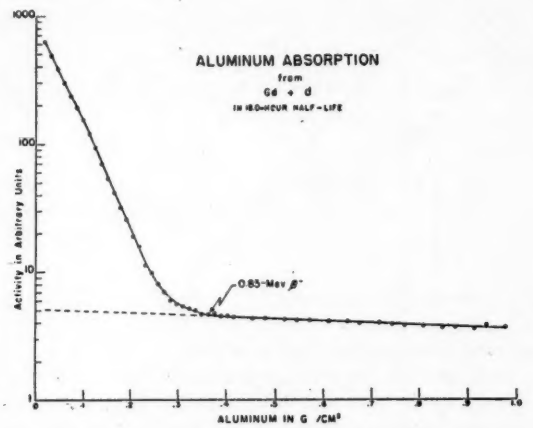

FIG. 5. Aluminum absorption curve showing 0.85-Mev β-particle associated with the decay of the 18.0-hour activity.

with the emission of β-particles of 1.4 Mev. By means of lead absorption measurements a γ-ray of approximately 0.9 Mev was found to be associated with this decay. When this activity was subtracted from the total activity curve shown in Fig. 6 an additional activity with a minimum half-life of 75 days was observed.

VI. DISCUSSION

Early investigators found that the use of a radon-beryllium source with as much as 500 millicuries of radon induced very weak activities

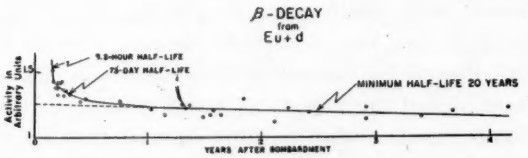

FIG. 6. β-particle decay curve of the rare earth activity induced by a deuteron bombardment of europium. The 75-day half-life was observed when the activity of the 20-year half-life was subtracted from the total β-particle activity shown in this Fig.

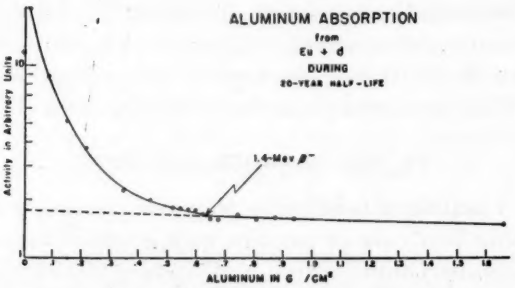

FIG. 7. Aluminum absorption curve showing 1.4-Mev β-particle associated with the decay of the 20-year activity.

in gadolinium. First experimenters using this technique found a weak gadolinium activity which decayed with a half-life of 8 hours.[1] Later, others used the same technique but did not confirm the presence of this half-life in gadolinium. In one case gadolinium was found to be inactive[2] and in another the induced activity was found to be 6.4 ± 0.3 hours.[4] In this latter experiment a 500-millicurie radon-beryllium source of neutrons was used with 14 grams of gadolinium oxalate to obtain an activity of 16 counts/minute with a Geiger counter. The use of cyclotron techniques to obtain greater induced activity in gadolinium also failed to confirm the 8-hour activity.[5] Half-lives of 3.5 minutes and 17 hours were obtained using both slow and fast neutrons. For the experiments described in this paper activities were obtained ranging from the equivalent of 60 counts/sec. to 18,000 counts/sec. on a Geiger counter.

In view of the manner in which neutron bombardments were carried out it is unlikely that contamination could have been added to the original material during preparation for bombardment. The specific purity of the gadolinium used to obtain the activity curves shown is given by Hilger laboratory report No. 11,817. The possibility that any of the periods observed might be due to impurities was further checked by performing each experiment at least twice with sample materials obtained on different shipments. This possibility is eliminated by four factors: the bombarding particle by which the activities were produced, the half-lives observed, the characteristic radiations of the observed activities, and a repetition of saturation intensity ratios over two or three bombardments performed in the same manner.

Since both the 18.0-hour and the 5.5-day activities are produced by slow neutron bombardment of gadolinium, assignment of either to Gd^{153}, Gd^{159}, or Gd^{161} is possible. Assignment of either activity to Gd^{153} is eliminated by the fact that both periods decay with the emission of a negative β-particle. Assignment of either activity to Gd^{159} is unlikely since neither could be produced by a fast neutron bombardment of Tb. Both the 18.0-hour and the 5.5-day activities are therefore assigned mass 161. This assignment is apparently substantiated by the appearance of both activities when dysprosium is bombarded with lithium neutrons. The saturation intensity ratio of the 18.0-hour half-life to the 5.5-day half-life produced by such a neutron bombardment of Gd_2O_3 was found to be 25. The large ratio eliminates the possibility that the 5.5-day activity is a daughter product of the 18.0-hour activity. Assignment of both to Gd^{161} is not supported by the fact that a deuteron bombardment of gadolinium produced the 5.5-day and the 72-day activities with equal intensities. Since the 72-day half-life is known to be produced by a $Gd^{160}(d,2n)Tb^{160}$ reaction, it appears most likely that the 5.5-day activity is produced by a $Gd^{160}(d,n)Tb^{161}$ reaction. Both the 18.0-hour and the 5.5-day activities are therefore tentatively assigned to Tb^{161}.

Fajans and Voigt found Eu^{154} decayed with a half-life of 4–8 years by the emission of a β-particle of 1.0 ± 0.1 Mev. This figure for the half-life of this activity was determined by observations made over a period of 8 months.[7] The half-life determined from Fig. 6 over the first 8 months is approximately 4 years. The fact that two activities are present in this decay is not evident until observations have been made for a number of years. Since the 75-day activity is present with comparatively small intensity, absorption measurements taken while the total activity was decaying with a half-life of 4–8 years would probably show a single "end point." The 20-year activity is therefore assigned Eu^{154}, which decays by the emission of a negative β-particle of 1.4 Mev and a γ-ray of approximately 0.9 Mev to Gd^{154}.

The 75-day activity could be assigned either to Gd^{151} or Gd^{153}. Since 75 days is a longer half-life than would be expected for Gd^{151}, it is tentatively assigned to Gd^{153}.

The authors are grateful for the support received from the Ohio State University Development Fund and the Graduate School.

Calculation of a Perturbing Central Field of Force from the Elastic Scattering Phase Shift

EGIL A. HYLLERAAS
University of Oslo, Oslo, Norway

(Received March 9, 1948)

It has been shown that the interaction potential between two particles can be uniquely determined from the supposed knowledge of the observed phase shifts for the whole energy range, but for only one particular angular momentum. Coulomb forces between charged particles, as well as all kinds of inelastic scattering, have so far not been considered.

IT is well known that the fraction of particles scattered by an angle ϑ through a unit solid angle by a central field of force is given by the expression

$$|(1/k)\sum_l(2l+1)P_l(\cos\vartheta)e^{i\eta_l}\sin\eta_l|^2, \quad (1)$$

where η_l is the so-called phase shift defined by the asymptotic behavior of the radial wave functions

$$\begin{aligned} &c_1r^{l+1}\leftarrow v_1\rightarrow\sin(kr-l(\pi/2)+\eta_l),\\ &c_2r^{-l}\leftarrow v_2\rightarrow\cos(kr-l(\pi/2)+\eta_l),\\ &0\leftarrow r\rightarrow\infty, \end{aligned} \quad (2)$$

v_1 and v_2 being themselves solutions of the radial wave equation for angular momentum l,

$$\begin{aligned} &\{L+V(r)\}v=0,\\ &L=(d^2/dr^2)-[l(l+1)/r^2]+k^2, \quad (3)\\ &k=(2\pi/h)p=2\pi/\lambda. \end{aligned}$$

As we see the phase shift η_l is uniquely determined by the interaction potential $V(r)$. Suppose, on the other hand, that the phase shift for a given l is known from scattering measurements for the whole (or at least the major) part of the energy range from zero to infinity, the question arises whether, conversely, the interaction potential is uniquely determined by the phase shift. The true answer to this question, of course, must be of some importance to the judgment of the expected usefulness or necessity of introducing the so-called S-matrix method in quantum mechanics.

On the suggestion of W. Pauli the problem has been successfully, but rather incompletely, dealt with by C. E. Fröberg[1] in the form of solution of a certain integral equation. Because of the lack of any convergence proof, or even a clear formulation of the method itself in higher approximations, his treatment of the problem can scarcely be considered more than a first approximation, corresponding to the Born approximation in scattering theory.

In this paper we shall try to give a detailed method for calculation of the interaction potential. The starting point is the phase shift as a function of the energy expressed by a definite integral over the potential function. Since the leading idea has been to consider this phase shift as analogous to the Fourier transform of a coordinate function in the ordinary theory of Fourier integrals, we shall start with some preliminary considerations which, I hope, will make the understanding easier.

Consider the Fourier transformations:

$$\begin{aligned} F(r)&=(4/\pi)\int_0^\infty G(k)\sin 2krdk,\\ G(k)&=\int_0^\infty F(r)\sin 2krdr. \end{aligned} \quad (4)$$

We can find the condition for the validity of these transformations in the whole region $0\leq r\leq\infty$, $0\leq k\leq\infty$, of the variables by introducing one of the transformations into the other. We shall then find that some improper product integrals have to be δ-functions. For instance, the integral

$$\begin{aligned} &\lim_{K\to\infty}(4/\pi)\int_0^K\sin 2kr\sin 2kr'dk\\ &=\lim_{K\to\infty}\left\{\frac{\sin 2K(r-r')}{\pi(r-r')}-\frac{\sin 2K(r+r')}{\pi(r+r')}\right\}\\ &=\delta(r-r')-\delta(r+r') \end{aligned} \quad (5)$$

[1] Carl-Erik Fröberg, Phys. Rev. **72**, 519 (1947).

is a difference of two δ-functions, the second of them being insignificant in the case of positive values of r. For $r=0$, however, the two terms are equal, leading to a zero value of the function $F(r)$ represented by the Fourier integral. This of course also follows directly from Eqs. (4).

Now introducing

$$f(r)=-F'(r), \quad F(r)=\int_r^\infty f(r)dr, \tag{6}$$

$f(r)$ being an integrable function in the region $r\to\infty$, we get

$$f(r)=-(4/\pi)\int_0^\infty G(k)(d/dr)\sin 2krdk,$$

$$kG(k)=\int_0^\infty f(r)\sin^2 krdr. \tag{7}$$

These transformations, of course, are equivalent to ordinary Fourier cosine integrals in the case of

$$F(0)=\int_0^\infty f(r)dr=0.$$

In the case of $F(0)\neq 0$, the transformations may give rise to some improper integrals. Therefore, when applying analogous formulae from the theory that is to follow one should examine separately the convergence of the integrals.

By introducing the expressions

$$u_1=v_1=\sin kr, \quad u_2=v_2=\cos kr,$$
$$Y_k(r)=u_1v_1, \quad Z_k(r)=u_1v_2+u_2v_1, \tag{8}$$

the transformations (7) obviously can be written

$$f(r)=-(4/\pi)\int_0^\infty G(k)Z_k'(r)dk,$$

$$kG(k)=\int_0^\infty f(r)\,Y_k(r)dr, \tag{9}$$

and this is the form we shall meet in the following transformations of a potential function to its scattering phase shift and *vice versa*.

We now make use of the solutions

$$C_1r^{l+1}\leftarrow u_1\to\sin(kr-l(\pi/2)+\xi(k)),$$
$$C_2r^{-l}\leftarrow u_2\to\cos(kr-l(\pi/2)+\xi(k)), \tag{10}$$
$$0\leftarrow r\to\infty,$$

of an auxiliary equation,

$$\{L+U\}u=0, \tag{11}$$

with some approximate potential function $U(r)$. With a good starting function the calculations would be easier. Usually, however, we shall have to start with the function $U=0$.

From Eqs. (3) and (11) we now easily obtain

$$k\sin(\eta-\xi)=\int_0^\infty (V-U)\,Y_k(r)dr, \quad Y_k=u_1v_1, \tag{12}$$

an equation which is well known and frequently quoted in the case of $U=0$ and $\xi=0$. Comparison with (9) suggests the existence of an inverted equation

$$V-U=-(4/\pi)\int_0^\infty \sin(\eta-\xi)Z_k'(r)dk,$$
$$Z_k(r)=u_1v_2+u_2v_1. \tag{13}$$

The condition for the validity of Eqs. (12) and (13) may be written

$$-(4/\pi)\int_0^\infty (1/k)\,Y_k(r)Z_{k'}'(r)dr=\delta(k-k') \tag{14}$$

or

$$-(4/\pi)\int_0^\infty (1/k)\,Y_k(r')Z_k'(r)dk=\delta(r-r'). \tag{15}$$

The equations are obviously equivalent, but so far it has not been possible to prove directly the validity of (15). Hence, we should have to prove Eq. (14), but we shall rather prove the equation

$$(4/\pi)\int_0^\infty (1/k)\,Y_k'(r)Z_{k'}'(r)dr=\delta(k-k'), \tag{16}$$

which differs from (14) only by the term

$$\lim_{R\to\infty}\left\{-\frac{4}{\pi}\frac{1}{k}Y_k(R)\sin(2k'R-l\pi+\eta(k')+\xi(k'))\right\}.$$

This term makes no difference because an integration with respect to dk' gives zero.

PROOF OF THE COMPLETENESS RELATION

The proof of Eq. (16) is based exclusively upon the differential equations (3) and (11), defining the functions u and v together with the asymp-

totic values of the functions when $r\to\infty$. In this way we avoid all kinds of complicated transformation theorems analogous to those already established, as for instance in the theory of Bessel functions.

To clarify the idea, consider once more the simplest case of $U=V=0$, $l=0$,

$$\begin{aligned} &Y_k'''+4k^2Y_k'=0, \quad (1/k)\,Y_k'\to\sin 2kr,\\ &Z_k''+4k^2Z_k=0, \qquad Z_k\to\sin 2kr,\\ &\qquad\qquad r\to\infty. \end{aligned} \tag{17}$$

If we replace k by k' in the last equation, multiply by $Z_{k'}$ and Y_k, respectively, subtract, and integrate, we obtain

$$\begin{aligned} \frac{4}{\pi}\int_0^R \frac{1}{k}Y_k'Z_{k'}dr &= \frac{Y_k'(R)Z_{k'}'(R)-Y_k''(R)Z_{k'}(R)}{\pi k(k^2-k'^2)}\\ &= \frac{\sin 2R(k-k')}{\pi(k-k')}-\frac{\sin 2R(k+k')}{\pi(k+k')}\\ &= \delta(k-k')-\delta(k+k'), \text{ when } R\to\infty. \end{aligned} \tag{18}$$

In the general case of arbitrary U, V, and l the functions Y_k and Z_k are obeying third-order equations only when $U=V$. When $U\neq V$ and, hence, u_1, u_2 is different from v_1, v_2, it can be shown that

$$\begin{aligned} &MY_k'+[4l(l+1)/r^3]Y_k+(U'+V')Y_k\\ &\qquad -(V-U)(u_1v_1'-u_1'v_1)=0,\\ &MZ_k+(u_1v_2''+u_1''v_2-2u_1'v_2'+u_2v_1''\\ &\qquad +u_2''v_1-2u_2'v_1')=0,\\ &M=(d^2/dr^2)-[4l(l+1)/r^2]+2(U+V)+4k^2. \end{aligned} \tag{19}$$

We shall also have use for the equations

$$\begin{aligned} &(V-U)\,Y_k+(d/dr)(u_1v_1'-u_1'v_1)=0,\\ &(V-U)Z_k+(d/dr)(u_1v_2'-u_1'v_2\\ &\qquad +u_2v_1'-u_2'v_1)=0, \end{aligned} \tag{20}$$

$$\begin{aligned} &Y_k\left[\frac{d}{dr}(MZ_k)-\frac{4l(l+1)}{r^3}Z_k-(U'+V')Z_k\right]\\ &\quad=[u_1v_2'-u_1'v_2+u_2v_1'-u_2'v_1](V-U)\,Y_k. \end{aligned}$$

We now change k into k' in Z_k and corresponding product functions with different subscripts, like u_1v_2. If we combine Eqs. (19) in the same way as Eqs. (17), we obtain, after some rearrangements,

$$\begin{aligned} &4(k^2-k'^2)\,Y_k'Z_{k'}+(d/dr)[Y_k''Z_{k'}-Y_k'Z_{k'}']\\ &\quad-(d/dr)[Y_k(u_1v_2''+u_1''v_2-2u_1'v_2'\\ &\qquad+u_2v_1''+u_2''v_1-2u_2'v_1')]\\ &\quad+(d/dr)[(u_1v_1'-u_1'v_1)(u_1v_2'-u_1'v_2\\ &\qquad+u_2v_1'-u_2'v_1)]. \end{aligned} \tag{21}$$

Upon integration from $r=0$ to $r=R$, and as $R\to\infty$, the two last terms disappear and we are left with an equation rather similar to Eq. (18). In fact, we get

$$\begin{aligned} &\frac{4}{\pi}\int_0^\infty \frac{1}{k}Y_k'Z_{k'}dr\\ &\quad=\lim_{R\to\infty}\left\{\frac{\sin(2R(k-k')+\eta_k+\xi_k-\eta_{k'}-\xi_{k'})}{\pi(k-k')}\right.\\ &\qquad\left.-\frac{\sin(2R(k+k')+\eta_k+\xi_k+\eta_{k'}+\xi_{k'})}{\pi(k+k')}\right\}\\ &\quad=\delta(k-k')-\delta(k+k'). \end{aligned} \tag{22}$$

Hence, the completeness of the product functional system and the validity of Eq. (13) have been proved.

METHOD OF SOLUTION

Starting from Eqs. (11) and (13), we introduce a known potential $U=V_0$, which may be equal to zero, and solve Eq. (11), obtaining thereby the approximate wave functions u_1 and u_2 with the approximate phase shift ξ. Now we replace the unknown functions v_1 and v_2 in Eq. (13) by u_1 and u_2, thus finding an approximate value of the potential difference $V-U$. By calling this V_1-U we have a first approximation V_1 of the unknown potential V.

In the next approximation we put $U=V_1$, and by solving anew Eq. (11), we obtain better approximate functions u_1, u_2 and a better approximate phase shift ξ. Writing again $v_1=u_1$ and $v_2=u_2$ in Eq. (13) we obtain an approximate value V_2-V_1 of the potential difference $V-V_1$ and so on.

This, of course, is an iteration method and we should have to prove its convergence or at least apply it to some elementary problem in order to illustrate how it works. Unfortunately, there is no simple potential law to which it could be

applied without entering into calculations containing non-elementary functions and integrals. However, there is an improper potential law to which the method—with some precautions—might be applied without leading to non-elementary calculations. This is the inverse-square distance law for the potential which, for convenience, we write in the form

$$V=-(2l+1+\epsilon)\epsilon/r^2 \tag{23}$$

so that the solutions of the wave equation (3)—apart from a factor $(\pi kr/2)^{\frac{1}{2}}$—are Bessel functions of kr with index numbers $\pm(l+\frac{1}{2}+\epsilon)$. The true phase shift now is $\eta=-(\pi/2)\epsilon$. Similarly, we may use an auxiliary potential

$$U=-(2l+1+\delta)\delta/r^2$$

corresponding to the approximate phase shift $\xi=-(\pi/2)\delta$.

The integral (13), of course, is then an improper, non-convergent integral. It can be made convergent, however, by the introduction of a convergence factor in the integrand. This amounts to the same as averaging over a great number of different values of the upper limit, $k=K$, of the integral when all these values tend to infinity. In this way we only eliminate oscillating terms with respect to the upper limit of the integral. With respect to the lower limit, $k\to 0$, the integral is convergent only if $|\epsilon-\delta|<2$, that is when the phase shift difference is smaller than π.

Putting now in the $(n+1)$th approximation $r^2U=r^2V_n=-(2l+1+\epsilon_n)\epsilon_n$, we find from (13) by making $\epsilon\to\epsilon_n$, that

$$\begin{aligned} r^2(V_n-V_{n+1}) &= (2l+1+2\epsilon_n)(2/\pi)\sin(\pi/2)(\epsilon-\epsilon_n) \\ &\approx (2l+1+2\epsilon_n)(\epsilon-\epsilon_n). \end{aligned} \tag{24}$$

On the other hand,

$$r^2(V_n-V)+(2l+1+\epsilon+\epsilon_n)(\epsilon-\epsilon_n). \tag{25}$$

Hence,

$$\begin{aligned} r^2(V_{n+1}-V) &= (2l+1+\epsilon+\epsilon_{n+1})(\epsilon-\epsilon_{n+1}) \\ &\approx (\epsilon-\epsilon_n)^2. \end{aligned} \tag{26}$$

By starting now from $U=V_0=0$, $\epsilon_0=0$, we obtain from (26)

$$\begin{aligned} &r^2(V_1-V)\approx\epsilon^2, && \epsilon-\epsilon_1\approx\epsilon^2/(2l+1), \\ &r^2(V_2-V)\approx\epsilon^4/(2l+1)^2, && \epsilon-\epsilon_2\approx\epsilon^4/(2l+1)^3, \\ &r^2(V_3-V)\approx\epsilon^8/(2l+1)^6, && \epsilon-\epsilon_3\approx\epsilon^8/(2l+1)^7, \\ &r^2(V_4-V)\approx\epsilon^{16}/(2l+1)^{14}, && \text{etc.} \end{aligned} \tag{27}$$

These results show clearly that the convergence is extremely good in all cases where the phase difference at the starting point is not too close to the very limit of convergence.

Now in the case of an ordinary integrable potential we may argue that if it is numerically smaller than a given inverse-square potential of the form (23) the convergence will be even better than in the case considered above in (27).

Hence if an approximate starting potential U can be found giving a phase shift difference $\eta-\xi$ numerically smaller than some given number in the entire energy region, we may be safe that the method outlined above is convergent. Thus it has been proved that a perturbing central field of force can be uniquely determined from the observed scattering phase shift.

Radiation from Electrons Accelerated in a Synchrotron

F. R. ELDER, R. V. LANGMUIR, AND H. C. POLLOCK
General Electric Company, Schenectady, New York

(Received March 15, 1948)

High energy electrons subjected to large radial accelerations radiate considerable energy in the optical spectrum. The distribution of energy in the light from a synchrotron beam has been measured and compared with theory at several electron energies up to 80 Mev. The results indicate reasonable agreement with theory. Measurement of total light output allowed an estimate of electron current in the beam. High speed photography of the light permitted observation of the size and motion of the beam within the accelerator tube.

1. INTRODUCTION

DURING the early operation of a 70-Mev synchrotron[1] in this laboratory, intense visible radiation from the high energy electrons was observed[2] through the glass wall of the accelerating tube. Almost fifty years ago Lienard[3] pointed out that electrons rotating in a circle should radiate energy and he gave a formula for the rate of radiation from the centripetal acceleration of an electron. The classical theory was developed considerably by G. A. Schott[4] in connection with early models of the atom. More recently it has been shown that radiative energy losses have an important effect on the operation of high energy electron accelerators,[5] and the theory has been further discussed by several authors.[6]

In betatrons and synchrotrons, in which the radiation almost entirely results from continuous centripetal accelerations of the order of 10^{19} cm/sec./sec., the energy loss per electron is proportional to the fourth power of the electron energy in the relativistic region. The radiation is emitted in a narrow cone around the instantaneous direction of electron motion. Experiments with Polaroid confirm that the light is polarized with the electric vector in the plane of the electron orbit. In our machine the beam is first visible at about 30 Mev as a dull red spot. At 80 Mev, the present peak energy, the light is very brilliant and a bluish-white color. The spectral distribution of the radiation has been determined during the acceleration of electrons to several different levels of peak energy and in this paper is compared with the theory.

2. THEORY

The energy radiated by an electron is distributed over many harmonics of the fundamental rotation frequency of the electron in its orbit (in our machine 163.5 megacycles). Except for the microwave region, the radiation is incoherent and the total radiation from the beam is just the power radiated by one electron times the number of electrons undergoing acceleration.

Professor J. S. Schwinger of Harvard has calculated the distribution of the energy radiated, and has kindly sent us his results (expressions (1) through (4)).

For an electron of constant energy

$$P(\omega)d\omega=(3\sqrt{3}/4\pi)\omega_0(e^2/R)(E/mc^2)^4 \times\left[\int_{\omega/\omega_c}^{\infty}K_{5/3}(x)dx\right](\omega/\omega_c)d\omega, \quad (1)$$

where $P(\omega)d\omega$ is the power radiated by one electron at the circular frequency ω in the range $d\omega$. R is the radius of the orbit in cm; ω_0 the angular velocity of the electron, V/R; e the electron charge in e.s.u.; E the total electron energy; and $K_{5/3}$ a cylinder function as defined in Watson's treatise on Bessel Functions. $\omega_c=\frac{3}{2}\omega_0(E/mc^2)^3$. ω_c is a critical frequency which roughly measures the upper limit of the spectrum. The expression for the total power ra-

[1] F. R. Elder, A. M. Gurewitsch, R. V. Langmuir, and H. C. Pollock, J. App. Phys. **18**, 810 (1947).
[2] F. R. Elder, A. M. Gurewitsch, R. V. Langmuir, and H. C. Pollock, Phys. Rev. **71**, 829 (1947).
[3] A. Lienard, L'Eclairage elec. **16**, 5 (1898).
[4] G. A. Schott, Ann. d. Physik **24**, 641 (1907); Phil. Mag. **13**, 189 (1907); G. A. Schott, *Electromagnetic Radiation* (Cambridge University Press, Teddington, England, 1912).
[5] D. Iwanenko and I. Pomeranchuk, Phys. Rev. **65**, 343 (1944); J. P. Blewett, Phys. Rev. **69**, 87 (1946).
[6] L. I. Schiff, Rev. Sci. Inst. **17**, 6 (1946); J. S. Schwinger, Phys. Rev. **70**, 798 (1946); L. Arzimovich and I. Pomeranchuk, J. Phys. USSR **9**, 267 (1945).

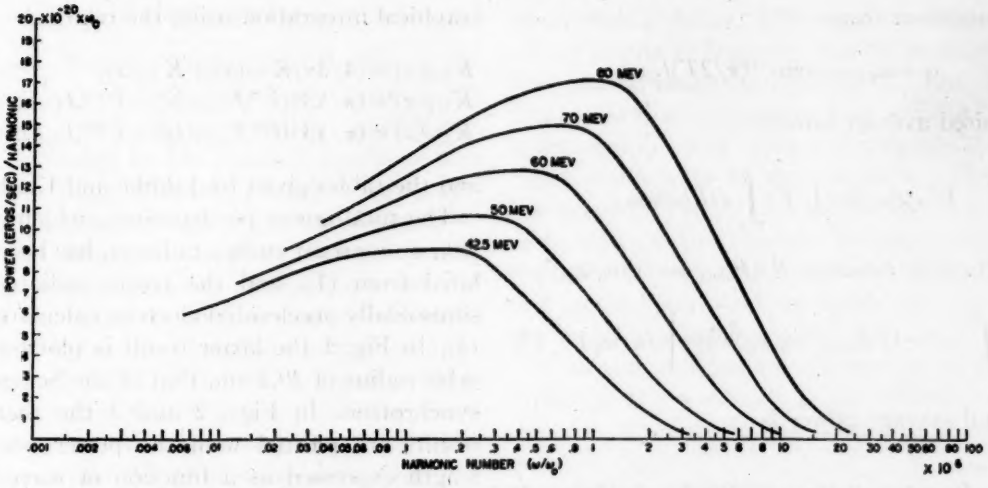

FIG. 1. Radiation loss per harmonic of an electron sinusoidally accelerated during $\frac{1}{4}$-cycle *vs.* harmonic nomber.

diated is:

$$P=\int_0^\infty P(\omega)d\omega=\tfrac{2}{3}\omega_0(e^2/R)(E/mc^2)^4. \qquad (2)$$

This is essentially the expression first derived by Lienard. Most of the energy is emitted in the region of the critical frequency and is contained in a cone of $\frac{1}{2}$-angle approximately equal to mc^2/E about the direction of electron motion.

The actual energy distribution observed with the synchrotron, however, is that of an electron of energy E, which varies sinusoidally, i.e., the average of (1) over an acceleration interval. If the magnetic field increases sinusoidally to its maximum value in the time T, $E=E_{\max}\sin(\pi/2T)t$ and

$$\omega_c=\tfrac{3}{2}\omega_0(E_{\max}/mc^2)^3\sin^3(\pi/2T)t=\omega_m\sin^3(\pi/2T)t.$$

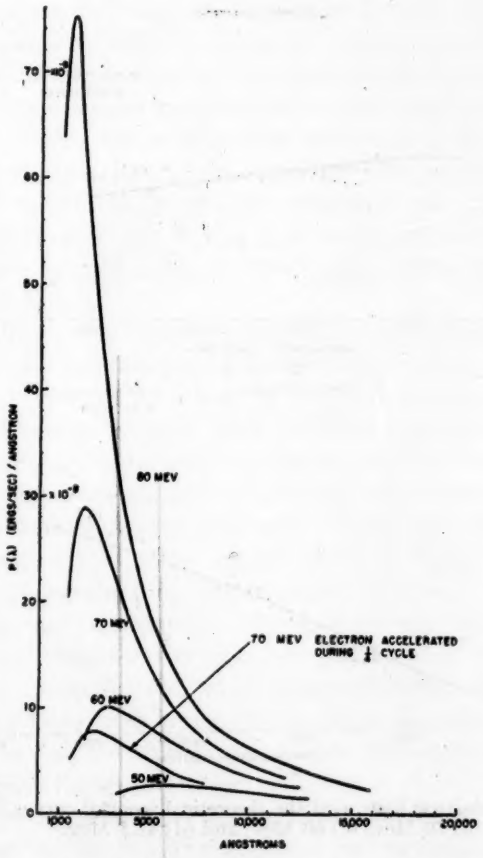

FIG. 2. Radiation loss per angstrom of a constant energy electron *vs.* wave-length.

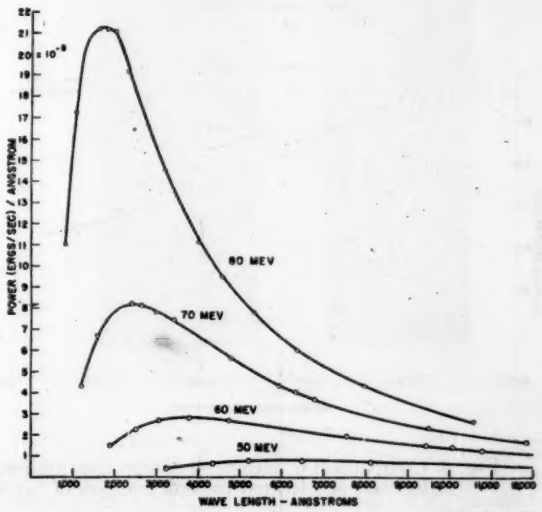

FIG. 3. Radiation loss per angstrom of an electron sinusoidally accelerated during $\frac{1}{4}$-cycle *vs.* wave-length.

It is convenient to use

$$\tau=\omega_m/\omega_c=\sin^{-3}(\pi/2T)t.$$

The desired average power,

$$\bar{P}(\omega)d\omega, \text{ is } (1/T)\int_0^t dt P(\omega)d\omega$$

$$\bar{P}(\omega)d\omega=(3\sqrt{3}/2\pi^2)\omega_0(e^2/R)(E_{\max}/mc^2)^4(\omega/\omega_m)^2$$

$$\times\left[\int_1^\infty(\tau^{\frac{2}{3}}-1)^{\frac{1}{2}}K_{5/3}[(\omega/\omega_m)\tau]d\tau\right](d\omega/\omega_m). \quad (3)$$

The total average power is

$$\bar{P}=\int_0^\infty\bar{P}(\omega)d\omega=(1/4)\omega_0(e^2/R)(E_{\max}/mc^2)^4. \quad (4)$$

The integral in Eq. (3) has been evaluated by graphical integration using the relations

$$\begin{aligned}K_{5/3}(x)&=(4/3x)K_{2/3}(x)+K_{1/3}(x),\\ K_{1/3}(x)&=(\pi/\sqrt{3})(i^{1/3}J_{-1/3}(ix)-i^{-1/3}J_{1/3}(ix)),\\ K_{2/3}(x)&=(\pi/\sqrt{3})(i^{2/3}J_{-2/3}(ix)-i^{-2/3}J_{2/3}(ix)),\end{aligned} \quad (5)$$

and the tables given by Jahnke and Emde.[7]

The total power per harmonic, which an electron at constant energy radiates, has been calculated from (1), and the power radiated by a sinusoidally accelerated electron calculated from (3). In Fig. 1 the latter result is plotted for an orbit radius of 29.2 cm, that of the Schenectady synchrotron. In Figs. 2 and 3 the theoretical results are plotted with the power per wave-length expressed as a function of wave-length. It is evident from these curves that the distribution of light energy is very different from that of the more conventional light sources.

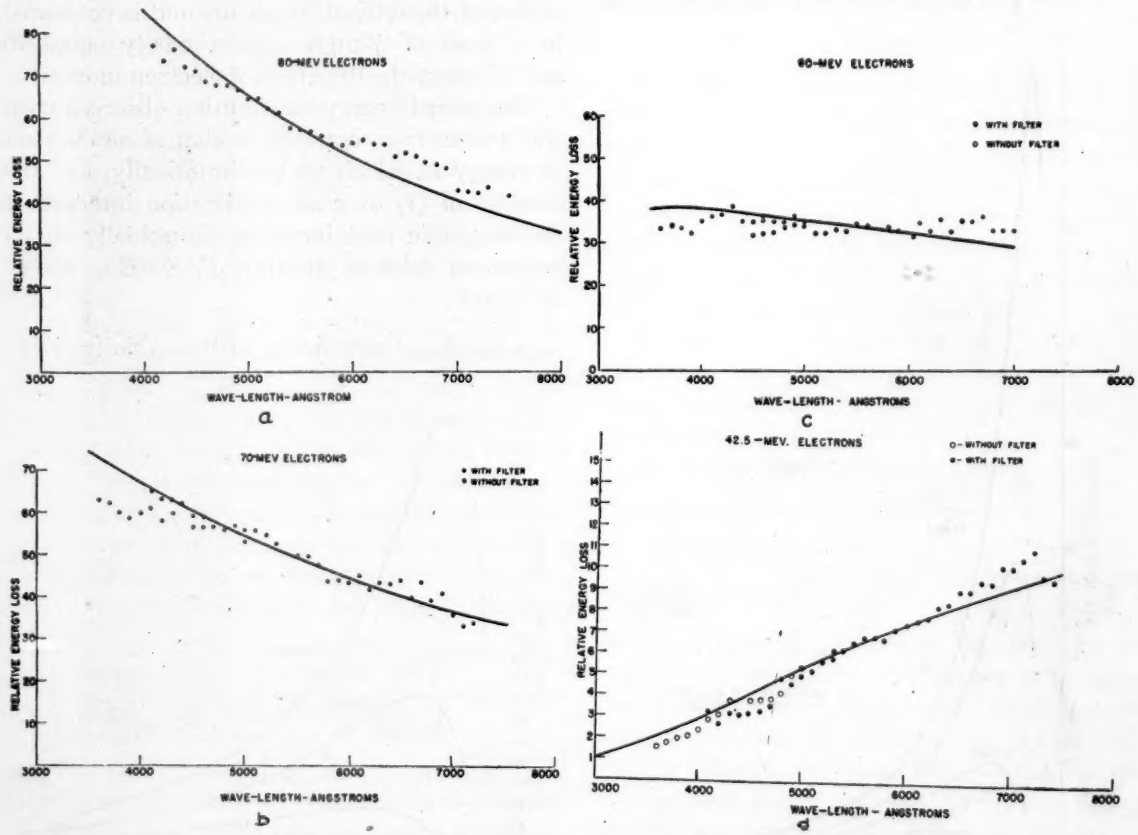

FIG. 4. Comparison of measured energy distribution of the electron light with the theoretical spectral curves. Electrons accelerated to peak energies of (a) 80 Mev, (b) 70 Mev, (c) 60 Mev, and (d) 42.5 Mev.

[7] E. Jahnke and F. Emde, *Tables of Functions* (Dover Publications, New York), 4th edition, p. 235.

3. EXPERIMENTAL

To verify that the spectral distribution of the radiation from the electron beam agrees with the theory, we used a recording spectroradiometer developed by Dr. Frank J. Studer of this laboratory. Light from the electrons leaves the accelerating tube through a quartz window and enters the spectroradiometer through a slit which is centered in and perpendicular to the plane of the orbit. In this instrument the light is reflected from a front-surfaced mirror on to a Wood grating of 15,000 lines per inch, which concentrates the reflected light into the first-order spectrum. An arrangement of gears rocks the grating and simultaneously traverses the spectrum with a 1P22 photo-multiplier tube. The photo-tube output is amplified and fed into a curve-drawing meter. The drives for the traverse and the recording meter are synchronized so that the two are in step at all times. The spectroradiometer was calibrated by making records with a standard tungsten lamp of color temperature 2848°K. From this record the sensitivity of the instrument was obtained throughout the wave-length range 3500 to 7000 angstroms. To prevent the second-order spectrum of short wave-length light from reaching the 1P22, a filter which cut off at 4200 angstroms was used in front of the slit during both the experimental runs and calibration in the region above this wave-length.

When using the synchrotron for x-ray production the radiofrequency acceleration voltage is usually turned off when the electrons are at desired energy and the orbit permitted to expand or contract to hit suitably placed targets. However, for these optical experiments, the electrons were accelerated to maximum energy and then decelerated to a low energy before turning off the r.f. accelerating voltage. Different peak energies were obtained by changing the excitation of the magnet. For each excitation level the peak magnetic field, which determines the electron energy, was measured by means of a search coil and an R-C integrating circuit. The machine is driven at 60 cycles/sec.

The agreement of theory and experiment is shown in Fig. 4. The theoretical curves obtained from Eq. (3) were arbitrarily matched with the experimental data at 5000 angstroms. The scatter of the points is probably due to fluctuations of the electron beam current during a run. We also took several spectrograms with a Hilger quartz spectrograph. The plates indicated the continuous character of the spectrum and showed the expected change in distribution of intensity with peak electron energy. However, the variation of plate sensitivity with wave-length made this method seem less attractive than the use of the spectroradiometer.

A measurement of the electron beam current, using Eq. (4), was made in the following way. A shielded Kipp thermopile, located 23 in. from

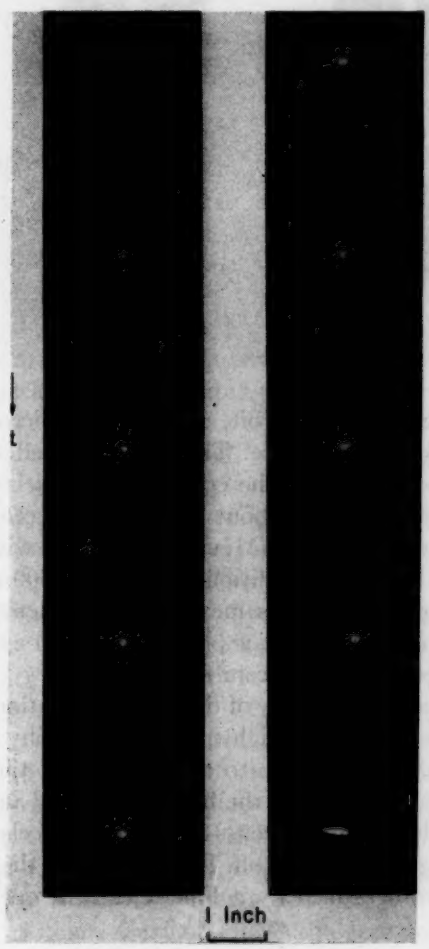

FIG. 5. Consecutive frames taken with Fastex Camera located in the plane of the orbit. The center of the orbit is to the right of the spot. The r-f was turned off before peak magnetic field (after frame 8). The orbit contracts (frame 9) and then expands, moving to the left in the final frame.

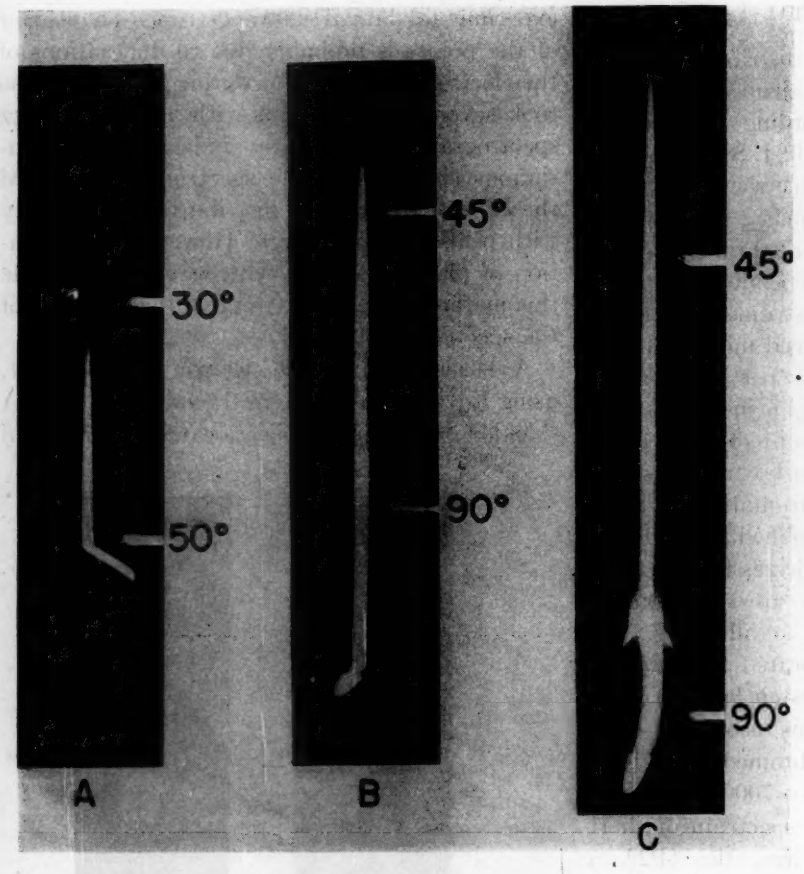

FIG. 6. Photographs of beam taken with a continuous drive camera. The numbers indicate electrical degrees after zero magnetic field. (a) Beam contracted at approximately 55 Mev. (b) Beam expanded by turning off r-f after peak magnetic field. (c) Radiofrequency turned off just before peak magnetic field corresponding to 70 Mev. Beam first contracts slightly and then expands to target. Some electrons are lost from the beam at the time of r-f turn off.

the center of the orbit, received 1.8 microwatts on its active surface. This corresponded to 3.3 milliwatts around the entire orbit, which is the power radiated by about 10^8 electrons accelerated each cycle. The 70-Mev x-ray output with the same injection conditions was about 300 roentgens per minute, as measured in a Victoreen *r* thimble mounted in a $\frac{1}{4}$-inch thick lead cylinder located one meter from the target.

The high intensity of the optical radiation from the beam permits high speed photography of the beam. It is possible to determine that the high energy diameter of the beam is about $\frac{1}{8}$ in., and to follow its movements after the r-f accelerating voltage was turned off. Figure 5 shows the beam as photographed by a Fastex camera operating at 3000 frames per second. A different display of the beam is shown in Fig. 6. These pictures were taken with a General Radio continuous drive camera in which the film moved perpendicular to the plane of the orbit with a uniform speed of 40 ft./sec.

ACKNOWLEDGMENTS

This work has been supported by the Office of Naval Research. We are very grateful to Professor J. S. Schwinger of Harvard University for sending us the equations quoted in this paper. Dr. E. A. Lewis of M.I.T. and Dr. H. Levine of Harvard have also sent us some of their theoretical results. Mrs. R. Wells of this laboratory assisted with the numerical calculations.

Radioactive Isotopes of Ru and Tc

D. T. EGGEN* AND M. L. POOL
Department of Physics, Ohio State University, Columbus, Ohio

(Received March 16, 1948)

A new isotope of Ru and one of Tc were found when Mo was bombarded with alpha-particles. The Ru activity decayed with a half-life of 1.65±0.05 hours. Positrons, x-rays, and gamma-rays were emitted with energies of 1.1 Mev, 0.7A, and 0.95 Mev, respectively. The Ru activity also was produced by fast neutron bombardment of Ru. The Tc activity decayed with a half-life of 20.0±0.5 hours and emitted x-rays of 0.7A and gamma-rays of 0.78 Mev. The Tc activity also was made by proton bombardment of Mo. Electromagnetically separated Mo^{92} of 92 percent abundance was bombarded with alpha-particles producing the 1.65-hour and 20-hour activities. Electromagnetically separated Mo^{94} of 75 percent abundance under alpha-particle bombardment made a 2.8-day activity. Thus the 1.65-hour, 20-hour, and 2.8-day activities can be assigned to Ru^{96}, Tc^{95}, and Ru^{97}, respectively.

I. INTRODUCTION

IT has been reported that a 2.8-day Ru activity produced by neutron[1,2] and deuteron[1] bombardments of Ru decays by K-electron capture into the 90-day daughter isotope, Tc^{97}. The 2.8-day activity emitted x-rays, 0.2-Mev electrons, and 0.23-Mev gamma-rays; the mass assignment was made to the isotope Ru^{97}. A 45-day Ru activity resulting from neutron[3] and deuteron[4] bombardment of Ru and also from U-fission[5] has been found to decay by emitting 0.2-Mev beta-particles and 0.56-Mev gamma-rays. A half-life of less than 90 minutes was reported following an alpha-bombardment of molybdenum.[6] A 52-day Tc activity which decays by K-electron capture has been produced by proton and deuteron bombardments of molybdenum.[7]

The above Ru and Tc activities have been essentially confirmed in this laboratory; while doing so, however, two new radioactive substances have been found, one in Ru and one in Tc. It is the purpose of this paper to report on their characteristic radiations, and to make mass assignments.

II. Ru FRACTION

Molybdenum sheet metal was bombarded by 20-Mev alpha-particles and 5-Mev protons. Immediately after the bombardments the Mo was dissolved in HCl and the active Ru and Tc were distilled as RuO_4 and $TcCl_3$ with an inactive Ru carrier into a concentrated solution of KOH containing a Re salt as carrier for the Tc. The Ru fraction was precipitated with alcohol and filtered. The supernate containing the active Tc was made $6N$ with H_2SO_4 and the Tc fraction was precipitated with H_2S.

The decay of the Ru fraction from a Mo+α bombardment is plotted in Fig. 1. Curve C in the insert represents a decay of the total radiation taken over a period of five months. When the intensity of the 45-day half-life material is subtracted from curve C, activities with half-lives of 2.8 days, 20 hours, and 1.65 hours are found. Curve A, representing the total radiation, is plotted over the first 40 hours of the decay. Successive subtractions show the relative ionization produced by the 1.65-hour, 20-hour, and 2.8-day activities in this sample. The time required to make the chemical separation was about 1.5 hours. Curve B shows the decay of the gamma-rays when the beta-particles and the x-rays were removed. It is observed that each of the above activities emits gamma-rays.

Lead absorption measurements taken during the 1.65-hour activity disclosed two gamma-rays

* Research fellow of the National Institute of Health.

[1] W. H. Sullivan, N. R. Sleight, and E. M. Gladrow, Phys. Rev. **70**, 778 (1946).

[2] E. E. Motta, G. E. Boyd, and A. R. Brosi, Phys. Rev. **71**, 210 (1947).

[3] K. Senma and H. Yamasaki, Phys. Rev. **59**, 402 (1941).

[4] E. Bohr and N. Hole, Arkiv. Math. Astro. Fys. **A32**, No. 15, 8 (1946).

[5] W. E. Grummitt and G. Wilkinson, Nature **158**, 163 (1946).

[6] L. D. P. King, W. J. Henderson, and J. R. Resser, Phys. Rev. **55**, 1118 (1939).

[7] J. E. Edwards and M. L. Pool, Phys. Rev. **72**, 384 (1947).

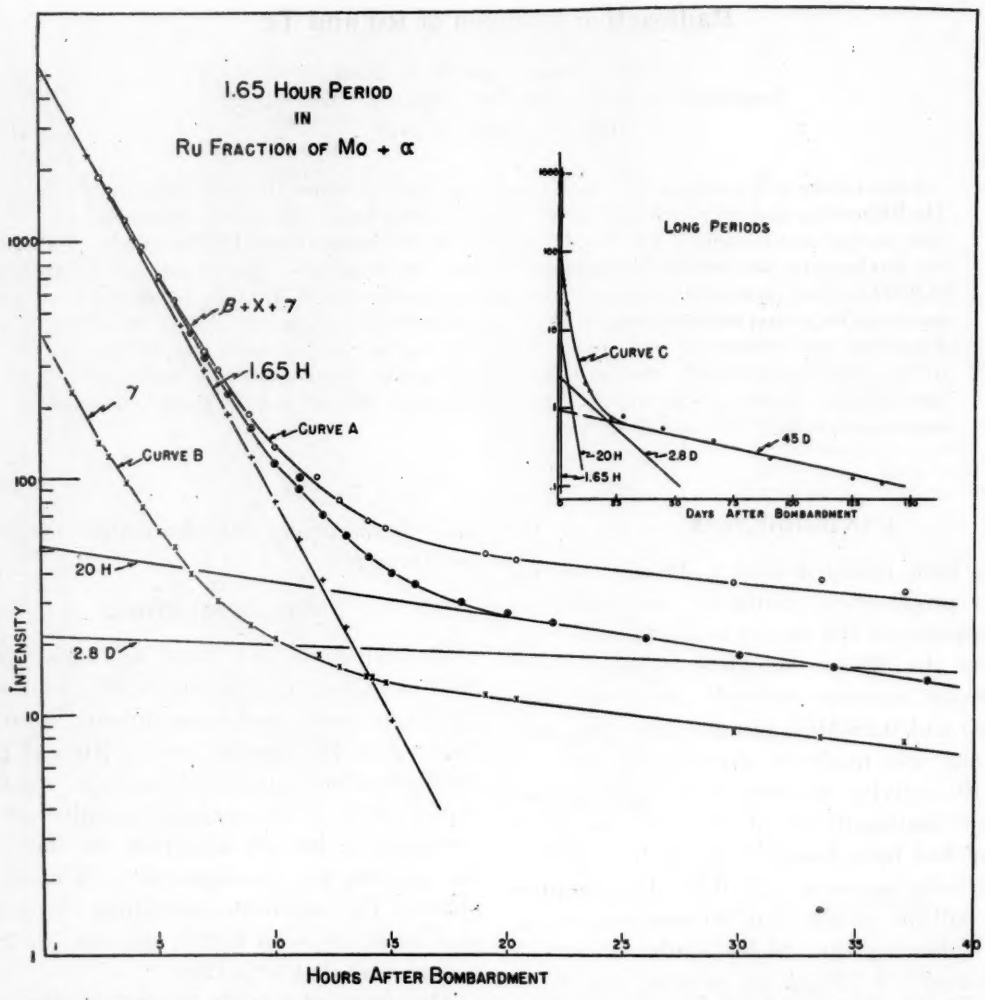

FIG. 1. Decay curves for (*A*) and (*C*) total radiation and (*B*) gamma-radiation of the Ru fraction of a Mo+α bombardment. The 1.65-hour Ru^{95}, 20-hour Tc^{95}, 2.8-day Ru^{97}, and 45-day Ru^{103} are shown with their relative ionization intensities.

with half-value thicknesses of 0.41 cm and 0.86 cm corresponding to energies of 0.52 Mev and 0.95 Mev, respectively. From Wilson cloud chamber observations, it is seen that the 1.65-hour substance decays by positron emission. Aluminum absorption measurements taken when the activity was mainly in the 1.65-hour period are plotted in Fig. 2. The curve shows that the positrons have a maximum range of 440 mg/cm² or a maximum energy of 1.1 Mev.[8] When the positrons are deflected from the ionization chamber by a strong magnetic field, it is possible to show by aluminum absorption measurements that x-rays are emitted. Such measurements are shown also in Fig. 2. The absorption coefficient obtained was about 5 cm²/g and therefore indicates x-rays of wave-length approximately 0.7A. K_α x-rays characteristic of the elements in the Tc region have wave-lengths near this value.

Decay measurements may be taken using the magnet as above. These measurements indicate the presence of a small amount of ionization caused by the x-ray radiation in the 1.65-hour activity; therefore, *K*-electron capture takes place as well as positron emission. The probability of decay by means of *K*-electron capture is of the same order of magnitude as that by positron emission.

In addition to the alpha-bombardment of

[8] N. Feather, Proc. Camb. Phil. Soc. **34**, 599 (1938).

molybdenum, ruthenium was bombarded by fast and slow neutrons. The fast neutrons produced the 1.65-hour, 2.8-day, and 45-day Ru activities. However, the slow neutron bombardment made only the 2.8-day and 45-day activities and not the 1.65-hour activity.

III. Tc FRACTION

The decay curves for the Tc fraction from a Mo+α bombardment are plotted in Fig. 3. The insert shows the decay curve of the total radiation taken over a period of five months. The long period denoted as the 52-day activity serves as the base line for curve *A*. Curve *A* shows the decay of the total radiation during the first nine days after bombardment.

Based upon measurements carried through ten half-lives, a value of 20.0±0.5 hours was found. Curve *B* shows the decay due to the total electromagnetic radiation only. In subtracting curve *B* from curve *A*, it is seen that the ionizing intensity caused by the negatively charged particles emitted during the decay of the 20-hour period is very small compared to that of the electromagnetic radiation. Aluminum absorption measurements were made on an electrometer particularly designed for low energy particles. A maximum energy of 200 kev was recorded.

Curve *C* shows the decay due to the electromagnetic radiation after passing through one-quarter inch of aluminum. This curve is caused primarily by gamma-rays and shows the presence of a gamma-ray in the 20-hour period. Lead absorption measurements give a half-value thickness of 0.69 cm, which indicates the energy of the gamma-ray is approximately 0.78 Mev. By taking the difference between curve *B* and curve *C*, it is observed that the intensity of the resulting x-rays decays with a half-life of 20 hours. Aluminum absorption measurements made on the electromagnetic radiation are plotted in Fig. 4. These measurements show a measured half-value thickness of 0.132 g/cm^2 corresponding to an x-ray wave-length of 0.72A.

It was pointed out in the Ru section that the Ru fraction from the Mo+α bombardment also contained a 20-hour activity. An additional observation is now presented that the relative amount of 20-hour material in the Ru fraction is dependent on the period of time between the end of the bombardment and the chemical separation of the Ru and Tc fractions. In a sample where the chemical separation was made 15 hours after bombardment, the 20-hour activity was almost absent in the Ru fraction and was correspondingly more abundant in the Tc fraction. It is therefore plausible to conclude that the 20-hour substance is the daughter product of the 1.65-hour Ru activity. The 20-hour Tc activity was also produced by a proton bombardment of molybdenum.

IV. ELECTROMAGNETICALLY SEPARATED ISOTOPES

Samples of $Mo^{92}O_3$ and $Mo^{94}O_3$** were bombarded with alpha-particles. The Mo^{92} was enriched to 92 percent, electromagnetically, and the Mo^{94} enriched to 75 percent. Equal masses of the two enhanced isotopes were bombarded under nearly identical conditions by rotating a target, having the two samples on opposite sides. The decay curves of these respective activities are shown in Fig. 5.

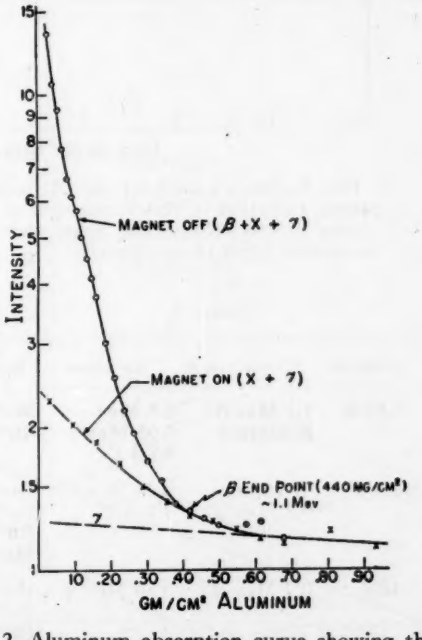

FIG. 2. Aluminum absorption curve showing the end-point energy of 1.1 Mev for the positrons in the 1.65-hour Ru^{95}. This curve also shows an x-ray of wave-length about 0.7A.

** Supplied by the *Y*-12 plant, Carbide and Carbon Chemical Corporation, through the Isotopes Division, United States Atomic Energy Commission, Oak Ridge, Tennessee.

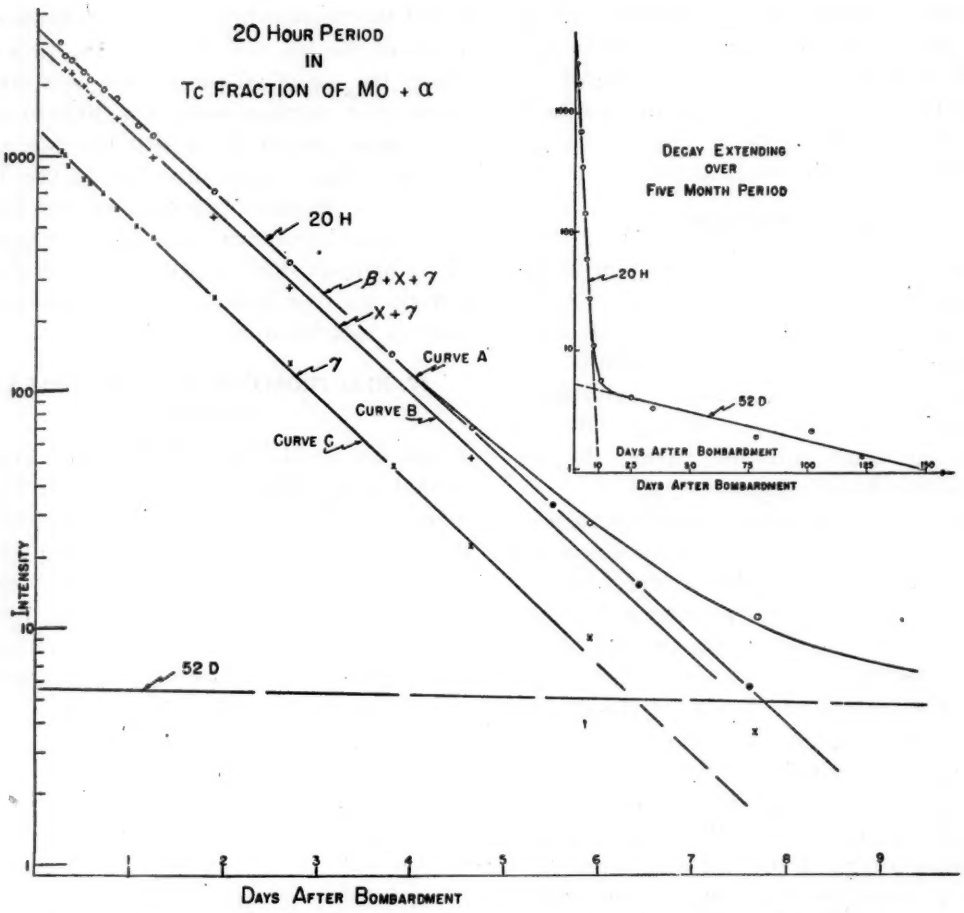

FIG. 3. Decay curves for the (*A*) total radiation, (*B*) total electromagnetic radiation, and (*C*) gamma-radiation of the Tc fraction of a Mo+α bombardment, showing the 20-hour Tc^{95} and 52-day Tc^{95} activities. The insert shows the intensity of the total radiation from the sample taken over a five month period.

TABLE I.

Isotope	Half-life	Characteristic	Radiations	Reaction
Ru^{95}	**1.65-h**	**1.1 Mev β^+ K-capture**	**0.5 Mev γ 0.95 Mev γ 0.7 *AX***	**$Mo^{92}(\alpha,n)$ $Ru^{96}(n,2n)$**
Ru^{97}	2.8-d	*K*-capture 0.2 Mev β^-	0.23 Mev γ 0.7 *AX*	$Ru^{96}(n,\gamma)$ $Ru^{96}(d,p)$ **$Ru^{98}(n,2n)$** **$Mo^{94}(\alpha,n)$**
Ru^{103}	45-d	0.2 Mev β^-	0.56 Mev γ	$Ru^{102}(n,\gamma)$ $Ru^{102}(d,p)$ **$Ru^{104}(n,2n)$** **$Mo^{100}(\alpha,n)$**
Tc^{95}	**20-h**	***K*-capture 0.2 Mev β^-**	**0.78 Mev γ 0.7 *AX***	**$Mo^{92}(\alpha,p)$ $Mo^{95}(p,n)$**
Tc^{95}	52-d	*K*-capture	0.25 Mev γ 0.84 Mev γ	$Mo^{95}(p,n)$ $Mo^{95}(d,n)$ **$Mo^{92}(\alpha,n)$**

The decay of the activity from the bombarded $Mo^{92}O_3$ definitely shows the 1.65-hour and 20-hour activities and an indication of a long period presumed to be the 52-day Tc activity. The decay of the activity from the bombarded $Mo^{94}O_3$ is predominately the result of a 2.8-day activity. A small amount of 1.65-hour activity is present in the decay of the Mo^{94} isotope and is probably caused by a small percentage of Mo^{92} in the sample.

V. MASS ASSIGNMENTS

Since the 1.65-hour positron activity of Ru was produced by alpha-bombardment of molybdenum and fast neutron bombardment of ruthenium but was not produced by slow neutron bombardment of ruthenium, the 1.65-hour ac-

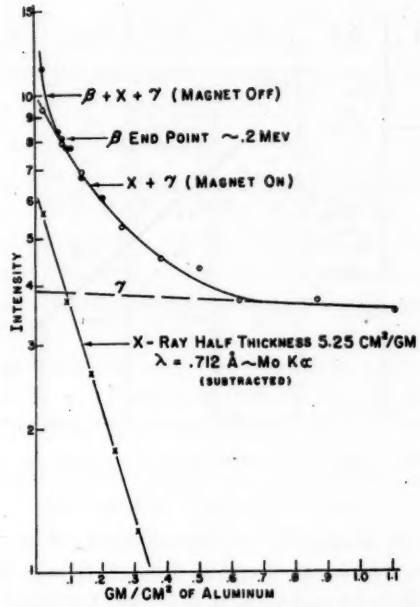

FIG. 4. Aluminum absorption curve taken during the 20-hour Tc^{95} period showing Mo $K\alpha$ x-rays.

tivity may be best assigned to Ru^{95}. The electromagnetically separated Mo^{92} bombarded with alpha-particles definitely confirms this assignment. Since the 20-hour Tc activity was shown to be produced by alpha-particle and by proton bombardments of molybdenum and also by the decay of the 1.65-hour Ru activity, the 20-hour activity is thus assigned to Tc^{95}. The alpha-particle bombardment of enriched Mo^{92} also confirms this assignment. The 2.8-day Ru activity which was produced by slow neutron and deuteron bombardments of ruthenium was assigned to Ru^{97}. The fast neutron bombardments of ruthenium and alpha-particle bombardments reported in this paper yield results which are consistent with this assignment. The alpha-particle bombardment of electromagnetically separated Mo^{94} confirms the assignment of the 2.8-day activity to Ru^{97}.

SUMMARY

The Tc region of a nuclear transmutation chart is shown in Fig. 6. In this chart, the isotopic positions of Tc^{95}, Ru^{95}, and Ru^{97} are indicated by heavy lines. New reactions are indicated by heavy arrows on which the nuclear reaction is noted.

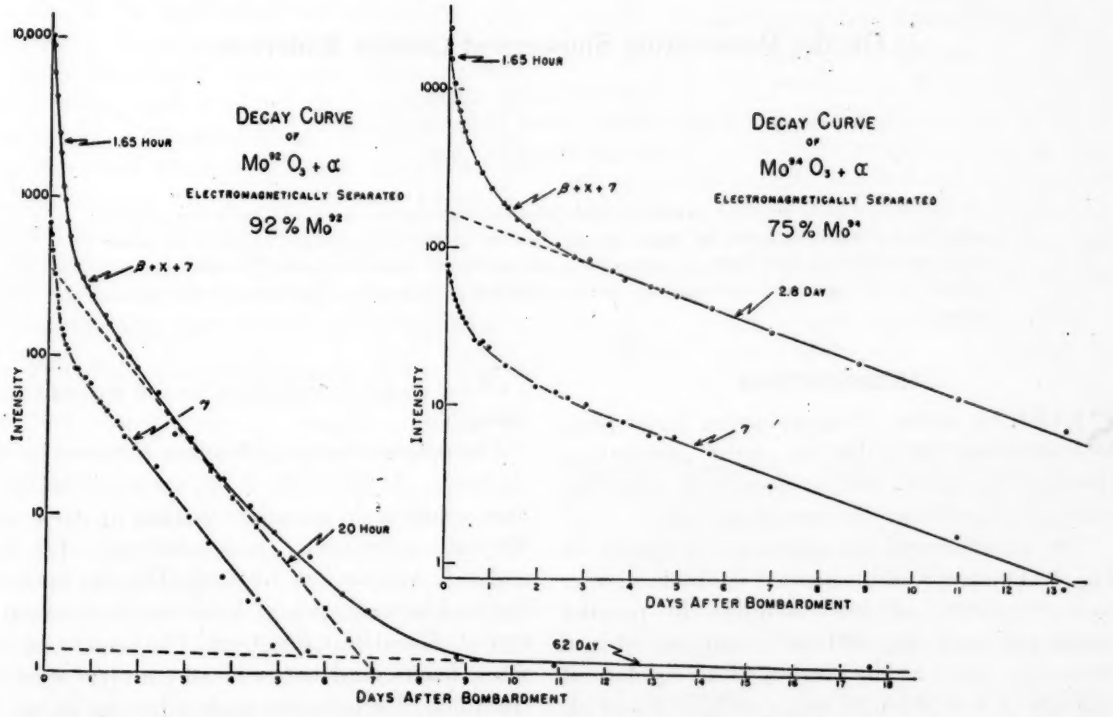

FIG. 5. Decay curves of the total radiation and gamma-radiation of electromagnetically separate Mo^{92} and Mo^{94} bombarded with alpha-particles. The 1.65-hour Ru activity and 20-hour Tc activity are found in the decay of the $Mo^{92}O_3+\alpha$ curves and the 2.8-day Ru activity is found in the $Mo^{94}O_3+\alpha$ curves.

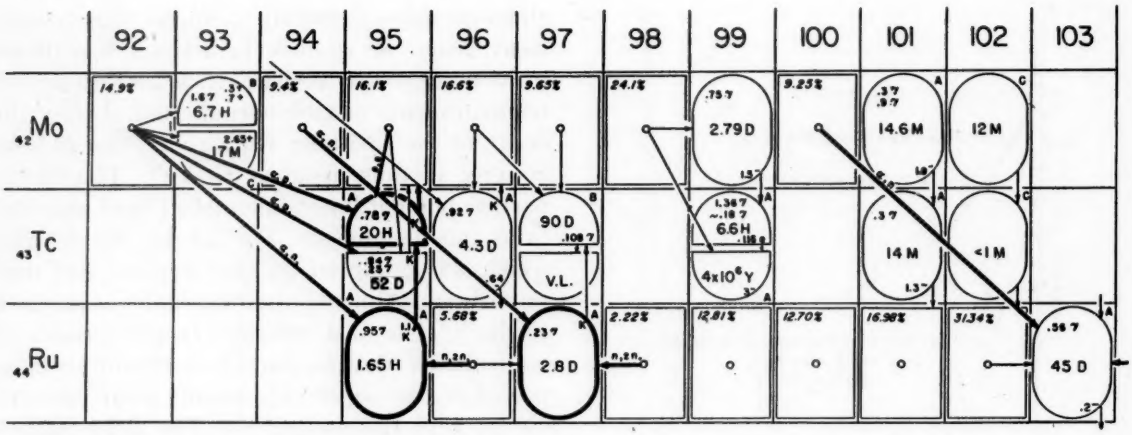

FIG. 6. The technetium region of the nuclear transmutation chart. Heavy lines and arrow indicate information reported in this paper.

Table I shows the characteristic radiations of the isotopes studied. The information reported in this paper is given in boldfaced type.

The support of The Ohio State Development Fund is gratefully acknowledged. The junior author wishes to express his gratitude for the fellowship awarded him by The National Institute of Health.

PHYSICAL REVIEW VOLUME 74, NUMBER 1 JULY 1, 1948

On the Penetrating Showers of Cosmic Radiation

G. COCCONI AND K. GREISEN
Laboratory of Nuclear Studies, Cornell University, Ithaca, New York
(Received March 17, 1948)

Experiments have been performed on the penetrating showers of cosmic radiation accompanied and not accompanied by extensive air showers. In the accompanied showers the penetrating particles are very likely to pre-exist in the air; in the unaccompanied showers they are created in the absorbers surrounding the counters by a nucleonic component of the cosmic radiation.

1. INTRODUCTION

SEVERAL series of experiments have been performed in order to study penetrating showers associated and unassociated with the extensive cosmic-ray showers at sea level.

The experimental arrangement is shown in Fig. 1. The trays of unshielded counters a, b, c, each consisting of four counters in parallel (surface of each tray 400 cm²), were placed in a horizontal plane at the vertices of an equilateral triangle of 4-m sides, in boxes of light material, maintained at constant temperature, on the roof of the laboratory. The three-fold coincidences $a+b+c$ ($\sim 6h^{-1}$) were due to the extensive air showers.

The penetrating particles were recorded by the six trays, A, B, C, D, E, F, each consisting of four counters in parallel (surface of each tray 400 cm²) arranged in three telescopes, AB, CD, and EF, surrounded by lead. The thickness of the lead between A and B was 6 cm, between C and D, E and F it was 1 cm. The screens on the sides, fronts, and backs of all counters were 11 cm thick. Underneath each telescope 6 cm of lead were placed. Above the telescopes the thickness T was varied in different series of

measurements from 10 to 31 cm. The axes of the telescopes AB and CD were 16 cm apart (6-cm Pb in between); the distance between the axes of AB and EF was 230 cm. The two lead boxes were placed inside the laboratory, about 3 m under the plane of the counters abc and roughly in the middle of the triangle abc.

The arrangement of the counters A, B, C, D was such that spurious coincidences $A+B+C+D$, due to a single penetrating particle crossing either AB or CD and generating a soft secondary, were avoided. In fact, the minimum amount of lead such a secondary would have had to penetrate was more than 8 cm.

2. PENETRATING SHOWERS ACCOMPANIED BY EXTENSIVE SHOWERS (PSA)

We call PSA the events in which at least two penetrating particles cross the recording system under lead, accompanied by the simultaneous discharge of the three counters a, b, and c. We recorded simultaneously the coincidences:

$a+b+c+A+B+C+D$ (narrow PSA),
$a+b+c+A+B+E+F$ (large PSA).

The aim of the experiment was to compare the frequencies of the narrow and large PSA. Measurements have been made with different thicknesses of the lead T above the telescopes. No appreciable differences were obtained in the counting rates with the different absorbers. In Table I the results of the different series are summed up. As the table shows, the frequencies of the narrow and large PSA are about the same.

We think that this result is understandable only by assuming one of the following hypotheses:

(a) PSA consist of particles pre-existing in the extensive showers, i.e., not locally generated in the lead.

(b) PSA consist of particles locally generated in the lead in a *non-multiple* process by some component of the extensive showers.

In fact, were the penetrating particles generated in the lead above the counters in multiple processes, the probability of coincidences $a+b+c+A+B+C+D$ would have been much larger than that of the coincidences $a+b+c+A+B+E+F$.

This result, in agreement with data obtained by Greisen and Treat at Echo Lake,[1] leads us to a conclusion about the origin of the PSA in complete disagreement with the previous view based on experiments performed by one of us,[2] as well as on experiments of Janossy[3] and Salvini and Tagliaferri;[4] all these experiments have been interpreted as indicating local multiple processes of generation of PSA.

We think that our present experiment faces the problem in a more direct way than our previous experiment[2] so that the present results have surely more weight than the previous ones. As for the experiments of Janossy[3] and of Salvini and Tagliaferri,[4] we want to note that their arrangement for detecting the penetrating showers probably did not completely avoid the penetrating showers not accompanied by extensive showers, which, as we shall see, are locally generated in the absorber.

On the basis of our experiment there is no way of discriminating between hypotheses (a) and (b). However, an indication in favor of hypothesis (a) may be derived from the fact that, as shown by reference 2 and confirmed by references 3 and 4, the frequency of PSA is independent of the atomic number Z of the absorber above the counters. Ferretti has shown[5] that if the penetrating particles are locally produced by the electrons and photons of the extensive showers, the independence of Z of their rate of production would indicate a cross section for the process proportional to Z^2, which would be hardly understandable. The independence of Z is instead to be expected in the case of hypothesis (a), since the absorption of the

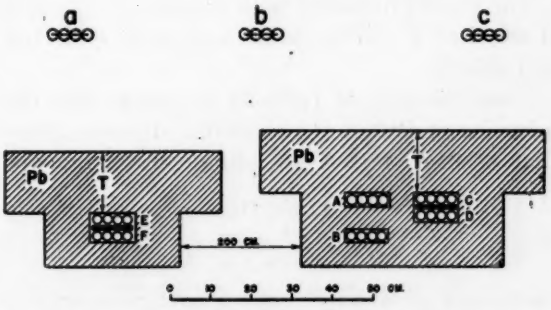

FIG. 1. Arrangement of the counters and the absorbers.

[1] J. Treat and K. Greisen, Phys. Rev.

[2] G. Cocconi and C. Festa, Nuovo Cimento **3**, 293 (1946).
[3] L. Janossy and Broadbent, Proc. Roy. Soc. **190**, 497 (1947).
[4] G. Salvini and G. Tagliaferri, Phys. Rev. **73**, 261 (1948).
[5] B. Ferretti, Nuovo Cimento **3**, 301 (1946).

TABLE I.

hours	$a+b+c+A+B+C+D$ (narrow PSA)	$a+b+c+A+B+E+F$ (large PSA)
1640	52	50

penetrating particles pre-existing in the shower is mass proportional.

3. PENETRATING SHOWERS NOT ACCOMPANIED BY EXTENSIVE SHOWERS (PSNA)

We call PSNA the events in which at least two penetrating particles cross the detecting system under lead, without simultaneous discharge of the counters *abc*.

While performing the PSA experiments, we also recorded the coincidences: $A+B+C+D$ and $A+B+E+F$. The PSNA were given by the differences:

$$(A+B+C+D)-(a+b+c+A+B+C+D)$$
(narrow PSNA),

and

$$(A+B+E+F)-(a+b+c+A+B+E+F)$$
(large PSNA).

While in PSA experiments the chance coincidences were completely negligible, in the PSNA experiments the chance coincidences due to two incoherent mesons crossing AB and one of the telescopes CD or EF are quite troublesome. In order to minimize their number, a coincidence circuit (blocking oscillators and crystal diode coincidences) was used with resolving time 1.2 μsec. The rate of chance coincidences $A+B+C+D$ or $A+B+E+F$ was $0.08h^{-1}$.

The results obtained with various thicknesses of the lead T above the telescopes are collected in Table II.

From the data of Table II it appears that the behavior of PSNA is completely different from that of PSA. PSNA are practically all narrow

TABLE II.

T (cm Pb)	hours	narrow PSNA observed	narrow PSNA corrected*	narrow PSNA rate h^{-1}	large PSNA observed	large PSNA corrected	large PSNA rate h^{-1}
6	122	224	214	1.75 ± 0.12	—	—	—
10	313	638	613	1.95 ± 0.08	38	13	0.04 ± 0.02
15	713	1475	1418	1.99 ± 0.05	62	5	0.007 ± 0.015
22	471	989	951	2.02 ± 0.07	33	0	0 ± 0.02
31	143	294	282	1.97 ± 0.12	20	3	0.02 ± 0.04

* "Corrected" figures refer to coincidences corrected for the chance coincidences.

TABLE III.

T	hours	narrow PSNA observed	narrow PSNA corrected**	narrow PSNA rate h^{-1}
Permanent 6-cm Pb	61	224	214	3.5 ± 0.23
6-cm Pb+72-g cm^{-2} Pb	207	852	820	3.97 ± 0.14
6-cm Pb+72-g cm^{-2} C	243	1561	1521	6.25 ± 0.16

** The correction indicated is for chance coincidences.

showers, which indicates that they are created locally in multiple processes in the lead above the detecting system. All the recorded $A+B+E+F$ coincidences may be accounted for by chance coincidences.

The frequency of the narrow PSNA remains practically constant ($\sim 2h^{-1}$) when the thickness T is varied from 10 to 31-cm Pb; from this the conclusion may be derived that either the primary radiation generating the PSNA or the particles of which PSNA consist have high penetrating power; but one has to remember that the variation of T causes a change in the angular spread of the recorded showers, so that a possible absorption may be masked.

An experiment has been performed in order to study the dependence of PSNA on the atomic number Z of the material in which their production take place. The frequencies of the PSNA have been compared under equivalent amounts of lead and carbon, placed above a permanent layer of 6-cm Pb.

In order to avoid the geometrical effect due to the different densities of these materials, the measurements with lead were performed with the permanent Pb always close above the telescopes, and the other 6-cm Pb arranged in 5 layers evenly distributed in the same space as that occupied by the equivalent amount of graphite (42 cm). In order to increase the counting rate, the telescope EF was placed inside the absorber, near AB, in the symmetrical position of CD. Coincidences $a+b+c+A+B+C+D$ and $a+b+c+A+B+E+F$ were recorded, as well as coincidences $A+B+C+D$ and $A+B+E+F$, in order to allow the discrimination of the PSNA.

The results are collected in Table III.

From these data it follows that (coinc. under C/coinc. under Pb) $=1.58\pm0.07$. This remarkable difference between the frequencies of the

showers under carbon and lead may be considered as a confirmation of the hypothesis formulated by several authors,[3,6,7] that the PSNA are generated by a nucleonic radiation, presumably the primary protons; the lower efficiency of Pb in producing PSNA would be due to the condensation effect of many nucleons in the heavy nucleus, as pointed out by Janossy.[8]

Following this interpretation, from our data it is possible to state that the cross section for the production of PSNA must not be much smaller than the geometrical cross section of the nucleons ($\sim 7.10^{-26}$ cm^2). This is in agreement with the cross section ($\sim 2.10^{-26}$ cm^2) required to explain the variation of the frequency of the PSNA with altitude above sea level.[6,7]

Finally, a test experiment has been made with all the counters of the trays *a*, *b*, *c* connected in parallel and acting as a single counter of 1200-cm^2 surface. With $T=15$ and 31-cm Pb, penetrating showers were recorded both accompanied and unaccompanied by at least one particle on the tray *abc*.

The counting rates obtained were practically the same as those recorded during the experiments described above. This demonstrates that the discrimination between PSA and PSNA did not depend on the particular arrangement of unshielded counters chosen for detecting the extensive showers.

[6] G. Wataghin, Nature **161**, 91 (1948).
[7] E. P. George and P. T. Trent, Nature **161**, 248 (1948).
[8] L. Janossy, Phys. Rev. **64**, 345 (1943).

4. CONCLUSIONS

Penetrating showers not accompanied by extensive showers and penetrating showers accompanied by extensive showers differ sharply in local behavior. The first ones are mostly generated locally in the absorber above the detecting system and their rate of production is weakly Z dependent (larger for smaller Z). The second ones, instead, are mostly generated in the air and their rate under absorbers of equal weight does not depend on Z.

We wish to emphasize that this distinction between the two kinds of showers rests on an experimental basis and does not imply any more fundamental difference between the showers than a difference in their place of origin, whether it is in the absorber or in the air far above the absorber.

With counter arrangements designed to detect narrow penetrating showers, the frequency of PSNA is much bigger than that of the PSA (with our arrangement 70 times). Therefore, most of experiments on penetrating showers in which no discrimination has been made between showers accompanied and not accompanied by extensive showers concern the PSNA. Hence, we want to emphasize that the conclusions derived therefrom refer to this type of shower.

We wish to thank Mr. E. D. Palmatier for assistance in the early stages of the experiment. This work has been supported in part by the Office of Naval Research.

Mass Temperature Coefficients of Cosmic-Ray Components

F. M. MILLICAN* AND D. H. LOUGHRIDGE
University of Washington, Seattle, Washington

(Received January 27, 1948)

The temperature pressure curve from U. S. Navy Raob data was integrated by an empirical formula determined graphically. The resulting average "mass temperature" of various fractions of the atmosphere was correlated by a method of least squares with the vertical cosmic-ray intensity of three components; hard, medium, and soft, shielded by 30.5, 20.5, and 0.5 cm of lead, respectively. The temperature coefficient was found to be an increasing function of the fraction of the atmosphere for larger fractions.

The temperature coefficients obtained for the fractions 1, 3/4, 6/10, and 1/4 are for the hard component: -0.25 ± 0.06, -0.18 ± 0.04, -0.15 ± 0.04, and -0.17 ± 0.04 percent per degree centigrade, respectively. The results for the medium component are: -0.61 ± 0.11, -0.43 ± 0.07, -0.34 ± 0.08, and -0.39 ± 0.08 percent per degree centigrade, respectively. Comparative results for data from a Millikan-Neher electroscope shielded by 12 cm of lead are: -0.25 ± 0.05, -0.17 ± 0.03, -0.16 ± 0.03, and -0.17 ± 0.03 percent per degree centigrade for the respective fractions listed above. The results for the soft component correlated so poorly that no values are quoted.

I. INTRODUCTION

INVESTIGATION into the correlation of cosmic-ray intensity with average "mass" temperatures of the atmosphere has been stimulated by Blackett's[1] theory on the temperature effect and the subsequent discovery of the "air-mass" effect by Loughridge and Gast.[2] Benedetto, Hess, and Altman,[3] using a counter telescope arrangement with an aperture of 0.297 steradian and shielded by approximately 22 cm of lead, have contributed to this study.

The authors have made a similar study employing a counter telescope of 18° zenith angle differentiating the hard, medium, and soft components shielded by 30.5, 20.5, and 0.5 cm of lead, respectively. This instrument has been described at length by Smith.[4] A "Millikan-Neher"[5] recording electroscope shielded by approximately 12 cm of lead was operated, but not concurrently with the telescope, to study the temperature coefficient for radiation from all directions. This instrument is described by Millikan and Neher.

II. MASS TEMPERATURES

Hess and Benedetto[3] suggested using an average temperature in which the temperature was weighted proportionally to the mass of air of a given temperature rather than to the space occupied by the band. They accomplished this by integrating the atmospheric pressure *vs.* temperature curve and dividing by the pressure over the particular fraction desired.

For the purpose of obtaining the mass temperature of various fractions for the present work, Raobs (radio observation, balloon soundings) taken at Sand Point Naval Air Station, Seattle, were obtained from the U. S. Weather Bureau, Seattle, Washington.

Atmospheric temperatures as a function of pressure of standard levels were plotted for arbitrarily chosen data scattered through the year as shown in Fig. 1. The pressure levels 1000, 850, 700, 500, 300, 200, and 100 are designated "standard" millibar levels whose temperatures are reported on all Raobs provided there is no equipment failure. To accomplish the graphical integration of the pressure-temperature curve, it was divided into pressure intervals such that the temperature of the standard millibar pressure

* Now at Naval Electronics Laboratory, San Diego, California.

[1] P. M. A. Blackett, Phys. Rev. **54**, 973 (1938).

[2] D. H. Loughridge and P. F. Gast, Phys. Rev. **58**, 583 (1940).

[3] V. F. Hess and F. A. Benedetto, Phys. Rev. **60**, 610 (1941); F. A. Benedetto, G. O. Altman, and V. F. Hess, Phys. Rev. **61**, 266 (1942).

[4] L. E. Smith, Jr., *Intensity Coefficients of Cosmic Ray Components* (University of Washington Thesis, 1945). H. T. Stetson, Sci. Mo. **58**, 207 (1944); Electronic Industries **94**, January (1944).

[5] R. A. Millikan and H. V. Neher, Phys. Rev. **50**, 15 (1936).

levels gave a fair representation of the average for that interval, as shown in Fig. 1 where the standard levels are indicated by S.L. The same division appeared satisfactory throughout the year. A weight (in terms of multiples of 50 millibars) was assigned to each standard millibar level and the following formulae derived for the average mass temperatures of the various fractions of the atmosphere:

$$T_{1/4}=[3(T_{850})+2(T_{1000})]/5,$$
$$T_{6/10}=[3(T_{700}+T_{850})+2(T_{1000})+4T_{500}]/12,$$
$$T_{3/4}=[3(T_{300}+T_{7000}+T_{850})+2(T_{1000})+4T_{500}]/15,$$
$$T_{1}=[3(T_{100}+T_{300}+T_{700}+T_{850})+2(T_{200}+T_{1000})+4T_{500}]/20.$$

$T_{1/4}$, $T_{6/10}$, $T_{3/4}$, and T_1 represent the mean mass temperatures of the lower 1/4, 6/10, 3/4, and 1 fractions of the atmosphere, respectively. T_{100}, T_{200}, T_{300}, etc., are the temperatures of the 100, 200, 300, etc., millibar levels as given on the Raob reports. The mean mass temperatures were determined for each day from the morning (0800) and evening (1800) reports. The values used in correlating were the average of these two taken to represent the daily mean centered about noon (1200).

The Raob balloons do not always reach the higher standard levels. Missing upper air data were filled in by interpolation and through reference to data from the Tatoosh station 150 miles NW of Seattle. The difference between the upper air at these two stations is usually small and changes slowly. A consideration of the formula for T_1, for example, will reveal that an error of five degrees in estimating T_{100} will cause an error in T_1 of but about three percent under average atmospheric conditions.

III. TREATMENT OF DATA

The data from the telescope and the electroscope were divided into periods for analysis as given in Table I.

The temperatures used represent the daily means centered about noon. The counts for each hour of the day were reduced to a standard barometer of 30 inches of mercury, using barometric coefficients as given by Smith[4] and Gast[6]

[6] P. F. Gast, *Various Factors Affecting Cosmic Ray Intensity* (University of Washington Thesis, 1941).

TABLE I. Periods for analysis of data.

Period	Cosmic-ray telescope	Number of days
I	July 4–July 24, 1946	21
II	Aug. 21–Sept. 7, 1946	18
III	Sept. 12–Oct. 2, 1946	21
IV	Oct. 3–Oct. 22, 1946	20
V	Oct. 26–Nov. 17, 1946	23
	Millikan-Neher Meter	
I	Jan. 4–Jan. 31, 1947	28
II	Feb. 2–Feb. 28, 1947	27
III	March 1–March 30, 1947	30

for the telescope and electroscope, respectively. These values are:

telescope:

hard——3.81 percent per inch of mercury,
medium——8.64 percent per inch of mercury,
soft——9.65 percent per inch of mercury,
Millikan-Neher——4.32 percent per inch of mercury.

The counts were then averaged about noon for each 24-hour period. It was these averages which were correlated with the temperature.

The correlations were by a method of least squares as given by Forsythe[7] and Doan.[8] The essential relations are given below:

(a). X = the deviation of the temperature from some value near the mean.
(b). Y = the deviation of the counts from some value near the mean.
(c). n = the number of days in the period.

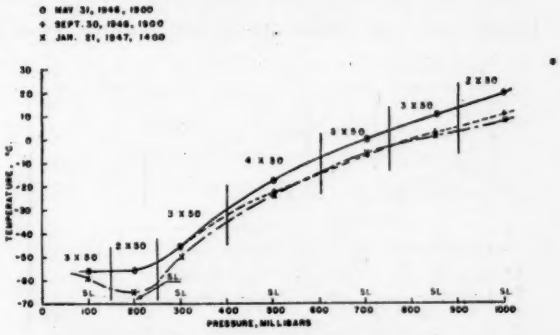

FIG. 1. Temperature-pressure curves from Raob reports.

[7] C. H. Forsythe, *Mathematical Analysis of Statistics* (John Wiley and Sons, Inc., New York, 1924), pp. 223.
[8] R. L. Doan, Phys. Rev. **49**, 107 (1936).

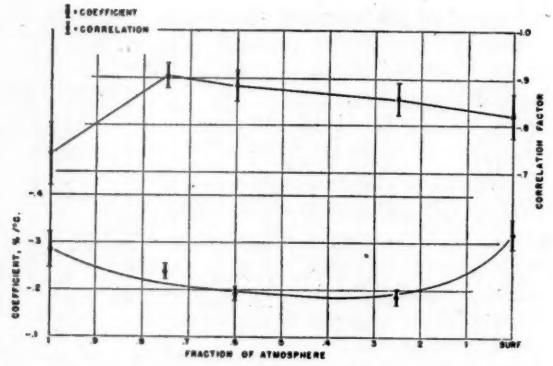

FIG. 2. Temperature coefficient *vs.* fraction of atmosphere, hard, Period I.

(d). $\bar{y}$ = the average of the daily counts being correlated.

(e). $\sigma_x = [(\Sigma X^2/n) - h^2]^{\frac{1}{2}}$ = standard deviation of temperature.

(f). $\sigma_y = [(\Sigma Y^2/n) - k^2]^{\frac{1}{2}}$ = standard deviation of counts.

(g). $\nu_{xy} = (\Sigma XY/n) - hk$ = product-moment.

(h). $r = \nu_{xy}/\sigma_x\sigma_y$ = correlation factor.

(i). $P_r = \pm 0.675(1-r^2)/(n)^{\frac{1}{2}}$ = probable error in r.

(j). $\alpha = 100\nu_{xy}/\sigma_x^2\bar{y}$ = temperature coefficient in percent per degree C.

(k). $P_\alpha = \pm 0.675(1-r^2)^{\frac{1}{2}}\sigma_y 100/(n)^{\frac{1}{2}}\sigma_x\bar{y}$ = probable error in α in percent per degree C.

(l). $h = \Sigma X/n$ = the displacement of the origin of the deviations from the mean.

(m). $k = \Sigma Y/n$ = the displacement of the origin of the deviations from the mean.

IV. EXPERIMENTAL RESULTS

On the basis of this work the values given below are the most probable values of the temperature coefficient for the fractions 1, 3/4, 6/10, and 1/4, respectively, for the hard component: -0.25 ± 0.06, -0.18 ± 0.04, -0.15 ± 0.04, and -0.17 ± 0.04 percent per degree centigrade, respectively. The values for the medium component are -0.61 ± 0.11, -0.43 ± 0.07, -0.34 ± 0.08, and -0.39 ± 0.08, percent per degree centigrade, respectively. The Millikan-Neher meter data led to -0.25 ± 0.05, -0.17 ± 0.03, -0.16 ± 0.08, and -0.17 ± 0.03 percent per degree centigrade for the respective fractions listed above. The correlations for the soft component were very low both positive and negative. It is felt that the results for the soft component should not be quoted pending further study.

Figures 2–7 show the variation in temperature coefficient with fraction of the atmosphere for various components and periods as indicated. In all cases the temperature coefficient is an increasing function of fraction of the atmosphere for higher fractions. For small fractions approaching surface temperature it is not possible

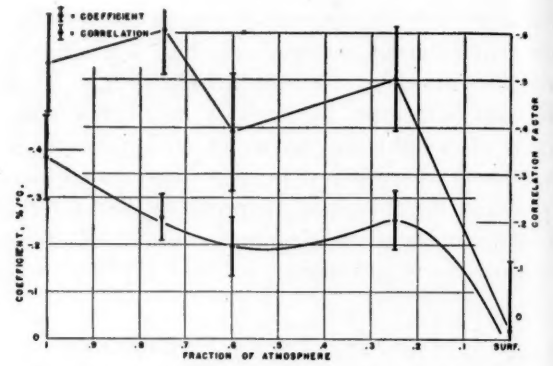

FIG. 4. Temperature coefficient *vs.* fraction of atmosphere, hard, Period III.

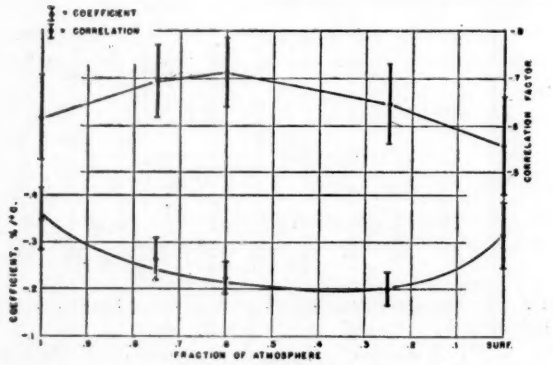

FIG. 3. Temperature coefficient *vs.* fraction of atmosphere, medium, Period I.

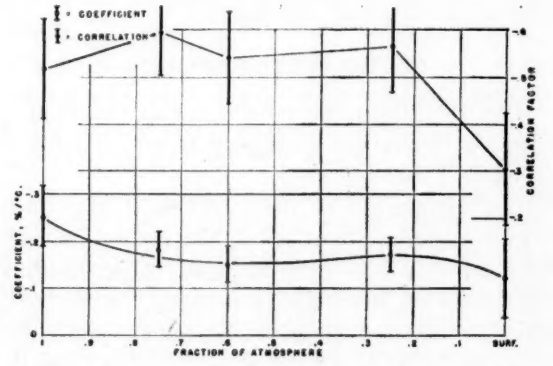

FIG. 5. Temperature coefficient *vs.* fraction of atmosphere, hard, average of Periods I, II, III, and V.

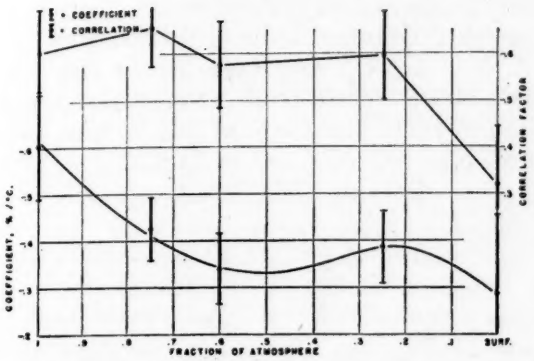

FIG. 6. Temperature coefficients *vs.* fraction of atmosphere, medium, average of Periods I, II, III, and V.

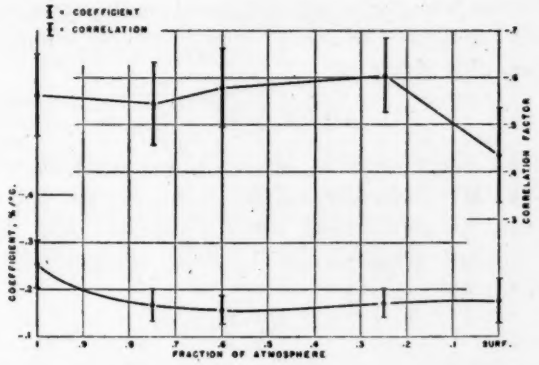

FIG. 7. Temperature coefficient *vs.* fraction of atmosphere, Millikan-Neher meter, average of Periods I, II, and III.

to predict whether the coefficient will rise or continue to fall. Figures 2–4 show cases of both possibilities. It appears certain, however, that the correlation falls off as the surface temperature is approached. Surface temperature is influenced by the local terrain more than the upper air. One would not expect surface temperature to correlate the same as upper air temperatures. The results for the Millikan-Neher meter vary in a manner similar to those from the telescope.

V. THEORETICAL DISCUSSION

Benedetto[3] made the assumption that an increase of intensity is linearly proportional to a downward shift of air mass. It then follows that:

$$dI/I = -dZ/L \qquad (1)$$

where

I = mesotron intensity,
Z = height of mesotron production level, and
L = mesotron mean free path.

The temperature coefficient may be defined as:

$$\alpha = (-1/I)\cdot(dI/dT) = (-1/I)\cdot(dI/dZ)\cdot(dZ/dT), \qquad (2)$$

and putting (1) in (2):

$$\alpha = +(1/L)\cdot(dZ/dT). \qquad (3)$$

Equation (3) then indicates that α is proportional to dZ/dT. In calculating the coefficient, the mass temperature of a certain fraction of the atmosphere was correlated with cosmic-ray intensity. So from Eq. (3), α is proportional to av.$[\partial Z/\partial T]_f \cdot$ Av.$[\partial Z/\partial T]_f$ is equal to dZ/dT averaged over the fraction in question.

It was remarked that Benedetto assumed that an increase in cosmic-ray intensity was linearly proportional to a downward shift in the mesotron producing layer. Assume that the layer is located at a height $Z=L$, the average path length above the earth's surface. The shape of the path-length distribution curve is complicated by the fact that the mesotrons have a finite lifetime. However, if the distribution curve does not differ markedly from a Gaussian curve, the mean free path length, L will intersect the distribution curve at a point where the slope is not changing rapidly. A number of independent experiments fix at least one mesotron producing level in the vicinity of the 100 millibar, 16 kilometer, level. As will be shown later in this section, this level rises but about 60 meters per degree centigrade. So for a normal temperature change of a few degrees, the change in height of the level is a small percentage of the height of the level. In view of this, the section of the distribution curve over which L varies will be nearly a straight line. Thus it appears that Benedetto's assumption of the linear proportionality between the number of particles reaching the surface and the height of the producing layer is a reasonable one.

It was decided to check the proportionality

TABLE II. Change in height of atmospheric layers.

Fraction	$[\partial Z/\partial T]_f$ m/°C	av. $[\partial Z/\partial T]_f$ m/°C
1/5	6.89	3.29
2/5	15.4	6.79
3/5	26.8	11.8
4/5	47.0	17.6

between the coefficients obtained in the present work and av.$[\partial Z/\partial T]_f$. The "law of atmospheres" is given by:

$$p = p_0 e^{-Mgh/RT} \tag{4}$$

where p=pressure at height h, p_0=pressure at $h=0$, M=molecular weight of air, R=gas constant, g=acceleration due to gravity, and T=absolute temperature of the air. Solving Eq. (4) for h,

$$h = (-RT/Mg)\ln(p/p_0). \tag{5}$$

If T is taken as the average mass temperature of the layer (p_0-p), Eq. (5) gives the height of the top of the layer. Taking small increments in h and T,

$$[\Delta h/\Delta T]_f = (-R/Mg)\ln(p/p_0), \tag{6}$$

where $[\Delta h/\Delta T]_f = [\partial Z/\partial T]_f$ = the change in the height of the top of the layer f with respect to temperature. Equation (6) may be integrated with respect to p to find the area under the $[\Delta h/\Delta T]_f$ *vs.* p curve as follows:

$$\text{Area}_f = \int_{p_f}^{p_0} [\Delta h/\Delta T]dp = -\int_{p_0}^{p_f} [\Delta h/\Delta T]dp. \tag{7}$$

Now, putting Eq. (6) in (7),

$$\text{Area}_f = (R/Mg)\int_{p_0}^{p_f} \ln[p/p_0]dp$$

$$= (R/Mg)[p\ln(p/p_0) - p]_{p_0}^{p_f}.$$

If the proper p limits are used and the area obtained divided by the interval in pressure, the result is the av.$[\partial Z/\partial T]_f$ for the fraction in question. The upper limits of the fractions 1/5, 2/5, 3/5, and 4/5 were taken as the 800, 600, 400, and 200 millibar levels, respectively. p_0 was taken as 1013. Equations (6) and (8) were used to compute $[\partial Z/\partial T]_f$ and av.$[\partial Z/\partial T]_f$ for each of these fractions. The results are given in Table II.

The ratio of av.$[\partial Z/\partial T]_{4/5}$ to av.$[\partial Z/\partial T]_{1/5}$ is 17.6/3.29. Reference to Benedetto's work shows a ratio of 24/17. It appears likely that the upper limits of his fractions are not those used in this paper. However, regardless, it is obvious that the two independent determinations of av.$[\partial Z/\partial T]_f$ are not in agreement. When one compares the values of av.$[\partial Z/\partial T]_f$ given in Table II with the values of the coefficients obtained in this work, it can be said that the temperature coefficient and av.$[\partial Z/\partial T]_f$ are both increasing functions of fraction of the atmosphere for higher fractions.

This work was made possible through a Frederick Cotrell grant-in-aide from the Research Corporation of New York. The aid of Professor L. A. Sanderman in overseeing the operation of the apparatus during the latter war years, when the authors were away from the campus, is appreciated. The writers thank David Dye, Glenn Loughridge, and Donald Nelson for aid in processing the data. They are also indebted to the Department of Terrestrial Magnetism of the Carnegie Institution of Washington for the generous loan of one of its Millikan-Neher type electroscopes.

The Use of the Double Crystal Spectrometer in the Analysis of Bragg Reflections at Very Small Angles*

PAUL KAESBERG, H. N. RITLAND, AND W. W. BEEMAN
University of Wisconsin, Madison, Wisconsin

(Received March 24, 1948)

A two-crystal spectrometer has been used to investigate x-rays scattered from the large periodicities in wet collagen. Positions and relative intensities are assigned to the first through the seventh orders and to the ninth order. Some advantages of this method over the usual diffraction methods are pointed out.

I. METHOD

THE customary x-ray diffraction methods, using slit or pinhole collimation and photographic registration, become increasingly difficult as the angle between the scattered radiation and the primary beam is decreased. At best, the conflicting demands of resolution and intensity can be compromised at exposure times of hours or days and resolutions of two or three minutes of arc. The very small apertures required are difficult to align, slit edge scattering is a problem, and little power can be dissipated in the small area of the target seen by the slits. Photographic registration, while it has the advantage of simultaneously collecting data at many scattering angles, is not well suited to accurate intensity measurements nor to the measurement of very low intensities. Some investigators have lessened these difficulties by the use of an evacuated camera and very long wave-length radiation,[1] or by the use of a curved crystal monochromator.[2]

The double crystal spectrometer as used in the present work[3] (see Fig. 1) is equivalent to a slit geometry of high resolution, but without the usual intensity difficulties since one can use a wide beam and, therefore, a large focal spot. The first crystal collimates the beam while the second crystal analyzes the angular distribution of the scattered x-rays near the parallel position. The resolution is limited only by the natural width of the parallel position rocking curve. The accuracy with which the angular position of the peaks may be determined is governed by the sharpness of the peak and the precision of the measurement of the angle of rotation of the second crystal.

A Ross-type mounting was used in the $(1,-1)$ position. The spectrometer crystals were of calcite, ground and etched, having a full width at half-maximum of 16 seconds for Cu K_α radiation. The angular position of the second crystal was measurable to within one-half second of arc. A metal, continuously pumped x-ray tube with interchangeable iron and copper targets was used for the present experiments. It was operated at 20 milliamperes and 31 kilovolts with electronic stabilization of current and voltage.[4] The beam irradiating the sample was approximately 4 mm wide, and 3 mm high. The former figure is the diameter of the focal spot. A thin glass window, argon-alcohol Geiger counter served to record the x-ray intensity reflected by the second crystal.

II. DISCUSSION

The fibrous proteins are among the best examples of very large periodicities to be found in nature. Among these, collagen has been investigated by means of the electron microscope,[5] and by means of x-rays,[6,7] and has been found to

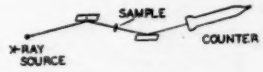

FIG. 1. The geometry of the two crystal spectrometer for small angle scattering.

* This research was supported in part by the Research Committee of the Graduate School from funds supplied by the Wisconsin Alumni Research Foundation.

[1] R. Hosemann, Zeits. f. Physik 114, 133 (1939).
[2] A. Guinier, Ann. de Physik 12, 161 (1939).
[3] I. Fankuchen and M. H. Jellinek, Phys. Rev. 67, 201 (1945); J. W. M. DuMond, Phys. Rev. 72, 83 (1947); W. W. Beeman and Paul Kaesberg, Phys. Rev. 72, 512 (1947).
[4] A. F. LeMieux and W. W. Beeman, Rev. Sci. Inst. 17, 130 (1946).
[5] C. E. Hall, M. A. Jackus, and F. O. Schmitt, J. Am. Chem. Soc. 64, 1234 (1942).
[6] R. S. Bear, J. Am. Chem. Soc. 66, 1297 (1944) and also 64, 727 (1942).
[7] O. Kratky and A. Sekora, J. mackromol. Chemie 1, 113 (1943).

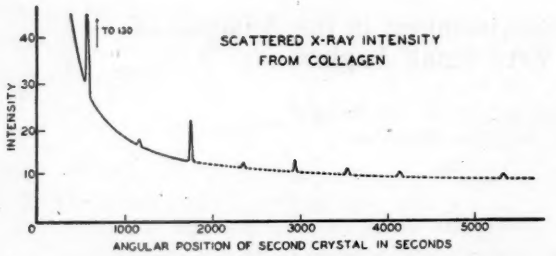

FIG. 2. Scattered intensity of x-rays from wet collagen. The full lines indicate the regions mapped carefully. Points in these regions were taken every five seconds of arc. Points in the dashed regions were taken every 100 seconds of arc.

have a particularly regular structure. The electron microscope studies indicate a fundamental periodicity varying from 522 to 902 angstroms in dried collagen. However, the preparation of the specimen for use in the electron microscope has a considerable effect on its structure. Several investigators have used x-ray diffraction cameras in the study of collagen. Bear[6] and Kratky and Sekora[7] have observed a first-order peak in the region corresponding to 640A for dried collagen, assigning its exact position by measurement of higher orders. Kratky and Sekora used dried kangaroo tail tendon, finding a spacing of 642A. Bear used, among other things, kangaroo tail tendon and beef tendon. He listed periodicities varying from 640 to 645A for air-dried samples, and from 675 to 680A for wet samples.

The collagenous tissues used in the present study were samples of beef tendon approximately

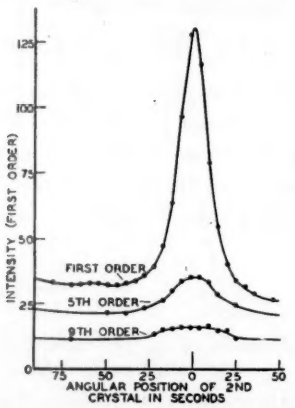

FIG. 3. Detailed curves with experimental points of the first, fifth, and ninth orders. The fifth and ninth orders are plotted to five times the vertical scale of the first order. The zero ordinate for the fifth and ninth orders is not shown, but is apparent from Fig. 2. The slight hump at the left base of the first order peak is from K_β radiation.

1 mm thick, soaked in water for several hours and then enclosed in cellulose tape. The specimens were placed midway between the spectrometer crystals (Fig. 1). The fiber axes were perpendicular to both the x-ray beam and the axis of rotation of the second crystal, thus permitting the observation of periodicities along the fiber axis.

Diffracted maxima corresponding to several orders were observed from the collagen. These are shown in Fig. 2. The relative intensities of the orders and the lattice spacing as determined from them are given in Table I; the mean value of the latter is 675A in satisfactory agreement with the results of Bear. It should be noted that the relative intensity of the first order (shown in more detail in Fig. 3) is much higher than that found by previous investigators. Another sample was examined in the first and third orders, yielding a spacing of 670A. The data for the first specimen were taken with an iron target; data for the second sample, as well as the data described below, were taken with copper radiation.

The resolution of the instrument and the regularity of the collagen lattice are apparent from the sharpness of the lower order peaks, which were about 20 seconds wide. This is very little more than the $(1,-1)$ width. The higher orders are somewhat wider, due in large part to the $K_{\alpha 1}$, $K_{\alpha 2}$ spacing, which is 10 seconds for iron radiation in the ninth order. In the first-order plot in Fig. 3, the K_β peak is clearly evident, though weak. Because of the high resolution one can examine the regions between the peaks carefully for further scattering. A check was made for evidence of diffuse small angle scattering of the type obtained with small, randomly spaced particles.[8] The region of the curve between the central maximum and the third-order peak showed no further evidence of scattering, the shape of the curve agreeing very closely with the rocking curve with no sample in place (corrected for absorption). Also the region 0–500 seconds with the fibers perpendicular to the beam but parallel to the axis of rotation of the second crystal was checked and was found to agree closely with the blank rocking curve.

Some observations were made of the position

[8] See, for example, R. Hosemann, Zeits. f. Physik 113, 751 (1939).

and intensity of the first-order peak as a function of the orientation of the fibers. When the sample was rotated about a vertical axis (parallel to the axis of rotation of the second crystal), the peak moved to larger angles; when rotated about a horizontal axis (parallel to the x-ray beam), the peak moved to smaller angles and widened considerably. In both cases, the height of the peak had decreased by half within 15 degrees of the normal specimen position. This made it difficult to determine the shifts quantitatively, since they are functions of the cosine of a small angle. They were consistent, however, with secant ϕ and cosine ϕ, respectively.

The total intensity available and the ratio of peak to background determine the counting time necessary for a given statistical accuracy. Figures 2 and 3 are from a run in which 6400 counts per point were taken. Counting times averaged between one and five minutes per point for the first three orders. Thus the neighborhood of the first-order peak could be mapped in less than an hour. A peak having an intensity equal to that of the first-order peak could be located easily if it were only 100 seconds from the primary beam, However, the eighth-order peak in this sample was so weak that it was not located, as the counting times for significant statistics would have been excessive.

TABLE I. Intensity in arbitrary units and lattice spacing obtained from various orders. The spacings were calculated from the angular separation of the given order from the central maximum (zero order).

Order	Intensity	Spacing
0	~100,000.0	—
1	100.0	674.7A
2	0.9	674.7
3	8.5	675.1
4	0.5	676.1
5	3.0	674.3
6	0.9	676.1
7	1.1	675.1
8	<0.2	—
9	1.1	675.1
		Av. 675.1A

It is evident that neither the full intensity nor angular precision of the instrument have been realized. The output of the tube could be increased by a factor of two to four without target damage. We believe our lattice spacings are dependable to within one quarter of one percent, but the lines are sufficiently sharp to permit measurements to one-tenth of one percent with a little extra care. The intensity might be considerably increased, with some loss of resolution, by grinding the crystals.

We are indebted to Dr. C. D. West of the Polaroid Corporation, who supplied us with the calcite crystals used on the spectrometer.

Molecular Spectroscopic Evidence of the Existence of Strontium Isotopes Sr^{88}, Sr^{87}, and Sr^{86}

L. H. AHRENS*
Department of Geology, Massachusetts Institute of Technology, Cambridge, Massachusetts
(Received March 2, 1948)

An analysis of certain heads of the sequence $v'-v''=+1(^2\Sigma\rightarrow{}^2\Sigma)$ in SrF arc emission spectra, revealed three components at each of the first heads, the displacements of which show the presence of three strontium isotopes at masses 88, 87, and 86. A quantitative determination of the abundance ratio, 88/86 gave a value of 8.52, which is in reasonably good agreement (+2.0 percent) with the abundance ratio of 8.38 determined mass spectrographically. The accuracy with which this ratio has been determined is considered to be within ±4–6 percent. Abundance ratios, 88/87 and 87/86 could be determined only approximately because of masking of the $Sr^{87}F$ component by the dominant $Sr^{88}F$ component. The spectra had been recorded using first order (dispersion, 0.848 A/mm), but if second order were used, this masking would be reduced to an insignificant amount. For geological age requirements, mass-spectrographic measurement of strontium isotope abundance ratios is preferable because as little as 0.3 mg of strontium salt is required, whereas using molecular spectra, far larger amounts are required. As the maximum concentration of strontium in the most ancient rubidium-rich minerals does not exceed 0.02 percent, inconveniently large quantities of mineral have to be employed to extract sufficient strontium for a molecular spectroscopic analysis.

1. INTRODUCTION

FOR the determination of geological age, the lead and helium methods are commonly used, but recently the strontium method has also been applied.[1,2] This last method is based on the natural β^--decay of $Rb^{87}\rightarrow Sr^{87}$; if the ratio Sr^{87}/Rb^{87} can be determined in a given mineral, the age of the mineral can be calculated since the decay constant of the transmutation is known. In a spectrochemical or chemical analysis the ratio Sr(total)/Rb^{87} can be estimated, and since primary (ordinary) strontium will be present in the mineral to a greater or lesser extent, relative abundance measurements have to be made of the strontium isotopes.

The common procedure is analysis by means of the mass spectrograph. This procedure is well adapted to strontium, but it was decided to explore other possible methods for showing and estimating different strontium isotopes. In the field of optical spectroscopy, Heyden and Kopfermann[3] have been able to show the presence of the three main strontium isotopes in common strontium and the presence of Sr^{87} only, in radiogenic strontium, by a hyperfine structure analysis of certain emission lines of strontium. This paper will describe some investigations that were carried out on molecular spectra.

2. CHOICE OF SUITABLE MOLECULAR SPECTRA

It is well known that molecular spectra are emitted by emitters of the type SrF, SrCl, SrBr, and SrI in flame sources and also in the arc. Spectra emitted by SrF are intense and clearly defined and can be conveniently produced using the common d.c. arc, whereas the other Sr halide spectra tend to be much weaker and diffused in this source because the energies of dissociation of SrI, SrBr and SrCl are much smaller than that of SrF. Furthermore, fluorine has only one isotope, which makes an examination of the spectra for isotope effects much simpler. SrF arc emission spectra were therefore selected to investigate the possibility of showing the presence of strontium isotopes, 88, 87, and 86 and to make relative abundance measurements on these isotopes.

3. EARLIER WORK

An earlier attempt had been made by Harvey[4] to show the presence of Sr^{86} and Sr^{88} by using SrF emission spectra. This author carried out his investigations in 1931, at which time the presence of Sr^{87} was still unknown. Harvey pointed out

* Research Fellow, South African Council for Scientific and Industrial Research.

[1] L. H. Ahrens, Trans. Geol. Soc. S. Africa, in press (1947).

[2] L. H. Ahrens, Bull. Geol. Soc. Am., in press.

[3] M. Heyden and H. Kopfermann, Zeits. f. Physik **108**, 232 (1937).

[4] A. Harvey, Proc. Roy. Soc. **A133**, 336 (1931).

that because of the small difference from unity of the isotope coefficient, ρ, for Sr^{88} and Sr^{86}, the detection of isotope heads in the sequence $v'-v''=0$ ($^2\Sigma\rightarrow{}^2\Sigma$) is not possible, whereas the separation in the squence $v'-v''=+1$ should be of the order of 1 cm^{-1}, that is, about 0.33A at the wave-length of these bands (~5700A). Using a 21-ft grating, Harvey recorded spectra in the 1st order; these spectra showed faint companion heads on the violet side of each main head in the $v'-v''=+1(^2\Sigma\rightarrow{}^2\Sigma)$ sequence. The measured shift, $Sr^{88}F-Sr^{86}F$ was found to be in reasonably good agreement with the theoretical shift as calculated from the equation, $\nu-\nu=(\rho-1)\nu_v$, using 17257 cm^{-1} for the system origin for computing ν_v.

4. PRESENT INVESTIGATION

Since the above investigation was carried out, Sr^{87} has been discovered, and although Harvey's results do appear to indicate the presence of Sr^{86}, they are not conclusive because no indication of the presence of Sr^{87}, which should have been apparent, was evident on his plates. It is quite probable that although the resolving power of the grating was sufficient, dispersion was not sufficient to register three separate isotope components for each head, and consequently in this investigation a greater dispersion has been used (see later discussion).

The isotope coefficients

$$\rho_1=(\mu^{Sr^{88}}/\mu^{Sr^{86}})^{\frac{1}{2}},\quad \rho_2=(\mu^{Sr^{88}}/\mu^{Sr^{87}})^{\frac{1}{2}},$$
$$\rho_3=(\mu^{Sr^{87}}/\mu^{Sr^{86}})^{\frac{1}{2}}$$

are given below. μ = reduced mass, calculated according to the equation $1/\mu=(1/m_1)+(1/m_2)$, where m_1 and m_2 are, respectively, the mass of a given strontium isotope and the mass of F.

$\rho_1=1.00207$, $\rho_2=1.00103$, and $\rho_3=1.00106$.

From the values of ρ calculation shows that $Sr^{88}F-Sr^{87}F$ and $Sr^{87}F-Sr^{86}F$ shifts are ~0.5 cm^{-1}, which corresponds to about 0.15A; a minimum resolving power of 40,000 and a large dispersion is therefore necessary to record the individual isotope heads.

A large (35 ft.) Paschen-type grating spectrograph, kindly placed at my disposal by Dean George R. Harrison of the Department of Physics, Massachusetts Institute of Technology, was used. Theoretical resolving power was 180,000 and dispersion 0.848 A/mm, in the 1st order.

A 1:1 mixture of SrF_2 and powdered carbon was placed in a cupped graphite anode and arced, using a d.c. source of excitation run at 6–7 amp. Thirty separate exposures, each of two minutes, were made (total exposure time one hour) and the spectra were recorded on Eastman Type 103-G spectroscopic plates.

Because of the astigmatism of the mounting, emulsion calibration (photographic response *vs.* intensity) could not be made using step weakeners, sectors, etc., and a separate calibration spectrum was made with the aid of a Wadsworth-type grating spectrograph (Cabot Spectrographic Laboratory, Department of Geology, Massachusetts Institute of Technology) using a rotating step sector and an iron arc as source. Calibration and analysis plates were developed under identical conditions.

5. RESULTS

Qualitative

According to Harvey,[4] the heads of the $v'-v''=+1$ sequence are, with the exception of the first two, close doublets, the separations of which increase towards the red. This doublet formation has been found to obscure the measurements of isotope displacements, and measurements could be made only on the first heads. In addition, the appearance of a background—the fine structure of preceding heads—is considerable for all heads with the exception of the first few. The head freest from background interference is the (2,1) head, and accurate displacements and relative intensity measurements could be made. Some measurements were also

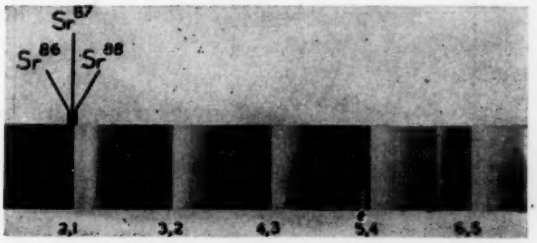

FIG. 1. SrF arc emission spectra of the sequence $v'-v''=+1(^2\Sigma\rightarrow{}^2\Sigma)$. $Sr^{88}F$, $Sr^{87}F$, and $Sr^{86}F$ components are particularly clear in the (2,1) head.

TABLE I.

	Calculated shift	Observed shift	
(2,1) head: $Sr^{88}F = 17771.28$ cm^{-1}			
	cm^{-1}	cm^{-1}	A
$Sr^{88}F - Sr^{86}F$	1.06	1.06	0.337
$Sr^{88}F - Sr^{87}F$	0.53	0.52	0.165
$Sr^{87}F - Sr^{86}F$	0.54	0.54	0.172
(3,2) head: $Sr^{88}F = 17959.56$ cm^{-1}			
$Sr^{88}F - Sr^{86}F$	1.04	1.03	0.326
$Sr^{88}F - Sr^{87}F$, $Sr^{87}F - Sr^{86}F$	Interference excessive.		

made on the (3,2) head, but attempts to measure isotope displacements on the other heads were fruitless because of extensive interference from head doubling and background fine structure. Figure 1 shows the (2,1), (3,2), (4,3), (5,4), and (6,5) heads; the presence of isotope heads may be seen best in the (2,1) heads.

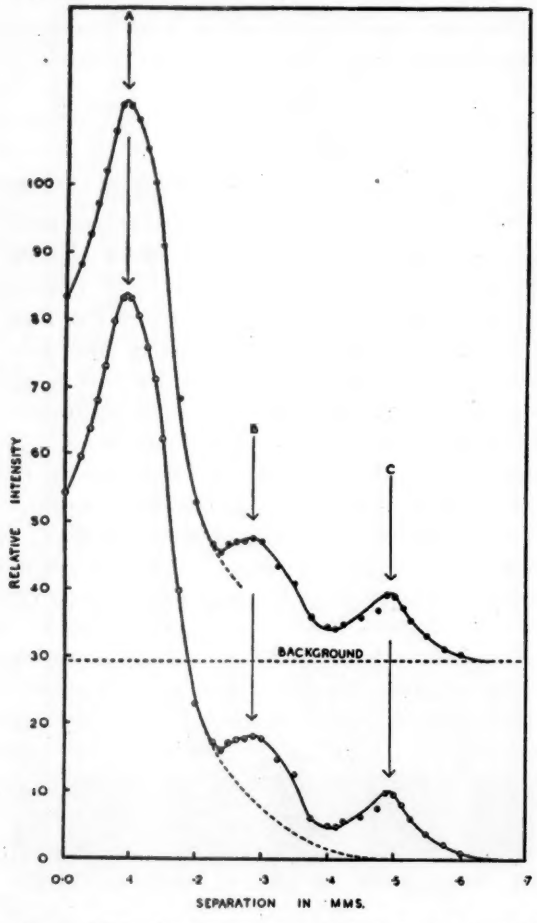

FIG. 2. Microphotometer trace of (2,1) head: $A = Sr^{88}F$ component, $B = Sr^{87}F$ component, and $C = Sr^{86}F$ component.

Band head displacements and intensity measurements were made with the aid of a Hilger non-recording microphotometer. The (2,1) and (3,2) heads were scanned by moving the plate at definite small intervals across the microphotometer light beam falling on the photo-cell and noting the galvanometer deflection at each setting. These deflections were converted to densities and by referring to the calibration curve (density *vs.* log intensity), the photographic response, measured as density, was converted into relative intensity units.

Figure 2 shows a plot of relative intensity (arbitrary units) *vs.* isotope head separation (in mm) for the (2,1) head. The upper curve is not corrected for background, whereas the lower curve has been corrected for background by a subtraction of background intensity from the total intensity at each reading. Three peaks are clearly in evidence, the separation of which could be measured accurately.

In Table I, theoretical and measured isotope displacements are given for the (2,1) and (3,2) heads. The wave numbers of the main ($Sr^{88}F$) heads, have been taken from Harvey.[4]

Because each isotope head in the (3,2) head appeared to be broader than in the (2,1) head, $Sr^{88}F$ masked $Sr^{87}F$ to a considerable extent; consequently, no sharp $Sr^{87}F$ peak could be obtained and hence only the $Sr^{88}F - Sr^{86}F$ displacement for the (3,2) head is given in Table I.

Where it has been possible to make accurate displacement measurements, agreement between calculated and observed results are very close, and the presence of the three peaks in Fig. 2 is due, therefore, to the three strontium isotopes of masses 88, 87, and 86. Another isotope of strontium (Sr^{84}), the relative abundance of which is 0.6 percent, has been found mass spectrographically, but because background and fine structure are relatively intense, the presence of this isotope could not be verified by using molecular spectra. Reference to Fig. 2 shows that for Sr^{86} (relative abundance ~10 percent) background intensity is about three times greater than that of the isotope head alone, and would thus be almost fifty times greater than the intensity of the $Sr^{84}F$ head alone.

Quantitative Relative Abundance Measurements

The relative abundance of the four known strontium isotopes (88, 87, 86, and 84) are, respectively, 82.6, 7.02, 9.86, and 0.56 percent according to mass-spectrographic data.

In Fig. 2, the predominance of Sr^{88} is easily seen and the ratio 88/86 may be determined with reasonable accuracy. Unfortunately, the ratio of 87 to either 88 or 86 could not be measured with precision because of masking of the $Sr^{87}F$ head by that of $Sr^{88}F$. If the spectra are recorded in the 2nd order, accurate measurements on the relative abundance of Sr^{87} could also be made.

From mass-spectrographic data, the abundance ratio $Sr^{88}/Sr^{86}=8.38$ and the ratio determined from molecular spectra is 8.52. Agreement is reasonably close as the difference is only 2.0 percent, but it is difficult to ascertain the accuracy of the latter determination. The experimental error limits are undoubtedly greater than 2.0 percent and are probably about ±4–6 percent.

The approximate ratio Sr^{88}/Sr^{87} was determined as 10.1 (±25 percent), whereas the mass-spectrographic ratio is 11.8. The accuracy with which this ratio could be determined could be increased very considerably by using 2nd-order spectra. However, further investigation on the use of the 2nd order was not continued, partly because of the difficulty with which this wavelength area of the spectrum could be recorded by using the available layout, and mainly because of the greater sensitivity of the mass spectrograph. According to recent investigations by Mattauch,[5] an accurate quantitative mass-spectrographic analysis may be made on as little as 0.3 mg of strontium salt. For these isotope investigations by the use of molecular spectra far greater amounts of strontium are required, and although the sensitivity obtained in this investigation could be enhanced, it would never be nearly as sensitive as the mass spectrograph. This drawback is a serious one for geological age measurements because the minerals on which age determinations are made contain at the most 0.02 percent Sr—usually much less—and consequently inconveniently large quantities of mineral would have to be worked up to produce a sufficient quantity of strontium for a strontium isotope analysis using SrF emission molecular spectra.

ACKNOWLEDGMENTS

Grateful acknowledgement is made to Dean G. R. Harrison for providing equipment facilities and for making useful suggestions for recording the spectra, and to Dr. Rand McNally, Jr. for aid and also for making useful suggestions.

[5] J. Mattauch, Am. angew. Chemie 2, 37 (1947).

Internal Conversion Electrons from Sm^{153}-47 Hour

R. D. HILL
Department of Physics, University of Illinois, Urbana, Illinois
(Received March 29, 1948)

The internal conversion electron spectrum of 47-hour beta-radioactive Sm^{153} has been investigated with a beta-ray spectrograph. Fourteen lines have been measured in the energy region up to 300 kev, nine of which can be attributed to internal conversions of two gamma-rays of 103 and 69.5 kev energy. Other lines are due to Auger electrons from Eu^{153}, and two weak lines are not assigned.

1. INTRODUCTION

A SUMMARY of data concerning the radioactivity of Sm^{153}-47 hour is given in the Plutonium Project Report.[1] Sm^{153} emits beta-rays with an upper energy limit of approximately 700 kev and gamma-rays of approximately 100 and 600 kev.[2-4] It has also been reported by Wu and Segrè[5] that 47-hour Sm emits x-rays, and Bothe[6] showed that these are characteristic of Eu (63) and therefore follow the beta-ray emission. Finally, Burson and Muehlhause[7] have found the existence of a high coincidence rate between the x-rays emitted from 47-hour Sm.

2. APPARATUS

The beta-ray spectrograph was a 180° focusing type with a maximum radius of curvature of 20 cm. The source, slit system, and photographic plate were mounted in an aluminum tray, which could be inserted, with suitable vacuum- and light-tight seals, in a brass box fitting between the poles of a permanent magnet. The magnet, of the double window yoke type, was formed by slabs of soft iron energized by short Alnico permanent magnets placed between the yoke and pole pieces. The poles were rectangular with sides of 30.5 cm by 51 cm, and the air gap of 7.5 cm had a field of approximately 102 oersteds. The field did not vary by more than 0.2 percent over an area within 4 cm of the pole-face edges. This area amply covered the space in which the electrons were bent to form spectra. The energy range of the spectrograph extended up to 300 kev.

TABLE I. Internal conversion lines from Sm^{153}-47 hour.

$H\rho$ (oersted cm)	E (kev)	Assignment	Gamma-ray energy (kev)
495	21.2	γ_1-K	21.2+48.6= 69.8
627	33.3	$K\alpha_{1,2}-L_I$	
637	34.5	$K\alpha_{1,2}-L_{III}$	
687	39.9	$K\alpha_{1,2}-M$	
808	54.3	γ_2-K	54.3+48.6=102.9
861	61.1	γ_1-L_I	61.1+ 8.1= 69.2
868	62.3	γ_1-L_{III}	62.3+ 7.0= 69.3
906	67.2	γ_1-M	67.2+ 1.8= 69.0
916	68.8	γ_1-N	68.8+ 0.4= 69.2
964	75.8	?	
1000	81.2	?	
1087	95.0	γ_2-L	95.0+ 8.0=103.0
1124	101.5	γ_2-M	101.5+ 1.8=103.3
1134	103.1	γ_2-N	103.1+ 0.4=103.5
Weighted means of gamma-ray energies:			γ_1= 69.4 kev
			γ_2=103 kev

3. RESULTS AND DISCUSSION

The measured $H\rho$ values of the observed conversion lines are shown in Table I. Some indication of the relative intensities of the lines can be gathered from Fig. 1.

Nine of the lines can be assigned to conversions of two gamma-rays of 69.5 and 103 kev. The absolute error of these energies may be of the order 1 kev. In obtaining these energies the electron work functions pertaining to Eu(63)

[1] Plutonium Project Report, Rev. Mod. Phys. **18**, 513 (1946).
[2] L. Winsberg and others, reference 1.
[3] L. C. Miller and L. F. Curtiss, reference 1.
[4] L. Meitner, Arkiv f. Mat. Astro. Fysik **A27**, 18 (1940).
[5] C. S. Wu and E. Segrè, Phys. Rev. **61**, 203 (1942).
[6] Bothe, Zeits. f. Naturforschung **1**, 179 (1946).
[7] Burson and Muehlhause, private communication.

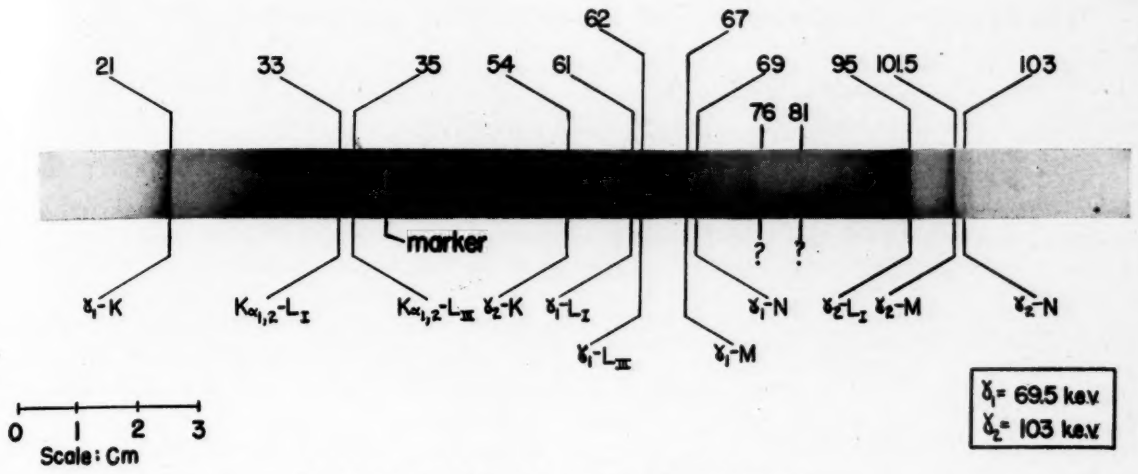

FIG. 1. Internal conversion electrons from Sm^{153}-47-hr.

have been used. It can be shown, in fact, that conversion of these gamma-rays in Sm(62), or in any element other than Eu, is inconsistent with the value of the magnetic field of the spectrograph.

The x-ray critical absorption energies can be used to obtain an accurate evaluation of the magnetic field. Once an assignment of the conversion lines has been made from an approximate value of the field, the accurate x-ray energy level values can then be used to calculate accurately the value of the field which will bring the gamma-ray energies derived from the K, L, M, N conversions into agreement. Check measurements of the well-known UX_1 conversion line at 92.5 kev[8,9] have also been made. Using the derived field of 101.8 oersteds, an energy of 92.0 kev was obtained for this line.

Other lines present in the Sm^{153} conversion spectrum are Auger lines arising from the internal conversion of Eu(63) x-rays. These lines at 33.3, 34.5, and 39.9 kev, although composite, show sharp edges where the more intense $K\alpha_1$ components are converted. Two other weak lines at 76 and 81 kev are unaccounted for. They appear, however, to be characteristic of Sm^{153}-47 hour.

There is no indication of conversion lines that might arise from combinations of the two observed gamma-ray lines, i.e., in the regions of $(103+69.5-K)$ and $(103-69.5-L)$.

ACKNOWLEDGMENTS

The investigation of samarium was performed at the suggestion of Dr. M. Goldhaber who arranged for the supply of pile-activated Sm_2O_3 from the Argonne National Laboratory, Chicago. The UX_1 sources were prepared by Mr. L. M. Smith. The Office of Naval Research supported this work under Contract N6-ori-71.

[8] L. Meitner, Handbuch der Physik **20** (1933).
[9] Bradt and Scherrer, Helv. Acta Phys. **19**, 307 (1946).

The Angular Distribution of Pair-Produced Electrons and Bremsstrahlung*

P. V. C. HOUGH
Laboratory of Nuclear Studies, Cornell University, Ithaca, New York
(Received March 8, 1948)

The Bethe-Heitler unscreened cross sections for pair production and bremsstrahlung have been integrated to give the angular distributions. For simplicity, results are restricted to large angles and high energies, but it is shown that extension to smaller angles requires that screening be considered at energies for which screening is important in the usual differential cross sections. The effect of the finite size of the nucleus is estimated and found to be large at the higher energies. It is shown that large-angle pair production will provide only a very small background for single meson production by quanta.

I. INTRODUCTION

THE basic cross sections for pair production and bremsstrahlung have been derived by H. A. Bethe and W. Heitler.[1,2] They have also carried out the complete angular integrations, in pair production, e.g., over the angles of both electron and positron; for convenience, however, new variables are introduced mixing the two sets of angles so that the integration over one pair is not obtained. We have carried out such an integration and have obtained, through suitable approximation, usable formulas for the high energy large-angle distribution of pair-produced electrons and bremsstrahlung.

Apart from the intrinsic interest in these distributions and the opportunity they provide for a detailed experimental test of the consequences of radiation theory, the results are of use for estimating the background of electrons against which one must look for mesons produced by quanta.

II. DISTRIBUTION OF PAIR-PRODUCED ELECTRONS

The fundamental cross section for pair production[3] given by Bethe and Heitler is differential in the angles of electron and positron and in the energy division between them, and we shall refer to it as the triple differential cross section. The result on integration over both pairs of angles we call the single differential cross section. As a consequence of Born's approximation, electron and positron coordinates enter symmetrically in the triple differential cross section; it is immaterial therefore which particle's angles are integrated over and the distribution obtained applies to either. For definiteness we integrate on positron coordinates. The notation throughout is that of Bethe and Heitler, *viz.*, E_+, p_+, θ_+ for the positron's energy, momentum $\times c$, and angle relative to the quantum's direction, with similar notation for the electron. k is the energy of the quantum.

The azimuthal integration is elementary and leads to eight integrals on the polar angle, of which the most complicated is the following:

$$\int_0^2 [(a+bx)x(2-x)dx/(x+\eta_+)^2X^{\frac{1}{2}}]. \qquad (1)$$

Here $x=1-\cos\theta_+$, $\eta_+=(E_+-p_+)/p_+$, X is a quadratic form in x, and a, b and the coefficients in X depend on E_+, E_-, p_+, p_-, and θ_-. The other integrals differ from (1) simply in the omission of various factors, e.g., in the denominator $x+\eta_+$ may occur to the first power or not at all, X may be raised to the $\frac{1}{2}$ power, etc. All have been evaluated exactly[4] with a resulting formula too complicated for convenient use. The high energy large-angle limit gives, however, our chief result, Eq. (2) below.

A second treatment[5] makes use of the large-angle high energy assumptions at the start and may be described with reference to the typical

* This work was supported in part by the Office of Naval Research.
[1] H. Bethe and W. Heitler, Proc. Roy. Soc. **146**, 90 (1934).
[2] W. Heitler, *The Quantum Theory of Radiation* (Oxford University Press, London, 1936), §§17, 20.
[3] See reference 2, p. 196, Eq. (7).
[4] I wish to thank Mr. E. S. Lennox for an independent exact calculation of these integrals which made possible the elimination of several mistakes.
[5] This method was suggested by Professor H. A. Bethe.

integral (1). With μ the electron rest energy, at high energies $\eta_+=\frac{1}{2}(\mu/E_+)^2$ and introducing $\delta\sim\mu/E_+$ we may break the integral $\int_0^2$ into $\int_0^\delta+\int_\delta^2$. In the first of these all factors in the integrand are put equal to their values at $x=0$, except $x/(x+\eta_+)^2$ which is easily integrated, and in the second η_+ is neglected compared to x. The latter approximation evidently requires only $(\mu/E_+)\ll 1$; the former demands that $(a+bx)/X^{\frac{1}{2}}$ does not vary rapidly for $x<\delta$. That this implies large E_- may be seen from Fig. 1. For the factor $(a+bx)/X^{\frac{1}{2}}$ is just the azimuthal integration of $1/q^4$, where $q=k-p_--p_+$, as shown by the circle. And this integral does not vary rapidly with θ_+ for $\theta_+\sim 0$ unless q is small there, i.e., unless θ_- or p_- is small.

We conclude, with reference to the triple differential formula, that when the rapid variation of $1/q^4$ and $1/(E_+-p_+\cos\theta_+)^2=1/E_+^2(x+\eta_+)^2$ can be separated, the integration is simple, and when not, it is complicated; the simple case is distinguished by simultaneous large θ_- and E_-.

The two methods agree in every detail, and we obtain for the probability per nucleus of electron production in solid angle $d\omega$ at angle θ (writing θ for θ_-) and in the energy interval dE_- at energy E_-, the following:

$$d\phi_-=\tilde{\phi}d(E_-/k)d\omega_-(\mu/k)^2(1/4\pi)S, \qquad (2)$$

where $\tilde{\phi}=(Z^2/137)(e^2/\mu)^2$, and S contains the angular variation.

$$S=(1+\gamma^2)\ln(2k/\mu)\cdot[\cot^2(\theta/2)/\sin^2(\theta/2)]+f(\gamma,\theta), \qquad (2a)$$

$$f(\gamma,\theta)=(1+\gamma^2)\ln\frac{\gamma}{(1+\gamma)^2}\cdot\frac{\cot^2(\theta/2)}{\sin^2(\theta/2)}+\frac{\gamma(5-2\gamma)}{4\sin^4(\theta/2)}+\frac{\gamma^2-2\ln(1+\gamma)}{\sin^2(\theta/2)}+\frac{\gamma^2\left[\frac{\gamma}{\rho^2}[2\sin^2(\theta/2)+\gamma]-1\right]}{8\sin^6(\theta/2)}+\frac{(1+\gamma)[3\rho^2-\gamma(2+\gamma)]\ln(\rho+\gamma/\rho-\gamma)}{2\rho^3\sin^2(\theta/2)} \qquad (2b)$$

with $\gamma=E_+/E_-$, and $\rho=|\mathbf{k}-\mathbf{p}_-|/E_-=[\gamma^2+4(1+\gamma)\sin^2(\theta/2)]^{\frac{1}{2}}$. We have separated in S the one term depending directly on k; the remainder, $f(\gamma,\theta)$, depends only on the ratio E_-/k. We have plotted f in Fig. 2 as a function of E_-/k for $\theta=45°$, 90°, 135°, and 180°. In addition, Fig. 3 shows S as a function of θ for representative E_-/k and $k=500\mu=255$ Mev.

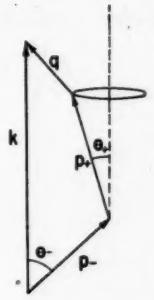

FIG. 1. Momentum diagram illustrating the discussion of the approximate integration.

Restrictions on the range of validity of (2) arise from two sources. The first is in the approximate integration, which, as shown by the reduction from the exact calculation, requires

$$E_-,\ E_+\gg\mu,\quad \theta\gg\mu/E_-. \qquad (3)$$

The second is the effect of screening by atomic electrons. Applying the considerations of Bethe and Heitler,[6] we find that the momentum transfer in a production process is large enough that screening may be neglected, provided

$$\theta\gg[(2\mu E_+/kE_-)(Z^{\frac{1}{3}}/137)]^{\frac{1}{2}}. \qquad (4)$$

The limitation on θ by (4) and by (3) are of the same magnitude for

$$(2E_+E_-/k\mu)\sim 137Z^{-\frac{1}{3}}, \qquad (5)$$

and this will be recognized as the boundary region where screening becomes important in the single differential cross section.[7]

Thus the extension of formula (2) to smaller angles by exact integration, which removes restrictions (3), is valid only for energies for which screening is not important in the single differential cross section. At the higher energies a small-angle formula requires introduction of the atom form factor, which is known only numerically; any but the simplest analytical approximation to the form factor would make it necessary to do all integrals numerically, and at best an analytical result would be much more complicated than (2).

[6] See reference 2, p. 168ff.
[7] See reference 2, p. 197, Eq. (11).

An exception to this generally unpleasant behavior at small angles is the case θ_- (θ in (2)) exactly zero. There the azimuthal dependence of the triple differential cross section disappears, and we get in the high energy, unscreened case simply

$$d\phi_-|_{\theta_-=0}=\bar{\phi}d\omega_-d\left(\frac{E_-}{k}\right)\frac{4}{\pi}\frac{E_-^2}{k^2}$$

$$\times\left(\frac{E_+^2+E_-^2}{\mu^2}\ln\frac{2E_+E_-}{\mu k}-\frac{(E_+-E_-)^2}{2\mu^2}\right). \quad (6)$$

The precise limitations on (6) are

$$E_-,\ E_+\gg\mu,$$
$$(2E_+E_-/k\mu)\ll 137Z^{-\frac{1}{3}}. \quad (7)$$

We see that the forward production emphasizes high energy electrons (similarly positrons) by a factor E_-^2/k^2 modifying a formula otherwise symmetrical in E_- and $k-E_-$. This emphasis must occur since we have seen (Fig. 4) that at large angles low energy particles are relatively more numerous, while the single differential cross section is symmetrical about $E_-=k/2$.

The cross section at large angles is extremely small. For example, if $k=255$ Mev, $\theta=90°$, the cross section per unit solid angle for production of electrons of energy $\geq\frac{1}{2}k$ is from (2) $(Z^2/137)\times(1.6\times10^{-7})$ barn, for Pb 0.8×10^{-5} barn. At 45° and for electrons of energy $\geq0.1k$, it becomes $\sim(Z^2/137)(10^{-4})$ barn, for Pb$\sim5\times10^{-3}$ barn.

For the large momentum changes here considered the modification of the Coulomb field resulting from the finite extent of the nucleus will give an additional very appreciable decrease in the cross section. The effect is estimated in Section IV below.

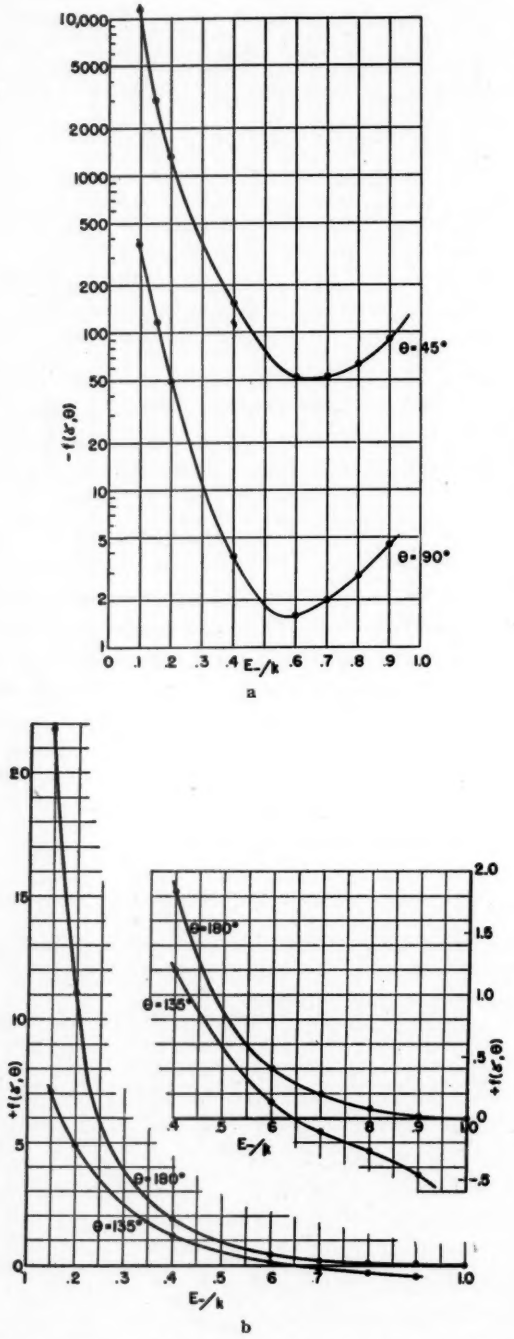

FIG. 2. The auxiliary function $f(\gamma,\theta)$, Eq. (2b) of the text. (a) $-f$ plotted semilogarithmically against E_-/k for $\theta=45°$, 90°. (b) $+f$ plotted linearly against E_-/k for $\theta=135°$, 180°. Insert: the same, with f-scale enlarged five times.

III. BREMSSTRAHLUNG DISTRIBUTION

Pair production and bremsstrahlung are just inverse processes, except that in pair production the initial electronic state is of negative energy. In the bremsstrahlung process, let E_0, p_0, θ_0 refer to the electron's initial energy, momentum $\times c$, and angle relative to the quantum; E, p, θ describe its state after radiating, and k is still the quantum energy. Then, as Bethe and Heitler have shown,[8] the bremsstrahlung cross section is obtained from the pair production by writing E_0 and p_0 for E_-, p_-, $-E$ and $-p$ for E_+, p_+,

[8] See reference 2, §20.

and multiplying by $k^2dk/p_0^2dE_-$ to provide the correct energy density of final states with electron and quantum present rather than electron and positron. It will be noted that following the above prescription the conservation of energy $E_-+E_+=k$ becomes $E_0-E=k$, which is right, and q^2 becomes $(k+p-p_0)^2$, still correct for the square of the momentum transferred to the nucleus. Thus, except for certain square roots of perfect squares taken in deriving (2), which now (notably in the arguments of logarithms) require absolute value signs, the bremsstrahlung angular distribution is obtained from (2) simply by writing $-\gamma$ for γ and (a review of the work shows) $-\rho$ for ρ, where now $\gamma=+E/E_0$ while ρ retains its significance: $\rho=|\mathbf{p}_0-\mathbf{k}|/E_0=[\gamma^2+4(1-\gamma)\sin^2(\theta_0/2)]^{\frac{1}{2}}$. With these definitions and dropping the 0-subscript so that now θ represents the angle of emission of k relative to p_0, we get

$$kd\phi_k=E_0\bar{\phi}d(k/E_0)d\omega_k(\mu/E_0)^2(1/4\pi)T, \quad (8)$$

$$T=(1+\gamma^2)\ln 2E_0/\mu \cdot[\cot^2(\theta/2)/\sin^2(\theta/2)]+g(\theta,\gamma), \quad (8a)$$

$$g(\theta,\gamma)=(1+\gamma^2)\ln\frac{\gamma}{1-\gamma}\cdot\frac{\cot^2(\theta/2)}{\sin^2(\theta/2)} - \frac{\gamma(5+2\gamma)}{4\sin^4(\theta/2)}+\frac{\gamma^2-2\ln(1-\gamma)}{\sin^2(\theta/2)} - \frac{\gamma^2\left\{\frac{\gamma}{\rho^2}[2\sin^2(\theta/2)-\gamma]+1\right\}}{8\sin^6(\theta/2)} - \frac{(1-\gamma)[3\rho^2+\gamma(2-\gamma)]\ln(\rho+\gamma/\rho-\gamma)}{2\rho^3\sin^2(\theta/2)} \quad (8b)$$

$kd\phi_k$ is proportional to the intensity of radiation emitted in energy interval dk at k and in solid angle $d\omega_k$ at angle θ. The angular dependence has again been separated into a term depending on the absolute value of the incident energy (here E_0) and $g(\gamma,\theta)$ which depends only on ratios of energies.

Figure 4 gives $g(\gamma,\theta)$ for four angles and a range of k/E_0, and for $E_0=255$ Mev Fig. 5 shows T as a function of θ for representative quantum energies.

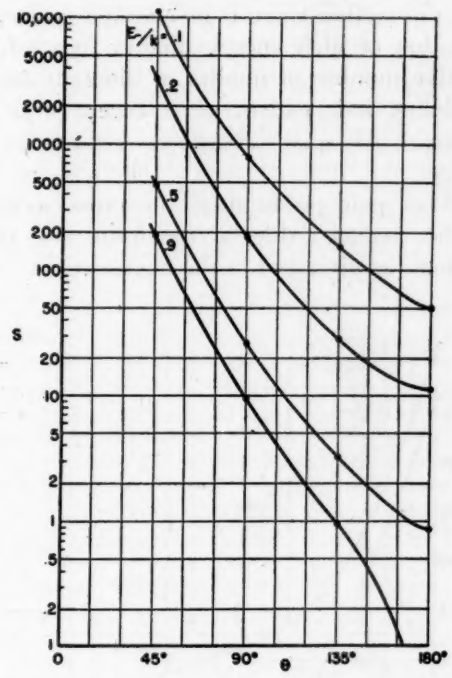

FIG. 3. S of Eqs. (2) and (2a) with $k=500\mu=255$ Mev. The numbers on the curves are E_-/k.

In complete analogy to (3) and (4), the restrictions on (8) are, from the approximate integration

$$E_0,\ E\gg\mu,\quad \theta\gg\mu/E_0, \quad (9)$$

and from screening

$$\theta\gg[(2\mu E/kE_0)(Z^{\frac{1}{3}}/137)]^{\frac{1}{2}}. \quad (10)$$

The cross section for radiation directly forward, corresponding to (6) above, is

$$kd\phi_k|_{\theta=0}=E_0\bar{\phi}d\omega_k d\left(\frac{k}{E_0}\right)\frac{4}{\pi} \times\left(\frac{E_0^2+E^2}{\mu^2}\ln\frac{2E_0E}{\mu k}-\frac{(E_0+E)^2}{2\mu^2}\right), \quad (11)$$

with restrictions

$$E_0,\ E\gg\mu,\quad (2E_0E/\mu k)\ll 137Z^{-\frac{1}{3}}. \quad (12)$$

One finds on comparing (8) and (11) at energies where both are valid that in contrast to

pair production there is no marked preferential radiation of high energy quanta forward. The relative number of quanta of different energies is almost independent of θ, except near 180° where hard quanta become relatively very scarce.

As in pair production, the cross section is further reduced due to the finite size of the nucleus, as discussed in the next section.

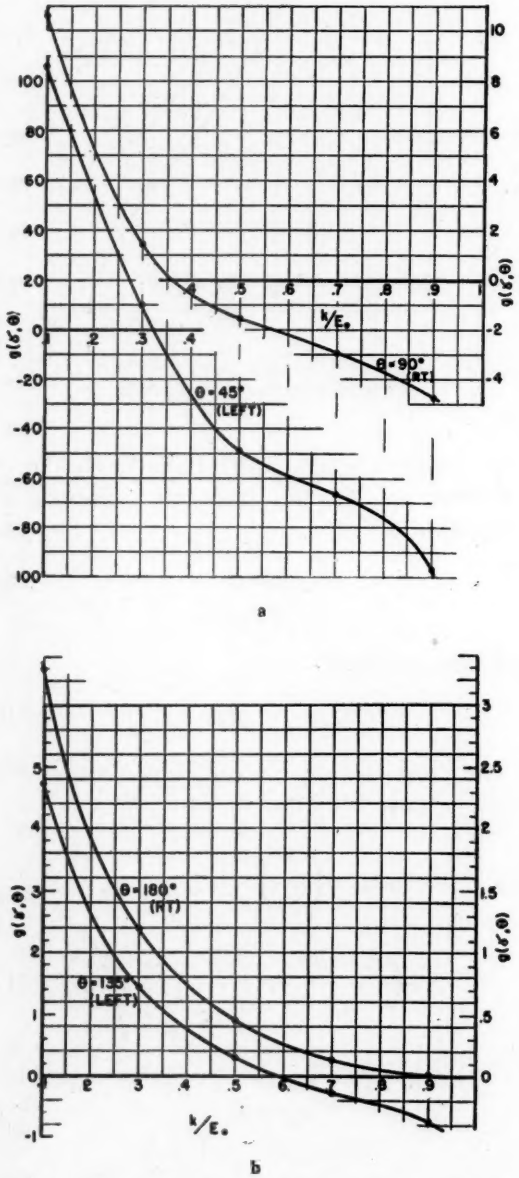

FIG. 4. The auxiliary function $g(\gamma,\theta)$, Eq. (8b) of the text. (a) g *vs.* k/E_0 for $\theta=45°$, 90°. (b) The same for $\theta=135°$, 180°.

It will be seen that while the bremsstrahlung distribution is simply obtained from the pair production, the third related distribution—of scattered radiating electrons—is not. A new integration is required, in which the angles relative to the quantum of both incident and scattered electron are varied, connected, however, by the requirement of fixed angle relative to each other.

IV. EFFECT OF THE FINITE EXTENT OF THE NUCLEUS

By confining ourselves to pair production and bremsstrahlung with large momentum transfer we need not consider screening by atomic electrons. But under this condition the effective impact parameter for both processes becomes of the order of the nuclear radius, and deviations from the Coulomb field on the inner side must be taken into account. For brevity we call the effect inner screening.

The original Bethe-Heitler cross sections are proportional to the square of the matrix element

$$V_q=\int V(\mathbf{r})\exp[i(\mathbf{q}\cdot\mathbf{r}/\hbar c)]d\tau$$

$$=4\pi(\hbar c/q)^2\int\rho(\mathbf{r})\exp[i(\mathbf{q}\cdot\mathbf{r}/\hbar c)]d\tau, \quad (13)$$

with $V(\mathbf{r})$ the potential and $\rho(\mathbf{r})$ the space density of electric charge. (The second well-known form follows from the first by writing $\exp[i(\mathbf{q}\cdot\mathbf{r}/\hbar c)]$ $=-(\hbar c/q)^2\nabla^2\exp[i(\mathbf{q}\cdot\mathbf{r}/\hbar c)]$, and using Green's theorem and Poisson's equation in that order.) Equation (13) is of the form $V_q^{\text{coul}}\cdot F(q)$ where V_q^{coul} corresponds to a pure Coulomb field and gives the usual cross sections, and

$$F(q)=\frac{1}{Ze}\int\rho(\mathbf{r})\exp(i\mathbf{q}\cdot\mathbf{r}/\hbar c)d\tau \quad (14)$$

is the nuclear form factor. The effect of inner screening is thus to multiply the triple differential cross section by the square of (14).

Instead of attempting to integrate these modified cross sections to find the angular distributions with inner screening, we may obtain a fair approximation to the result by multiplying the distributions (2) and (8) by $|F(q)|^2$ at the q

which gives maximum contribution to the unscreened integrals. Unfortunately, as discussed in Section II, there are two such q's, the first when p_+ is parallel to k (in bremsstrahlung p parallel to k) and the second when q itself is a minimum. Calling them q_1 and q_2, respectively, one finds that in pair production $q_1 \simeq q_2$ for much greater ranges of the variables than in bremsstrahlung—in the latter case the approximate equality holds only for large θ and $E \ll E_0$. For this reason we limit ourselves in the following to the case of pair production.

From the definition of q_1 and q_2

$$q_1 = 2E_- \sin(\theta/2),$$
$$q_2 = (k^2 + p_-^2 - 2kp_- \cos\theta)^{\frac{1}{2}} - p_+.$$

In rough approximation, $q_2/q_1 = 1 - [1 - (E_-/k)] \times [1 - \sin(\theta/2)]$. At high k the contribution from around q_1 predominates, but only by virtue of a coefficient $\ln(k/\mu)$, and for quanta of a few hundred Mev or less it is best to use in (14) $\bar{q} = q_1 - (\frac{1}{3})(q_1 - q_2)$

$$\bar{q} = 2E_- \sin(\theta/2)\{1 - \tfrac{1}{3}[1 - (E_-/k)] \times [1 - \sin(\theta/2)]\}. \quad (15)$$

One may expect a relative error in $\bar{q}$

$$\delta\bar{q}/\bar{q} \sim \tfrac{1}{2}[1 - (E_-/k)][1 - \sin(\theta/2)]. \quad (16)$$

It is clear that for suitable angles and energies (16) can be made small, so that a given electron energy and angle correspond in (14) to a quite definite q. The nuclear charge distribution may thereby be explored, but since elastic electron scattering by nuclei gives the same information with less theoretical ambiguity and experimental difficulty we shall not consider this point in detail.

The effect on the pair-production cross section may be estimated sufficiently accurately by taking for the nucleus a uniform sphere of charge of radius R. Equation (14) gives

$$F(q) = (3/\alpha^2)[(\sin\alpha/\alpha) - \cos\alpha], \quad (17)$$

where $\alpha = Rq/\hbar c = R/\lambda$, λ the wave-length $\div 2\pi$ corresponding to the momentum q/c. This $|F(q)|^2$ is plotted semilogarithmically in Fig. 6. To show what α's may be obtained we note that $\hbar c/E_- = 2.0 \times 10^{-13}$ cm for $E_- = 100$ Mev, hence

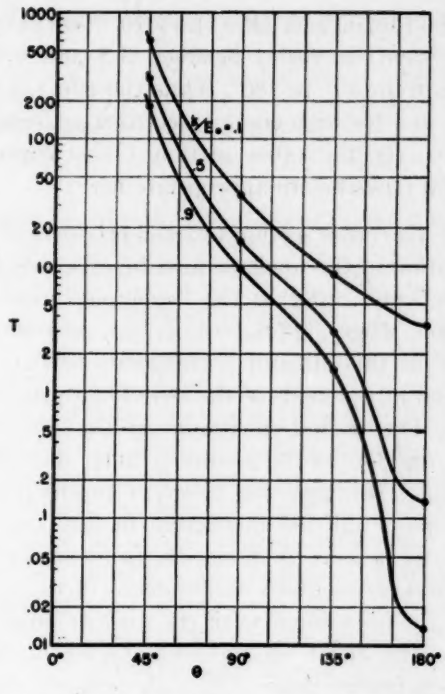

FIG. 5. T of Eqs. (8) and (8a), with $E_0 = 500\mu = 255$ Mev. The numbers on the curves are k/E_0.

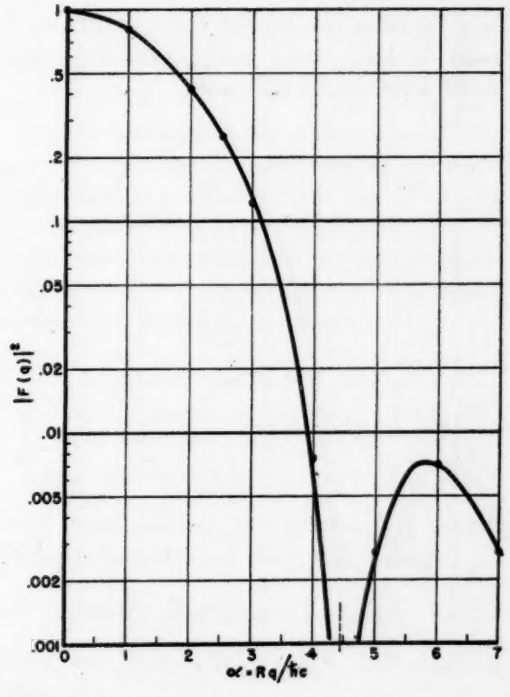

FIG. 6. $|F(q)|^2$ from Eq. (17), plotted semilogarithmically against $\alpha = Rq/\hbar c$, where R is the nuclear radius and q/c the momentum transfer.

for the Pb nucleus ($R=(1.5\times10^{-13}$ cm$)A^{\frac{1}{3}}=8.9\times10^{-13}$ cm) α varies between 3.5 and 9 as θ ranges from 45° to 180°. Thus the effect is very large, and for high energy electrons a strong decrease over the cross section (2) is expected. Several remarks are appropriate here:

(a) The cross section for pair production with excitation of the nucleus must be expected to be of the same order as the "coherent" pair production when $|F(q)|^2\sim1/Z$, for a reduction factor of this amount corresponds to pair production in the fields of the individual protons.

(b) The second maximum in the $|F(q)|^2$ of Fig. 6 is due to the assumed sharp edge of the nucleus. Although the coherent production for such q's is half the incoherent or less, one may hope to observe a deviation from smooth decrease experimentally and correlate its magnitude with the indefiniteness of the nuclear boundary.

(c) The effect on the form factor of an increased proton density near the edge of the nucleus has been shown to be slight, and there seems small chance to detect such an increase by pair-production measurements.

(d) Since single meson production by quanta will not be coherent, for detection of mesons the decrease in large angle pair production caused by inner screening is pure gain.

V. MESON DETECTION

Estimates[9] of the total cross section per nucleon for single meson production by quanta of energy ~250 Mev are 5×10^{-29} cm² or greater. For such energies the production will occur over quite a large solid angle, and we may take as a minimum for the cross section per unit solid angle at $90°\sim10^{-30}$ cm². The Pb nucleus thus provides a cross section of 10^{-28} cm² or more. We may compare this with the analogous pair-production cross section from Section II of 0.8×10^{-29} cm² per unit solid angle at 90°, for $k=255$ Mev, and for electrons of energy $\geq\frac{1}{2}k$. Adding in positrons of the same energy gives a cross section of a few $\times10^{-29}$ cm². (Electrons and positrons of lower energy can easily be screened from mesons by magnetic selection.) Considering inner screening this cross section drops to less than 10^{-30} cm². We conclude that pair production will not directly produce a background nearly as large as the expected meson yield.

VI. ACKNOWLEDGMENT

I wish to thank Professors Robert R. Wilson and H. A. Bethe for suggesting this work, and Professor Bethe for his continuing interest and very helpful advice.

[9] See e.g., L. W. Nordheim and G. Nordheim, Phys. Rev. **54**, 254 (1938).

Enumeration of Potentials for Which One-Particle Schroedinger Equations Are Separable

L. P. EISENHART
Fine Hall, Princeton, New Jersey
(Received March 2, 1948)

IN 1891 Stäckel[1] solved the problem of determining the quantities H_i in the Hamiltonian equation

$$\sum_i (1/H_i^2)(\partial\theta/\partial x_i)^2 + V - \alpha_1 = 0,$$

where α_1 is a constant, so that the variables are separable, that is, so that the solution is of the form $\theta = \sum_i X_i$, where X_i is a function of x_i alone. The complete solution is: given any n^2 functions φ_{ij}, where φ_{ij} is a function of x_i alone, φ^{ij} is the cofactor of φ_{ij} in the determinant $\varphi(\neq 0)$ of the functions φ_{ij}; then $H_i^2 = \varphi/\varphi^{ij}$. The potential function V in any such coordinate system is

$$V = \sum_i (f_i(x_i)/H_i^2), \tag{1}$$

when f_i is an arbitrary function of x_i.

In 1927 Robertson[2] showed that for the Schroedinger equation

$$\sum_i (1/H)(\partial/\partial xi)[(H/H_i^2)(\partial\psi/\partial xi)] + k^2(E-V)\psi = 0,$$
$$H = \prod_i H_i, \quad (i = 1, \cdots, n),$$

to admit by separation of the variables a solution of the form $\prod_i X_i$, where X_i is a function of x_i alone, the functions H_i must be of the Stäckel form, the potential function be of the form (1), and the Stäckel determinant φ be such that

$$\varphi = \prod_i (H_i/\theta_i), \tag{2}$$

where θ_i is a function of x_i at most.

In 1934 I showed[3] that a necessary and sufficient condition that functions H_i be of the Stäckel form is that the following equations be satisfied:

$$(\partial^2 \log H_i^2/\partial x_i \partial x_j) + (\partial \log H_i^2/\partial x_j)(\partial \log H_j^2/\partial x_i) = 0, \quad (i \neq j)$$

$$\frac{\partial^2 \log H_i^2}{\partial x_j \partial x_k} - \frac{\partial \log H_i^2}{\partial x_j}\frac{\partial \log H_i^2}{\partial x_k} + \frac{\partial \log H_i^2}{\partial x_j}\frac{\partial \log H_j^2}{\partial x_k} + \frac{\partial \log H_i^2}{\partial x_k}\frac{\partial \log H_k^2}{\partial x_j} = 0, \quad (i, j, k \neq).$$

Proceeding from this result I derived all the real forms of H_i for Euclidean 3-space, ten in number in addition to the Cartesian case $H_i = 1$; and showed that the condition (2) is automatically satisfied in Euclidean 3-space. In a note in this journal[4] I listed the ten possible forms of H_i.

For each of the ten possible forms Eq. (1) gives the expression for the potential function V in the particular coordinates x_i of each canonical form. Recently Professor Wigner raised the question as to whether it is possible to obtain the expression for V in Cartesian coordinates in each of the ten cases, as a possible aid to those making an investigation of particular problems. This paper gives an answer to this question, deriving the possible forms of V in Cartesian coordinates x, y, z.

What follows after the expressions for the H's in each case are the expressions of Cartesian coordinates x, y, z in terms of the corresponding x_i. Then follow xi as functions of x, y, z, except in the last two cases where a general solution is impossible. For the possible cases the form of V is given in Cartesian coordinates.

I. $H_1^2 = 1, \quad H_2^2 = x_1^2, \quad H_3^2 = 1,$
$x = x_1 \cos x_2, \quad y = x_1 \sin x_2, \quad z = x_3,$
$x_1 = (x^2+y^2)^{\frac{1}{2}}, \quad \tan x_2 = y/x, \quad x_3 = z,$
$V = \varphi[(x^2+y^2)^{\frac{1}{2}}] + [\psi(y/x)/(x^2+y^2)] + f(z),$

where here, and in what follows, φ, ψ, and f are arbitrary functions of their arguments.

II. $H_1^2 = H_2^2 = \frac{1}{2}a^2(\cosh 2x_1 - \cos 2x_2), \quad H_3^2 = 1,$

where here, and in later cases, a is an arbitrary constant.

[1] Paul G. Stäckel, Ueber die Integration des Hamilton—Jacobischen Differential gleichunger Mittelst separation der variabeln, Habilitationschrift, Halle.
[2] H. P. Robertson, "Bemerkung über separierbare Systeme in der Wellenmechanik," Math. Ann. **98**, 749–752 (1927).
[3] L. P. Eisenhart, "Separable systems of Stäckel," Ann. Math. **35**, 284–305 (1934).
[4] L. P. Eisenhart, "Separable systems in Euclidean 3-space," Phys. Rev. **45**, 427–428 (1934).

$x=a\cosh x_1\cos x_2$, $y=a\sinh x_1\sin x_2$, $z=x_3$,
$\sinh^2 x_1=A+B$, $\sin^2 x_2=-A+B$, $x_3=z$,

where

$$A=(1/2a^2)(x^2+y^2-a^2),\quad B=(A^2+(y^2/a^2))^{\frac{1}{2}},$$
$$V=[a^2/(A^2+(y^2/a^2))^{\frac{1}{2}}]\times[\varphi(A+B)+\psi(-A+B)]+f(z).$$

III. $H_1^2=H_2^2=x_1^2+x_2^2$, $H_3^2=1$,
$x=\frac{1}{2}(x_1^2-x_2^2)$, $y=x_1x_2$, $z=x_3$,
$x_1^2=x+(y^2-x^2)^{\frac{1}{2}}$, $x_2^2=-x+(y^2-x^2)^{\frac{1}{2}}$, $x_3=z$,
$V=[1/2(y^2-x^2)^{\frac{1}{2}}][\varphi(x+(y^2-x^2)^{\frac{1}{2}})^{\frac{1}{2}}+\psi(-x+(y^2-x^2)^{\frac{1}{2}})^{\frac{1}{2}}]+f(z)$.

Before proceeding with the other cases we remark that it is evident from the expressions in Cases I, II, and III that, if one puts $z=x_3=0$, one has cases of separable systems in Euclidean 2-space. It can be shown that these are the only possibilities.

IV. $H_1^2=1$, $H_2^2=x_1^2$, $H_3^2=x_1^2\sin^2 x_2$,
$x=x_1\sin x_2\cos x_3$, $y=x_1\sin x_2\sin x_3$, $z=x_1\cos x_2$,
$x_1=r=(x^2+y^2+z^2)^{\frac{1}{2}}$, $\cos x_2=z/r$, $\tan x_3=y/x$,
$V=\varphi(r)+(1/r^2)\psi(z/r)+[f(y/x)/(x^2+y^2)]$.

V. $H_1^2=H_2^2=x_3^2[k^2cn^2(x_1,k)+k'^2cn^2(x_2,k')]$, $H_3^2=1$,

where the constants k and k' of the elliptic functions are in the relation $k^2+k'^2=1$.[5]

$$x=x_3dn(x_1,k)sn(x_2,k'),$$
$$y=x_3sn(x_1,k)dn(x_2,k'),$$
$$z=x_3cn(x_1,k)cn(x_2,k').$$

Making use of the relations

$$sn^2+cn^2=1,\quad dn^2+k^2sn^2=1,\quad dn^2-k^2cn^2=k'^2,$$

we obtain from the above

$$k^2cn^2(x_1,k)=A+B,\quad k'^2cn^2(x_2,k')=-A+B,\quad x_3^2=r^2,$$

where

$$A=(1/2r^2)(k^2x^2-k'^2y^2+(k^2-k'^2)z^2),$$
$$B=(A^2+(k^2k'^2z^2/r^2)^{\frac{1}{2}},$$
$$V=(1/2r^2B)[\varphi((A+B)^{\frac{1}{2}}/k)+\psi(-A+B)^{\frac{1}{2}}/k')]+f(r).$$

[5] Cf. Benjamin O. Peirce, *A Short Table of Integrals* (Ginn and Company, Boston, 1929), pp. 84–87.

VI. $H_1^2=H_2^2=x_1^2+x_2^2$, $H_3^2=x_1^2x_2^2$,
$x=x_1x_2\cos x_3$, $y=x_1x_2\sin x_3$, $z=\frac{1}{2}(x_1^2-x_2^2)$,
$x_1^2=r+z$, $x_2^2=r-z$, $\tan x_3=y/x$,
$V=(1/2r)[\varphi((r+z)^{\frac{1}{2}})+\psi((r-z)^{\frac{1}{2}})]+[1/(x^2+y^2)]f(y/x)$.

VII. $H_1^2=H_2^2=a^2(\sinh^2 x_1+\sin^2 x_2)$,
$H_3^2=a^2\sinh^2 x_1\sin^2 x_2$,
$x=a\sinh x_1\sin x_2\cos x_3$, $y=a\sinh x_1\sin x_2\sin x_3$,
$z=a\cosh x_1\cos x_2$,
$\sinh^2 x_1=A+B$, $\sin^2 x_2=-A+B$, $\tan x_3=y/x$,

where

$$A=(1/2a^2)(r^2-a^2),\quad B=(A^2+(x^2+y^2)/a^2)^{\frac{1}{2}},$$
$$V=(1/2a^2B)[\varphi((A+B)^{\frac{1}{2}})+\psi((-A+B)^{\frac{1}{2}})]+f(y/x)/(x^2+y^2).$$

VIII. $H_1^2=H_2^2=a^2(\sinh^2 x_1+\cos^2 x_2)$,
$H_3^2=a^2\cosh^2 x_1\sin^2 x_2$,
$x=a\cosh x_1\sin x_2\cos x_3$, $y=a\cosh x_1\sin x_2\sin x_3$,
$z=a\sinh x_1\cos x_2$,
$\cosh^2 x_1=A+B$, $\cos^2 x_2=-A+B$, $\tan x_3=y/x$,

where

$$A=(1/2a^2)(r^2-a^2),\quad B=(A^2+(z^2/a^2))^{\frac{1}{2}},$$
$$V=(1/2a^2B)[\varphi((A+B)^{\frac{1}{2}})+\psi((-A+B)^{\frac{1}{2}})]+f(y/x).$$

IX. $H_i^2=[(x_i-x_j)(x_i-x_k)/f(x_i)]$,
$f(x_i)=4(\alpha-x_i)(\beta-x_i)(\gamma-x_i)$, $(i,j,k\neq)$,
$x^2=[\prod_i(\alpha-x_i)]/(\alpha-\beta)(\alpha-\gamma)$,
$y^2=[\prod_i(\beta-x_i)]/(\beta-\alpha)(\beta-\gamma)$,
$z^2=[\prod_i(\gamma-x_i)]/(\gamma-\alpha)(\gamma-\beta)$,

where $\alpha>x_1>\beta>x_2>\gamma>x_3$. From these expressions we have

$$x^2/(\alpha-x_i)+y^2/(\beta-x_i)+z^2/(\gamma-x_i)=1\quad(i=1,2,3);$$

consequently, the x_i are roots of the cubic

$$t^3-at^2+bt-c=0,\qquad\text{(i)}$$

where

$$a=\alpha+\beta+\gamma-r^2,$$
$$b=\alpha\beta+\beta\gamma+\gamma\alpha-(\beta+\gamma)x^2-(\gamma+\alpha)y^2-(\alpha+\beta)z^2,\qquad\text{(ii)}$$
$$c=\alpha\beta\gamma-\beta\gamma x^2-\gamma\alpha y^2-\alpha\beta z^2.$$

If in Eq. (i) we put

$$t=u+(a/3)\qquad\text{(iii)}$$

the resulting equation in (ii) is

$$u^3-pu^2+q=0, \quad p=\tfrac{1}{3}a^2-b, \qquad q=-(2/27)a^3+(ab/3)-c. \tag{iv}$$

For $q=0$, which is an equation of the third degree in x^2, y^2, z^2, the expressions for x_i are

$$x_1=(a/3)+(p)^{\frac{1}{2}}, \quad x_2=a/3, \quad x_3=(a/3)-(p)^{\frac{1}{2}};$$

p must be positive. Also there are the conditions $\alpha>x_1>\beta>x_2>\gamma>x_3$ to be satisfied. In this case

$$H_1^2=2p/f(x_1), \quad H_2^2=-p/f(x_2), \quad H_3^2=2p/f(x_3),$$

where $f(x_i)=4(\alpha-x_i)(\beta-x_i)(\gamma-x_i)$, and thus $f(x_1)$ and $f(x_3)$ are positive, and $f(x_2)$ negative,

$$V=(1/p)[(\varphi_1 f(x_1)/2)-\varphi_2 f(x_2)+(\varphi_3 f(x_3)/2)],$$

where φ_i is an arbitrary function of x_i.

When p and q are different from zero the cubic equation (i) above, having three real solutions, $x_1>x_2>x_3$, is irreducible, that is, it is impossible to find x_i as functions of x, y, and z. However for particular numerical values of p and q, such that p and $(p^3/27)-(q^2/4)$ are positive, real solutions of Eq. (iv) are[6]

$$2(p/3)^{\frac{1}{2}}\cos(\theta/3), \quad 2(p/3)^{\frac{1}{2}}\cos[(\theta+2\pi)/3], \quad 2(p/3)^{\frac{1}{2}}\cos[(\theta+4\pi)/3],$$

where θ is given by

$$\cos\theta=-(3q/2p)(3/p)^{\frac{1}{2}}.$$

By means of a table of cosines θ can be found, and then the numerical values of the three roots of Eq. (iv). This process yields a numerical expression for V involving three arbitrary functions of constants x_i.

X. $$H_i^2=(x_i-x_j)(x_i-x_k)/f(x_i), \qquad f(x_i)=4(\alpha-x_i)(\beta-x_i),$$

where $x_1>\alpha>x_2>\beta>x_3$.

$$x=(x_1+x_2+x_3-\alpha-\beta)/2, \qquad y^2=[\textstyle\prod_i(\alpha-x_i)]/(\beta-\alpha), \qquad z^2=[\textstyle\prod_i(\beta-x_i)]/(\alpha-\beta).$$

From these expressions we have

$$y^2/(\alpha-x_i)+z^2/(\beta-x_i)=2x-x_i, \quad (i=1,2,3).$$

Consequently, the roots x_i are solutions of an equation of the form (iv), where in this case

$$a=-(2x+\alpha+\beta), \quad b=\alpha\beta+2x(\alpha+\beta)-y^2-z^2, \qquad c=\beta y^2+\alpha z^2-2x\alpha\beta.$$

Unless $q=0$, the equation is irreducible. The procedure in this case is the same as with type IX where now a, b, c are the new functions of x, y, and z.

The foregoing results are the solution of the problem in one system of Cartesian coordinates. They are such that

$$H_i^2=(\partial x/\partial x_i)^2+(\partial y/\partial x_i)^2+(\partial z/\partial x_i)^2 \equiv\sum(\partial x/\partial x_i)^2,$$
$$\sum(\partial x/\partial x_i)(\partial x/\partial x_j)=0 \quad (i\neq j),$$

where $\sum$ denotes summation over x, y, and z.

There is, however, no preferred system of Cartesian coordinates. If x, y, z and $\bar{x}, \bar{y}, \bar{z}$ are two such systems, they are related as follows:

$$x=a_1{}^1\bar{x}+a_2{}^1\bar{y}+a_3{}^1\bar{z}+b_1,$$
$$y=a_1{}^2\bar{x}+a_2{}^2\bar{y}+a_3{}^2\bar{z}+b_2,$$
$$z=a_1{}^3\bar{x}+a_2{}^3\bar{y}+a_3{}^3\bar{z}+b_3,$$

where the a's and b's are constants, the former subject to the conditions

$$\textstyle\sum_i a_j{}^i a_k{}^i=\delta_{jk}, \quad \sum_i a_i{}^j a_i{}^k=\delta^{jk},$$

where

$$\delta_{jk}, \ \delta^{jk} \text{ are 1 for } j=k; \ 0 \text{ for } j\neq k.$$

In view of these conditions we have

$$H_i^2=\sum(\partial x/\partial x_i)^2=\sum(\partial\bar{x}/\partial x_i)^2,$$

$$0=\sum(\partial x/\partial x_i)(\partial x/\partial x_j) =\sum(\partial\bar{x}/\partial x_i)(\partial\bar{x}/\partial x_j) \quad (i\neq j).$$

Accordingly, the general form of V is obtained by substituting the above expressions for x, y, z, interims of $\bar{x}$, $\bar{y}$, and $\bar{z}$, in the previous results.

[6] Cf. H. B. Fine, *College Algebra* (Ginn and Company, Boston, 1905), pp. 483–491.

Waves and Electrons Traveling Together—A Comparison between Traveling Wave Tubes and Linear Accelerators

L. BRILLOUIN
Cruft Laboratory, Harvard University, Cambridge, Massachusetts
(Received February 7, 1948)

A general theory is needed that would include both extreme cases of traveling wave amplifiers and linear accelerators without introducing any restriction on the magnitudes of either fields or space charge. A special case is given as an example and represents a curious sort of electromagnetic shock waves.

I. GENERAL DISCUSSION

THERE is a variety of structures where the electronic engineer uses a flow of electrons and an electromagnetic wave traveling in the same direction with the same velocity. Such is the case in all the "traveling wave" tubes, and in many other structures with drifting electrons. The multicavity magnetron has many points in common with the traveling wave devices, but for the fact that the magnetic field bends the trajectories and the cavities slow down the propagation of electric fields.

On quite a different scale, waves and particles (ions) traveling together are found in most large scale modern accelerators. Whenever the word "synchro" is used in the title, it simply means some device of this type; synchro-betatron, synchro-cyclotron, etc., are well-known examples of the fact. As for the linear accelerators, they represent a structure exactly similar to the traveling wave amplifier tube, but for a different scale.

A comparison of these two classes of devices immediately leads to the question: how is it possible that they be used for exactly opposite purposes? (A) In the traveling wave amplifiers, or the magnetrons, the synchronization of waves and electrons results in an energy transfer from the electrons to the wave and a powerful amplification of the wave. (B) Linear accelerators and "synchro-" devices are built for the opposite purpose, namely, an energy transfer from the wave to the particles, resulting in an acceleration of the ions.

How is this apparent contradiction to be solved? The answer is double: traveling wave tubes work with high space charge and weak waves, the velocity of the wave being maintained constant. "Synchro-" devices, on the contrary, use very low space charge and high power waves, the velocity of the waves being progressively increased.

In the first case, theory and experiment show that the net result is a light bunching of the electrons in the beam and a large amplification of the wave. In the second case, a strong bunching of the particles is soon obtained, the ion bunches being afterward accelerated when the wave velocity is increased.

This confronts the theoretician with a very interesting task of discussing in general terms, without all the approximations used by the engineers, a problem of waves and charged particles traveling together, when both the wave and the space-charge density may be large.

When an attempt is made at such a theoretical discussion, two points appear clearly of importance: *I.* Means providing for the lateral stability of the beam are essential, in order to prevent electrons (or ions) from escaping sidewise. *II.* The whole problem with space charge is very strongly non-linear. The two extreme cases (A) and (B) correspond to simple approximations that allow for a reduction to linear equations.

Many non-linear problems have general characteristics in common; a final stage of the motion is reached that may be very unsensitive to the initial conditions. The question of whether such a stable final motion can be found in the present problem will now be discussed, and a composite stable wave with space charge suggested for that purpose.

2. SLOW GUIDED WAVE

Let us first consider a *TM* wave propagating along a suitable wave guide, with a velocity lower

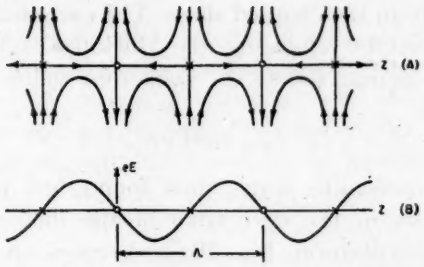

FIG. 1. ○—stable positions; ×—unstable positions along the Z axis.

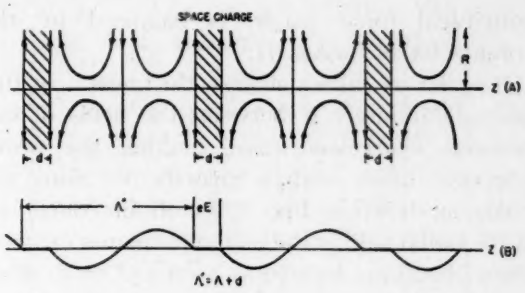

FIG. 2.

than c, and no space charge. The field distribution in space is shown on Fig. 1A, while Fig. 1B represents the intensity of the E_z field along the z axis, as a function of z. Let us now introduce charged particles e, and assume the arrows to show the direction of the force eE acting on the moving particles e of the beam. As long as longitudinal motions along the axis only are considered, the positions marked with a circle are stable positions and those marked with a cross are unstable. But if one looks at the upper drawing of Fig. 1A, he immediately notices that for transverse motions the crosses are stable and the circles unstable. This first discussion shows that a complete stability of the composite system (wave plus particles) cannot be achieved unless some special means are provided to insure transverse stability of the beam. Transverse stability may result from magnetic forces, as in the betatron or synchrotron; it can also be obtained in the case of a linear accelerator by using a longitudinal magnetic field or a system of electrostatic lenses. We shall consider the case of a stabilizing longitudinal magnetic field H as a workable theoretical problem (although in many practical problems the field strength needed for stability might be impossible to obtain!).

For a TM wave without space charge, propagating in the z direction with a velocity $W<c$, the fields are given by the following formulae

$$
\begin{aligned}
&K^2=\omega^2[(1/W^2)-(1/c^2)]=4\pi^2[(1/\Lambda^2)-(1/\lambda^2)]\\
&\Lambda=2\pi(W/\omega)=\text{wave-length of the slow wave},\\
&\lambda=2\pi(c/\omega),\\
&E_z=AJ_0(jKr)\exp\{j\omega[t-(z/W)]\},\\
&E_r=A(\omega/KW)J_1(jKr)\exp\{j\omega[t-(z/W)]\}\\
&\quad\approx Aj(\omega/2W)r\exp\{j\omega[t-(z/W)]\}\\
&\quad\text{for small } Kr\ (J_0J_1,\ \text{Bessel functions})
\end{aligned}
\tag{1}
$$

in the case of circular symmetry. In some instances it may be found convenient to refer the wave to a frame of reference moving with the velocity W, and with respect to which the wave is at rest. This can be obtained by a relativistic transformation, or by taking

$$
\begin{aligned}
&\omega=0,\quad W_0=0,\quad \Lambda=\Lambda_0 \text{ finite},\quad \lambda=\infty,\\
&\qquad K=K_0=2\pi/\Lambda_0,\\
&E_{0z}=A_0J_0(jK_0r)\exp(-jK_0z),\\
&E_{0r}=A_0J_1(jK_0r)\exp(-jK_0z)\\
&\qquad\approx\tfrac{1}{2}A_0jK_0r\exp(-jK_0z)
\end{aligned}
\tag{2}
$$

in our general formulae (1). The radial field E_r (or E_{0r}) is proportional to the radial distance r from the z axis, so long as Kr remains small. For larger distances, the J_1 Bessel function is needed.

We shall discuss in the next section the properties of a composite wave, carrying a certain amount of space charge, and we shall limit our problem to the case of a wave of small radius R, where the preceding approximation can be used without practical error.

According to the preceding remarks, a constant longitudinal magnetic field shall be used to stabilize the space-charge.

3. SPACE-CHARGE DISTRIBUTION IN THE BEAM WITH MAGNETIC STABILIZATION

This problem has a well-known solution;[1] with a uniform space-charge density ρ rotating about the axis with a constant angular velocity ω_H, and giving a radial distribution of electric field E_r,

$$
\begin{aligned}
&\omega_H=-\tfrac{1}{2}\mu_0(e/m)H,\quad \rho=2\epsilon_0(m/e)\omega_H^2,\\
&E_r=(m/e)\omega_H^2r=\tfrac{1}{4}(\mu_0H)^2(e/m)r.
\end{aligned}
\tag{3}
$$

The radial force eE_r on the moving particles plus

[1] L. Brillouin, Phys. Rev. **67**, 260 (1945).

centrifugal force $m\omega_H^2 r$, is balanced by the Lorentz force $+\mu_0 e\omega_H r H$.

Now let us take a slice of thickness d in this beam, and insert it between the fields of our previous chargeless wave, making the whole structure move with a velocity W along the z axis, as shown on Fig. 2. We obtain continuity of the radial field in the boundary planes (at $t=0$, these planes are located at $z=0$ and $z=d$) when we take

$$\tfrac{1}{2}Aj(\omega/W)=\tfrac{1}{4}(\mu_0 H)^2(e/m), \qquad (4)$$
$$A=-\tfrac{1}{2}(eW/m\omega)j(\mu_0 H)^2.$$

The radial fields are matched across the boundary planes, when the beam is fine enough, and $KR\ll 1$.

The *composite wave* represented in Fig. 2 is *stable*, and propagates along the z axis with the velocity W. Its wave-length is

$$\Lambda'=\Lambda+d, \qquad (5)$$

and its total current averages

$$I=\rho W(d/\Lambda')\pi R^2. \qquad (6)$$

The magnitude H of the stabilizing magnetic field determines the value of the electric field in the chargeless region and also the space-charge density in the charged slices. The current can be adjusted by changing the thickness d of the space-charge slices. Its maximum value is, of course,

$$I_{\max}=\rho W\pi R^2. \qquad (7)$$

The composite wave thus found has discontinuities in the derivative of the longitudinal field distribution (Fig. 2B) and represents a sort of *electromagnetic shock wave*. It yields a rigorous solution of the wave equation with space-charge and represents a generalization of the solutions obtained for the two extreme special cases of the traveling wave amplifier or the linear accelerator. The solution obtained here should correspond to the final stage of complete bunching of the particles by the wave, after oscillations of the particles about their equilibrium positions (the circles of Fig. 1) have died out, and the field rearrangements have been completed.

Of course, the solution is valid only at a certain distance of the boundary of the wave guide, and would be seriously distorted in the neighborhood of the boundary, according to the type of guide structure used to slow down the waves.

PHYSICAL REVIEW VOLUME 74, NUMBER 1 JULY 1, 1948

On the Neutron-Proton Force*

JOHN M. BLATT
Laboratory for Nuclear Science and Engineering, Massachusetts Institute of Technology, Massachusetts
(Received March 22, 1948)

IT has been pointed out[1] that neutron-proton scattering experiments at energies below about 10 Mev do not give any *detailed* information about the neutron-proton force. They only determine the strength and range of the force, not its exact distance dependence.

J. Schwinger[2] has developed a powerful variational approach to scattering theory. This method, applied to the case of the scattering of neutrons by protons, leads to great simplifications in the analysis of the experiment. Schwinger was able to prove rigorously that to a good approximation the shape of the well does not matter for the scattering. The well is described phenomenologically by the scattering length[3] to which it gives rise (evaluated at zero energy) and by an *equivalent range*, r. This equivalent range depends both upon the width and the depth of the well, becoming smaller as the well is made deeper. For a square well of range b, the equivalent range r equals b if the depth of the well is such as to give a resonance level in the scattering exactly at zero energy. For the triplet state, therefore, $r<b$, for the singlet state, $r>b$. It is the great advantage of this analysis, how-

* The research described in this article was supported in part by Contract N5ori-78, U. S. Navy Department.
[1] J. Smorodinsky, J. Phys. U.S.S.R. **8**, 219 (1944); **11**, 195 (1947).
[2] J. Schwinger, Phys. Rev. **72**, 742 (1947).
[3] E. Fermi and L. Marshall, Phys. Rev. **71**, 66 (1947).

ever, that we are *not* required to refer everything back to a square well. On the contrary, we can analyze the scattering experiments in order to find the equivalent ranges in the triplet and singlet states, without knowing the well shape. Of course, if we have reason to suspect (from some other evidence) that a particular well shape is the one realized in nature, then we can very easily find the depth and range of this particular well necessary to give the observed scattering length and equivalent range. The present work is based upon this method. It will be reported more fully following publication of Schwinger's basic work.

Schwinger's analysis shows that the phase-shift is given by

$$k\cot\delta=-a^{-1}+(\tfrac{1}{2})rk^2 \\ +\text{terms of order } (r^3k^4). \quad (1)$$

The notation is as follows:

$k=Mv/2h$ = wave number of the neutron in the center-of-gravity system,

a = scattering length,[3] (positive for a bound state) evaluated at zero energy,

r = effective range.

In the *triplet state*, there exists a relation between the scattering length a_t and the effective triplet range r_t since we know the binding energy of the deuteron. This relation is

$$(a_t)^{-1}=\alpha[1-(\tfrac{1}{2})r_t\alpha \\ +\text{terms of order } (r_t\alpha)^2], \quad (2)$$

where $\alpha=2.29\times10^{12}$ cm^{-1} is the reciprocal "radius of the deuteron." The effective triplet range r_t depends upon the range and depth of the nuclear force in the triplet state; the latter two are related through the binding energy of the deuteron. Figure 1 shows the resulting relation between the range b of the force and the effective triplet range r_t if a square well shape is assumed for the distance dependence of the force. It will be seen that b/r_t approaches unity as r_t approaches zero.

As regards the *singlet state*, we know that the singlet scattering length a_s is negative (virtual state) and the effective singlet range r_s is intrinsically positive. For a square well shape we have the relation

$$b\cong r_s[1+(4/\pi^2)(r_s/a_s)]. \quad (3)$$

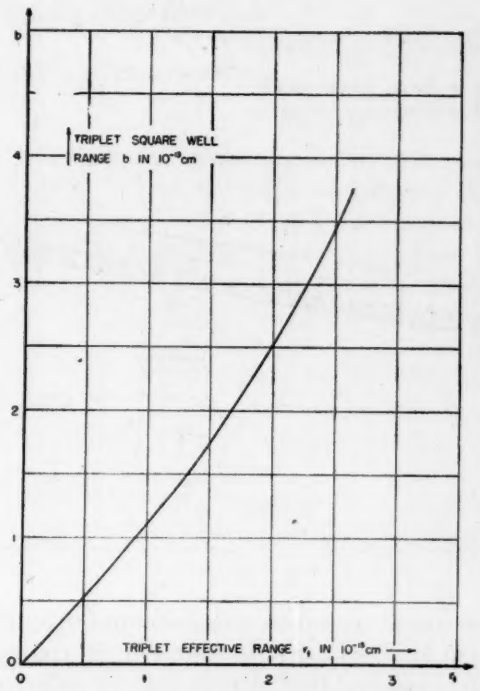

FIG. 1. Abscissa: effective range in the triplet state. Ordinate: the square-well range corresponding to this effective range. The depth of the square well is adjusted for each range to give the observed binding energy of the deuteron.

This is a small correction (about 5 percent for $r_s=2.6\times10^{-13}$ cm) in the negative direction (a_s is negative).

The magnitude of the higher terms in (1) and (2) depends upon the shape of the well. The terms are small if the potential falls off sharply outside its range, large if there is a long tail.

If we neglect the higher order terms, the neutron-proton cross section implied by (1) is

$$\sigma=\tfrac{3}{4}(4\pi)[(-a_t^{-1}+\tfrac{1}{2}r_tk^2)^2+k^2]^{-1} \\ +\tfrac{1}{4}(4\pi)[(-a_s^{-1}+\tfrac{1}{2}r_sk^2)^2+k^2]^{-1}. \quad (4)$$

r_t, r_s and a_s are independent constants; a_t is given by (2).

The experiments[4] are not sufficiently accurate to test the validity of Eq. (4). In particular, the assertion of Bohm and Richman[5] that a long-tailed well is necessary to fit the data is true only if one insists (as they did) upon assuming the neutron-proton range to equal the proton-proton range in both spin states. There seems to

[4] C. L. Bailey, W. E. Bennet, T. Bergstrahl, R. G. Nucholls, H. T. Richards, and J. H. Williams, Phys. Rev. **70**, 583 (1946); D. Frisch, Phys. Rev. **70**, 589 (1946).

[5] D. Bohm and C. Richman, Phys. Rev. **71**, 567 (1947).

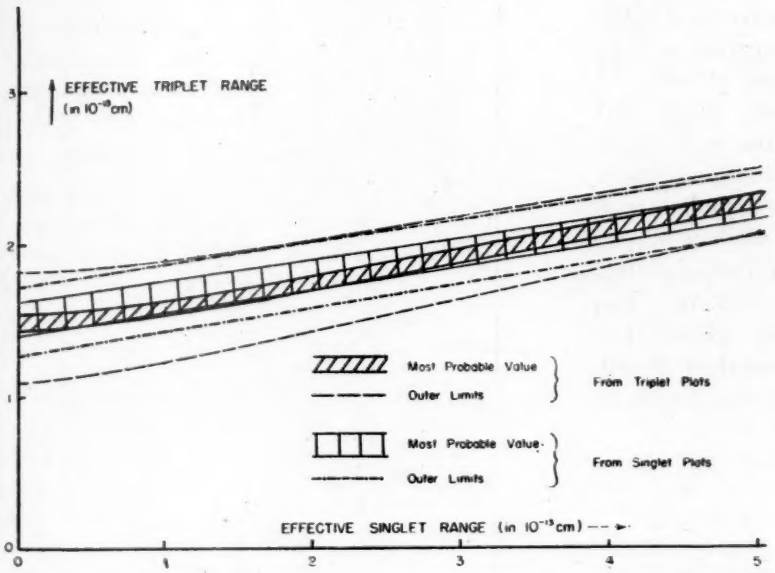

FIG. 2. Abscissa: effective range in the singlet state. Ordinate: effective range in the triplet state. The curves define the regions of best fit to the neutron-proton scattering data at energies below 6 Mev. The singlet plots use energies below about 2 Mev, the triplet plots use energies between 1 Mev and 6 Mev, approximately.

be no cogent reason for this assumption, and the present analysis did not use it. On the contrary, *we assumed that the potential falls off sufficiently sharply so that the higher terms in (1) can be neglected.* (They are completely negligible for a square well shape at energies below 10 Mev.)

Our analysis of the scattering data proceeds as follows:

I. Singlet plots.—Assume a value for r_t, compute a_t from (2), use the experimental cross section to compute $(-a_s^{-1}+\frac{1}{2}r_sk^2)$ from (4), plot against k^2. This is feasible for energies below about 2 Mev.

II. Triplet plots.—Assume values for a_s and r_s, use the experimental cross section to compute $(-a_t^{-1}+\frac{1}{2}r_tk^2)$ from (4), plot against k^2. This is feasible for energies above about 1 Mev.

I gives a_s and r_s as functions of r_t (incidentally, the value of a_s depends practically exclusively upon the epithermal cross section, and r_t enters only insofar as it affects the triplet scattering length a_t and, through it, the triplet epithermal cross section). We can use the results of the singlet plots to draw a curve of mutually compatible values of r_s and r_t in the r_s-r_t plane.

II gives r_t as a function of a_s and r_s. Since r_t is mostly determined from the high energy points, it is only slightly dependent upon the choice of a_s, as long as this choice is kept reasonable. Hence we can use the results of the triplet plots to draw another (independent) curve of mutually compatible values of r_s and r_t in the r_s-r_t plane. The curves are independent because entirely different energy ranges are used in their determination.

The two curves should cross somewhere in the r_s-r_t plane, their intersection point determining both effective ranges. Since the data are not infinitely accurate, each "curve" is really a region of compatibility, and the intersection of these two regions would then determine a region of values of r_s and r_t consistent with all the scattering data. This region would narrow down to a point as the data become more accurate.

Such a plot is shown in Fig. 2. It is seen that the regions of compatibility determined from the singlet and triplet plots overlap completely. (This is an unlucky accident, and wouldn't have happened if the singlet state were real, for example.) It seems out of the question to increase the accuracy of the experiments to the point where *these* two regions are narrowed down until they give a unique point of intersection. *Hence, scattering experiments alone are not sufficient to determine even the effective ranges of neutron-proton forces in the two spin-states.* They only give a functional relation between r_s and r_t.

It might be interesting to see whether the scattering data alone are consistent with the assumption of a square well potential with the *same* range b in both spin states. If we try $b=2.8\times10^{-13}$ cm, the value initially assumed by

Bohm and Richman, Fig. 1 gives $r_t = 2.15 \times 10^{-13}$ cm and formula (3) yields $r_s = 2.94 \times 10^{-13}$ cm. The corresponding point on Fig. 2 is right on the outer limit of the allowed region, and is therefore a very poor fit to the data. On the other hand, if we assume $b = 2.6 \times 10^{-13}$ cm, the effective ranges are $r_t = 2.03 \times 10^{-13}$ cm and $r_s = 2.72 \times 10^{-13}$ cm. The corresponding point on Fig. 2 is somewhat above the shaded (best) region, but well inside the outer limits. Hence the scattering data alone do not exclude this hypothesis. We might remark here that if one takes only the proton-proton scattering data of Herb, Kerst, Parkinson, and Plain[6] and does not use the data of Hafstad, Heydenberg, and Tuve,[7] then $b = 2.6 \times 10^{-13}$ cm is in good agreement with the proton-proton scattering data.

More information can be obtained from a direct measurement of the *coherent neutron-proton scattering amplitude at low energies, f:*

$$f = 2(\tfrac{3}{4}a_t + \tfrac{1}{4}a_s). \qquad (5)$$

There are two methods for measuring f: scattering of neutrons by parahydrogen and scattering of neutrons by crystals containing hydrogen atoms. The results are:

$f = -(3.95 \pm 0.12) \times 10^{-13}$ cm parahydrogen,[8]
$f = -(4.72 \pm 0.40) \times 10^{-13}$ cm crystals.[9]

The parahydrogen value is subject to many systematic errors (admixture of orthohydrogen, uncertainty in the capture cross section, etc.), so the quoted statistical error may be misleading. It should be noticed that these two determinations of f are inconsistent. The stated experimental errors do not overlap.

The epithermal cross section σ_0 is given from (4):

$$\sigma_0 = \tfrac{3}{4}(4\pi a_t^2) + \tfrac{1}{4}(4\pi a_s^2). \qquad (6)$$

σ_0 has been determined by the scattering of epithermal neutrons from crystals and by the use of neutron velocity spectrometers. The values are:

$\sigma_0 = (20.2 \pm ?) \times 10^{-24}$ cm^2, crystals;[10]
$\sigma_0 = (20.6 \pm 1.0) \times 10^{-24}$ cm^2, velocity spectrometer;[11]
$\sigma_0 = (20.0 \pm 0.15) \times 10^{-24}$ cm^2, velocity spectrometer.[12]

Some crystal measurements have been made with neutrons from the indium resonance. This energy (1.44 ev) is low enough to introduce a systematic error into σ_0, tending to make the measured value too high. (The author wishes to thank Dr. McDaniel and Dr. Jones for pointing out this source of error.)

Knowing f and σ_0, we can determine a_s and a_t. The value of a_t then gives the effective triplet range r_t by Eq. (2). In Fig. 3 we show curves of constant r_t in the $\sigma_0 - f$ plane.

We have also indicated some of the experimental results on Fig. 3. The top three horizontal lines give the crystal measurement of f (the

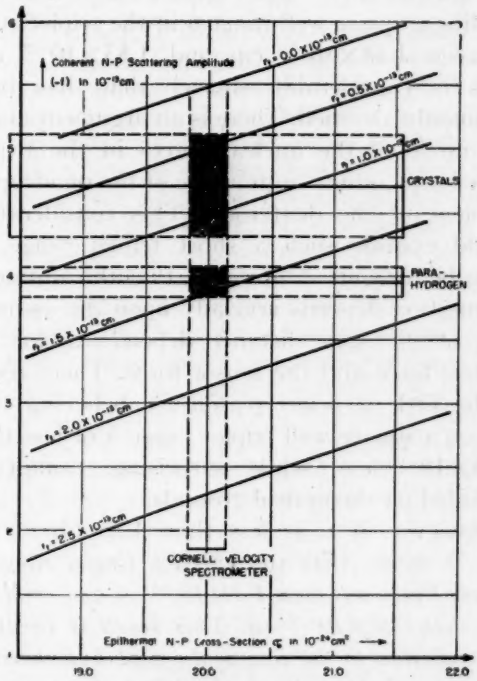

FIG. 3. Abscissa: epithermal N–P scattering cross section, σ_0. Ordinate: (negative) coherent epithermal N–P scattering amplitude, $(-f)$. The slanted curves give the theoretical relation between σ_0 and $(-f)$ for assumed values of the effective range r_t in the triplet state. The horizontal lines indicate measured values of $(-f)$, the vertical lines indicate the measured value of σ_0. (In each case the center line is the most probable value, the dashed lines on either side represent the claimed experimental error.)

[6] R. G. Herb, D. W. Kerst, D. B. Parkinson, and G. J. Plain, Phys. Rev. **55**, 998 (1939).
[7] N. P. Heydenberg, L. R. Hafstad, and M. A. Tuve, Phys. Rev. **56**, 1078 (1939).
[8] R. B. Sutton, T. Hall, E. E. Anderson, H. S. Bridge, J. W. deWire, L. S. Lavatelli, E. A. Long, T. Snyder, and R. W. Williams, Phys. Rev. **72**, 1147 (1947).
[9] G. C. Shull, E. O. Wollan, G. A. Morton, and W. L. Davidson, Phys. Rev. **73**, 262 (1948).
[10] J. Marshall, Phys. Rev. **70**, 107A (1946).
[11] W. W. Havens, L. J. Rainwater, and C. S. Wu, Bull. Am. Phys. Soc. **23**, No. 2, 37 (1948).
[12] B. D. McDaniel and W. Jones, private communication.

center line corresponds to the most probable value, the dashed lines to the limits of error), the bottom three horizontal lines give the parahydrogen measurement of f. The three vertical lines correspond to the Cornell measurement of σ_0.

Consider first what happens if we accept the crystal measurement of f. Figure 3 shows that then r_t is less than 1.2×10^{-13} cm, and may be as low as 0.35×10^{-13} cm. On the other hand, Fig. 2 cannot be reconciled with a triplet range less than 1.2×10^{-13} cm. There is no overlap here. *The crystal measurement of f, in conjunction with the Cornell measurement of σ_0, is inconsistent with the scattering data.*

The situation is somewhat better if we accept the parahydrogen determination of f. Figure 3 then shows that r_t must lie between 1.30×10^{-13} cm and 1.55×10^{-13} cm. Figure 1 shows that this implies a square well range b in the triplet state between 1.48×10^{-13} cm and 1.83×10^{-13} cm. This is considerably shorter than has been commonly assumed. There is an argument about the range of the nuclear forces in the triplet state based on the finite value of the quadrupole moment of the deuteron.[13] This consideration would exclude such a short triplet range. It must be recognized, however, that the argument in question depends crucially upon the assumption of the *same* distance dependence for the central force and the tensor force. There seems to be little *a priori* reason for believing this. Hence a square well triplet range b of less than 1.83×10^{-13} cm, while surprising, cannot be excluded on theoretical grounds.

However, if r_t is less than 1.55×10^{-13} cm, Fig. 2 shows that the *effective singlet range r_s is very likely less than 1.2×10^{-13} cm and certainly less than 2.0×10^{-13} cm. This result is in direct contradiction to the commonly used hypothesis of the charge-independence of nuclear forces in the singlet state.* It might be pointed out that the argument from the mirror nuclei is not relevant here. In mirror nuclei we can compare the effects of neutron-neutron and proton-proton forces. Here we are comparing neutron-proton and proton-proton forces.

It is, of course, possible that the real neutron-proton well shape is of the long-tail kind so that our whole analysis is invalid. Estimates show that the well would have to be very long-tailed indeed to make the present experimental data consistent. It is premature, however, to consider this possibility seriously until the value of f is beyond doubt.

In view of the importance of the measurement of f for our understanding of the nature of nuclear forces, it is strongly suggested that it be redetermined with a view toward narrowing down the limits of error (as well as eliminating possible systematic errors). Figure 3 gives an indication of the accuracy necessary to narrow down the effective triplet range within reasonable limits. Here is a case where *a gain of a factor 5 (or even 2 or 3) in the accuracy of the experiments would make a lot of difference.* In view of an unexpectedly large absolute value of the coherent scattering amplitude f, it is very encouraging that there are two completely independent ways of measuring this quantity.

The author thanks Professor J. Schwinger and Professor V. Weisskopf for some valuable discussions concerning this problem and Professor McDaniel and Dr. Jones for permission to quote their measurement of σ_0.

Note Added In Proof.—After this manuscript had been sent off, a detailed paper on crystal diffraction studies has come out from the Oak Ridge Laboratory.[14] According to this paper, the best value for the coherent neutron-proton scattering amplitude f is $f=(3.96\pm0.20)10^{-13}$ cm. The difference between this value and the one reported earlier is due to the fact that the thermal motion of the protons in the crystal lattice had been taken into account incorrectly at first.

This result changes the conclusion of this note somewhat. We may now consider the value of f reasonably well established (even though a better accuracy would be very desirable) and we can therefore state the conclusion in a more definite way:

If the nuclear potential is not "long-tailed," the effective triplet range is between 1.30 and 1.55 $\times10^{-13}$ cm, and the effective singlet range is less than 2.0×10^{-13} cm (in contradiction to the hypothesis of the charge-independence of nuclear forces).

An analysis of the data with arbitrary well-shapes is now in progress.

[13] J. Schwinger, Phys. Rev. **60**, 164 (1941).

[14] Shull, Wollan, Morton and Davidson, Phys. Rev. **73**, 842 (1948).

Letters to the Editor

PUBLICATION of brief reports of important discoveries in physics may be secured by addressing them to this department. The closing date for this department is five weeks prior to the date of issue. No proof will be sent to the authors. The Board of Editors does not hold itself responsible for the opinions expressed by the correspondents. Communications should not exceed 600 words in length.

Evidence for Neutrons Associated with the Stopping of Sea Level Mesons in Lead*

R. D. SARD, W. B. ITTNER III, A. M. CONFORTO,** AND M. F. CROUCH***
Washington University, St. Louis, Missouri
May 17, 1948

WE are carrying out an experiment designed to bring to light neutrons emitted by nuclei that have captured negative light mesons. In our first measurements we have found a time correlation between the stopping of a penetrating charged particle, indicated by a Geiger-Mueller tube anticoincidence, and the detection of a neutron.

The arrangement used is shown in Fig. 1. Counter trays A and B select a cone of charged particles capable of penetrating 12.7 cm Pb. Some of these stop in the 7-cm Pb absorber, resulting in failure of tray C to discharge except in the small (2 percent) fraction of the cases in which a decay electron reaches C. Tray C more than covers the cone defined by A and B. The circuit records coincidences (AB) (B within 0.7 μsec. before to 1.0 μsec. after A) as well as anticoincidences $(AB-C)$ (C within 2.1 μsec. before to 7.2 μsec. after the coincidence (AB)). Underneath C is placed a group of slow neutron counters, N, surrounded by paraffin. These are proportional counters coated on the inside with boron enriched in B^{10}.[1] They are connected in parallel to the input of an amplifier and pulse-shaping circuit biased to respond only to input pulses stronger than about 20 millivolts. The output drives a recording circuit giving the N counting rate.

An anticoincidence $(AB-C)$ initiates a rectangular pulse 80 μsec. in length. This "gate" is placed in coincidence with the N pulse; the coincidence output drives a recording circuit giving the $(AB-C:N)$ rate. This coincidence circuit responds only when the neutron pulse occurs within 4 to 84 μsec. after the (AB) coincidence. Thus N pulses simultaneous with $(AB-C)$, such as might be produced by an electron shower that happens to miss C, cannot contribute to the $(AB-C:N)$ rate. As it takes several microseconds for a neutron of several Mev to be brought to thermal speed in the paraffin and the mean life of the thermal neutron is of the order of 150 μsec., the late start incurs only a small loss of counts from neutrons associated in time with the incident charged particle.

The dimensions of the paraffin "moderator" were those determined empirically to give maximum neutron counting rate for the fission neutrons from a 41- ×51-cm tray of uranium oxide placed at the level of the middle of the 7-cm Pb absorber.

Our preliminary results are given in Table I. Subtracting the $(AB-C)$ rate without the lead absorber from the rate with it in place, one obtains 0.86/min. for the apparent rate of stopping in the lead. This gives an absorption coefficient of 3.8×10^{-4} per g/cm², in excellent agreement with counter telescope data.[2] Apparently 55 percent of the anticoincidences recorded are not due to the stopping or scattering of particles in the lead absorber, corresponding to an anticoincidence efficiency of 96.5 percent.

In order to separate N pulses due to neutrons from N pulses due to showers and contamination, data were taken with and without 1-mm cadmium shields around the counters. The sixth and seventh rows give the $(AB-C:N)$ rates in the two cases. There is seen to be a definite effect, far exceeding the expected accidental rate of $1.89\times7.43\times80\times10^{-6}=1.12\times10^{-3}$ per hour.

The one $(AB-C:N)$ count in the absence of absorber (eighth row) could be accidental or due to a particle stopped in the G-M tube walls (0.8-mm brass) or aluminum shielding (1.6 mm).

Since a considerable fraction of the anticoincidences are not due to stopping in the lead, it is not yet certain on the basis of the data thus far discussed that the neutrons are associated with meson stoppings. In order to settle this point, data were taken with no voltage on counters C. The $(AB:N)$ rate so obtained should be almost thirty times higher than the $(AB-C:N)$ rate if the effect is due to penetrating events, while it should be the same if the effect is due *entirely* to mesons stopped in the lead. As shown in the ninth and tenth rows, the neutron coincidence rate is about doubled. We take this to mean that the stopping of mesons in the lead results in the production of neutrons. The doubling of the rate could be due to neutrons produced by or contained in penetrating ionizing events[3] or to neutrons produced by mesons stopping beneath the C tray, in the paraffin or the neutron counters themselves (these would be detected with considerably higher efficiency than neutrons made in the lead). Ac-

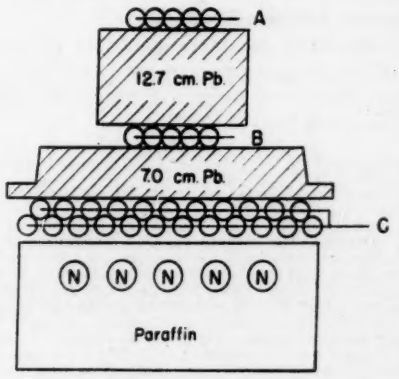

FIG. 1. Counter arrangement. Search for fast neutron associated with meson stopping.

TABLE I.

	Counts	Duration	Rate
(AB)	765,606	26,920 min.	28.44±0.03/min.
$(AB-C)$ with 7-cm Pb absorber	26,313	13,925 min.	1.89±0.01/min.
$(AB-C)$ sans 7-cm Pb absorber	7,859	7,597 min.	1.03±0.01/min.
N with 7-cm Pb absorber	116,666	15,707 min.	7.43±0.02/min.
N with 1-mm Cd sheaths around N counters	6,744	5,850 min.	1.15±0.01/min.
$(AB-C:N)$ with 7-cm Pb absorber and sans Cd sheaths	61	181.33 hr.	0.34±0.04/hr.
$(AB-C:N)$ with 7-cm Pb absorber and with Cd sheaths	0	50.75 hr.	—
$(AB-C:N)$ sans 7-cm Pb absorber and sans Cd sheaths	1	44.13 hr.	0.02±0.02/hr.
$(AB:N)$ with 7-cm Pb absorber and sans Cd sheaths	56	80.45 hr.	0.70±0.09/hr.
$(AB:N)$ with 7-cm Pb absorber and with Cd sheaths	0	46.75 hr.	—

cording to present views, there should be no neutrons from mesons stopped in paraffin.

The ratio of particles stopped in the lead to neutron coincidences is 51.6:0.34, or 152. Allowing for a 20 percent positive excess, we conclude that there is one neutron coincidence per 61 negative mesons stopped. The solid angle subtended by the neutron detecting arrangement is approximately π-steradians. If there is one neutron produced per negative meson stopped, the efficiency of the neutron detecting arrangement is 6.5 percent per incident neutron. Before any conclusion can be drawn as to the multiplicity of the neutron production, it will be necessary to determine experimentally the efficiency of the neutron detecting arrangement for incident neutrons of various energies. We are preparing to do this for Po-Be and Ra-Be neutrons. It is also not entirely impossible that the neutron coincidences are due to stopped protons, which may amount to as much as 5 percent of the number of stopped mesons.[4] This would, however, imply an improbably high efficiency for the neutron detecting arrangement.

We are continuing our investigation of the effects reported, and are, in particular, trying to find out whether the neutrons result from capture or decay (neutral mesons producing neutrons?).

* Research assisted by the Office of Naval Research through Contract N6onr-202, T.O. 3.

** International Study Fellow of the American Association of University Women.

*** Now at Harvard University, Cambridge, Massachusetts.

[1] We are indebted to the Argonne National Laboratory for the loan of these counters; we understand that their efficiency for room-temperature neutrons incident at right angles to the axis is about 10 percent.

[2] B. Rossi, N. W. Hilberry, and J. B. Hoag, Phys. Rev. **57**, 464 (1940).

[3] V. Tongiorgi [Phys. Rev. **73**, 923 (1948)], using a technique similar to ours, finds neutrons associated with extensive showers. We have recently taken data with extra anticoincidence counters of the C group, C^1, placed next to trays A and B. The $(AB-C^1:N)$ rate is not significantly less than the $(AB:N)$ rate, indicating that the doubling cannot be ascribed to showers incident on the apparatus.

[4] B. Rossi, *Interpretation of Cosmic Ray Phenomena* (Technical Report No. 7 of the Massachusetts Institute of Technology Laboratory of Nuclear Science and Engineering, March 22, 1948).

The Isotopic Constitution of Praseodymium and Neodymium

MARK G. INGHRAM, DAVID C. HESS, JR., AND RICHARD J. HAYDEN
Argonne National Laboratory, Chicago, Illinois
May 17, 1948

OUR mass spectrometric measurements of rare earth isotopic constitutions[1,2] have been extended to include praseodymium and neodymium. Methods of analysis were similar to those discussed in the first reference.

Praseodymium was first studied by Aston,[3] who reported a single isotope of mass 141. He gave no upper limits for possible existence of other stable isotopes. No other studies of this element have been reported.

For this investigation a nitric acid solution of praseodymium oxide (Hilger Laboratory No. 1533) was pipetted onto a tungsten filament and heated in air to form an adherent oxide coat. This filament was then inserted into the source of a 60° mass spectrometer. Upon heating, ion currents were obtained at masses 157, 158, and 159, corresponding to $Pr^{141}O^{16+}$, $Pr^{141}O^{17+}$, and $Pr^{141}O^{18+}$. Negligible ion currents were observed of the type Pr^{141+}. From the ratios of the ion currents observed we can conclude that other stable praseodymium isotopes, if they exist, are present to less than the following percentages:

138	<0.002 percent	142	<0.005 percent
139	<0.003 percent	143	<0.010 percent
140	<0.005 percent	144	<0.001 percent
		145	<0.001 percent

The limits of the abundances of the isotopes at masses 142 and 143 were obtained by comparison of the observed ion currents with those predicted from the known abundances of O^{17} and O^{18} and, therefore, these limits are not as low as are the rest. Assuming a packing fraction of -3.0×10^{-4} and a conversion factor of 1.000275, the chemical atomic weight is 140.92, which is in complete agreement with the international chemical value.

Neodymium was first investigated by Aston[4] who found isotopes at masses 143, 143, 144, 145, and 146. Later Dempster[5] discovered rarer isotopes at masses 148 and 150. Mattauch and Hauk[6] on the basis of photometric analysis of photographic plates gave the abundances shown in Table I.

For this investigation neodymium oxide (Hilger Laboratory No. 6783) was applied to the source in a manner similar to that used for praseodymium. The ion currents consisted principally of NdO^+ ions with very much weaker currents of the type Nd^+. The results tabulated in Table I are the average of 200 separate determinations in the oxide position. A typical recorder curve is shown in Fig. 1. The uncertainty quoted is not the mean deviation of these results, but is larger than this by an amount sufficient to

TABLE I. Isotopic constitution of neodymium.

Observer	142	143	144	145	146	148	150
Mattauch and Hauk	25.95	13.0	22.6	9.2	16.5	6.8	5.95
This work	27.13 ±0.2	12.20 ±0.1	23.87 ±0.2	8.30 ±0.05	17.18 ±0.2	5.72 ±0.06	5.60 ±0.06

include possible systematic errors in the mass spectrometer.[1] The actual mean deviations are about one-third of the deviations quoted in this table. The following upper limits were set for the existence of other neodymium isotopes:

138	<0.002 percent	149	<0.005 percent
139	<0.02 percent	151	<0.002 percent
140	<0.004 percent	152	<0.002 percent
141	<0.01 percent	153	<0.002 percent
147	<0.01 percent	154	<0.002 percent

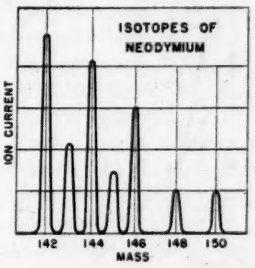

FIG. 1. A typical recorder curve for neodymium. For clarity the mass numbers shown are those of the neodymium isotopes and are sixteen units less than those of the NdO^+ ions actually recorded.

The high limits at masses 139 and 141 are due to lanthanum and praseodymium impurities in the neodymium sample. The fact that the small ion currents observed at these masses were not due to Nd isotopes was proved by the observation that the ratios of these ion currents to those of the neodymium isotopes varied with time. Assuming a packing fraction of -2.7×10^{-4} and a conversion factor of 1.000275, the chemical atomic weight is 144.25, which is in good agreement with the international chemical value of 144.27.

[1] Inghram, Hayden, and Hess, Phys. Rev. **72**, 967 (1947).
[2] Inghram, Hess, and Hayden, Phys. Rev. **73**, 180 (1948).
[3] J. G. Aston, Phil. Mag. **49**, 1191 (1925).
[4] J. G. Aston, Nature **132**, 930 (1933).
[5] A. J. Dempster, Phys. Rev. **51**, 589 (1937).
[6] Mattauch and Hauk, Naturwiss. **25**, 780 (1937).

Beta- and Gamma-Spectra of Cs^{137}

J. TOWNSEND, G. E. OWEN, MARSHALL CLELAND, AND A. L. HUGHES
Washington University, St. Louis, Missouri
May 8, 1948

AN investigation in this laboratory on the absorption of gamma-rays called for the use of radioactive isotopes emitting monoenergetic gamma-rays. Among those used was Cs^{137}, a fission product of high specific activity, produced by the Clinton Laboratories at Oak Ridge, Tennessee. According to the Radioactive Iostope List issued by the Atomic Energy Commission (September 1947), Cs^{137} emits two groups of beta-rays with maximum energy of 0.84 Mev (50 percent) and 0.5 Mev (50 percent), respectively, and one gamma-ray of energy 0.75 Mev. These values were determined by absorption methods. It was considered advisable to investigate the radiations

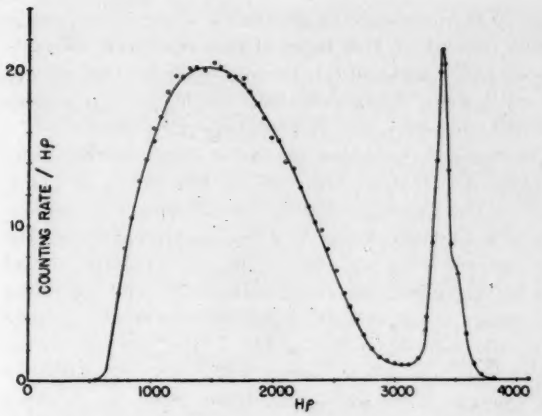

FIG. 1. Cs^{137} β-ray spectrum.

emitted by means of beta-ray spectrographs to check these results.

Two beta-ray spectrographs were used: a thin magnetic lens spectrograph and a small 180° spectrograph. The spectrographs had been previously calibrated by measurements of the spectra of ThB, P^{32}, and Cu^{64}. (In the case of the small 180° spectrograph the magnetic field was also directly measured.)

In order to remove any possible rare earth impurities from the source material, a fluoride precipitation was carried out. The beta-source was a deposit about 2 mg/cm² thick on a mica backing about 1 mg/cm² thick.

The beta-ray spectrum is shown in Fig. 1. The shape suggests a beta-spectrum of a simple type on which is superposed at the high energy end a strong internal conversion line. A Kurie plot is reproduced in Fig. 2. It indicates a maximum energy of 0.550 ± 0.005 Mev for the beta-ray spectrum. The linearity of the Kurie plot, above 0.1 Mev, indicates that we have but one beta-ray group. (The departure from linearity below 0.1 Mev is due to the fact that no great pains were taken to use very thin supports or very thin windows.) In particular, we find no indication of a beta-ray group with a maximum energy

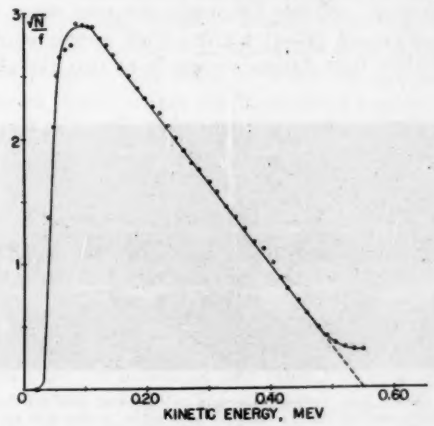

FIG. 2. Kurie plot from Fig. 1.

above 0.55 Mev, as was implied by the absorption measurements referred to. It is believed that absorption methods cannot easily distinguish between a single beta-ray group, on which there is superposed near the high energy end an internal conversion line, and two beta-ray groups.

The internal conversion line has an energy of 0.626 Mev. Adding to this, 0.037 Mev, the binding energy of the K shell for Ba, we find for the energy of the converted gamma-ray 0.663 ± 0.006 Mev. A direct measurement of the gamma-ray energy was made by placing a radiator of lead 0.2 mm thick in front of a sample of Cs^{137} and measuring the energy of the photoelectrons ejected. On adding 0.088 Mev, the binding energy of the K shell in lead to the measured photoelectron energy 0.577 Mev, we obtain for the energy of the gamma-ray 0.665 Mev. No evidence for the presence of any other gamma-ray could be found. The internal conversion coefficient was found to be 0.12.

In summary, this investigation shows that the radiation from Cs^{137} consists of a simple beta-ray spectrum with an end point at 0.550-Mev energy and a single gamma-ray of 0.663-Mev energy, 12 percent of the gamma-ray being internally converted. The monoenergetic nature of the gamma-ray combined with the long half-life of Cs^{137}, 33 years, suggests its use as a gamma-ray standard. Coincidence studies are being made to secure information as to the decay scheme of this isotope. The work was carried out under contract with the Office of Naval Research.

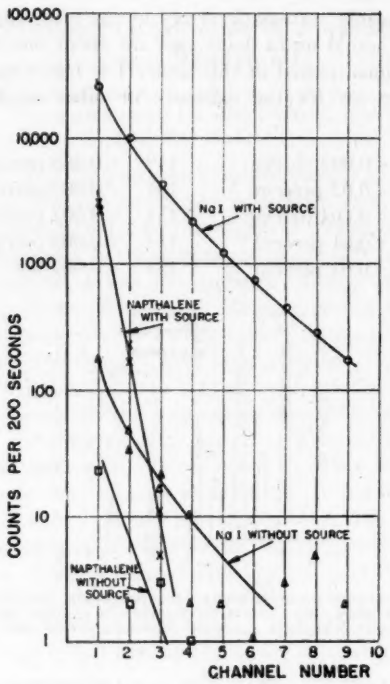

FIG. 2. Differential bias curves for pulses from NaI(Tl) and naphthalene. Channel 1 records pulses in the range 5–10 volts. Channel 2, 10–15 volts, etc.

Alkali Halide Scintillation Counters

ROBERT HOFSTADTER
Princeton University, Princeton, New Jersey
May 20, 1948

IT has been shown by J. W. Coltman, H. Kallman, M. Deutsch, and G. B. Collins[1] that beta-particles and gamma-rays can be detected by the scintillations which these ionizing radiations produce in certain crystals. Among the most successful for practical applications are naphthalene and perhaps anthracene.[2] Such crystals are not particularly suitable for many purposes since their densities are small (about 1 g/cc), their atomic numbers low, and their light flashes are small, so that the photomultiplier detector must be cooled to reduce background noise pulses.

FIG. 1. Oscilloscope screen photographs taken at random for 1/30 second. Above, pulses due to NaI(Tl) and below, pulses due to naphthalene under identical circumstances. Sweep calibration: total length of sweep equals 4.3 microseconds.

From the known properties of the alkali halide phosphors[3] it occurred to the author that these materials, of moderate density (2.0 to 4.5 g/cc), medium atomic numbers, great transparency, and beautiful form, might be very suitable for scintillation counters. The time during which light flashes are emitted is also known to be small, although phosphorescence is observed in some specimens.[4]

The author had in his possession a crystal of potassium iodide with a small thallium impurity (probably 0.1 percent or so) which was kindly provided him a year ago by Mr. Frank B. Quinlan of the General Electric Company. This crystal had been grown in 1938 by Dr. Frederick Seitz and Mr. Quinlan. Accordingly, the author, with the help of Mr. J. C. D. Milton, made an attempt to detect gamma-rays with this crystal and a 931A type photo-multiplier. The attempt was successful and will be described at a later time.

Since potassium is radioactive and, moreover, since the pulses observed in KI were somewhat smaller than those observed with naphthalene samples, the author prepared some powder samples of NaI plus thallium. The results were very encouraging, for pulses caused by alpha-particles were equal, if not greater, than those observed with ZnS (silver), which is known to be a very efficient phosphor. The powder sample proved to be hydroscopic when exposed to air and, in addition, a yellow film formed on the surface. In a few hours the pulses due to alpha-particles were considerably smaller than the original ones.

Another NaI sample was made in vacuum in a 0.5-inch quartz tube with the result that a mass (~8.0 g) of extremely luminescent small crystals was produced. The crystals are about one or two millimeters on a side. When the quartz tube containing the crystals was placed close to a photo-multiplier, very large pulses were observed from radium gamma-rays. These pulses were larger than those observed with a clear piece of naphthalene (5.8 g) of comparable size. Of course, this NaI sample is completely unaffected by atmospheric conditions and is quite convenient for normal handling. A comparison of results is shown in Figs. 1 and 2. Figure 1 shows oscilloscope pictures of 1/30-second random exposures taken under identical circumstances with the NaI sample and with naphthalene. The source was 0.1-millicurie radium at 16 cm, filtered by 3/32-inch brass. Figure 2 shows a differential bias curve taken under identical conditions for the two materials. From the rise times of the pulses in NaI there is some evidence that the light flashes are emitted in about one microsecond or less. All work reported has been carried on at room temperature.

Further work in progress is designed to produce large single crystals of this and other alkali halides with thallium impurities. A neutron counter using a lithium halide seems to be a reasonable possibility.

In tests made by placing crystals of NaI, KI, and naphthalene on photographic plates (Eastman 103-O) much greater light output was observed from NaI and KI than from naphthalene samples of comparable size. Apparently, naphthalene is not an efficient phosphor.

A sample of NaI in a quartz tube gave measurable blackening of a photographic plate when the combination was exposed for thirty minutes to the gamma-rays of 1.8 millicuries of radium at a meter distance.

A more complete description of these results is being prepared.

The author wishes to thank Professors J. A. Wheeler and R. Sherr for interesting discussions, and Professors M. G. White and H. W. Fulbright for loan of equipment used in these tests.

[1] J. W. Coltman and F. H. Marshall, Phys. Rev. **72**, 528 (1947); H. Kallman, Natur und Technik (July 1947); M. Deutsch, Nucleonics **2**, 58 (1948); G. B. Collins and Rosalie C. Hoyt, Phys. Rev. **73**, 1259 (1948).
[2] P. R. Belland R. C. Davis, Bull. Am. Phys. Soc. **23**, No. 3, 52 (1948). X12.
[3] R. Hilsch, Zeits. f. Physik **44**, 860 (1927); W. von Meyeren, Zeits. f. Physik **61**, 329 (1930).
[4] E. H. Hutten and P. Pringsheim, J. Chem. Phys. **16**, 241 (1948).

An Example of the Beta-Decay of the Light Meson*

E. C. Fowler, R. L. Cool, and J. C. Street
Lyman Laboratory of Physics, Harvard University, Cambridge, Massachusetts
May 17, 1948

THE photographs of Fig. 1 show two views of a large Wilson cloud chamber containing a horizontal lead plate at the top one cm thick, eight aluminum foils each 0.020 cm thick, and two lead plates at the bottom each 0.9 cm thick. The photograph at the left is taken at 21° to that side of normal, while the right view is taken from a symmetrical position on the other side.

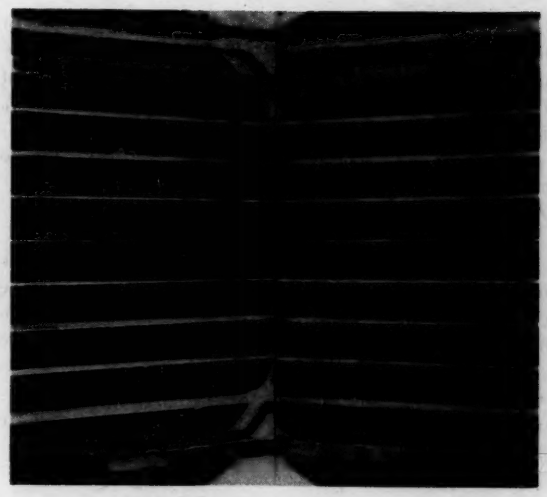

FIG. 1. A meson stops in a foil at the top of the chamber and its decay electron, after penetrating 7 foils, stops in the upper lead plate at the bottom of the chamber. The bright vertical line seen here is a thin wire used as a reference marker.

The nearly horizontal dense track which is seen between the top lead plate and the first aluminum foil, and which appears to stop in the foil, is probably that of a light meson. The density of ionization is between five and ten times the minimum for a singly charged particle. An electron with this ionization would scatter markedly and would have a range of less than two cm in the gas. Hence the observed particle cannot be an electron. A proton with this ionization has a range of more than 0.25 cm of aluminum, and so would be expected to pass through the foil. Reconstruction of the track in space shows that the point where it appears to stop in the foil is well within the region of good illumination. If the scattering of the particle inside the foil is neglected, it has a range of less than 0.10 cm of aluminum. A meson of mass $200m_e$ with this range ionizes 8 times the minimum. Therefore, it seems reasonable to assume that the stopped particle is a light meson.

From the point where the meson stops a particle ionizing less than 2 times minimum is seen to go downward. Its track appears to stop in the upper lead plate at the bottom of the chamber. The point at which the particle strikes the plate is well within the illuminated region. A proton which has a range of less than 0.9 cm of lead ionizes more than 4 times minimum; therefore the observed secondary particle cannot be a proton. In all known cases of the decay of a heavy meson to a light meson (the π–μ-decay) the light meson has an energy of 4 Mev, ionizes 5 times minimum, and has a range of 0.07 cm of aluminum.[1] The event observed here cannot be a π–μ-decay. It seems reasonable, however, to interpret this event as the beta-decay of a light meson. It is evident that the secondary particle ionizes near the minimum and that it is appreciably deflected by scattering in the aluminum foils. Taking this particle to be an electron, it is possible to estimate its

energy from the size of the deflections. The energy loss of the electron by ionization is 0.1 Mev per foil, the loss resulting from radiation may be neglected. The deflection of the particle caused by scattering in the gas is less than $\frac{1}{10}$ that caused by scattering in the foils.

The mean square average angle of deflection due to multiple scattering in a material of thickness t is[2-5]

$$(\Theta^2)_{Av}=(E_s^2 t/p^2\beta^2),$$

where Θ is the total deflection of the incident particle due to multiple small angle scattering, t is the thickness of the scatterer in radiation lengths, E_s is 21 Mev/c, p is the momentum of the particle in Mev/c, and β is v/c, the relative speed of the particle. The deflection angle in space has been computed for the scattering at each foil from measurements on the photographic negatives. The results are tabulated below:

Foil No.	Angle
2	0.015 radian
3	0.062
4	0.059
5	0.018
6	0.047
7	0.121
8	0.033

The value of the kinetic energy corresponding to the average of the squares of these angles is 15 Mev, and the standard deviation in this result is ±3 Mev.[6] It is difficult to evaluate a possible systematic error caused by the distortions of the track by movements of the gas in the chamber. Measurements have been made on the tracks of penetrating particles which have been observed near the location of the electron track shown here. The observed angles of deflection for a typical track correspond to an energy of 110 Mev for an electron. This indicates that the distortional error in the energy determination is probably within the statistical error stated above.

This picture was made near sea level in Cambridge. The dimensions of the chamber are 18 inches in diameter by 8 inches deep, and the chamber was counter-controlled, though the event discussed could not have been selected by the counters.

* The work described in this letter was supported in part by Contract N5ori-76, Task Order IV, U. S. Navy Department, Office of Naval Research.

[1] C. M. G. Lattes, G. P. S. Occhialini, and C. F. Powell, Nature **160**, 486 (1947).
[2] E. J. Williams, Proc. Roy. Soc. **A169**, 531 (1939).
[3] E. J. Williams, Phys. Rev. **58**, 292 (1940).
[4] B. Rossi and K. Greisen, Rev. Mod. Phys. **13**, 240 (1941).
[5] H. A. Bethe, Phys. Rev. **70**, 821 (1946).
[6] Two previous measurements of the energy of decay electrons, 24 and 25 Mev, have been reported by C. D. Anderson. C. D. Anderson *et al.*, Rev. Mod. Phys. **20**, 334 (1948).

On the High Energy Part of the K^{40} β-Spectrum

S. Franchetti and M. Giovanozzi
Università di Firenze, Instituto di Fisica, Arcetri, Firenze, Italy
March 19, 1948

In recent years some work has been performed on the subject of both the β- and γ-radiation from K^{40} disintegration. Several workers have attributed the γ-rays to the excited nucleus of A^{40} which would form from K^{40} by K-capture. The chief argument for this attribution is that the γ-quantum would have an energy larger than the maximum energy liberated in β-disintegrations, i.e., the upper limit E_0 of the β-spectrum (and cannot be emitted "in cascade" with the β-disintegrations, as these largely outnumber the γ-emissions).

The data on the γ-quantum appear to converge on the value 1.5×10^6 e.v. Concerning E_0, O. Hirzel and H. Wäffler[1] find a value $(1.41\pm0.02)10^6$ ev, and Dželepov *et al.*[2] find $(1.35\pm0.05)\times10^6$ ev. The first datum is obtained by comparison of the absorption curve with that of the Na^{24} electrons; the second is obtained by a special magnetic spectrograph using a coincidence method of counting.

However, the writers[3] investigating the high energy part of the β-spectrum with the aid of a cloud chamber have found a substantially larger value, that is, $(1.7\pm0.1)\times10^6$ ev, for the upper limit. As the substance employed (KCl) was carefully tested for radioactive impurities with negative result, this cause of error must be discarded and is, moreover, quite unlikely because of the regular shape of the spectrum and the agreement of the total activity with known data.[4]

Figure 1 shows the results in the form of a Fermi plot

Table I.

Energy intervals	Effect	Zero effect	Energy intervals	Effect	Zero effect
0.84 – 0.95	50	7	1.27 – 1.37	13	2
0.95 – 1.05	48	0	1.37 – 1.48	5	0
1.05 – 1.16	26	2	1.48 – 1.58	2	0
1.16 – 1.27	27	7	1.58 – 1.68	4	2
			1.68 – 1.79	1	2

(energy includes rest mass). The dimensions of the rectangles give (double) average errors. The dashed line is what should be expected for a value $E_0=1.4\times10^6$ ev, in the hypothesis that the spectrum is similar to that of an "allowed" transition, at least in the high energy region. This is what is suggested by our results, if one keeps in mind that a deviation from the straight line in qualitative agreement with that observed is due to the well-known[5] distortion introduced by the thickness of the source (33 mg/cm²) and of the supporter. The same distortion prevents saying anything definite on the lower energy part of the spectrum.

The explanation of the above-mentioned lower values of E_0 is very likely to be found in the fact that the percentage of electrons beyond 1.4×10^6 ev[6] is very small (order of 1 percent) so that it easily gets lost, especially in absorption methods, if the zero effect of the revealing device is not very low. The cloud chamber has this advantage, as is shown by the values[7] in Table I taken from our work:

(The zero effect is given by the amount of tracks which would be obtained without KCl, the number of expansions being the same as for the effect.)

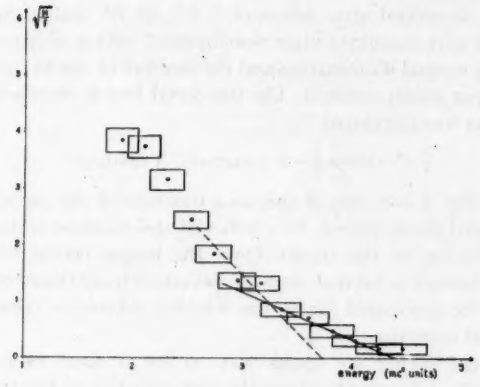

FIG. 1. End of the K^{40} β-spectrum.

The conclusion we draw is that the γ-quantum might as well be attributed to the β-disintegration of K^{40}. If this is so we should expect a weak band in the β-spectrum with an end point at $(1.7\pm0.1-1.5)\times10^6$ ev $=(0.2\pm0.1)\times10^6$ ev. A confirmation of this might be seen in an integral curve obtained by D. Bocciarelli,[4] using a magnetic deflection method (with counter revelation) with a relatively thin layer of KCl (7 mg/cm²). This curve shows in the region of $H\rho=1300$ an inflection which appears to be just above statistical errors.

[1] E. Gleditsch and T. Gráf, Phys. Rev. **72**, 640 (1947); O. Hirzel and H. Wäffler, Helv. Phys. Acta **19**, 216 (1946).
[2] Dželepov, Kopjova, and Vorobiov, Phys. Rev. **69**, 538 (1946).
[3] S. Franchetti and M. Giovannozzi, Rend. Acc. Linc. **1**, 1078 (1946).
[4] For instance, Mühlhoff, Ann. d. Physik **7**, 205 (1930); D. Bocciarelli, Rend. Acc. Linc. **15**, 686 (1932).
[5] A. W. Tyler, Phys. Rev. **56**, 125 (1939).
[6] This value lies very near the inflection point of a Fermi curve with $E_0=1.7\times10^6$ ev.
[7] These values correspond to the last 9 points on the diagram. The energy intervals cannot, however, be exactly compared, as in drawing the diagram corrections have been introduced for the slight shift of the high energy part of the spectrum owing to the absorption in the emitting layer.

Inelastic Scattering of Neutrons

J. M. CASSELS AND R. LATHAM
Cavendish Laboratory, Cambridge, England
May 13, 1948

A THEORETICAL paper by Weinstock[1] discusses the scattering of neutrons by polycrystalline materials, taking into account the lattice vibrations. The scattering is inelastic when the neutron gains or loses energy to the lattice, and the cross section for this process is obtained by assuming the Debye approximation to describe the frequency spectrum of the thermal oscillators.

We have made use of his work to calculate the inelastic scattering cross section (E_{in}) of iron at five temperatures, for incident neutron wave-lengths (λ) ranging from 1.79 to 20A (Fig. 1). Since iron has four stable isotopes, one of which possesses a spin, we have examined the theory to see which scattering cross section is relevant. At these energies, it seems that the inelastic scattering is a function only of the cooperative cross section $S=4\pi(\Sigma_r p_r a_r)^2$, where a_r is the bound scattering length and p_r the effective abundance of the rth nuclear state; p_r contains spin-dependent factors if the nucleus concerned has a spin.

The theoretical results are, accordingly, expressed as percentages of S. At 1.79A they agree closely with those already computed by Weinstock. We have, following him, retained only the K_1 term in Eq. (52); a trial for 10A and 800°K showed that the K_2 and K_3 terms were each about 5 percent of the K_1 term and of opposite sign to each other, so that this approximation is probably well justified throughout. For $\lambda>4.1$A, the inelastic scattering is entirely due to processes in which the neutron gains energy; at very long wave-lengths the K's decrease linearly so that E_{in} becomes proportional to λ.

We have attempted to test the theory by measuring at two temperatures the total cross section of iron in the 5–8A region, with the aid of the Cavendish Laboratory velocity selector. These wave-lengths are more than 4.1A, or twice the maximum Bragg spacing, so that there is no ordered elastic scattering.

There remain nuclear capture, nuclear disorder scattering, and inelastic scattering processes. The capture cross section has been taken[2] as 1.22λ barn. The disorder scattering cross section ($s=4\pi\{\Sigma_r p_r a_r^2-(\Sigma_r p_r a_r)^2\}$) we have found to be about 0.8 barn by another type of experiment[3] which measures, for $\lambda>4.1$A, the scattered rather than the transmitted neutrons. In such an experiment, the effect of the inelastically scattered neutrons is much reduced, because they have gained energy in the collision and are hence less efficiently detected by a "thin" BF_3 counter.

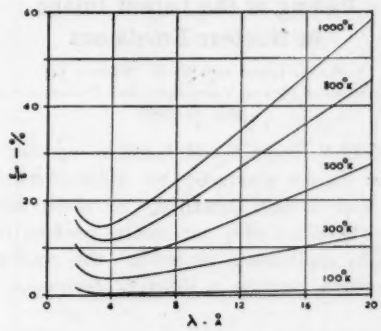

FIG. 1. Theoretical inelastic scattering of iron.

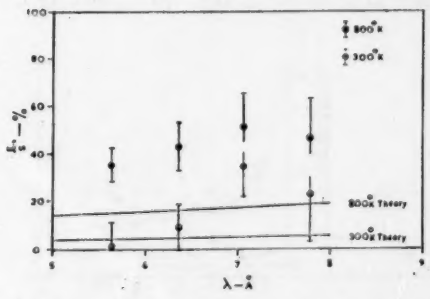

FIG. 2. Comparison of theoretical and experimental inelastic scattering.

The disorder scattering arising from magnetic effects would be negligible even if the atomic spins were oriented at random, and this is, of course, not the case since both temperatures are below the Curie point.

We accordingly obtain the inelastic scattering by subtracting the other two contributions to the total cross section; it is shown in Fig. 2 as a percentage of $S=10.2$ barns. The value of S is determined from the amorphous scattering cross section ($\sigma=4\pi\Sigma_r p_r a_r^2$) by means of the relation $\sigma=S+s$, taking[3] σ as 11.0 barns.

The rather large nuclear capture (approximately $\frac{3}{4}$ of the total cross section) makes it difficult to obtain really accurate values, but the experiment so far shows that the inelastic scattering is rather more than the theory predicts, and perhaps has a different energy dependence in this region.

The discrepancies are probably caused by departures from the Debye spectrum, which are, of course, to be expected.[4-6] More accurate experimental data should indicate quantitatively the modifications required, since by varying the temperature and neutron wave-length it is possible to weight the contributions from different parts of the spectrum.

[1] R. Weinstock, Phys. Rev. 65, 1 (1944).
[2] L. J. Rainwater, W. W. Havens, Jr., and C. S. Wu, Phys. Rev. 73, 1265 (1948).
[3] R. Latham and J. M. Cassels, Nature 161, 282 (1948).
[4] M. Blackman, *Reports on Progress in Physics* (Physical Society, London, 1941), Vol. 8, p. 11.
[5] W. V. Houston, Rev. Mod. Phys. 20, 161 (1948).
[6] R. B. Leighton, Rev. Mod. Phys. 20, 165 (1948).

Fading of the Latent Image in Nuclear Emulsions

W. A. LAMB AND F. W. BROWN III
Naval Radiological Defense Laboratory, San Francisco, California
May 21, 1948

RECENTLY Yagoda and Kaplan[1] reported that the latent image produced by alpha-particles in an emulsion with a high percentage of silver halide fades with time. Qualitatively, our results confirm this work, and it seems appropriate we publish this confirmation of the phenomena because a different technique was employed.

Eastman NTA plates (emulsion No. 359938) were irradiated identically with Po^{210} alpha-particles. Some of these were developed immediately as controls and the remainder were stored at 0°C, 20°C, and 40°C. Plates were developed after delays of 5, 12, 20, 29, and 46 days; these were examined after development with a microscope using normal illumination and the number of tracks (about 200 per plate) counted. The fractional loss in numbers of tracks was computed

$$(N \text{ control} - N \text{ counted})/N \text{ control},$$

and Fig. 1 is a plot of this as a function of the period of delayed development. It is believed this increase is due to the fading of the tracks. Only the longer period trends are deemed to be real, and the deviation from these trends may be accounted for by the inherent subjective errors of visual counting.

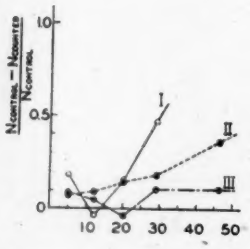

FIG. 1. Period of delayed development in days.

Experiments are under way to see if there is a significant difference between the rate of fading of the tracks of other highly ionizing particles and that of images produced by visible light.

[1] H. Yagoda and N. Kaplan, Phys. Rev. 71, 910 (1947).

Wide Range Frequency Modulation*

K. R. MACKENZIE
*University of California at Los Angeles*** *and*
Radiation Laboratory, Department of Physics, University of California, Berkeley, California
May 21, 1948

THE cyclotron frequency-modulation systems, so far proposed, utilize mechanical variation of capacity. This capacity is most effective when placed at the leading edge of the dee. In this position, however, many difficulties are introduced. A system has been developed at the Radiation Laboratory, in which the variable capacitor is outside the magnetic field.[1] Tests made with a one-half scale model of the proposed system for the 184-inch cyclotron show that a frequency range of 2.4 to 1 can be covered continuously. This range can be shifted approximately 10 percent by addition of fixed inductance or capacity. Since the frequency ranges required for protons and deuterons in the 184-inch magnetic field are 22.9 to 15.8 megacycles, and 11.5 to 9.8 megacycles, respectively, it seems that the cyclotron can accelerate either type of ion by making minor adjustments, or possibly both ions at once if so desired. Recent measurements on the 184-inch cyclotron indicate that the required frequency range need be only a few percent greater than the theoretical range, and also the shape of the frequency time curve is not critical.

A schematic diagram is shown in Fig. 1(a). It resembles the arrangement used on the Berkeley 37-inch and 184-inch cyclotrons in which the dee and rotary capacitor are joined by a transmission line and form an electrical half-wave system.[2] In the new system the capacitor is grounded, not directly, but through a large rectangular cross-section line, somewhat less than a $\frac{1}{4}$ wave-length at the upper frequency limit. The lower frequency limit is now greatly extended, since the capacitor and transmission line eventually pass through series resonance. The voltage distributions corresponding to f, $\frac{3}{4}f$, $\frac{1}{2}f$, and $\frac{1}{4}f$ are shown in Fig. 1(b) for the expected condition where the minimum ca-

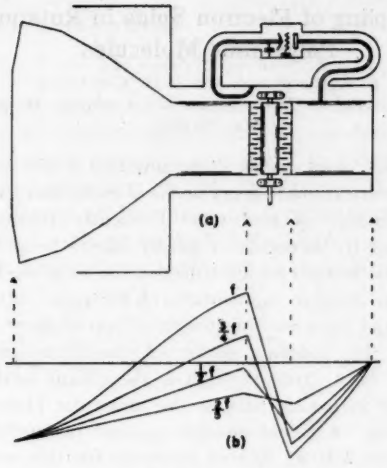

FIG. 1.

pacity of the condenser is one-half the effective dee capacity.

The condenser consists of a rotor with six rows of teeth, approximately 50 teeth per row, which mesh with two stator rows. The rotor is held on a high inductance frame, which reduces the frequency range slightly, but provides a rigid support. The final maximum and minimum capacities will probably be around 2500$\mu\mu$fd and 100$\mu\mu$fd.

Power is supplied by two grounded grid 9C21 tubes, coupled to the system by transmission lines as shown in Fig. 1. There are three fundamental modes, but with this coupling scheme the two undesired modes will produce voltages at the tubes with the wrong phase relation. Phase shift between filament and plate r-f voltages (in the correct mode) is controlled by a condenser between filament and grid. Amplitude modulation throughout either the proton or deuteron ranges can be held to about 20 percent by choosing the correct lengths and impedances of the plate and filament lines and the large cross-section line from the rotary condenser to ground. Peak power will be around 200 kw, but it is planned to pulse the oscillator over only the needed range. Dimensions have been determined from the model with a fair degree of accuracy, and engineering drawings for the 184-inch installation are now well under way.

* This paper is based on work performed under Contract No. W-7405-eng-48B, with the Atomic Energy Commission in connection with the Radiation Laboratory of the University of California, Berkeley, California.

** Present location.

[1] K. R. MacKenzie, Phys. Rev. **73**, 540 (1948).
[2] F. H. Schmidt, Rev. Sci. Inst. **17**, 301 (1946).

Energy of the Be^7 Gamma-Ray

DANIEL J. ZAFFARANO, BERNARD D. KERN, AND ALLAN C. G. MITCHELL
Department of Physics, Indiana University, Bloomington, Indiana

May 8, 1948

WHEN Li is irradiated by deuterons, a radioactive Be^7 is formed according to the reaction $Li^6(d,n)Be^7$, which has a half-life of approximately 43 days. This isotope decays by K-capture to Li^7, either directly to the ground state or to an excited state with the subsequent emission of a gamma-ray. The energy of this gamma-ray has been measured by several investigators who give values for the energy lying between 453 kev and 485 kev, each author giving his estimated error in the neighborhood of 10 kev. The results obtained by the various authors and the methods used are shown in Table I.

In addition the energy of the excited state of Li^7 has been determined by studying the reactions $Li^6(d,p)Li^7$, $B^{10}(n,\alpha)Li^7$, and $Be^9(d,\alpha)Li^7$.[1] A study of these reactions showed that there were two groups of protons from the first reaction, and two groups of alpha-particles in the second two reactions. From a measurement of the energies these two groups of particles, from any of the three reactions, the energy of the excited state of Li^7 can be determined. The results of these determinations are also given in Table I.

Since the magnetic lens determinations by Siegbahn and Rubin show considerable disagreement, we have made another determination of the energy of this gamma-ray using a magnetic lens. Be^7 was produced in the Indiana University cyclotron by bombarding lithium for 500 microampere-hours with 11.5-Mev deuterons. The chemi-

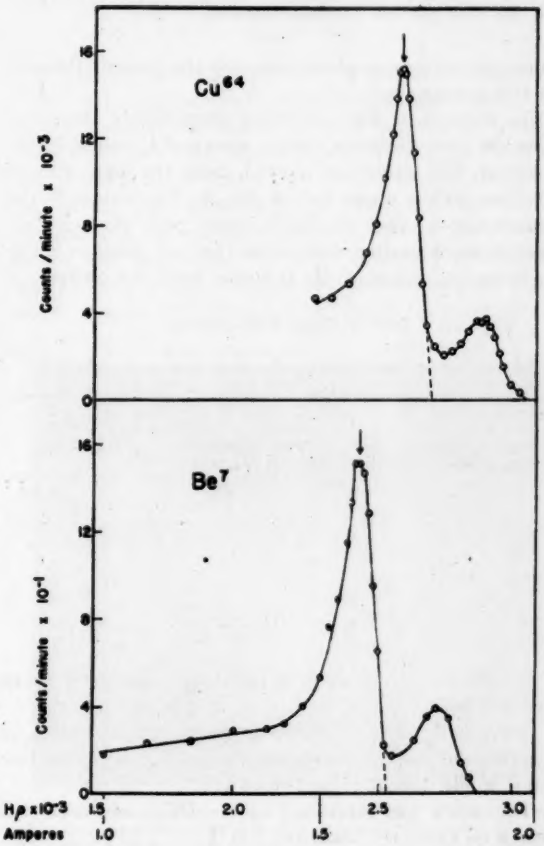

FIG. 1.

cally purified Be^7 source was placed in a capsule having an end plate of 1-mil copper on which was placed a lead radiator whose surface density was of 21 mg/cm². The energy of the photoelectrons produced by the gamma-ray in the lead radiator was measured in the magnetic lens. The results are shown in Fig. 1, in which the number of

TABLE I. Energy of the excited state of Li^7.

Reaction	$E\gamma$(kev)	Method	Reference
(a) From the measurement of gamma-rays.			
$Be^7(k,\gamma)Li^7$	425±25	Lead absorption	a
$Be^7(k,\gamma)Li^7$	485±5	Coincidence absorption of Compton electrons	b
$Be^7(k,\gamma)Li^7$	453±5	Photoelectrons in magnetic lens	c
$Be^7(k,\gamma)Li^7$	476±10	Lead absorption	d
$Be^9(d,\alpha)Li^7$	480±10	Photoelectrons in magnetic lens	e
(b) From measurement of particle ranges.			
$Li(d,p)Li^7$	455±15	Proton ranges	a
$B^{10}(n,\alpha)Li^7$	480	Alpha-particle ranges	f
$Be^9(d,\alpha)Li^7$	494±16	Alpha-particle ranges	g
$Be^9(d,\alpha)Li^7$	490±10	Alpha-particle ranges	h

[a] L. H. Rumbaugh, R. B. Roberts, and L. R. Hafstad, Phys. Rev. **54**, 657 (1938).
[b] I. Zlotowsky and J. H. Williams, Phys. Rev. **62**, 29 (1942).
[c] K. Siegbahn, Arkiv f. Mat., Astr. o. fys. **34**, No. 6 (1946).
[d] S. Rubin, Phys. Rev. **69**, 134A (1946).
[e] T. Lauritsen, W. A. Fowler, C. C. Lauritsen, and V. K. Rasmussen, Phys. Rev. **73**, 636 (1948).
[f] M. S. Livingston and J. G. Hoffman, Phys. Rev. **53**, 227 (1938).
[g] E. R. Graves, Phys. Rev. **57**, 855 (1940).
[h] E. N. Strait, C. G. Stergiopoulos, A. Sperduto, and W. W. Beckner, Bull. Am. Phys. Soc. **23**, No. 3, 30 (1948), J6.

counts per minute is plotted against the current through the coil in amperes.

The instrument was calibrated immediately thereafter using the photoelectrons from a source of Cu-annihilation radiation. The results are plotted, using the same scale of abscissae, in the upper half of Fig. 1. The results of the measurements taken on the K-photo peak of each line, together with another calibration run, are given in Table II. Since the value of $H\rho$ is linear with the current, it

TABLE II. Energy of Be^7 gamma-ray.

Type of radiation	i(K peak) amp.	i(K-edge) amp.	$H\rho$ peak edge gauss-cm		Energy peak edge kev	
Annihilation rad. run 1	1.685±0.002	1.746±0.002				
Annihilation rad. run 2	1.685±0.002	1.748±0.002				
Be^7 gamma-ray	1.585±0.005	1.658±0.002	2436	2457	470	478
		Mean			474±4	

follows that

$$(H\rho)_{\mathrm{Be}}=(H\rho)_{\mathrm{ann}}\times\frac{i_{\mathrm{Be}}}{i_{\mathrm{ann}}}.$$

The value of the energy of annihilation radiation is taken as 510.8 kev.

There is a slight difference in the result depending on whether the peak or the edge of the line is taken. The best value would appear to be 474±4 kev.

This work was supported by the Office of Naval Research on Contract N6ori-48, T.O. I.

[1] E. Segrè, Chart of Isotopes, Revised May 15, 1945.

Coupling of Electron Spins in Rotating Polyatomic Molecules

R. S. HENDERSON AND J. H. VAN VLECK
Department of Physics, Harvard University, Cambridge, Massachusetts
May 21, 1948

RECENT observations have revealed a fine structure in the rotational energy levels of molecules possessing an odd number of electrons.[1] Evidently the magnetic field set up by molecular rotation effects a splitting of these levels through its influence on the coupling between the orbital angular momentum of electrons within the molecule and the non-vanishing resultant of their spins.

Taking this coupling to be of the Russell-Saunders type, one may carry through a theoretical analysis by associating with that part of the molecular Hamiltonian representing rotational energy, a small perturbing term of the form $A(\mathbf{L}\cdot\mathbf{S})$. Matrix elements for this composite operator are most easily obtained in a representation based on the wave functions of a symmetric rotor. If the molecule under consideration lacks an axis of symmetry, one must eventually transform to the representation characteristic of an asymmetric rotor in the manner set forth by Wang.[2] The electronic angular momentum $\mathbf{L}$ is not itself quantized; rather, it is best pictured as being compounded with the angular momentum of the rotating molecule to produce a quantized resultant, $\mathbf{J}$ (Hund's "case b"). The term $A(\mathbf{L}\cdot\mathbf{S})$ emerges, in consequence, as a highly off-diagonal matrix, furnishing no first-order corrections to the rotational energy. But further application of perturbation analysis[3] turns up a second-order correction consisting of two parts, namely,

$$A\left\{\frac{\alpha W+\beta\Sigma_\kappa T^2(\kappa,\kappa')K^2}{J(J+1)}+\gamma\right\}C, \tag{1}$$

$$A^2\left\{\frac{\alpha' W+\beta'\Sigma_\kappa T^2(\kappa,\kappa')K^2}{J(J+1)}+\gamma'\right\}\times\left\{\frac{\frac{3}{8}C(C+1)-\frac{1}{2}S(S+1)J(J+1)}{(2J-1)(2J+3)}\right\}, \tag{2}$$

with C standing for $F(F+1)-S(S+1)-J(J+1)$ and $\mathbf{F}=\mathbf{J}+\mathbf{S}$.

The first part has its origin in cross terms connecting the spin coupling energy with rotational distortion of the orbital motion of electrons. The second bears a strong resemblance to expressions commonly derived in calculations on quadrupole coupling, and is conveniently designated as a "pseudoquadrupole" term.[4] Here K is the quantum number typical of symmetric rotors, in the mathematical description of which it represents quantized angular momentum about the axis of symmetry. The quantities $T(\kappa,\kappa')$ are elements of Wang's transformation matrix. The symbol W stands for the unperturbed energy of rotation, the Greek letters for constants of the molecule.

In the case of chlorine dioxide, one has $S=\frac{1}{2}$, and the quadrupole-like expression vanishes. Furthermore, the molecule is not far from being symmetrical, which makes it possible to determine W and $T(\kappa,\kappa')$ by ordinary per-

turbation methods.[5] The fine structure formula then assumes the following form

$$\{aK^2[J(J+1)]^{-1}+b+cf(J,K)\}C,$$

where a, b, and c are constants and $f(J,K)$ is a rather complicated function which takes into account the small departure from molecular symmetry. This expression can be fitted handsomely to the data presented in Coon's paper.[1] Indeed the leading (and dominant) term closely approximates his empirical formula, $a'(2K-J)$, for values of J and K large in comparison with their difference.

[1] J. Coon, J. Chem. Phys. **14**, 665 (1946).
[2] S. C. Wang, Phys. Rev. **34**, 249 (1929).
[3] E. C. Kemble, *Fundamental Principles of Quantum Mechanics*, see Section 48c, p. 394, on Van Vleck's method.
[4] H. M. Foley, Phys. Rev. **72**, 504 (1947).
[5] E. E. Witmer, Proc. Nat. Acad. **13**, 60 (1927).

On the Fine Structure in the Inversion Spectrum of Ammonia

R. S. HENDERSON
Department of Physics, Harvard University, Cambridge, Massachusetts
May 21, 1948

SIMMONS and Gordy[1] report that interactions involving the nuclear quadrupole moment do not altogether account for the fine structure appearing in the inversion spectrum (microwave) of $N^{15}H_3$, and suggest that coupling of the nuclear dipole moment with the magnetic field set up by molecular rotation may be responsible for the discrepancies brought to light by their measurements.

A theoretical expression describing the effect of such coupling in molecules possessing a non-vanishing resultant of electron spins has recently been put forward by the writer.[2] This can be taken over bodily in dealing with cases where nuclear rather than electron spins interact with electronic orbital angular momenta. In the present instance one has only to replace S by I and add the resulting expression to the formula used by Simmons and Gordy in their calculations. Over and above terms representing quadrupole (or pseudoquadrupole) coupling, there then appears the following correction to the rotational energy

$$\{aK^2[J(J+1)]^{-1}+b\}[F(F+1)-J(J+1)-I(I+1)],$$

which owes its simple form to the fact that the ammonia molecule is symmetrical about an axis through the nitrogen atom.

The extent to which this improves the agreement between calculated and observed separations of satellites from their main lines is set forth in Table I. The columns list discrepancies between observed values of $\Delta\nu$ and $\Delta\nu'$, and those calculated with and without inclusion of the dipole term in the fine structure formula. It is seen that these can be reduced so that they compare in magnitude and scatter with experimental errors, estimated by Simmons and Gordy as ranging from ±5 kc/sec. to ±30 kc/sec.

Constants used in obtaining these figures were (mc/sec.):

$$eQ\partial^2V/\partial z^2=4.10 \quad \text{with} \quad a=0.0057, \quad b=0.0011,$$

TABLE I.

		Discrepancies (kc/sec.)						Discrepancies (kc/sec.)			
		in $\Delta\nu$		in $\Delta\nu'$				in $\Delta\nu$		in $\Delta\nu'$	
J	K	New	Old	New	Old	J	K	New	Old	New	Old
1	1	−6	+3	+9	−6	8	8	−3	+42	−6	−75
2	2	+12	+25	+1	−24	9	9	−17	+34	+17	−58
3	3	+1	+17	0	−32	2	1	−11	+10	−8	−15
4	4	+13	+36	0	−40	4	3	−7	+22	−2	−30
5	5	+15	+43	−17	−63	5	4	−13	+20	+2	−34
6	6	+10	+42	−6	−63	6	5	−8	+30	+3	−43
7	7	−12	+28	−19	−80	7	6	−15	+28	+6	−47
						4	2			−22	−43

and

$$eQ\partial^2V/\partial z^2=4.08$$

when the quadrupole term stands alone.

We wish to acknowledge the kind assistance of Professor Townes, at whose suggestion this work was undertaken.

[1] J. W. Simmons and W. Gordy, Phys. Rev. **73**, 713 (1948).
[2] Previous communication.

Distortion of Progressive Ultrasonic Waves*

J. C. HUBBARD, J. A. FITZPATRICK, B. T. KANKOVSKY, AND WILLIAM J. THALER
The Catholic University of America, Washington, D. C.
May 22, 1948

THE subject of plane waves of sound of finite amplitude has received attention from the time of Riemann and was considered at some length by Rayleigh,[1] who predicted that, neglecting viscosity, the "crests of the velocity curve would gain continually on the troughs and must at last overtake them." R. D. Fay[2] has provided an analysis, including a consideration of the viscosity effect, and has shown that there is a gradual transfer of energy from lower to higher frequencies, so that a wave tends toward the distortion predicted by Rayleigh. Be-

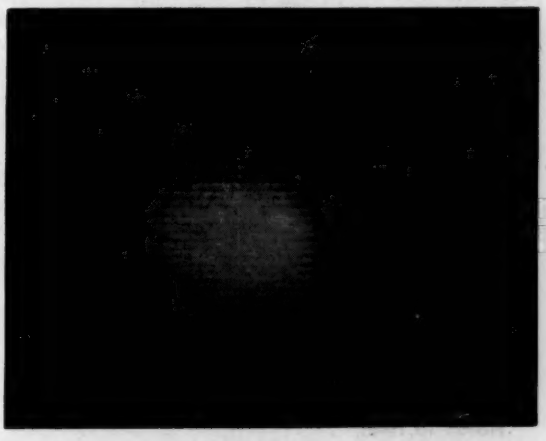

FIG. 1. Shadow photograph by collimated light of sound waves in air of frequency 405 kc/sec., at 27°C, the source being an x cut quartz plate with a peak voltage of 350 volts on the electrodes. Distortion of plane waves leaving the source is shown.

cause energy in the higher frequencies is more rapidly attenuated than in the lower, a dynamically stable wave form which is a function of the attenuation results. Not much of a specific nature seems to be known regarding the effect upon progressive change in wave form, although the effect has received much attention in connection with shock waves, and with the characteristics of sound produced by electroacoustic apparatus such as loud-speakers and signaling apparatus.

The development of short time spark shadow photography[3] has recently made it possible to photograph progressive sound waves in air in the millimeter wave-length region.[4] An outstanding characteristic of such photographs is the change in wave form which, after appearing to be symmetrical near the source, becomes sharpened on one side and, so far as has been determined, remains so for all intensities that can be photographed. An important problem was therefore to determine the respective thresholds of intensity at which, by several methods, distortion of wave form could be detected.[5] It became immediately apparent that some thresholds lie at relatively low intensity and that it is difficult to photograph ultrasonic waves at intensities low enough to avoid such a distortion. The characteristic appearance of a spark shadow photograph of a system of plane waves taken with light made parallel by a corrected lens is shown in Fig. 1. The duration of the spark is less than 10^{-7} sec. This is for air at 27°C, the frequency being 405 kc/sec. The ultrasonic wave-length is thus about 0.857 mm, and the travel during illumination 0.035 mm. A trace of this negative, kindly made by the Naval Ordnance Laboratory with a Leeds and Northrup recording microphotometer, is shown in Fig. 2. It will be observed that the waves, leaving the source with approximately a symmetrical form, almost immediately change to a form having a steeper front, suggesting the initial stages of shock wave formation.

A partial confirmation of these effects is provided by viewing the spectra produced by the negative used as an optical grating in a spectrometer of small aperture. The portion of field comprising the first eleven wave-lengths shows only the central image and two first-order spectra, the midportion of the negative shows the first and second orders very clearly, the third order being faintly visible, while the remainder shows only first and second orders.

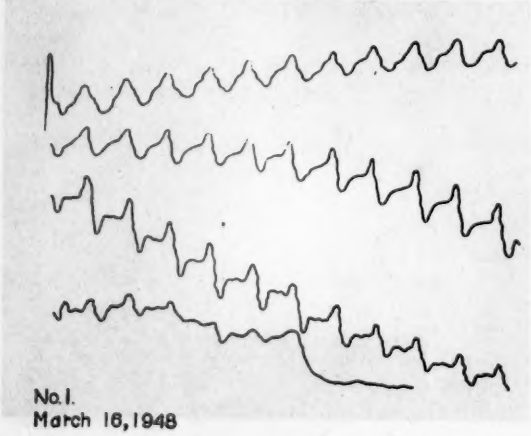

FIG. 2. Microphotometer trace of the negative of Fig. 1, starting from source, showing progressive change of symmetrical wave form into one with steeper fronts and increased harmonic content.

Spark shadow photographs of ultrasonic waves in water, glycerine, and carbon tetrachloride have also been made. below 75°C in water the phenomena are similar to those described in air, but the initial regime of symmetrical waves is very short. For normal liquids the temperature coefficient of sound velocity is negative and the order of events is reversed, the rear of the wave is steepened and the wave develops a saw tooth in reverse, or a sharp reduction in pressure is followed by a relatively long recovery. These and other examples of interest, both from the standpoint of difference of C_p and C_v, and that of temperature coefficient of velocity of sound, are being studied. The consequences of this behavior are especially significant for all types of ultrasonic measurement, and may well account for the many discrepancies in measured values of ultrasonic absorption, and to some extent as well for ultrasonic velocity. No doubt the characteristic emulsifying and other effects of intense sound or ultrasonic waves will be found to be closely connected with the effects described here. A more extended account of these experiments is being prepared.

* Supported by contract with the Office of Naval Research.

[1] Lord Rayleigh, *Theory of Sound* (MacMillan Company, Ltd., London, 1878), Vol. 2, p. 36.
[2] R. D. Fay, J. Acous. Soc. Am. 3, 222 (1931).
[3] J. W. Beams, A. R. Kuhlthau, A. C. Lapsley, J. H. McQueen, L. B. Snoddy, and W. D. Whitehead, Jr., J. Opt. Soc. Am. 37, 868 (1947).
[4] J. C. Hubbard, C. R. Larkin, and I. F. Zartman, J. Opt. Soc. Am. 37, 832 (1947).
[5] J. A. Fitzpatrick, B. T. Kankovsky, and W. J. Thaler, Bull. Am. Phys. Soc. Abstract K2, April 29 (1948).

Velocity and Two-Directional Focusing of Charged Particles in Crossed Electric and Magnetic Fields

N. SVARTHOLM
Nobel Institute for Physics, Academy of Sciences, Stockholm, Sweden
May 17, 1948

FROM mass and β-spectroscopy two types of focusing devices are well known: the homogeneous magnetic field where focusing occurs after 180° and the electrical radial field with a focusing angle equal to $\pi/\sqrt{2}\sim 127°$. In the high precision mass spectrographs of Aston, Dempster, Bainbridge-Jordan, and Mattauch-Herzog, sector fields of both kinds are used in order to achieve both velocity and direction focusing. Another focusing principle, the two-directional focusing in an inhomogeneous magnetic field, proposed by K. Siegbahn and the present author,[1] has been applied in the construction of a new β-spectrometer in this Institute. The field strength decreases with increasing radius as follows.

$$H(r)=H_0[1+\alpha_1(r-r_0)/r_0+\alpha_2(r-r_0)^2/r_0^2+\cdots], \quad (1)$$

where $\alpha_1=-\frac{1}{2}$, $\alpha_2\sim\frac{3}{8}$, and $r_0=50$ cm.

In the present note it will be pointed out that if a magnetic field of the general shape (1) is combined with a

radial electric field of the form

$$E(r)=E_0[1+\beta_1(r-r_0)/r_0+\beta_2(r-r_0)^2/r_0^2+\cdots], \quad (2)$$

then radial and axial focusing occurs after the angles

$$\phi_r=\pi/[1+(\kappa-1)(\kappa-2)+\alpha_1\kappa+\beta_1(1-\kappa)]^{\frac{1}{2}} \quad (3)$$

and

$$\phi_z=\pi/[\kappa-1-\alpha_1\kappa-\beta_1(1-\kappa)]^{\frac{1}{2}}, \quad (4)$$

respectively. The quantity $\kappa=er_0H_0/mv_0$ is the ratio between the magnetic force and the centrifugal force. This result includes the following special cases: radial ($\phi_z=\infty$), axial ($\phi_r=\infty$), and two-directional ($\phi_r=\phi_z$) focusing in an electric field ($\kappa=0$), in a magnetic field ($\kappa=1$), and that special combination of an electric and a magnetic field where velocity focusing of the first order is achieved ($\kappa=2$). In this combination of fields an energy spread δE gives a resolving power proportional to $(E/\delta E)^2$ instead of $E/\delta E$ in all other cases. According to Eq. (4), the condition for radial focusing is $\beta_1=2\alpha_1-1$. For a homogeneous magnetic field ($\alpha_1=0$) and an electric cylinder field ($\beta_1=-1$) this focusing principle was proposed by Bartky and Dempster[2] and applied by Shaw[3] in the determination of e/m for electrons, and by Bondy and Popper[4] in a mass spectrometer with large primary energy spread. Two-directional focusing ($\phi_r=\phi_z=\pi$) occurs in the case $\kappa=2$ when $\beta_1=2\alpha_1$ and includes the following subcases.

(a) $\alpha_1=\beta_1=0$: a homogeneous magnetic field combined with a radial electrical field independent of r.

(b) $\alpha_1=-\frac{1}{2}$, $\beta_1=-1$: an electric cylinder field combined with a magnetic field of the type $1/(r)^{\frac{1}{2}}$.

(c) $\alpha_1=\frac{1}{4}$, $\beta_1=\frac{1}{2}$, and $\beta_2=2\alpha_2+\frac{1}{2}$: this special case gives, in addition to first-order velocity focusing, second-order focusing in radial as well as axial directions.

As an immediate consequence of these principles it should be possible to increase the resolving power of a Bleakney or Nier spectrometer by introducing two deflectors of approximately parabolic profile according to the case (a) above. It remains to be seen whether there is any possibility of applying these principles to a high precision instrument. There are, in principle, some definite advantages but possibly also some practical disadvantages. A detailed discussion will be given at a later occasion.

[1] N. Svartholm and K. Siegbahn, Arkiv f. Mat., Astr. o. fys. Bd 33A, No. 21, and Nature 157, 872 (1946); N. Svartholm, Ark. f. Matem., astr. o. fysik, Bd 33A, No. 24.
[2] N. Bartky and A. J. Dempster, Phys. Rev. 33, 1019 (1929).
[3] A. E. Shaw, Phys. Rev. 44, 1006 (1933), and 54, 193 (1938).
[4] H. Bondy and K. Popper, Ann. d. Physik 17, 425 (1933).

On γ-Induced β-Disintegration: Experimental*

R. L. Burling and F. N. D. Kurie
Department of Physics, Washington University, St. Louis, Missouri
May 13, 1948

An endoergic β-decay, induced by γ-radiation, will be energetically possible if the energy of the incident photons is greater than the sum of the rest energy of a positron-electron pair (1.02 Mev) and the mass difference between the initial and final atoms (assuming neutrinos of zero rest mass). Thus the product of an element of atomic number Z and mass number A which decays by the reaction

$$(Z)^A\rightarrow(Z+1)^A+e^-+\nu+Q$$

might undergo a reaction

$$(Z+1)^A+\gamma\rightarrow(Z)^A+e^++\nu,$$

(ν standing for a neutrino). In view of the probable radioactivity of the neutron,[1] the particular case $Z=0$ corresponds to the photo-disintegration of the proton. In spite of the small cross section predicted for such a process,[2] it was thought worth while to verify experimentally that the cross section was small compared to that for the production of photo-neutrons in deuterium and beryllium, by comparing the neutron yield in the three cases.

The thresholds for the photo-disintegration of the proton, deuteron,[3] and beryllium[5] are 1.77, 2.19, and 1.63 Mev, respectively. The first figure is the neutron-hydrogen mass difference of 0.75 Mev[3], plus the rest mass of a pair, 1.02 Mev. Cl^{38}, having a γ-ray capable of disintegrating H and Be but not D, would be a good source for the purpose, but was not available in sufficient strength; so Mn^{56}, with γ-rays at 0.845, 1.81, 2.13, and 2.7 Mev[4,5], was used. Two of these γ-rays could presumably produce photo-neutrons from either H or Be but not from D, while the last could produce them from all three.

A Mn^{56} source having a γ-ray strength of the order of $\frac{1}{3}$ rhm was surrounded by sufficient Lucite to reduce the energy of the fastest β-particles to below 2 Mev, and was placed at the center of a cylindrical vessel containing 22.5 liters of distilled water. Neutrons were detected by means of a silver cylinder which was placed between the γ-ray source and the water for three minutes, and then quickly transferred to a position in which it surrounded a thin-walled glass Geiger-Mueller counter.

Adding the counts obtained in three 30-second counting periods (each following a three-minute exposure) in each case, the counts, corrected for a background of 27 ± 2 counts, for activity remaining in the silver from previous runs, and for decay of the γ-ray source, were: with 1250 moles of distilled water, 7 ± 6; after replacing 25 g of the water by D_2O and stirring, 51 ± 9; and after replacing 750 cc of that water by an acid solution of the beryllium chloride containing $6\frac{1}{4}$ moles of Be, 552 ± 23. Using the second of these counts to correct the first and third for photo-neutrons attributable to the deuterium present, taking into account the numbers of atoms present in the same volume in the three cases, and assuming that an increase equal to one-third of the background count would have been observable in the case of hydrogen, the ratio of photo-neutron production per atom in H to that in Be must be less than 5×10^{-5}, while the ratio for Be to D is 5.

The latter ratio gives no information relative to cross sections, since the number of photons with energy sufficient to disintegrate D is smaller than the number able to disintegrate Be; it may be compared with the value of 7.7 for the same ratio, obtained by Russell *et al.*[6] (the ratio of their neutron yields per Curie-second has been multiplied by the ratio of the number of atoms of D to the number of atoms of Be used). Considering differences in

geometry and in the degree of moderation of the neutrons, precise agreement is not to be expected.

The ratio of 5×10^{-5} should, however, be considered as an upper limit to the ratio of the cross section for photo-disintegration of the proton to that for Be, since the same two γ-rays (1.81 and 2.13 Mev) are involved in both cases. The cross section for the Be (γ,n) reaction appears to vary with photon energy in an unknown manner. Russell *et al.*[6] give $>10\times10^{-28}$ and 3.3×10^{-28} cm^2 as the cross sections at 1.67 and 2.5 Mev, respectively. Assuming a value of the order of 8×10^{-28} cm^2 near 1.81 and 2.13 Mev, an upper limit of 4×10^{-32} cm^2 can be set for the cross section for photo-disintegration of the proton by photons of energy in the neighborhood of 2 Mev.

The authors wish to express their indebtedness to A. A. Schulke for his assistance in providing the radioactive source used.

* The research described in this paper was supported, in part, by the Research Corporation and by the Navy Department under Contract N6ori-117, T.O. 1.

[1] A. H. Snell and L. C. Miller, Bull. Am. Phys. Soc., Washington Meeting 1948, abstract F12.
[2] H. Primakoff, Phys. Rev. **74**, 110 (1948).
[3] W. E. Stephens, Rev. Mod. Phys. **19**, 19 (1947).
[4] L. G. Elliot and M. Deutsch, Phys. Rev. **64**, 321 (1943).
[5] A. Wattenberg, Phys. Rev. **71**, 497 (1947).
[6] B. Russell, D. Sachs, A. Wattenberg, and R. Fields, Phys. Rev. **73**, 545 (1948).

On γ-Induced β-Disintegration: Theoretical*

H. PRIMAKOFF
Department of Physics, Washington University, St. Louis, Missouri
May 13, 1948

IN conjunction with the experiment performed by Dr. Kurie and Dr. Burling, and described in the present issue of the Physical Review,[1] a calculation has been made of the cross section for neutron (and positron) production due to irradiation of hydrogenous materials by γ-rays. The reaction treated is

$$\gamma+P\rightarrow N+e^++\nu, \tag{1}$$

where γ, P, N, e^+, and ν refer to the γ-ray, proton, neutron, positron, and neutrino, respectively; the cross section obtained on the basis of the Fermi theory of β-decay is $\sim10^{-46}$ cm^2 at the γ-ray energies used. Thus, Burling and Kurie's failure to detect any γ-induced neutrons in their experiment and their estimate of an upper limit to the cross section as $\sim10^{-32}$ cm^2 is in agreement with the β-decay theory.

The numerical value for the cross section quoted above is obtained with the use of time dependent perturbation theory to calculate the corresponding transition probability, the scalar interaction between the electron-neutrino and proton-neutron fields being assumed. In this perturbation theory, the reaction in Eq. (1) is treated as a two-step process: $P\rightarrow N+(e^+)'+\nu$ followed by $(e^+)'+\gamma\rightarrow e^+$ and $\gamma\rightarrow e^++e^-$ followed by $P+e^-\rightarrow N+\nu$, the matrix elements, the energy denominators, the density of final states, the summations over intermediate states and over the spins and polarization of the P, N, e^+, ν, and γ being all evaluated in the usual way. The resultant expression for the cross section of (1), σ_γ may be written as

$$\begin{aligned}\sigma_\gamma&\sim(2\pi^3\cdot30)^{-1}(2\pi e^2/\hbar c)G^2(\hbar/m_ec)^2\\&\quad\times\{[[E_\gamma-(M_Nc^2-M_Pc^2)]/m_ec^2]^5(m_ec^2/E_\gamma)\}\\&\sim(2\pi e^2/\hbar c)(\hbar(T')^{-1}/m_ec^2)(\hbar/m_ec)^2(m_ec^2/E_\gamma)\end{aligned} \tag{2}$$

for $M_Nc^2-M_Pc^2\ll E_\gamma\ll M_Pc^2$. (For $E_\gamma\gg M_Pc^2$ the γ-energy dependent quantity in the curly brackets is replaced by $\sim[M_Pc^2/m_ec^2]^2$.) In Eq. (2), e, $\hbar$, c have their usual significance; M_P, m_e, M_N are the proton, electron, and neutron rest masses, respectively; E_γ is the γ-ray energy; G is the (dimensionless) interaction constant between the electron-neutrino and proton-neutron fields; T' is the mean life of a completely allowed β-decay process with an energy release equal to $E_\gamma-(M_Nc^2-M_Pc^2)$; one has $\sigma_\gamma\sim10^{-46}$ cm^2 for $E_\gamma\leqq2$ Mev. Other types of interaction between the light and heavy particle fields, e.g., polar vector, should yield comparable values for σ_γ.

In conclusion it might be of interest to give the results of a calculation for the cross section of the electron capture reaction:

$$e^-+P\rightarrow N+\nu, \tag{3}$$

i.e., the creation of neutrons and neutrinos as a result of electron-proton collisions. The corresponding cross section, σ_e (calculated in a manner analogous to that of σ_γ, though, of course, the reaction now involves a single step process), is

$$\sigma_e\sim(2\pi)^{-1}G^2(\hbar/m_ec)^2\{E_e-[(M_Nc^2-M_Pc^2)/m_ec^2]\}^2, \tag{4}$$

for an electron energy $E_e\ll M_Pc^2$. (For $E_e\gg M_Pc^2$, the electron-energy dependent quantity in the curly brackets is replaced by $\sim[M_Pc^2/m_ec^2]^2$.) Thus $\sigma_e\sim2\times10^{-45}$ cm^2, for $E_e\leqq2$ Mev. A cross section of essentially the same value also applies to the neutrino capture reaction, $\nu+P\rightarrow N+e^+$,[2] in which the roles of the neutrino and electron are interchanged (relative to Eq. (3)).

* The research described in this paper was supported in part by Contract N6ori-117, U. S. Navy Department.
[1] R. L. Burling and F. N. D. Kurie, Phys. Rev. **74**, 109 (1948).
[2] See the general discussion of the absorption of neutrinos in matter by H. R. Crane, Rev. Mod. Phys. **20**, 292–4, (1948) in which an estimate, due to Bethe, of 10^{-44} cm^2 is quoted for the cross section of the neutrino capture reaction, and where it is concluded on the basis of an analysis of various experiments and of geophysical evidence that the neutrino capture cross section (by typical nuclei) is probably smaller than 10^{-36} cm^2.

Attempt to Detect Neutral Particles Produced by Exchange of Charge with Cosmic-Ray Mesons

ROGERS D. RUSK AND ALMA ROSENBAUM
Mount Holyoke College, South Hadley, Massachusetts
May 17, 1948

RECENT experiments at Berkeley[1] indicate the existence of exchange of charge between protons and neutrons. In such an exchange the particle may suffer little loss of energy or deviation in angle. The same type of exchange might be expected to occur between charge and neutral mesons if the latter exist. During the course of some experiments on absorption and scattering an attempt was made to detect the production of high speed neutral particles in heavy elements by cosmic-ray mesons

which have penetrated a considerable layer of absorbing material in the laboratory. If such particles were produced by an exchange process, their detection would depend on the life of the neutral particle and the frequency of occurrence of the exchange.

Recently de Vos and du Toit[2] reported an effect which they ascribed to neutral particles in incident cosmic rays detected by means of paraffin placed either above or below the first tube of a coincidence counter. In the present experiment measurements were made to see if the ionizing rays which have already passed through the first tube of a coincidence-anticoincidence arrangement would produce an effect in iron or lead which would then be sensitive to the presence of a light substance such as paraffin. Measurements with iron were of interest because of the observations that negative mesons absorbed in iron do not give evidence of ionizing decay products.

Four Geiger-Mueller tubes $18\times 2\frac{1}{4}$ inches were used in a vertical array. The second tube from the top was connected in anticoincidence. Layers of iron, lead, and paraffin were used in thicknesses of 10, 7, and 3.7 centimeters, respectively. Above the lowest tube 7 centimeters of lead served to insure that the rays which were counted after passing through the absorbing material were penetrating rays, presumably mesons. With lead or iron above the anticoincidence tube and paraffin below it, as many as 20 percent more counts was registered than when the position of the heavy absorber and paraffin were reversed. Comparison measurements with layers of one material in different positions, however, indicated that these large differences were mostly due to scattering and absorption depending on the position and nature of the material. The differences in counts which were obtained were always in the direction to be expected if a neutral ray from iron or lead passed through the anticoincidence tube and produced an ionizing ray in the paraffin, but it is obvious that the probability of such a twofold occurrence would be small unless the separate probabilities were fairly large.

Because of low counting rate, in spite of large tubes, the measurements were made over a period of several months and the total counts for each of a considerable number of combinations was of the order of 600. Upon subtracting the corrections for scattering and absorption a small effect remained which was of the order of magnitude of the statistical error. However, in repetitions of the measurement this difference was always in the same direction and could be explained by the presence of neutral mesons. Since the heavier meson is now thought more probably to interact with nuclei, the effect may not be measurable with the lighter meson. It may be concluded from the measurements that exchange, if present, is small but not completely ruled out. On account of the size of the tubes and their arrangement, shielding from side showers and accidental counts was impractical. A more exact check of the possibility of the above exchange phenomena might be made if adequate shielding could be provided.

[1] B. J. Moyer, R. Hildebrand, N. Knable, T. J. Parmley, and H. York, Bull. Phys. Soc. **22**, 4 (1947); J. Hadley, C. E. Leith, and H. York, Phys. Rev. **73**, 5, 541 (1948).
[2] P. J. G. de Vos and S. J. du Toit, Phys. Rev. **70**, 229 (1946).

The Polarization of Neutrons by Magnetized Iron

J. M. Cassels
Cavendish Laboratory, Cambridge, England
May 13, 1948

RECENT measurements of the amorphous[1] and disorder[2] scattering cross sections of iron for slow neutrons permit a redetermination of the mean scattering length of the iron nuclei.

The new value is

$$\langle a_r\rangle_{Av}=(1/2\pi^{\frac{1}{2}})(11\cdot 0-0\cdot 8)^{\frac{1}{2}}\times 10^{-12}=9\cdot 01\times 10^{-13}\text{ cm}.$$

The significance of this result in the present context lies in the fact that p, the magnetic scattering cross section which determines the magnitude of neutron polarization effects,[3] is proportional to $\langle a_r\rangle_{Av}$.

Since Halpern, Hamermesh, and Johnson[3] used a value $\langle a_r\rangle_{Av}=7\cdot 33\times 10^{-13}$ cm, their theoretical values of p should be raised by a factor $1\cdot 23$; the theoretical "single transmission effects" are correspondingly increased by a factor $(1\cdot 23)^2=1\cdot 51$.

This modification removes about half of the discrepancy between the observations of Fryer[4] and the theoretical values, as recalculated by Hamermesh.[5] Little further increase can be expected in $\langle a_r\rangle_{Av}$, since the disorder scattering adopted here has already a very small effect, and the amorphous scattering cross section is not likely to be much in error.

[1] L. J. Rainwater, W. W. Havens, Jr., and C. S. Wu, Phys. Rev. **73**, 1265 (1948).
[2] J. M. Cassels and R. Latham, Phys. Rev. **74**, 103 (1948).
[3] O. Halpern, M. Hamermesh, and M. H. Johnson, Phys. Rev. **59**, 981 (1941).
[4] E. M. Fryer, Phys. Rev. **70**, 235 (1946).
[5] M. Hamermesh, Phys. Rev. **61**, 17 (1942).

Cloud-Chamber Study of Electrons from Meson Decay*

Jacob L. Zar, Joseph Hershkowitz, and Evelyn Berezin
New York University, New York City, New York
May 24, 1948

AN experiment is under way to determine the energy spectrum of electrons arising from decay of mesons at sea level. Three cloud-chamber tracks have been obtained. Range and scattering observations are consistent with energies of 13, 18, and 50 Mev.

The experimental arrangement is shown in Fig. 1. The telescope accepts mesons through angles of 30° and 95° parallel and perpendicular to the plane of the figure, respectively. The cloud chamber, C.C., is rectangular, $10\times 16\times 4\frac{1}{2}$ in., and contains nine $\frac{1}{8}$- and $\frac{1}{4}$-in. aluminum plates. It is set off by a fourfold coincidence event $(ABCD-X)$ within a resolving time of 30 μsec. Mesons are absorbed in a carbon plate, D, 2 cm thick by $4\frac{1}{2}\times 10$ in. Counters, E, have $\frac{1}{32}$-in. copper walls.

The telescope recorded 485 incident mesons per hour. Calculations, neglecting scattering, lead to a conservative estimate of $\frac{1}{2}$ percent for the fraction of mesons stopped. The solid angle subtended by the set of side counters is 2.3

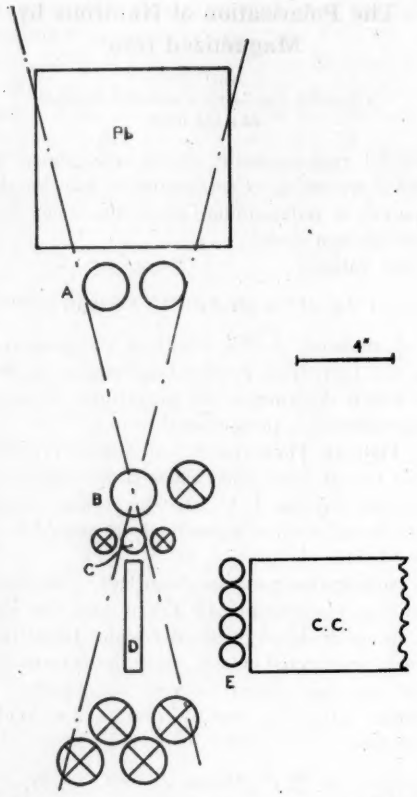

FIG. 1. Cosmic-ray telescope. Counters *ABC* and *E* are in coincidence. Crossed counters are anticoincidence. *D* is 2-cm carbon absorber. C.C. is cloud chamber.

steradians; hence, the expected number of expansions was about one in two hours. The number actually occurring was one per hour. Two hundred hours of operation were selected during which the apparatus was performing properly. Only 17 pictures were obtained which could in any way be interpreted as decay electrons. Of these, 12 penetrated only the first or second compartments of the cloud chamber and are classified as doubtful. Two more tracks appear to be electrons which left the chamber without stopping or scattering. Descriptions of the other three tracks are given below.

A track was identified as a decay electron by its ionization and scattering. Neon lights, photographed with the track, indicated which of the side counters was discharged by the decay electron and served as a further check on the identification of the particle. The energy of the electron was determined from its range by the Bethe-Block formula,[1] including radiation loss.

Track F2-9 stops in the third plate and shows some scattering. Its range is 1.58 ± 0.32 cm Al $+0.16$ cm Cu $+1\pm1$ cm carbon. This is consistent with an energy of 13 ± 3 Mev.

Track F2-11 penetrates two plates and shows large scattering in the gas of the second compartment. It was assumed that as it left the chamber through the side wall, it had negligible energy. Its range is 1.96 cm Al $+0.25$ cm Cu $+1\pm1$ cm carbon, which corresponds to an energy of 18 ± 4 Mev.

Track F4-5 penetrates eight plates showing scattering and leaves the chamber without stopping. From the scattering formula of Williams,[2] $E\bar{\alpha}_1$ is a constant for a given plate, where $\bar{\alpha}_1$ is the average projected angle of scattering and E the energy. The values of $E\alpha_1$ for this track were computed from seven observations of the scattering. Comparison of the average $E\alpha_1$ with the Williams value gave 15 ± 5 Mev for the most probable energy with which the electron left the chamber. This corresponds to an initial energy for the electron of 50 $(+15, -10)$ Mev.

A particle detected only in the first compartment was counted as natural background and not identified as a decay electron. The average energy for a particle to penetrate the second compartment where the criteria for decay electrons could be applied was 14 Mev for most of these experiments. If all decay electrons had energies greater than this value, we should have observed at least 50 tracks. This estimate is based on the solid angle subtended by the third plate at the carbon absorber and the calculated value of $\frac{1}{2}$ percent for the number of mesons stopped. Actually, only five possible, and twelve additional, doubtful decay tracks were found.

If the Fermi density correction[3] is appreciable, the ranges of the decay electrons for a given disintegration energy would be increased, and the number expected in the chamber on the basis of the Bethe-Bloch formula is presumably a lower limit. The energies given here would then have to be corrected downward for this effect.

The results here cited would appear difficult to reconcile with a monochromatic energy for μ-meson electron decay. A possible explanation is an energy distribution for decay electrons with a maximum frequency below 14 Mev.

We gratefully acknowledge the assistance of Professor I. S. Lowen, who suggested this problem.

* This work is supported by the Office of Naval Research.

[1] W. Heitler, *Quantum Theory of Radiation* (Oxford University Press, London, 1936).
[2] E. J. Williams, Proc. Roy. Soc. **169**, 531 (1939).
[3] O. Halpern and H. Hall, Phys. Rev. **73**, 477 (1948).

Lines of Methane at 7.7μ in the Solar Spectrum*

MARCEL V. MIGEOTTE**
Mendenhall Laboratory of Physics, Ohio State University, Columbus, Ohio
May 17, 1948

IN an earlier publication,[1] the presence of 13 lines of methane was reported in the 3.3μ region of the solar spectrum. Many lines were also found in the 7.7μ region, showing a possible correspondence between the laboratory data obtained on CH_4 by A. H. Nielsen and H. H. Nielsen[2] and the solar observations of A. Adel[3] published in 1941. However, identifications in this region are complicated by the presence of water vapor lines.

Recently, we have obtained improved spectra of water vapor, under laboratory conditions, between 7.2 and 8.2μ by using a more sensitive detector.

The introduction of methane into the optical path gave spectra which permitted a direct comparison with previously obtained solar spectra in the 7.7μ region.

This comparison has shown that methane is responsible

for several unidentified lines observed by A. Adel,[3] in Flagstaff, between 7.2 and 8.1μ.

Details concerning the identification of the 7.7μ fundamental band of CH_4 in the solar spectrum will be published in the Astrophysical Journal.

* Supported by Air Material Command, Wright Field, Dayton, Ohio.
** From the Institut d'Astrophysique de Cointe, University of Liege (Belgium).

[1] Marcel V. Migeotte, Phys. Rev. **73**, 519 (1948); Ap. J., in print.
[2] A. H. Nielsen and H. H. Nielsen, Phys. Rev. **48**, 864 (1935).
[3] A. Adel, Ap. J. **94**, 451 (1941).

On the Intrinsic Moment of the Electron

J. BARNÓTHY
Institute for Experimental Physics, University of Budapest, Budapest, Hungary
May 20, 1948

IN a recent paper Foley and Kusch[1] have reported observations which give, for the g value of the electron,

$$g_S = 2.00244 \pm 0.00006.$$

It is perhaps of interest to mention that in a paper[2] dealing with an attempt to seek the solution of the problem of elementary particles with the help of a non-Euclidian geometry, I obtained for the g value (reference 1, Eqs. (10) and (8)), if the proper mass defect of the electron is also considered (Eqs. (14), (12)):

$$g_S = 2(\mu)_s^* = (\beta_s I_s/S_s)(m_s^*/m_s) = 2.00343.$$

This value is in agreement with the experimental result, and it does not involve the existence of an intrinsic moment of the electron.

[1] H. M. Foley and P. Kusch, Phys. Rev. **73**, 412 (1948).
[2] J. Barnóthy, Papers of Terrestrial Magnetism, Hungary, No. 2, (1947). See review in Nature **160**, 847 (1947).

On a Refinement of the W.K.B. Method

ISAO IMAI
Physical Institute, Faculty of Science, University of Tokyo, Tokyo, Japan
May 17, 1948

AS is well known, the W.K.B. method is a very powerful mathematical tool in the application of quantum mechanics. Moreover, it can also be applied with success to problems in other fields of mathematical physics, e.g., propagation of electromagnetic waves, high speed flow of gases, etc. The method is essentially concerned with the asymptotic solution of the second-order differential equation:

$$d^2\Phi/dx^2 + k^2 P(x)\Phi = 0 \quad \text{for} \quad k \to \infty. \tag{1}$$

According as $P(x)$ is positive or negative, the solution Φ is known to behave like a sine or an exponential function. The connection between the regions where $P(x)$ is positive and negative can be established by the various procedures due to Kramers,[1] Zwaan,[2] Langer,[3] and Furry.[4] But none of these procedures except Langer's provides a reliable information as to the behavior of Φ near the turning point, at which $P(x)$ changes the sign.

In an attempt to apply the W.K.B. method to the two-dimensional flow of a compressible fluid, the present writer developed a procedure which turned out to be essentially the same as that adopted by Langer. Recently a further refinement of the procedure has been achieved so as to give better approximation to Φ in the neighborhood of the turning point.

If we introduce the variables z and Ψ, defined by

$$z = \int P^{\frac{1}{2}} dx, \quad \Phi = P^{-\frac{1}{4}}\Psi, \tag{2}$$

Eq. (1) becomes

$$d^2\Psi/dz^2 + (k^2 - Q)\Psi = 0, \tag{3}$$

where

$$Q = P^{-\frac{1}{4}} d^2(P^{\frac{1}{4}})/dz^2 = -P^{-\frac{1}{2}} d^2(P^{-\frac{1}{4}})/dx^2. \tag{4}$$

Except in the immediate neighborhood of the turning point Q is finite, so that for $k \to \infty$ (3) may be asymptotically solved by

$$\Psi \sim Ae^{ikz} + Be^{-ikz} \quad \text{or} \quad A'e^{k|z|} + B'e^{-k|z|}, \tag{5}$$

according as P is positive or negative.

Next, taking $x = 0$ to be a turning point, let us assume that $P(x)$ can be developed in a power series near $x = 0$,

$$P = a_1 x + a_2 x^2 + a_3 x^3 + \cdots. \tag{6}$$

Then, we have, by (2) and (4),

$$z = (2/3)a_1^{\frac{1}{2}} x^{\frac{3}{2}}\{1 + (3a_2/10a_1)x - \cdots\}, \tag{7}$$

$$Q = -(5/36)z^{-2}\{1 + (48/175)(3a_2^2 - 5a_1a_3)a_1^{-4}(3a_1z/2)^{4/3} - (64/375)(14a_2^3 - 35a_1a_2a_3 + 25a_1^2a_4)a_1^{-6}(3a_1z/2)^2 + \cdots\}. \tag{8}$$

Now, it can be shown without difficulty that the differential equation

$$d^2\Psi_1/dz^2 + \{\kappa^2 + (5/36)z^{-2} + \lambda(3z)^{-1}\}\Psi_1 = 0 \tag{9}$$

is satisfied by

$$\Psi_1 = z^{1/6}\xi^{\frac{1}{2}} Z_{\frac{1}{3}}(3^{-1}\kappa\xi^{\frac{3}{2}}), \quad \xi = (3z)^{\frac{1}{3}} + \lambda\kappa^{-2}, \tag{10}$$

where $Z_{\frac{1}{3}}$ is the Bessel function of order $\frac{1}{3}$.

Comparison of (3), (8), and (9) shows that Ψ_1 provides a very good approximation to Ψ, if we take

$$\lambda = (12/35)(3a_2^2 - 5a_1a_3)(2a_1^3)^{-4/3},$$
$$\kappa^2 = k^2 - (4/75)(14a_2^3 - 35a_1a_2a_3 + 25a_1^2a_4)a_1^{-4}.$$

Thus

$$\Phi_1 = P^{-\frac{1}{4}} z^{1/6}\xi^{\frac{1}{2}} Z_{\frac{1}{3}}(3^{-1}\kappa\xi^{\frac{3}{2}}) \tag{11}$$

is a very good approximation to Φ in the neighborhood of $x = 0$. It may be interesting to note that Φ_1 is a one-valued function of x.

If k and hence κ are large, (10) reduces to

$$\Psi_1 = z^{\frac{1}{2}} Z_{\frac{1}{3}}(kz), \tag{12}$$

which is just the same as Langer's result. It should be remarked, however, that the above reduction is valid only so long as z and hence x are not too small except when λ vanishes exactly. In fact, Langer's expression (12) satisfies Eq. (9) with $\lambda = 0$, which can be an approximation to (3) only to the order of z^{-2}. Further it may be mentioned that the connection formulas can be readily obtained from (11) by use of the asymptotic expression for the Bessel function.

Details of the analysis as well as applications will be given elsewhere.

[1] H. A. Kramers, Zeits. f. Physik **38**, 518 (1926).
[2] A. Zwaan, Thesis, Utrecht (1929).
[3] R. E. Langer, Trans. Am. Math. Soc. **33**, 23 (1931); **34**, 447 (1932); Phys. Rev. **51**, 669 (1937).
[4] W. H. Furry, Phys. Rev. **71**, 360 (1947).

Proceedings of the American Physical Society

Minutes of the Meeting of the Ohio Section at Columbus on March 13, 1948

FAIR weather, good roads, the promise of seventeen contributed papers, a special lecture, and a scheduled discussion of the problem of registration of physicists in Ohio were sufficient reasons to bring a large number to the 1948 Winter Meeting of the Ohio Section, held on March 13 at Columbus. There were more than 200 in attendance, coming from all corners of the State. The item of business of some general interest, namely, the question of registration of physicists, was settled for the present by deciding against the promotion of a State Register of Physics. There was enough discussion so that all seemed satisfied with this solution.

The special lecture was delivered by J. G. Daunt (Ohio State University) under the title "The behavior of the helium isotopes in the liquid phase." Titles of the contributed papers are appended.

LEON E. SMITH, *Secretary-Treasurer*

1. **Slave Sweep Circuits for Nuclear Research.** R. J. WATTS, *Ohio State University.*

2. **Disintegration by Consecutive Electron Capture in Nucleus 131.** FU-CHUN YU AND J. D. KURBATOV, *Ohio State University.*

3. **Study of Metastable and Resonance Atom Populations in Gas Discharges.** CARL KENTY, *General Electric Company.*

4. **The Structure of Evaporated Cobalt Films.** C. S. SMITH, J. C. HART, E. C. CRITTENDEN, AND L. O. OLSEN, *Case Institute of Technology.*

5. **Methods of Observing Microwave Absorption Lines.** DUDLEY WILLIAMS, *Ohio State University.*

6. **The Piezoelectric Measurement of Acoustic Absorption and Reflection in Fluids.** JOSEPH L. HUNTER, *John Carroll University.*

7. **Method for the Absolute Measurement of Dynamic Properties of Linear Structures at Sonic Frequencies.** W. JAMES LYONS AND IRVEN B. PRETTYMAN, *Firestone Company.*

8. **Demonstration of Some Optical Phenomena Using 3.2-cm Microwave Source.** MILAN J. KRASNICAN, *Antioch College.*

9. **Description of a Klystron Oscillator for Microwave Demonstrations and Measurements.** HARDY TROLANDER, *Antioch College.*

10. **The Physical Properties of Water Substance Near the Critical Temperature.** G. E. OWEN, *Antioch College.*

11. **The Infra-Red Spectrum of Dimethylacetylene.** ABNER WOLLAN, *Ohio State University.*

12. **A Physical Science Course.** OLIVER S. LOUD, *Antioch College.*

Special Lecture: The Behavior of the Helium Isotopes in the Liquid Phase. JOHN G. DAUNT, *Ohio State University.*

13. **The Absorption of Incident Quanta By Atoms.** JOHN A. VICTOREEN, *Victoreen Instrument Company.*

14. **Measurement of the Coefficient of Expansion of Microgram Samples of Metals.** R. E. BROCKLEHURST AND L. F. VASSAMILLET, *Monsanto Company.*

15. **Dynamical Parallaxes and the Apparent Failure of the Mass Luminosity Law.** ALLEN HYNEK, *Ohio State University.*

16. **A Vacuum Double Crystal X-Ray Spectrometer.** C. H. SHAW AND J. N. COOPER, *Ohio State University.*

17. **The Ohio State Electrostatic Generator.** J. N. COOPER AND C. H. SHAW, *Ohio State University.*

Minutes of the Meeting of the Ohio Section at Toledo on May 8, 1948

THE Ohio Section of the American Physical Society held its 1948 Spring Meeting as a joint meeting with Section F of the Ohio Academy of Science on May 8 at the University of Toledo, Toledo, Ohio. Pleasant weather was a contributing factor in the attendance of over one hundred.

New Officers selected for the coming year were: PAUL B. TAYLOR (Wright Field, Dayton), as *Chairman;* DONALD DOOLEY (Hiram College) as *Vice Chairman.* LEON E. SMITH was re-elected as *Secretary-Treasurer.*

Abstracts of nearly all of the papers presented are appended.

LEON E. SMITH, *Secretary-Treasurer*

ABSTRACTS

1. A "Brittleness" Testing Device for Small Glass Tubing. CHARLES D. SPENCER, *Lamp Development Laboratory, General Electric Company.*—Glass tubing is manufactured by automatic machine methods. The tensile strength and the cross-bending strength of such tubing varies through wide limits depending on the amount and severity of the surface damage which results from the mechanical contacts established on the glass surface by the drawing machines, the cutting-off mechanisms, and the sorting devices. A simple testing machine is described by means of which a "Factor of Merit" can be assigned to glass tubing according to the extent and the severity of the surface damage that occurs during fabrication.

2. The Absorption and Fluorescence Spectra of Tetraphenylisoporphine and Tetraphenylisoporphine Zinc Salt. H. V. KNORR, *Antioch College.*—The molecular absorption coefficients of tetraphenylisoporphine and tetraphenylisoporphine zinc complex salt have been measured by a method previously described[1,2] with some slight modifications in the apparatus. The dispersing instrument used was a modified Gaertner spectrometer L235 with glass optics. The detecting device was an electron multiplier tube RCAIP22. Anhydrous benzene was used as a solvent. The molecular absorption coefficients are shown in Table I:

TABLE I.

Tetraphenylisoporphine		Tetraphenylisoporphine zinc salt	
wave-length (mμ)	α	wave-length (mμ)	α
655	82.0×10^3	628	105.0×10^3
600	13.5×10^3	600	32.2×10^3
545	23.5×10^3	578	18.7×10^3
518	33.5×10^3	530	12.0×10^3
420	360.0×10^3	426	700.0×10^3

The fluorescence spectrum of tetraphenylisoporphine in benzene solution was excited by means of an AH4 mercury arc lamp. The maxima of the principal fluorescence bands are located at 656.6 mμ and 723.3 mμ.

[1] V. M. Albers and H. V. Knorr, J. Opt. Soc. Am. **28**, 121 (1938).
[2] V. M. Albers and H. V. Knorr, J. Chem. Phys. **9**, 497 (1941).

3. The Illuminant Problem in the Spectrophotometry of Fluorescent Materials. W. R. KOCH, *Wright-Patterson Air Force Base.*—The colors of many aircraft materials have been specified satisfactorily in terms of spectrophotometric measurements. However, the apparent spectral reflectance data for fluorescent materials depend upon the energy distribution of the illuminant as well as upon the position of the dispersing element in the spectrophotometer. Spectral data on three fluorescent materials used for signal and identification purposes were obtained by a Keuffel and Esser instrument in which the monochromator is between the sample and the observer. Brightness measurements relative to magnesium oxide were made at individual wave-lengths for direct sunlight and various laboratory illuminants. Tungsten illumination corresponding to I.C.I. Illuminant "A" did not show the effective luminosity which is the significant characteristic of materials. Spectral curves for non-fluorescent U. S. Air Force No. 508 International Orange and one of the fluorescent signal colors were similar for tungsten illumination, whereas the spectral curves for the two materials were radically different under direct sunlight. Introduction of a calibrated filter in the sample beam indicated that the maximum spectral reflectance of the fluorescent material was more than twice that of magnesium oxide. In order to avoid the inconvenience and lack of reproducibility inherent in the use of sunlight for laboratory tests, the RS-type sunlamp under standardized conditions was selected to provide spectral data which are suitable for procurement specification purposes.

4. Specular Infra-Red Spectral Reflectance for the Analysis of Organic Materials. GEORGE RAPPAPORT, *Wright-Patterson Air Force Base.*—Organic as well as inorganic compounds exhibit selective reflection maxima in the infra-red region of the spectrum. The reflecting power of a compound at various wave-lengths in the infra-red is related to its molecular structure. Although the spectral reflectance is usually low, it increases rapidly in the neighborhood of the frequency of a strong vibration. Thus, reflectance maxima can be observed at frequencies which correspond to strong, fundamental oscillations of molecules. A Perkin-Elmer infra-red spectrometer has been modified to give reflectance data by substituting a reflecting surface made from the material under investigation for the plane mirror in the source box. The reflecting surfaces were prepared by compressing the crystals of organic compounds into thin disks on a 20-ton press. The reflection maxima of several crystals and plastic sheets, such as sulfanilic acid, urea, polymethyl metacrylate, cellulose acetate, polystyrene, etc., were determined. For the determination of the fundamental frequencies and the identification of insoluble solid bodies by means of infra-red spectroscopy the reflection method has provided data unobtainable by conventional methods.

[1] C. Schaefer, "The infrared spectra of solid bodies," published in *Molecular Spectra and Molecular Structure* (Faraday Society, London, 1929), p. 844.

5. Utilizing the Vernier Principle for Precise Readings of Slide Rule Settings. ROGER C. WICKENDEN, *Miami University.*—The vernier principle may be employed to increase the accuracy of silde rule settings without the use of any attachments. Proper setting of the C scale enables it to be used as a vernier to read the D scale. Also, the B scale may be used as a vernier to read the A scale. Any desired ratio of divisions on the vernier to divisions on the scale may be obtained.

6. Acoustic Interpretation of Interferometer Data. JOSEPH L. HUNTER, *John Carroll University.* It may be shown that a resonant liquid column of variable length coupled to a vibrating piezoelectric crystal causes the crystal to present to the associated electrical circuit an impedance which may be represented as a pure resistance in parallel with a pure capacitance. The capacitance is the dielectric capacitance of the crystal and the resistance is found, electrically, to increase with increasing column lengths. The paper deals with the interpretation of this increase of resistance as due to attenuation in the liquid, and discusses the quantitative determination of attenuation from the curve of resistance *versus* path length.

7. Present Problems in Conduction of Electricity in Gases. W. M. BRUBAKER, *The Westinghouse Company.*—(No abstract submitted.)

8. A Combination Electron Diffraction and X-Ray Tube. JOHN E. EDWARDS AND KARL A. DAVIS, *Ohio University.*—A combination electron diffraction and x-ray tube has been constructed so as to utilize the same high potential and evacuating systems. The electron diffraction unit was adapted to fit in place of the target assembly in a three-electrode x-ray tube similar to that designed by Dershem.[1] The rough electrostatic focusing of the x-ray filament assembly provides an adequate supply of electrons to the collimators. A grid attached to the filament assembly serves to shift the focal spot to the position of the first collimator and to control the exposure times. A rotating disk in the diffraction unit provides space for five exposures and a fluorescent viewing screen.

[1] E. Dershem, Rev. Sci. Inst. 7, 86 (1936).

9. The Optics of Curved Glass. D. W. DUNIPACE, *Libbey-Owens-Ford Glass Company.*—Glass is characterized by its capacity to transmit vision. In many applications the glass elements produce desirable changes in the brightness or apparent dimensions of the image transmitted, while windows characteristically produce a minimum of change. In the case of optical instruments, the dependence of transmission and optics on the glass composition and optical design is well known. A window is also an optical element and its performance depends on its design. The key to this dependence is Snell's law: $n_i \sin i = n_r \sin r$. Simplified equations can be developed for the deviation of light rays through windows. The deviation effects due to thickness, wedge, and curvature in glass windows have been represented graphically. An example is given in which seriously deficient performance was overcome by proper design of a curved glass window. Approximate relations have been developed in the same or similar form by others, but it has seemed of interest to illustrate their application to windows. It is thus shown that the optical performance is a consequence of the glass shape, so that optics, as well as other architectural features, should be considered in the design of curved glass windows.

10. The Discoloration of Glass by Radium Radiations. W. J. ARNER AND D. E. SHARP, *Libby-Owens-Ford Glass Company.*—Spectral curves and data are presented on the development of color in a borosilicate glass caused by radioactive rays over a long period of time.

11. Effects of Milling on Zinc Beryllium Silicate Phosphors. SHANNON JONES, *Lamp Development Laboratory, General Electric Company.*—Data are presented on the effects of varying times of dry pebble millings on various synthetic zinc beryllium silicate phosphors. The phosphors vary in their degree of sintering as originally prepared, and relations between milling times and changes in effective particle sizes, as indicated by an air permeation method, are discussed. Data on relations between particle sizes as reduced by milling and the apparent fluorescent brightness of these phosphors are presented.

12. Recrystallization of Zinc at Room Temperature. NORMAN GOSS, *S.O.M. Center.*—The recrystallization of cold-rolled zinc was observed at room temperatures by the x-ray diffraction pinhole method. The cold reduced specimen was 0.002″ thick and mounted directly on the pinhole. Molybdenum radiation was used and no filter was employed. X-ray patterns were taken each 24 hours for 28 days. The changes in the recrystallization were very rapid the first 72 hours after which the changes in grain growth were very slow. Even after 28 days recrystallization was not complete at a room temperature of about 72°F. Heating the sample in boiling water did complete recrystallization with increase in grain size. Evidence is presented to prove that the grains which first form are perfect, but due to growth forces and constraints resisting their growth, distortion by block dislocation occurs. Several other observations were noted in this study.

13. X-Ray Diffraction Evidence for ZnS Formation in Zinc Activated Rubber Vulcanizates. W. L. DAVIDSON, *The B. F. Goodrich Research Center.*—With regard to the ultimate fate of the zinc in soluble zinc activated rubber stocks, certain workers believe that it appears finally as ZnS via the following reaction sequence:

$$2R+2S\rightarrow 2R-S^{-}+Zn^{++}\rightarrow$$
$$R-S-Zn-S-R+S\rightarrow R-S-S-R+ZnS,$$

where R = allyl rubber radical or ion and S = activated sulfur. Arguing from the absence of ZnS lines in x-ray diffraction patterns of such stocks, recent workers claim that the last step pictured does not occur; the zinc remains in combination with rubber as a mercaptide.

It has been shown that in the presence of a long chain fatty acid soap ZnS is soluble in rubber. Such is not the case, however, when a short chain fatty acid soap is used. To determine if ZnS solubility might explain the negative x-ray results, we have carried out diffraction studies on stocks compounded from acetone extracted rubber and activated with zinc acetate, zinc benzoate, or zinc propionate. In all three cases we have obtained the characteristic diffraction pattern of β-ZnS from the cured stocks, thus proving that ZnS is formed and that the final step above is a possible one. Studies are continuing on the mechanism whereby ZnS can be made soluble in rubber.

14. Formation of Radioactive Zinc Dimethyl Dithiocarbamate in the Vulcanization of Rubber. I. G. GEIB, *The B. F. Goodrich Research Center.*—When a stock containing rubber, zinc oxide, tetramethylthiuram monosulfide (TMTM) and sulfur is cured, zinc dimethyldithiocarbamate (ZnDMDC) is formed.[1] If radiosulfur is employed, the ZnDMDC is found to be radioactive. Mechanisms for the formation of ZnDMDC are discussed. That rubber is not necessary was confirmed by forming radio ZnDMDC by heating TMTM, radiosulfur, and zinc oxide. The observed activity of the ZnDMDC is higher than that predicted for a mechanism in which zinc and sulfur add directly to the TMTM molecule. ZnDMDC, which is quite stable thermally, is one of the most active accelerators for the vulcanization of rubber. Radio ZnDMDC should be valuable in future tracer studies on the mechanism of acceleration and vulcanization.

[1] Clark, Le Tourneau, and Ball, Ind. Eng. Chem. **35**, 198 (1943).

MINUTES OF THE MEETING OF THE SOUTHEASTERN SECTION AT OAK RIDGE, TENNESSEE, ON APRIL 9–10, 1948

THE fourteenth annual meeting of the Southeastern Section of the American Physical Society was held at Oak Ridge, Tennessee, on Friday and Saturday, April 9–10, 1948. A record number of 442 registered, and the total attendance was estimated to be 525. There were 410 people at the annual dinner on Friday night.

The regular program consisted of seventy-two papers, abstracts for sixty-four of which are printed below. Abstracts of the other papers will be printed in the *American Journal of Physics.*

The Program Committee, with Dr. C. K. Beck as Chairman, arranged an excellent program of invited papers. These consisted of the following: words of welcome by R. C. Cook of the Atomic Energy Commission; "University Scientists and Government Research Laboratories" by Frank P. Graham, President of the University of North Carolina; "Nuclear Magnetic Resonance" by K. K. Darrow of Bell Telephone Laboratories, Secretary of the American Physical Society; "Reflections of Low Speed Electrons from Polycrystalline Platinum" by C. J. Davisson of the University of Virginia; "Interim Report on Stroboscopic X-Ray Diffraction in Vibrating Crystals" by R. Pepinsky of the Alabama Polytechnic Institute; and "Low Temperature Experiments with Liquid Helium" by J. G. Daunt of Ohio State University. On Saturday afternoon, the visitors were taken on a conducted tour of the Oak Ridge area.

At the business meeting, the election of the following officers for the Section was announced: *Chairman*, E. S. Barr; *Vice Chairman*, Philip Rudnick; *Secretary*, Eric Rodgers; *Treasurer*, H. F. Henry; *Member of the Executive Committee*, C. K. Beck. D. R. McMillan was elected to the Executive Committee to fill the unexpired term of E. S. Barr.

Eric Rodgers, *Secretary*

ABSTRACTS

1. An Improved Axial Magnetic Suspension.* J. F. DILLON AND J. W. BEAMS, *University of Virginia.*—Previous experiments[1] have shown that the axial magnetic suspension offers almost negligible resistance to rotation of symmetrical rotors. Consequently, rotors suspended in a good vacuum can be driven in synchronism with a piezoelectrically controlled circuit without "hunting."[2] As a result, a large number of investigations requiring extremely constant speed rotating mirrors or centrifuges of various weights are possible. In this paper a number of improvements in the axial magnetic suspension will be described. Details of an axial magnetic suspension will be given with which rotors weighing from about 0.1 g to roughly 10^4 grams have been stably suspended. It is possible to suspend smaller or larger rotors by changing the "pick up" or the supporting magnet respectively.

* This work was carried out under the Contract NOrd-7873 with the Bureau of Ordnance, U. S. Navy.

[1] Beams, Young and Moor, J. App. Phys. **17**, 886 (1946).

[2] Beams, Wash. Acad. Sci. **37**, 221 (1947).

2. A Coil System for Producing Longitudinal Magnetic Gradients. W. C. WINELAND, T. M. HAHN, JR.*, AND L. R. BOYD, *Naval Ordnance Laboratory.*—Several types of coil systems have been developed at the Naval Ordnance Laboratory for producing uniform magnetic gradients. One of these, the Gradhelm, which has been previously described,[1] produces uniform transverse and longitudinal gradients of the field components transverse to the major axis of the system. The present coil system, or "Solengrad," yields a uniform longitudinal gradient of the axial component of field. It consists essentially of a set of series-connected square coils of varying numbers of turns spaced uniformly along their common axis. The numbers of turns on the central coils form an arithmetic progression, and the turns on the outermost coils are chosen so as to cause the gradient at the center of the system to be equal to that on the axis at a considerable distance from the center. Details of the design, construction and calibration are given for one such system, 28 feet long, which produces a gradient uniform to within one percent over an axial distance of twelve feet.

* Now at the Massachusetts Institute of Technology.
[1] Shortley and May, J. App. Phys. **16**, 841 (1945).

3. Current Amplifiers for Use with Magnetic Generators. H. E. WOLF, H. SMALL, AND J. H. BUEHLER, *Naval Ordnance Laboratory.*—Two types of current amplifiers are employed to supply the current required for magnetic generators. Both circuits are characterized by linear operation and high stability. The first circuit is a single-ended amplifier of the cathode-follower type. A bank of parallel-connected Type 6L6 tubes controls the current through the load which is in the common cathode circuit. With eight tubes, this amplifier is capable of supplying a peak-to-peak output current of approximately 500 μa to a 100-ohm load. The d.c. component of output current makes this type of amplifier inconvenient when the device being investigated is affected by background field comparable in magnitude with signal fields. To eliminate the background current, a balanced current amplifier has been designed which uses Type 6A3 tubes connected in push-pull. The input voltage is supplied by means of a bridge network, and the maximum peak-to-peak current out put is approximately 200 μa. The applicability of this amplifier is limited in being unusable with single-ended inputs.

4. Controls for Generators of Influence Signals. B. P. RAMSAY, J. H. BUEHLER, AND C. E. MOLINEUX, *Naval Ordnance Laboratory.*—Controls for influence generators consist of a signal simulator, a transit-speed regulator, a power-supply, and an amplifier. Signal simulators differ in regard to the basic control element which is employed and the mechanism by which the signal pattern is impressed upon it. The potential-divider and the photoelectric cell are basic elements which have been found most practical. The transit-speed with which the signal pattern is impressed upon the simulator is regulated satisfactorily by a gear train. Variable-speed friction-drive motors, and field-controlled direct current motors with speed indicators are objectionable for routine measurements in which exact reproducibility of transit-speed is desirable, but are employed when it is necessary to vary the transit-speed by small increments. Several circuits have been found suitable for the power supply and amplifier in transmitting the simulator signal to the influence generator. The controls described here have been employed with generators of static influence-signals, such as magnetic ship-signatures, and for modulating monochromatic carrier waves. They are not suitable for low speed signals of complex frequencies, or for high speed signals of any type.

5. Note on the d.c. Characteristics of the String Galvanometer. II. G. W. CRAWFORD, *North Carolina State College* AND F. T. ROGERS, JR., *University of North Carolina.*—In an earlier analysis[1] of the d.c. performance of a practical commercial form the Einthoven galvanometer, it was assumed that the tension in a string would be given, in terms of the string's elongation $(L-l)$, by $T=t+\delta(L-l)+\Delta(L-l)^2$, a non-linear elastic relation. Measurements have now been made[2] on 0.0004-inch diameter string of gold-plated copper, about 30 mm long: tensions have been measured to ± 1 dyne on the average, from zero to about 400 dynes; extensions have been obtained to ± 0.01 mm on the average, from zero to about 4 mm. Typical of results is the set of values, $t \sim 150$ dynes, $\delta \sim 1.25 \times 10^4$ dynes/cm and $\Delta \sim 2 \times 10^6$ dynes/cm^2; these values are quite concordant with some assumed in reference 1, and to that extent they indicate the general adequacy of the equation.

[1] Rogers, Rev. Sci. Inst. **12**, 351 (1941).
[2] G. W. Crawford, Phys. Rev. **74**, 119 (1948).

6. Sampling Specimens from an Ultra-Centrifuge by Quick Freezing. M. L. RANDOLPH, *Tulane University.*—Previous methods of pipetting or lifting off layers of solution after ultra-centrifugation in the quantity type rotor unavoidably cause some stirring on introducing the sampling devices.[1] Furthermore, incomplete removal of the top layers contaminates the lower layers. Therefore, a quick-freezing technique is suggested. After centrifugation, the sample tubes are put in metal tubes surrounded by a freezing mixture of "dry ice" and alcohol. These metal tubes are an eight inch shorter and a few mils greater in diameter than the sample tubes, with alcohol furnishing intimate contact. Cooling fins are provided. Within two minutes an entire sample is frozen solid and may be cut into sections in a lathe. Thermal insulation between the chuck jaws and sample tube is desirable. After cutting through the plastic wall and a few mils into the frozen solution, the section of sample is neatly broken off and allowed to melt at room temperature. Some changes in biological samples due to freezing and thawing may occur, but do not seem serious. Distinct layers, otherwise unnoticed, may appear following freezing and suggest points for cutting. Preliminary results with normal and pathologic human sera obtained with the cooperation of Dr. Roy H. Turner and associates of the Tulane Medical School will be presented.

[1] Hughes, Pickels and Horsfall, J. Exp. Med. **67**, 941 (1938). Chiles and Severinghaus, J. Exp. Med. **68**, 1 (1938).

7. A Knudsen Type Vacuum Gauge. J. T. MEERS AND L. A. PARDUO, *University of Kentucky.*—DuMond and Pickle[1] first investigated the usefulness of an all metal Knudsen type gauge for indicating continuously the pressure in systems where very low pressures are not maintained. Two gauges were constructed with some modification after the model of these investigators. They were calibrated by comparison with a McLeod gauge and an ion gauge. Curves obtained by plotting deflections of the Knudsen against the readings of the McLeod and the ion gauges showed very satisfactory reproducibility. The gauges were observed over a period of several months and their features noted. (1) The scale is nearly linear. (2) It gives a continuous reading of pressure and the time lag between pressure change and the response of the gauge is of the order of one second. (3) No auxiliary equipment is needed and there is no need for replacements of internal parts. One minor objection is that the gauge requires a solid support near the vacuum system.

[1] DuMond and Pickle, Rev. Sci. Inst. 6, 363 (1935).

8. New Data on Convection in Sands. H. L. MORRISON, *North Carolina State College.*—Since earlier work[1] has indicated the probable partial inadequacy of the only extant theory[2] of the minimum temperature gradient (β_c) required to produce thermal convection currents in liquids in porous media (possibly because the theory neglects the temperature-dependence of viscosity), a new series of measurements has been initiated for establishing the correct law for β_c by experiment. Using water in unconsolidated sands, the new data indicate in accord with the theory, that $\beta_c \propto 1/k$, where k is the sand permeability; they also indicate, again in accord with the theory, that β_c does not depend upon the horizontal extent of the sand. Present efforts are being directed toward determining the dependence of β_c on the depth (D) of the sand, for the theory indicates this to be a very strong dependence ($\beta_c \propto 1/D^2$). These measurements are being made under conditions where D and the horizontal extent are of the same order of magnitude, and where the vertical temperature gradient is a constant plus a cosine-of-distance.

[1] H. L. Morrison, J. App. Phys. 18, 849 (1947).
[2] C. W. Horton and F. T. Rogers, Jr., J. Appl. Phys. 16, 367 (1945).

9. A Mechanical Analysis of the Closure Movements of Venus' Fly Trap. OTTO STUHLMAN, JR., *University of North Carolina.*—The Venus' fly trap is a bivalve shaped structure formed at the end of the spatulated petiole of *Dionaea muscipula*, one of the "carnivorous" plants normally found near Wilmington, N. C. Closure (0.5 sec.) was analyzed with a moving picture camera. Angular closure was directly proportional to the square of the time. The basic movements simulate the motion of a rigid body rotating about a vertical axis under the action of constant normally directed forces. The forces maintaining the trap in its open position can be attributed to the action of an internal hydrostatic pressure localized in the layers of cells forming the inner epidermis. Speed and symmetry of closure can be controlled by the pattern of excitation, originating at the three spike-like organs located on the inner surfaces of the lobes. An excitatory wave-front in the form of an electrical transient, originating, at any one of the three excitatory organs, spreading over the lobes can account for the pattern and speeds of closure. Speed of wave-front about 5 cm/sec. A hydrostatic analogue, in the form of the response mechanism of the Bourdon gauge, is proposed as possessing the necessary and sufficient properties to account for all mechanical motions.

10. A Tensiometer for Elastic Properties of Very Small Wires. G. W. CRAWFORD, *North Carolina State College.*—In order to obtain direct measurements of increasing tension with elongation of small wires (0.0004-inch diameter), an apparatus has been constructed which consists of a vertical aluminum frame on each end of which are mounted micrometer calipers. A very light weight tensile spring, which can be calibrated, is fastened to the upper caliper; attached to its lower end is a light weight aluminum wire of U-shape, the coiled ends of which dip into two vessels containing a viscous fluid to damp out inevitable vibratory oscillations of the system. The very small test wire is fastened between the calibrated spring and the lower caliper. In use, the upper end of the test wire is adjusted always to a zero position as judged by a microscope; elongation is thus measured by the lower caliper, tension by the upper, to average precisions of 0.01 mm and 1 dyne, respectively. Provision is also made for mounting a magnetron magnet on the frame so as to immerse the test wire in a magnetic field, and for a mirror and micrometer microscope which allow observation of the behavior of the test wire when carrying a current in the magnetic field.

11. A Cathode-Follower Type of Dual-Coincidence Circuit. ARTHUR LINZ, JR., AND F. T. ROGERS, JR., *University of North Carolina,* AND G. W. CRAWFORD, *North Carolina State College.*—In a dual-triode gate-circuit[1] as used for detecting twofold coincidences, pulses P are applied to the two grids, and the resulting pulse V across the cathode resistor is used as an indication of grid-pulse coincidences. Let V_1 be the cathode resistor pulse when only one grid is pulsed, and let V_2 be the corresponding pulse caused by the simultaneous pulsing of both grids. Careful measurements have been made to demonstrate how V_2/V_1 depends upon $P<0$: for small values of P, this ratio is 2 or less as required by linear circuit theory; for large values of P, however, it rises to values as high as 8, indicating that the circuit is operating in a far from linear manner. The transition between these two limiting conditions is smooth and monotonic; and it seems possible to provide a graphical treatment of the nonlinear case which, merging into the linear at small P-values, should allow prediction of the V_2/V_1 ratio for a given circuit and known tube characteristics.

[1] Walter Jordan, invited paper read at Southeastern Section meeting on April 4, 1947.

12. Incremental Regulation by Carbon-Pile Type of Voltage-Regulator. V. E. SCHERRER AND F. W. ROGERS, JR., *University of North Carolina.*—In the simple d.c. voltage-regulator described elsewhere,[1] the output-voltage

is considered to be a function of the input-voltage and the equivalent load-resistance, and it is the purpose of the device to minimize $\partial E/\partial V$ and $\partial E/\partial Z$. In terms of the usual symbols, it can readily be shown that

$$\partial E/\partial V = Z_T/\phi, \quad (1)$$

$$\partial E/\partial Z = (V-E)/\phi, \quad (2)$$

where

$$\phi = Z_T + g + Eg'/Z_c. \quad (3)$$

It can also be shown from these equations that g or g' should be as large as practicable, but that perfect regulation is not practical. Tests have indicated that Eqs. (1)–(3) are quite valuable in predicting the incremental regulation for a regulator for which g and the constants are known.

[1] E. E. Caldwell and F. T. Rogers, Jr., Phys. Rev. **74**, 120 (1948).

13. Compensation of Circuits for Variations of Temperature. G. L. JENKINS AND F. T. ROGERS, JR., *University of North Carolina.*—The general features of the process of compensating a circuit of resistance $R_0[1+\alpha \times(T-T_0)]$ by means of a sintered oxide element which has resistance $r_0 \exp[-\beta(1/T-1/T_0)]$, are well known and have been published in various places. Because of the dissimilar characters of these T-functions, however, such compensation is generally not exact; instead, and as an example, if these two units are connected in series and then attached to an e.m.f. E, the current I which flows is temperature sensitive because

$$\partial I/\partial T = -I^2\{R_0\alpha - (\beta r_0/T^2)\exp[-\beta(1/T-1/T_0)]\}/E.$$

Hence the detailed behavior of the resulting "compensated" circuit is a matter which has to be adjusted through the above equation so as most nearly to satisfy applicable requirements, often a matter of compromise. The problem of compensation is further complicated because transients in heat flow (including the effects of self-heating in the elements themselves) may at times render the temperatures of the two units almost random variables.

14. Output Voltage from Carbon-Pile Type of Voltage-Regulator. E. E. CALDWELL AND F. T. ROGERS, JR., *University of North Carolina.*—A simple type of d.c. voltage-regulator[1] consists of a passive non-linear quadripole circuit which, attached to an input-voltage V, delivers a nearly constant output-voltage E, to a load Z. The series element in this quadripole is a carbon-pile resistor R, which is operated magnetically by the current i_c in a solenoid which is a following shunting element of resistance Z_c; there may be a second shunting element as well, but this is combined in the equivalent circuit into Z. Taking $R=g(i_c)$ in the steady state and $i_c=E/Z_c$ and letting $Z_T=Z_cZ/(Z_c+Z)$, it can readily be shown that

$$E\cdot g(E/Z_c)+E\cdot Z_T = V\cdot Z_T. \quad (1)$$

Equation (1) is useful because, solved numerically for E for a given g-function, it predicts the performance of such a regulator using that g-function. It is not difficult to predict E to within average uncertainties of two or three percent in some instances, by Eq. (1).

[1] W. G. Neild, Trans. A.I.E.E. **63**, 839 (1944).

15. A Study of the Mean Radiant Temperature and the Air Temperature in a Panel Heated House. CLYDE B. CRAWLEY, *University of Kentucky.*—The mean radiant temperature of a room may of course be higher or lower than the air temperature. The two temperatures ought not to differ greatly except for sudden changes in outside temperature. Data are given for a panel heated house to substantiate this point. A method of estimating the mean radiant temperature from a simple temperature reading is also given. The air temperature is first obtained with a thermometer at rest. The thermometer is then whirled rapidly in the air and the temperature read a second time. It is found that the mean radiant temperature is approximately equal to the first temperature. A table is given showing the relation between the mean radiant temperature and these two air temperatures.

16. The Formation of Spiral Marks on Fractures. ARTHUR E. RUARK, *The Johns Hopkins University.*—Fractures of glass and plastics show spiral marks called *ripples* (not to be confused with ribs, which are halting points of fracture, according to Poncelet and Murgatroyd). Wallner's explanation of ripples is, that when a fracture-front ruptures a serious flaw, an elastic wave is produced, which interacts with the spreading fracture, changing its characteristics at points on the locus of their intersection. This locus is a ripple. The ripple shape should depend only on the ratio of the elastic-wave speed and the fracture speed. There is evidence that the latter is nearly constant, so that ripple shapes can be used to measure the wave-speed. This varies from one case to another. I have made observations which suggest two modifications. (1) The speed of the finite, complex elastic disturbance is not equal to that of an infinitesimal disturbance, in analogy to plastic waves in metals. (2) As in metals, a flaw may rupture *before* the main fracture strikes it. These factors provide the flexibility needed for full elucidation of the behavior of these finite waves in brittle materials. Specimens will be shown.

17. Speed of Propagation of Fractures in Glass Plates.* V. E. SCHERRER AND ARTHUR LINZ, JR., *University of North Carolina.*—Measurements have been made of the progress of cracks across glass plates, with the object of obtaining information which bears upon the relation of fracture dynamics to initial applied stresses. Each crack was made to break a number of electric circuits (colloidal graphite) on the surface of a plate; and the circuit-breaks were recorded by means of a spark chronograph. Plate dimensions of 30 cm by 60 cm with a thickness of 0.3 cm have been studied to date; fracture along a surface scratch has been initiated in most instances by bending, although attempts have been made to cause fracture largely by tension. The data indicate that the velocity of fracture-head starts at a low value, accelerates, and then levels off at a value somewhat less than the velocity of sound. Similar tests are also under way using steel plates in tension.

* This research is being done under contract with the Office of Naval Research.

18. Failure of Metals Subjected to Repeated Plastic Strains.* J. P. PARKER, T. E. PARDUE, AND J. L. MELCHOR, *University of North Carolina.*—A research program has been initiated to determine the behavior of metals when subjected to repeated plastic strains. The experimental procedure consists of rotating a specimen in an R. R. Moore testing machine modified so as to permit the application of loads which stress the material at the outer surfaces of the metal plastically, in cyclic tension and compression. Measurements are made of the torques, strains and number of cycles to failure; these data provide a basis for approximate calculation of total work and work per unit volume necessary to produce failure. Preliminary tests indicate fundamental differences in the performances of three representative materials, cold rolled steel, cast iron and cast aluminum; graphs are presented to illustrate these differences.

* This work was financed by the Office of Naval Research.

19. Possible Method for Measurement of Speed of Brittle Fracture in Steel.* ARTHUR LINZ, JR., AND V. E. SCHERRER, *University of North Carolina.*—Two points, A and B, are placed close together at the center of one edge of a thin rectangular conductor. It has been found by experiment that if the plate is cut in two, starting between A and B and proceeding perpendicularly to the opposite edge, the resistance between the points A and B varies almost linearly with the length, x, of cut, until near the end of the cut: $R=R_0+A\cdot x$, $0<x<0.95d$, where d is the width of the plate. It has been suggested by Dr. F. T. Rogers, Jr. that a voltage developed across such a resistance in the case of a thin plate of steel might be used to study the speed of a brittle fracture across the plate; the discussion will relate to work which has been done in accord with this suggestion.

* This research is being done under contract with the Office of Naval Research.

20. Conditions for Brittle Fracture of Mild Steel. VICTOR SCHERRER AND JOSEPH W. STRALEY, *University of North Carolina.*—Measurements are being conducted to ascertain the conditions under which brittle fracture of notched steel plates may be initiated. Plates 12 inches wide and notched on both sides have been placed in a large testing machine and broken under tension. All fractures seem to start in a ductile or fibrous fashion but a portion may have the cleavage appearance associated with brittle fracture whose width depends on the conditions of the test. The likelihood of brittle fracture is increased if the plates are sharply notched on both sides and if the plate is quite thick at the notch. The dependence on speed in the ductile zone is now being studied by means of a spark chronograph. Speeds in the ductile region vary widely from a few hundred feet per second to several thousand feet per second. Speeds in the brittle region seem in every case to exceed the speeds attained in the ductile region.

21. Creeping Cracks in Slow-Bend Fracturing of Mild Steels.* MARGUERITE M. ROGERS, *University of North Carolina.*—If a slow-bend test specimen[1,2] is halted immediately after precracking, is stained, and then is reloaded to a torque value *below* the maximum which is necessary to cause ductile failure to continue in the ordinary way, it is found[3] that the specimen will begin to yield. If the applied torque is held constant, the creep of the specimen seems to accelerate until the creeping crack so formed develops sufficient speed to cause brittle failure to occur. Data on these creeping cracks will be given.

* This work is being done under contract with the Office of Naval Research.
[1] P. E. Shearin, Phys. Rev. **71**, 832 (1947).
[2] M. M. Rogers and P. E. Shearin, Phys. Rev. **73**, 656 (1948).
[3] This phenomenon was predicted for this particular type of specimen by Dr. G. R. Irwin.

22. The Maximum Normal Stresses in Mild Steel During Bending.* W. J. BYATT AND F. T. ROGERS, JR., *University of North Carolina.*—It is found in the series of tests which are presently under way,[1] that the maximum torque (T) supported by a four-notch type of mild-steel specimen, decreases roughly linearly with increasing depth (x) of the crack in the specimen. Considerable plastic working and deformation occur in these specimens during bending, leading not only to advancement of the crack but also to slight changes in lateral dimensions, to gradual closure of the "back notch," and so on. It does not seem possible to explain this relation of T to x by means of elastic-type maximum normal-stress functions, however non-linear, because they lead to a strongly quadratic relation. Instead it seems that non-linearities and drastic displacements of the neutral surface from the center of retained area, may have to be combined to produce a normal-stress function which satisfies present ideas as to maximum possible local stresses in tension and compression, and which still relates T to x according to the experimental data. The discussion will relate to what can be inferred as to the maximum normal-stress function from the necessary relations[2] involving integrals over the retained cross-sectional area.

* This work is being done under contract with the Office of Naval Research.
[1] F. T. Rogers, Jr., Phys. Rev. **74**, 122 (1948).
[2] S. Timoshenko, *Strengths of Materials* (D. Van Nostrand and Company, Inc., New York, 1930), p. 234.

23. Characteristics of Curved Tubes.* H. A. JARRELL, AND T. E. PARDUE, *University of North Carolina.*—The behavior of curved tubes, whose bend radius is large compared to the tube radius, has been given by von Karman[1] for loads applied in the plane of the bend and by Vigness[2] for loads applied transverse to the plane of the bend. These theoretical results are in good agreement with experimental data. The increased use of bends whose bend radius is comparable to the tube radius (used in high temperature high pressure steam systems) makes it imperative that an extension of the earlier work be carried out to include the effects of the short bend radius. Theoretical analyses have

been made[3–5] and an experimental verification is now being carried out. Reasonable agreement is observed between the theoretical and experimental data.

* This work was financed by U. S. Navy Contract N7onr-284, T. O. 4.
[1] Th. von Karman, "Ueber die Formanderung Dunnwandiger Rohre, insbesondere federnder Ausgleichrohre," Zeitschrift des V.D.I. **55**, 1889–95 (1911).
[2] Irwin Vigness, "Elastic Properties of Curved Tubes," Trans. A.S.M.E. **65**, 105 (1943).
[3] Discussion by H. E. Jenks of paper "Design of Steam Piping to Care for Expansion," by W. H. Shipman, Trans. A.S.M.E., paper FSP-51-52, 1929.
[4] P. S. Symonds and T. E. Pardue, "Characteristics of Short Radius Tube Bends," Second Partial Report (Theoretical), NRL Report No. 0-2761, Feb. 18, 1946.
[5] Leon Beskin, "Bending of Curved Thin Tubes," J. App. Mech. **12** (1945).

24. Effects of Relaxing Materials in Force-Transmitting Linkages.* EMILY JONES AND F. T. ROGERS, JR., *University of North Carolina.*—The problem is considered of relating the displacement $s(t)$ of the driving member in a mechanical system, to the yield $S(t)$ of the driven member, when the driving force $F(t)$ is transmitted between the two by means of a series linkage containing both elastic and time-dependent quasi-elastic members. A first-order differential equation can be set up to relate $F(t)$ and the correction $c(t)=S(t)-s(t)$, which involves various stiffness moduli and relaxation constants appropriate to the linkage. Using constants which apply to the North Carolina slow-bend test-gear,[1] it is possible to obtain c-values which agree favorably with values of $S-s$ which were observed directly at a later date. Apart from the actual numerical values for $c(t)$, it is significant that even well-designed linkages may exhibit relaxation phenomena (perhaps due to inevitable local imperfections of construction) which cannot be neglected if $S(t)$ is sought in terms of an observed $s(t)$.

* This work is being done under contract with the Office of Naval Research.
[1] F. T. Rogers, Jr., Phys. Rev. **74**, 122 (1948).

25. Strain-Aging Effects in the Slow-Bend Fracturing of Mild Steels.* MARGUERITE M. ROGERS, *University of North Carolina.*—The slow-bend fracturing apparatus and the method of staining specimens to correlate crack-depth with work-input, which are used in this series of tests, have been described elsewhere.[1,2] A series of specimens of mild steel was fractured at 120°F, with different time-intervals between the precracking and the succeeding stages of fracture. These time-intervals varied from 10 minutes to 3 days. The work required to fracture the specimen in a ductile fashion, as a function of crack-depth, decreased sharply with increased time of aging, although the torque required to advance the crack in the usual way increased (as would be expected); and both of these phenomena were strikingly evident on the autographic records of the test-data. Presumably the limiting case of this age-hardening would be brittle failure, corresponding to no absorption of energy; but this would require very long aging.

* This work is being done under contract with the Office of Naval Research.
[1] P. E. Shearin, Phys. Rev. **71**, 832 (1947).
[2] M. M. Rogers and P. E. Shearin, Phys. Rev. **73**, 656 (1948).

26. Quantitative Data from a Slow-Bend Test of Mild Steel.* F. T. ROGERS, JR., *University of North Carolina.*—The subject test and its notched design of mild-steel specimen have been described elsewhere;[1–4] both applied torque (T) and energy absorbed (W) are observed in terms of each specimen's deformation (s) and resulting crack-depth (x), under various conditions of temperature, etc. One major part of the problem of quantitative interpretation lies in relating x to s in accord with the experimental data. Another major part, the fact that W is found to be nearly linear in x, has been attributed[4] to the volume-extent of work-hardening. A third part involves the relation of T (roughly) linearly to x, as observed experimentally, and seems to require a non-linear normal-stress pattern.[5] Data are available on other not so obvious phenomena, such as relaxation, lateral deformation, stored elastic energy, crack creepage;[6] and these also require quantitative interpretations.

* This work is being done under contract with the Office of Naval Research.
[1] P. E. Shearin, paper read 18 October 1947 at ASM and Case Institute Seminar of Fracturing, Chicago.
[2] M. M. Rogers and P. E. Shearin, Phys. Rev. **73**, 656 (1948).
[3] M. M. Rogers and P. E. Shearin (to be published).
[4] P. E. Shearin, Phys. Rev. **71**, 832 (1947).
[5] W. J. Byatt and F. T. Rogers, Jr., Phys. Rev. **74**, 121 (1948).
[6] Marguerite M. Rogers, Phys. Rev. **74**, 122 (1948).

27. Reversal of Secondary Series. M. S. MCCAY, *Virginia Polytechnic Institute.*—The absorption spectra of secondary series have never been fully developed in terrestrial sources in a manner comparable to the reversed series obtained from stellar sources. Approximate simulation of stellar conditions under which reversal occurs is realized in various reported schemes. The shielded, field-free center of a HF discharge as a source of such absorptions will be discussed, as will the applicability of the method to the determination of band lines, exact intensity distributions and effective "rotation temperatures" of molecules.

28. Absorption Spectrum of Benzotrifluoride Vapor in the Near Ultraviolet.* H. SPONER AND D. S. LOWE, *Duke University.*—The absorption spectrum of benzotrifluoride vapor at 2740–2450A was photographed in a medium Hilger quartz spectrograph. The band system can be interpreted in terms of an electronic transition A_1-B_1. The 0,0 band appears strongly at 37819 cm^{-1} and happens to coincide with the location of the 0,0 band in fluorobenzene. Several progressions of totally symmetric vibrations occur involving particularly frequencies of 750, 928 and 961 cm^{-1}. The first of these is assigned to the C–CF_3 vibration. Other prominent bands result from vibrations which correspond to the degenerate ϵ_g^+ vibration in benzene responsible for the appearance of the spectrum of that molecule. Bands corresponding to the excitation of ground state frequencies up to 1336 cm^{-1} have been observed at higher pressures and found to coincide with Raman frequencies. As may be expected, the general appearance of the spectrum resembles that of toluene, although there are interesting differences in finer details.

* This work was supported by the Office of Naval Research.

29. Methods in Microwave Spectroscopy.* MYER KESSLER AND WALTER GORDY, *Duke University.*—A filtering circuit will be described that eliminates spurious signals caused by impedance mismatch in the microwave line while allowing amplification of a sharp signal caused by molecular absorption at low pressures. A method will also be discussed for increasing the sensitivity of the system by modulating the microwave source so that a tuned receiver can be employed. Absorption spectra of certain molecules will be given to illustrate the methods.

* The research described in this abstract was supported by a Frederick Gardner Cottrell grant-in-aid from the Research Corporation of New York.

30. Frequency Stabilization of Microwave Oscillators by Spectrum Lines.* JOSÉ L. GARCÍA QUEVEDO AND WILLIAM V. SMITH, *Duke University.*—A 2K50 microwave oscillator has been electronically coupled to the NH_3 3.3 rotational spectrum line at 23,870 megacycles in such a manner as to maintain the frequency of the oscillator at the spectrum line frequency. Details of its construction, operation and observed discriminator slope as a function of pressure and input power are discussed. The discriminator used with an amplifier of 2000 gain reduce drifts by factors of 250 to 1000 compared to an unstabilized tube. Saturation of the ammonia absorption line at high powers sets an upper limit to the attainable stability for a given discriminator.

* The research described in this abstract was supported by Contract No. W-28-099-ac125 with the Army Air Forces, Watson Laboratories, Air Material Command.

31. Microwave Spectra of Cyanogen Halides.* A. G. SMITH, H. RING, W. V. SMITH, AND W. GORDY, *Duke University.*—The microwave absorption spectra of BrCN, ClCN, and ICN have been observed in the millimeter wave-length region. The rotational transitions studies were $J=3$ to $J=4$ for BrCN, $J=2$ to $J=3$ for ClCN, and $J=4$ to $J=5$ for ICN. In each case the fine structure caused by nuclear quadrupole interactions was observed and compared with the theory of Bardeen and Townes. Doubling due to the isotope effect was noted in the cases of BrCN and ClCN. From the measurements it is possible to evaluate the moments of inertia of the molecules, the nuclear spins of the halogens, and the quadrupole coupling factors.

* The research described in this abstract was supported by Contract No. W-28-099-ac125 with the Army Air Forces, Watson Laboratories, Air Materiel Command and a Frederick Gardner Cottrell grant-in-aid from the Research Corporation of New York.

32. Saturation Effect in the Microwave Absorption of Ammonia.* ROBERT L. CARTER AND WILLIAM V. SMITH, *Duke University.*—Attenuation and line width for the NH_3, 3,3 inversion spectrum line at 23,870 megacycles are measured over a power range of from 10 milliwatts per cm^2 to 10^{-3} milliwatts per cm^2, at several pressures below 10^{-3} mm Hg. The peak like attenuation exhibits saturation at high powers in good agreement with theory. Measurement of the increase in line width accompanying saturation leads to an estimate of the collision cross section somewhat smaller than that deduced from collision broadening data.

* The research described in this abstract was supported by Contract No. W-28-099-ac125 with the Army Air Forces, Watson Laboratories, Air Materiel Command.

33. Structure of the Inversion Spectrum of Ammonia.* JAMES W. SIMMONS AND WALTER GORDY, *Duke University.*—Measurements of the fine structure in the ammonia inversion spectrum have been extended into the millimeter-wave region to the 16,16 line at 39944 mc/sec. The relative intensities and positions of the lines are compared with calculated values. The hyperfine structures of 15 lines have been measured. A systematic disagreement is shown to exist between the theoretical and observed separations of the hyperfine components. There is good agreement between the observed and calculated intensities of the hyperfine structure.

* The research described in this report was supported by Contract No. W-28-099-ac125 with the Army Air Forces, Watson Laboratories, Air Materiel Command.

34. Some New Measurements on the Infra-Red Spectrum of HF.* ROBERT M. TALLEY AND ALVIN H. NIELSEN, *University of Tennessee.*—In 1919 Imes[1] observed the fundamental vibration-rotation band of HF at 2.52mμ. Serious overlapping of this band, particularly of the P branch, with the atmospheric water vapor absorption at 2.7mμ prevented accurate measurements of the frequencies of the lines. In 1923 the first overtone was detected at 1.27mμ by Schaefer and Thomas.[2] Kirkpatrick and Salant[3] photographed and resolved beautifully the second and third overtones. There are certain discrepancies between their constants and those computed from Imes' work. With a sample of HF furnished by the K-25 Laboratories of Carbide and Carbon Chemicals Corporation at Oak Ridge the fundamental has been remeasured with a 7200 line-per-inch grating on an automatically recording infra-red spectrograph.[4] It is proposed also to measure the first overtone with high dispersion. Facilities for drying the air in the spectrograph permit much better identification and frequency measurement of the lines in the present data. It is hoped that these measurements will resolve earlier discrepancies.

* The research discussed in this abstract was supported by a Frederick Gardner Cottrell grant-in-aid from the Research Corporation of New York.

[1] E. S. Imes, Astrophys. J. **50**, 251 (1919).
[2] Schaefer and Thomas, Zeits. f. Physik **12**, 330 (1923).
[3] D. E. Kirkpatrick and E. O. Salant, Phys. Rev. **48**, 945 (1935).
[4] A. H. Nielsen, J. Tenn. Sci. **XXII**, No. 4, 241 (Oct., 1947).

35. The Infra-Red Spectrum of HCl in Solution with Dioxane, Di-Ethyl Ether, and Ethyl Acetate. JACK L. PARNELL AND JOSEPH W. STRALEY, *University of North Carolina.*—A study has been made of the infrared spectrum of HCl when in solution in benzene with dioxane, di-ethyl ether, or ethyl acetate. Interest in this problem arose from the observation by Gordy and Martin[1] that subsidiary bands at longer wave-lengths seem to be present. These bands are in addition to those normally expected

to arise as a result of the known tendency of these materials to form weak bonds with protons. A reexamination of the spectrum confirms the existence of these bands shifted approximately 0.4 microns farther into the infrared. A tentative explanation of the cause of this phenomenon will be presented.

[1] Gordy and Martin, J. Chem. Phys. 7, 99 (1939).

36. A Study of Short-Distance Propagation of 147-MC Radio Waves. ROBERT N. WHITEHURST, *University of Alabama.*—In an attempt to investigate the propagation of VHF radio waves over a path which is slightly below line of sight, a 147 mc. transmitter and a continuously-recording receiver have been set up at points approximately one and one-half miles apart. A hill higher than either of the two stations lies between them.

An introductory study of the effects of polarization and antenna height and orientation will be presented. Continuous recordings of field strength have now been obtained for periods up to five days duration in order to study the effects of meteorological factors. It is expected that results obtained from these recordings will also be presented.

37. Durable and Optically Improved Front Surfaced Mirrors Processed Exclusively by Thermal Evaporation. R. W. BOYDSTON, *Georgia School of Technology.*—During World War II, the writer analyzed existing front surfaced mirrors, evaluated their virtues and disadvantages for military use in precision Fire Control instruments. Such analyses revealed that no desirable mirror existed. Research to develop a truly desirable type was undertaken. This paper describes these situations, and culminates in the author's method of processing, and the properties of the evolved "standard" mirror adopted by Army Ordnance in specification FXS-670, and elsewhere, with reasons for the same. All Army Ordnance mirror-making facilities learned these techniques and complied. The durable and optically improved first surface mirrors demanded are described. The method applies to evaporated aluminum, silver, etc., reflectors and consists of a one-half wave-length thickness evaporated layer of durably processed magnesium fluoride overlaying, protecting and enhancing the optical properties of the resultant reflectors. Spectrophotometric curves and durability data are included. Overcoated hard and durable silver front surfaced mirrors, having reflections of 99.2 percent, and similarly treated aluminum mirrors, withstanding terrific abuse with reflections of 93 percent, are produceable.

38. Characteristics of an Acoustic Interferometer. NEWTON UNDERWOOD, *Carbide and Carbon Chemicals Corporation.*—A quartz crystal which sets up vibrations in the liquid is driven by the beat frequency between two other crystal controlled oscillators as devised by McMillan and Lagemann. A reflector is moved down through the liquid by means of a micrometer screw. Each time the reflector is at a nodal point, mechanical resonance occurs. This reacts on the crystal and results in a voltage drop of about 5 percent. Spurious nodal points sometimes appear. This may be remedied in three ways: (1) improve the stability of the acoustic coupling between the crystal and the liquid by driving through a wave plate (thickness equal to the sonic wave-length in the material), (2) keep the liquid surface non-parallel to the plane of the bottom, (3) slope the back surface of the reflector or make it a wave-length in thickness. One of the advantages of the oscillator drive of McMillan and Lagemann is its great stability and insensitiveness to changing experimental conditions. The pressure on the interferometer crystal was varied from 6 plus or minus 2 gmf to 6000 plus or minus 20 gmf, without changing the voltage dips in shape or absolute magnitude in a detectable manner.

39. Ultrasonic Velocity in Some Liquid Fluoro-Carbons.* R. T. LAGEMANN, JOHN EVANS, AND NEWTON UNDERWOOD, *Emory University.*—The velocity of compressional waves has been measured for some liquid fluorocarbons using a movable-reflector acoustic interferometer and a beat frequency oscillator. The frequency employed was 500,000 c.p.s., and, in most cases, the temperature was maintained at 60°C. Included in the compounds was a series of polymers of various molecular weights. It was found that the complete substitution of fluorine for hydrogen in the molecules studied results in remarkably low values of the ultrasonic velocity, approaching, in fact, the range of velocities found for gases. For example, in the completely fluorinated compound, hexadecafluoroheptane, the velocity was found to be only 444 m/sec. at 60°C. The study of a few of the compounds over the temperature range 20° to 70°C showed the velocity to be a linear function of the temperature. The variation of ultrasonic velocity with molecular structure will be discussed.

* Work done under contract with the Carbide and Carbon Chemicals Corporation, Oak Ridge, Tennessee.

40. Temperature Coefficient of Ultrasonic Velocity. D. R. MCMILLAN, JR. AND W. E. WOOLF, *Emory University.*—The velocity of ultrasonic waves was measured in twenty single-component liquids at 10°C intervals over the range of temperatures from 0°C to 60°C. An acoustic interferometer of the movable reflector type was employed for all measurements. Compressional waves were produced in the liquid contained in the interferometer by an x-cut quartz crystal which was driven by a 500 Kc/sec. crystal-controlled oscillator. The ultrasonic velocity was found to vary linearly with temperature for all liquids included in this study. The average temperature coefficient of velocity, defined here as dV/dt, was calculated for each compound from the observed data. A general decrease in the absolute value of this coefficient with increasing molecular weight was obtained. The results are tabulated and illustrated by graphs.

41. A Device for Determining Particle Size Distribution in Smokes. J. E. RHODES, JR., *Georgia School of Technology.*—A practical device for determining the particle size distribution in a smoke has been developed. Its

operation depends upon the fact that the velocity of thermal diffusion of a smoke particle in a gas is a function of its size. The particle bearing gas is passed at a known rate between two parallel walls whose temperatures are each maintained constant, and different from each other so that a temperature gradient is established in the gas. Smoke particles diffuse to and deposit on the cold wall. An examination of the variation of density of particles (number of particles per unit area, irrespective of their sizes) along the wall will yield the particle size distribution in the smoke. Particle densities can be obtained from microscopic counts, and particles can be counted that are too small to be resolved. An operator with experience can determine approximate distributions without laborious microscopic counting. The relation between particle density as function of position on the cold wall and the particle size distribution has to be determined with homogeneous smokes of known particle sizes.

42. Hard and Durable Non-Absorbing Optical Beam Splitters Produceable by Evaporated Multilayer Thin Filming Methods. R. W. BOYDSTON, *Georgia School of Technology.*—Strictly non absorbing beam splitters, impossible with metallized films, fit for outside, exposed optical surfaces, are described. Any prescribed reflectance, zero to 100 percent, or reflectance *vs.* wave-length curves, may be obtained by simple evaporations of alternate low and high index films. The author's processing methods and products replaced all means previously used expensively in complex, long drawn-out, and unsatisfactory procedures. During World War II such evaporatable multilayer films were impossible, since only magnesium fluoride, $N_D = 1.38$, properly processed, was satisfactorily durable. Other films were little more than laboratory curiosities. No technique had evolved giving additional materials required durabilities. Notwithstanding potential optical properties, zinc sulphite ($N_D = 2.37$) films were universally reported hopelessly non-durable. This paper describes the author's processing of ZnS in single or multiple layers with MgF_2 to possess amazing tenacities, toughness, hardness, and chemical durabilities. This disadvantage of ZnS films solved, they were applicable singly or in multiple with MgF_2 to give durable beam splitters, filters, dichroic reflectors, etc., having predictable optical properties. Inside and outside vacuum procedures, products, scientific and engineering applications, are revealed. Uses to date are extensive but strictly military. Spectrophotometric curves, durability data, support presented facts.

43. A Current Integrator for Small Currents. H. G. FLANARY, F. B. PAULS, AND L. A. PARDUE, *University of Kentucky.*—To record accurately the total charge received by a target from an ion source in a high voltage machine such as a Van de Graaff generator an integrating device is needed. This is usually accomplished by measuring the charge received by a condenser.[1] The integrator being described here consists essentially of a 1000$\mu\mu$f mica condenser and a $\frac{1}{4}$-watt neon glow bulb connected in parallel. The charge given up by the condenser in falling from the breakdown potential of the neon bulb to the extinction potential flows to ground through a resistance. The potential drop across the resistance constitutes a pulse which is amplified, shaped and observed on a mechanical recorder. A scaling circuit is used to scale the number of pulses down to a rate acceptable to the recorder when large currents are observed. This integrator is suitable for measuring pulsating currents from 10^{-8} amperes to 5×10^{-5} ampere. The counting rate and current show good linearity. Measurements on an ion source usable in the high voltage terminal of a generator will be discussed.

[1] R. E. Watt, Rev. Sci. Inst. **17**, 334 (1946).

44. Supercooling of Water. R. HOWARD AND C. B. CRAWLEY, *University of Kentucky.*—It is reported that waters from different sources have in general different spontaneous freezing points which are reproducible within small limits, provided the samples have not been subjected between measurements to temperatures much above room temperature. The spontaneous freezing points of some samples are constant for a period of months. Other samples have spontaneous freezing points which are erratic in time. Over a range extending from room temperature to temperatures somewhat above 100°C, the higher temperature to which a sealed sample of water is raised, the lower the spontaneous freezing point thereafter. Water can be held below 0°C for days without freezing. Data are given on the spontaneous freezing points of mixtures of waters as a function of concentrations. It is planned to investigate the relation between x-ray diffraction patterns and spontaneous freezing points. Finally, it is also planned to investigate the effect of centrifuging on the spontaneous freezing point. These investigations follow N. Ernest Dorsey's work as reported in Research Paper RP1105 of the National Bureau of Standards.

45. Crystal "Growth" in the Electron Microscope. A. C. MENIUS, JR. AND T. J. TURNER, *Clemson Agricultural College.*—Recently several observers[1–3] have noticed that objects viewed in the electron microscope change in size and shape when left in the electron beam for short times. This "growth," which is apparently due to some contamination, is critical since observations are therefore limited to a few seconds for any one object. Due to the importance of this phenomenon, a series of measurements have been made using zinc oxide crystals, in an attempt to determine the source of this contamination. The following results were obtained: (a) the growth is a linear function of time up to at least twenty minutes; (b) in contradiction to most observers[2] the growth seems to be independent of the distance of the specimen from the grid; (c) the rate of growth instead of increasing with beam current[2] reaches a maximum at about 0.25 μa and then decreases with current; (d) in agreement with other observers[3] the contamination appears less dense than the zinc oxide crystals.

[1] Watson, J. App. Phys. **18**, 153 (1947).
[2] Cosslett, J. App. Phys. **18**, 844 (1947).
[3] Watson, J. App. Phys. **19**, 110 (1948).

46. The Correlation of the Bioelectric Potential of Corn Seeds with X-Ray Dosage. M. W. JONES, J. G. JONES AND A. A. BLESS, *University of Florida.*—The current theories explaning the origin of the bioelectric potential are outlined. A description of the equipment used in the potentials of corn seeds is given with a resume of the difficulties encountered in its operation. The x-ray equipment and the mode of radiation of the seeds is described. Data and corresponding curves showing the rise of the bioelectric potential with growth of the seeds for the first 48 hours are given. The results of the irradiation of the seeds are tabulated and curves are drawn showing the decrease of the potential with increase of dosage. A summary of the observed results is given and from these results a discussion of the correlation of x-ray dosage, the growth of the seeds and their potentials is given.

47. Production of Short X-Ray Pulses by a Resonant Cavity Electron Accelerator.* L. B. SNODDY AND J. W. BEAMS, *University of Virginia.*—A reentrant copper lined cavity resonator tuned to approximately 400 megacycles is driven by a Western Electric 7C22 pulse operated twin triode. Such a resonator is essentially two quarter wave transmission lines back to back. Consequently, when resonance occurs an alternating high potential exists across the two ends of the "lines" or "gap" inside the cavity.[1] The 7C22 tube is pulsed with about 18,000 volts for sufficient time to permit the oscillations in the unloaded resonant cavity to build up to maximum amplitude. At this point a short duration vacuum spark is produced on one of the electrodes of the "gap" inside the cavity by a special transmission line arrangement. This gives a large burst of electrons which are accelerated across the gap and impinge upon a target. This in turn produces a short intense pulse of x-rays. Measurement showed that about 1.2 Mev electrons were produced. The duration of the x-ray pulse can be controlled by the characteristics of the transmission line feeding the vacuum spark.[2]

* This work was carried out under Contract NOrd-7873 with the Bureau of Ordnance U. S. Navy.
[1] Hereford, J. App. Phys. 18, 956 (1947).
[2] Beams, Kuhlthau, Lapsley, McQueen, Snoddy and Whitehead, J. Opt. Soc. 37, 868, (1947).

48. Operation of Grid-Controlled Fine-Focus X-Ray Tube.* H. M. LONG, JR. AND R. PEPINSKY, *Alabama Polytechnic Institute.*—Constructional details and modifications are described of the fine-focus, grid-controlled x-ray tube reported earlier from this laboratory,[1] and operating characteristics gathered over a two-year period are presented. Using the fine focal spot and a single pinhole at a distance of 11 cm. from it to produce near-parallel collimation (divergence about 20 feet of arc) of the primary x-ray beam, a d.c. tube current of 0.2 μa produces a beam of approximately the same intensity as is available in a beam of similar divergence from a General Electric CA-6 diffraction tube, viewed at the same angle with respect to the target surfaces, when the latter tube is operated at the same d.c. high voltage as the fine-focus tube but at 20 μa tube current. Operation of the tube under periodic grid pulsing is described.

* Development supported by U. S. Army Signal Corps.
[1] R. Pepinsky, Phys. Rev. 69, 546 (1946).

49. Some Observations on Geiger Counters for Periodically Pulsed X-Ray Photon Counting.* P. JARMOTZ AND R. PEPINSKY, *Alabama Polytechnic Institute.*—Carrying further the measurements recently described by Pepinsky, Jarmotz, Long and Sayre,[1] it has been possible directly to measure the time lag between the appearance of an x-ray photon in a Geiger counter and the arrival of the discharge at the central wire. The x-ray tube is pulsed as previously indicated, and an oscilloscope sweep synchronized to the pulses. The pulses to the x-ray tube grid are applied to one vertical oscilloscope plate, and the output of the Geiger tube circuits to the other. A lag of about 1.5 microseconds is observed in the counter pulse, in the case of the new commercial North American Philips "Norelco" mica-window counters radiated with CuKα along a path about 2 mm from the central wire. A coincidence circuit is used to reduce the counter background noise (due to cosmic rays and radioactive contamination). The counter tube amplifier is gated on only during the time when a discharge due to an x-ray pulse can occur. A hundred-fold reduction of background counts is readily achieved, and the detection of very weak diffracted intensities is consequently greatly facilitated.

* Development supported by U. S. Army Signal Corps.
[1] Pepinsky, Jarmotz, Long and Sayre, Rev. Sci. Inst. 19, 51 (1948).

50. Extensional and Thickness Vibrations of Two-Dimensional Crystals.* NICHOLAS CHAKO, *Alabama Polytechnic Institute.*—An investigation has been initiated of the modes of vibration of crystals of various types of symmetry, and a comparison of the results is made with the isotropic plate. Plates of rectangular as well as circular shape have been studied. It is found that for crystals belonging to group VII one obtains independent vibrations along the two axis (radial motion of the particles). For large amplitudes the vibrations in the two directions are coupled and the frequencies are no longer simple harmonic. For crystals of lesser symmetry than quartz, such as rochelle salt, the higher harmonics are in general not integral multiples of the fundamental, although for higher order vibrations the frequencies approach a simple harmonic relationship. For circular plates of quartz one can apply Love's theory, since both the dilatation and rotation vectors satisfy an equation of the type of wave motion with different propagation constants. The results, as one would expect, give a transcendental equation (of the Bessel type) for the determination of frequencies.

* This development supported by U. S. Army Signal Corps.

51. Quantitative Determination of Electron Densities and Contour Line Delineation in the Auburn Electronic Fourier Synthesizer for Crystal Structure Analyses.* R. PEPINSKY AND D. SAYRE, *Alabama Polytechnic Institute.*—By means of a clamping pip voltage detector applied directly to the intensity-modulating cathode-ray tube grid

signal, it is possible to sample quantitatively (within 1 to 2 percent) the projected electron density at any point of the planar map presented by the Auburn Fourier synthesizer for crystal structure analyses.[1] The point of sampling is indicated as a bright or dark pip directly superposed on the CR tube pattern, and the density at the sampled point appears as a meter reading. The accuracy of the measurement is independent of the CR tube screen, and depends only on the oscillators, amplitude potentiometers and subsequent amplifiers. Using simple coincidence circuits set at predetermined voltage levels, it has also been possible to accurately delineate contour lines of electron density directly on the oscilloscope screen. Photographs of contour-line patterns so obtained are presented.

* Development supported by Mathematics Section, Office of Naval Research.
[1] R. Pepinsky, J. App. Phys. **18**, 601 (1947).

52. Photoelectric Two-Dimensional Fourier Analyzer.* D. SAYRE AND R. PEPINSKY, *Alabama Polytechnic Institute.*—The coefficients ΩH_1H_2 of a two-dimensional Fourier series representing a function $\Omega(s_1\bar{a}_1+s_2\bar{a}_2)$, periodic in s_1 and s_2 with periods 1, are calculable from the relation:

$$\Omega H_1H_2=\int_0^1\int_0^1\Omega\cos 2\pi(H_1s_1+H_2s_2)ds_1ds_2 + i\int_0^1\int_0^1\Omega\sin 2\pi(H_1s_1+H_2s_2)ds_1ds_2.$$

Several photoelectric methods are described for evaluating ΩH_1H_2. These depend upon the preparation of photographic transparencies corresponding to Ω, and the multiplication and integration of these over a unit of Ω with a "fringe" corresponding to $\cos 2\pi(H_1s_1+H_2s_2)$ or the corresponding sine. In particular, the Fourier synthesizer for crystal structure analysis under construction at Alabama Polytechnic Institute[1] facilitates this evaluation for cells of any axial ratios and angles, and for H_1 and H_2 values between -20 and 20. The transparencies corresponding to Ω can be obtained radiographically, as will be described elsewhere.[2]

* Development supported by Office of Naval Research.
[1] R. Pepinsky, J. App. Phys. **18**, 601 (1947).
[2] R. Pepinsky (in press).

53. A Counter for Low Energy Ionizing Particles. H. C. THOMAS AND N. UNDERWOOD, *Vanderbilt University.*—A counter which combines large solid angle, low operating voltage, ease of changing source, and ability to detect particles of low energy is described. By means of a revolving plate a sample may be rotated to a position inside the counting chamber through which helium is slowly passing. A large solid angle with low operating voltage is achieved by placing side by side several semicylindrical cathodes whose central wires are electrically connected. Fe^{55} which has a half-life of about four years was used as a sample with which to examine the operational characteristics of the counter.

54. A Simplified Low Pressure Cloud Chamber. ARTHUR WALTNER, *University of North Carolina.*—Low pressure cloud chambers have been of somewhat complicated design.[1] Construction details are given for a simplified low pressure cloud chamber capable of operation at pressures of a few centimeters of Hg. Expansion is initiated by releasing a compressed coil spring held in the "set" position by an electromagnet. The region below the diaphragm is partially evacuated, making it possible to control the rapidity of the expansions by varying the pressure in this region. Electronic photo-flash tubes are used for illumination. Electronic timing circuits provide a variable interval between expansions and a variable delay between the expansion and the photography of tracks.

[1] J. Petrova, Zeits. f. Physik **55**, 621 (1929).

55. Investigation of the Fading of Latent Images of Neutron-Induced Proton Tracks in Special Fine Grain Particle Emulsions. J. S. CHEKA, *Oak Ridge National Laboratory.*—While latent images in ordinary photographic emulsions are very stable, those of nuclear particle tracks in "particle" emulsions are unstable and "fade," i.e., become undevelopable in comparatively short times. The present paper describes the results of investigation of this phenomenon as applied to monitoring of neutron exposures of personnel at Oak Ridge National Laboratory. Several Eastman emulsions of the type NTA and a few specimens of type NTB were tested. It was found that different emulsion batches showed different fading rates. Shorter tracks faded faster than long tracks, consequently, overall drop in density of developable tracks after periods of delay was a function of original distribution of track lengths. Assuming that sensitivity of individual grains was lost with a fixed half-life, decay rates of tracks of various lengths were calculated by Dr. W. S. Snyder of the University of Tennessee. Results showed good agreement with experimental data. Retention rate of recognizable tracks was increased by the use of longer development time. Stale developing solution was found to lose efficiency in bringing out latent tracks.

56. The Energy Dependence of Film Meters. L. J. DEAL, J. H. ROBERSON, *Oak Ridge National Laboratory,* AND F. H. DAY, *National Bureau of Standards.*—Since the earliest use of x-rays, photographic films have been used for detecting the stray radiation exposures of operating personnel. At the start of the Atomic Energy Project a film meter was devised to more accurately measure gamma-radiation. The meter contains a dental x-ray film packet, half of which is covered with a 1-mm cadmium shield to reduce the abnormally high absorption for wave-lengths near the K edge of silver. In order to study the wavelength dependence of the film meter, arrangements were made with the National Bureau of Standards to use their free air chamber and high voltage x-ray machine. Films were exposed to doses of 0.1*r*, 0.5*r*, and 1.0*r* over the range from 10 to 1400 kv. After developing the films under standard conditions, the films were read with an Ansco-Sweet densitometer. Plots were made of the density *versus* the voltage of the x-ray machine. These curves show the following results. The film meters seem to be independent of quantum energy above 350 kv. Between 150 and 300 kv

the shielded film meter reading shows a maximum at about 200 kv, which is roughly 30 percent higher than values in the high energy range. In the unshielded portion of the films the density for a given dosage is a maximum at 90 kv, some 600 percent higher than the density for tube voltages above 400 kv.

57. Focusing Properties of the Electrostatic Analyzer. W. A. BOWERS, *University of North Carolina.*—Numerical integrations of the equations of motion of a relativistic charged particle in a radial electric field inversely proportional to the distance from a fixed axis have been carried out in order to check the validity of the first order focusing theory.[1] This theory predicts perfect focusing of a monoenergetic beam of particles emitted from a line source parallel to the axis, and travelling approximately in a circle about that axis. Results of the numerical integrations show that the focal line is smeared out into a region whose dimensions depend on beam energy, distance of the source from the analyzer, and angular width of beam subtended by the analyzer. In a typical case, with $\beta^2=0.5$, the source distance equal to the radius of the analyzer, and an angle of about 10° subtended by the analyzer at the source, the width of the focal line is about 3 percent of the radius of the analyzer.

[1] F. T. Rogers, Jr. and C. W. Horton, Rev. Sci Inst. **14**, 216 (1943).

58. The Use of Auger Electrons in Coincidence Experiments. S. K. HAYNES AND H. C. THOMAS, *Vanderbilt University.*—Since no energetic charged particle accompanies every disintegration of a nucleus which decays by orbital capture, the study of the decay schemes of such nuclei by coincidence methods is more difficult than the study of those of positve and negative beta-ray emitters. If a very thin source is placed inside a low pressure chamber containing two windowless counters and if both receive particles from the front side of the source, not only x-rays but also Auger electrons can be counted and coincidence experiments can be performed. Experiments on Fe^{55} are underway. The theory has been worked out assuming that only one excited state of Mn^{55} is involved in the decay scheme. Due to large differences in the absorbability of the four different radiations, namely Auger electrons, x-rays, conversion electrons, and gamma-rays, the effects of each can be separated by absorption. Solution of four single counting equations and three coincidence equations yields both the conversion coefficient for the gamma-ray transition and the branching ratio between disintegrations to the ground state and disintegrations which leave Mn^{55} in an excited state.

59. "Band Width" for Energy in the Electrostatic Analyzer. MARY JANE AULD AND F. T. ROGERS, JR., *University of North Carolina.*—Let particles of rest-mass m_0 and charge e traverse the field (average value X) of an electrostatic analyzer of small aperture and small optical power; let ξ be the kinetic energy of particles, in units of m_0c^2. Let $\sigma \ll D$ be the separation of plates, where D is the average length ($r_0\Phi$) in X of paths which completely traverse the field; and let $\zeta = XeD/m_0c^2$. Then for such particles incident on the analyzer's field normally to x direction, approximate calculations indicate that only those particles which have energies in the band $W \leqq (2\sigma/\zeta D)\xi^2(2+\xi)^2/[1+(1+\xi)^2]$, centered at, will be able to pass through the analyzer; particles with other energies will collide with one of the plates. For particles entering in other directions, the band width is generally less than the equation indicates, because of the relatively great thickness (in the particle-optical sense) of the electrostatic lens.

60. Considerations on the Use of Field-Deflections for Determining the Mass of the Meson.* F. T. ROGERS, JR., *University of North Carolina.*—Since the electrostatic analyzer now seems capable of producing predictable focusing of particles of relativistic speeds,[1] it is worth while to examine the application of an earlier experiment[2] on the beta-particles of RaB, to the low energy particles of the cosmic radiation. Such an experiment would be quite large-scale, and would provide values N and n, respectively, for mv^2/e and mv/e, as

$$N = XR, \quad n = B\rho, \tag{1}$$

from which

$$v = N/n, \quad m/e = n^2/N. \tag{2}$$

The analyzer would largely eliminate uncertainties due to scattering in the entrance-slit window,[3] so that both N and n could be obtained for individual particles to within a fraction of one percent. Recent suggestions* relative to the enhancement of usable intensity of mesons for such an apparatus, make it appear possible to obtain intensities comparable to those in other present-day experiments.

* The basic parts of this paper were discussed on February 4, 1948 before the joint Duke-Carolina colloquium. The author is particularly indebted to Dr. L. W. Nordheim and to Dr. O. K. Rice in this connection.

[1] W. A. Bowers, Phys. Rev. **74**, 128 (1948).
[2] Marguerite M. Rogers, A. W. McReynolds, and F. T. Rogers, Jr., Phys. Rev. **57**, 379 (1940).
[3] F. T. Rogers, Jr., Phys. Rev. **73**, 656 (1948).

61. Composite Particles. NATHAN ROSEN, *University of North Carolina.*—In view of the large number of different particles that have been found in nature, one is led to consider the possibility that only a few of them are elementary particles, the others being built up from these. A reasonable assumption is that particles of spin 0 and 1 are formed by a combination of two particles each of spin ½. In accordance with this idea, a system of two interacting particles of spin ½ is treated relativistically. The starting point is similar to that of Kemmer,[1] except that the rest mass of each particle and the total momentum are taken to have arbitrary values. However, the sixteen-component wave function, instead of being expressed in terms of an irreducible representation, is expressed by means of a set of tensors of various ranks. The interaction between the particles can be treated relativistically by the use of the ideas of "statistical geometry."[2] The tensor equations are set up and some of the properties of the solutions are investigated.

[1] N. Kemmer, Helv. Phys. Acta **10**, 47 (1947).
[2] N. Rosen, Phys. Rev. **72**, 298 (1947).

62. A Densely Crowded Group of Galaxies in Serpens. C. K. SEYFERT, *Vanderbilt University.*—A new, unusually crowded group of six external galaxies has been found at the Vanderbilt Observatory on photographs taken at the Harvard Observatory. This sextet of galaxies is in the constellation Serpens and is contained within a volume of space two minutes of arc in diameter. If we assume for the average galaxy in the sextet a normal intrinsic luminosity of 10^8 times the luminosity of the sun and a mass of 2 times 10^9 solar masses for each of the members, the apparent luminosity leads to a distance of 40 million light years and to an average density of the material in the group 7×10^{-21} g/cc. If the individual galaxies are giants or dwarfs in luminosity and hence in mass, the computed distance will be correspondingly increased or decreased, but the computed density will remain essentially unchanged. A comparison of this group with other similar systems indicates that the density of material in the Serpens sextet is greater than that in any other known cluster or group of galaxies.

63. Effect of Rapidity of Expansion on Cloud-Chamber Operation. ARTHUR WALTNER, *University of North Carolina.*—The effect of the composition of the cloud-chamber liquid on the cloud and ion limits is well known.[1] For a given mixture these limits are, however, a function of the rapidity of the expansion. This effect has been studied by varying the rapidity of the expansion and recording the cloud limit, ion limit, and the optimum expansion ratio. It is observed that the cloud limit varies over a wide range whereas the ion limit remains essentially constant. Results are presented graphically and show the optimum expansion ratios for different expansion velocities. Expansion times are calculated from the forces acting and the mass of the moving system.

[1] N. N. Das Gupta and S. K. Ghosh, Rev Mod. Phys. 18, 235 (1946).

64. Present Problems in the Use of the Electrostatic Analyzer. MARY JANE AULD, *University of North Carolina.*—Following the original calculations[1] which showed that a non-relativistically monoenergetic bundle of particle-rays could be focused by a radial inverse-first-power electrostatic field, first-order relationships of more generality were established[2] and were extended to relativistic energies.[3] In the meantime the electrostatic analyzer was widely used, for purposes which generally involved increasing particle-speeds and higher precisions. There are, therefore, present problems having to do with the physics of the instrument itself, such as: the effects of stray-fields,[4] and of "non-uniformities" of field resulting from inevitable constructional non-perfections or from methods[5] of minimizing scattering; scattering; second-order aberrations in general;[6] and ultimate limits to operations, resulting from cold-field emission. It is the purpose of this note to invite attention to the need for resolving such problems.

[1] Hughes and Rojansky, Phys. Rev. 34, 284 (1929).
[2] Herzog, Zeits. f. Physik 97, 596 (1935).
[3] Rogers and Horton, Rev. Sci. Inst. 14, 216 (1943).
[4] Cf. the servo-operated automatic field-plotter under construction by the Department of Electrical Engineering of North Carolina State College, Raleigh, North Carolina.
[5] W. A. Backus, Phys. Rev. 68, 59 (1945).
[6] W. A. Bowers, Phys. Rev. 74, 128 (1948).